THE SELECTIVE RECRUITMENT OF REGULATORY T CELLS TO HUMAN COLORECTAL CANCER

by

STEPHEN THOMAS WARD

A thesis submitted to the University of Birmingham for the degree of

DOCTOR OF PHILOSOPHY

School of Immunity & Infection
College of Medical & Dental Sciences
University of Birmingham
March 2014

ABSTRACT

Regulatory T cells (Treg) are enriched in tumour tissue relative to other compartments. Anti-tumour immunity is promoted through their depletion. It is hypothesised that Treg are recruited to human colorectal cancer (CRC) via a specific combination of chemokine receptors and integrins, blockade of which reduces tumour Treg recruitment, ameliorating the anti-tumour immune response.

A systematic examination was conducted of receptors expressed by CRC-isolated Treg and the cognate ligands expressed by CRC. The effects of receptor inhibition were tested in murine models of colorectal cancer.

Human CRC-infiltrating Treg exhibit a specific chemokine receptor signature, expressing significantly higher levels of CCR5 than conventional T cells. CRC expresses the ligands for CCR5 at significantly higher levels than distal tissue. Isolated Treg migrated towards CCR5 ligands in vitro and suppressed allogeneic T cell proliferation. CCR5 inhibition in murine models of CRC led to delayed tumour growth but had no effect on tumour Treg infiltration compared with vehicle control.

CCR5 inhibition is unlikely to provide any significant reduction in the infiltration of Treg into human CRC. Given the effects CCR5 inhibition had on tumour growth, CCR5 antagonists command further investigation into their potential role as novel therapeutic agents in the treatment armoury against human CRC.

This thesis is dedicated to my wife, Jennifer, to my children, Max and George and to my parents, Thomas and Maureen, without whose support and understanding this work would not have been possible.

Acknowledgements

I would like to acknowledge the help, support and direction of my supervisors, Professor David Adams, Dr Bertus Eksteen and Professor Antal Rot, and the assistance offered to me by Dr Christopher Weston and Dr Stuart Curbishley. I thank Mr Tariq Ismail for his supervision and mentorship over the entire course of my PhD.

Funding from the Bowel Disease Research Foundation and Medical Research Council is gratefully acknowledged.

Acknowledgement is given to the body of consultant colorectal surgeons and consultant pathologists at the Queen Elizabeth Hospital Birmingham, in relation to their help obtaining human tissue samples.

Finally, gratitude is extended to all the patients who consented to donating blood and surplus tissue in support of this research.

Publications arising from this thesis

Ward ST, Weston CJ, Hepburn E, Damery S, Hejmadi RK, Morton DG, Middleton G, Ismail T, Adams DH. Evaluation of serum lysyl oxidase as a blood test for colorectal cancer. *EJSO 2013; 40(6): 731-8*

Ward ST, Li KK, Curbishley SM. A method for conducting suppression assays using small numbers of tissue-isolated regulatory T cells. *MethodsX 2014; 1: 168-74*

Ward ST, Li KK, Hepburn E, Weston CJ, Curbishley SM, Reynolds GM, Hejmadi RK, Bicknell R, Eksteen B, Ismail T, Rot A, Adams DH. The effects of CCR5 inhibition on regulatory T cell recruitment to colorectal cancer. *Br J Cancer* (accepted, October 2014)

Ward ST, Weston CJ, Shepherd EL, Adams DH. Evaluation of serum and tissue levels of VAP-1 in colorectal cancer. (Submitted to PLOS-ONE).

CONTENTS

List of Figures

List of Tables

Chapter 1
General introduction

Introduction to colorectal cancer

Colorectal cancer (CRC) is a common form of malignancy in developed countries. In the United Kingdom (UK), the disease incidence is approximately 38,000 new cases per year, making CRC the third most common malignancy after breast and lung (1). CRC is deadly in one third of patients due to metastases at the time of diagnosis, local recurrence or the development of metachronous metastases following resection of the primary tumour (2).

CRC genetics

Normal colonic glandular epithelial cells can transform into invasive adenocarcinomas due to acquired genetic and epigenetic changes in a process known as the adenoma-carcinoma sequence. Genetic alterations at different stages of neoplastic development were characterised by Vogelstein & Fearon (3), leading them to propose the following model (see Figure 1-1).

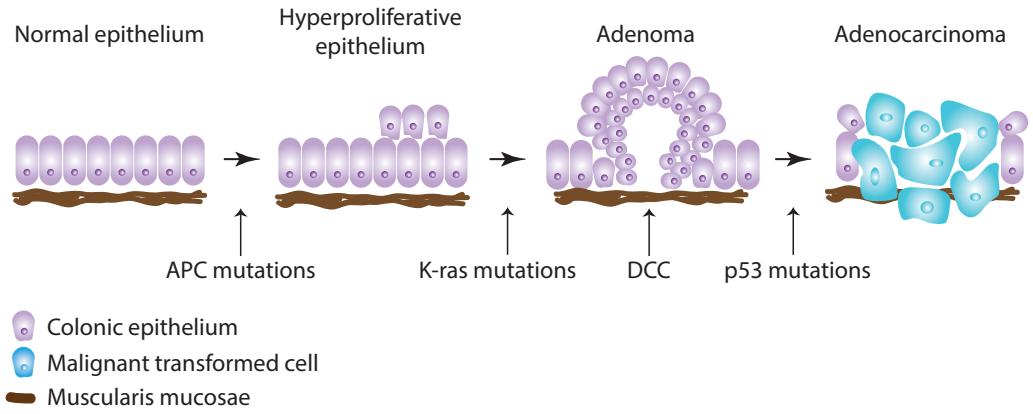

Figure 1-1: The adenoma-carcinoma sequence. Acquired genetic and epigenetic changes transform the normal colonic epithelium into invasive adenocarcinoma.

The two major molecular pathways that lead to these genetic changes are chromosomal instability (85%) and microsatellite instability (15%). The typical genetic changes associated with chromosomal instability are alterations in chromosome number (aneuploidy), losses of portions of chromosome 5q, 18q and 17p and mutations of the KRAS oncogene.

Wnt signalling

Mutations in the APC gene occur in 85% of CRC and is an initiating event in the adenoma-carcinoma sequence (4). ß-catenin localises to the nucleus where it binds to transcription factors regulating genes involved in cellular activation. APC forms part of a ß-catenin degradation complex along with axin and GSK-3 and thereby prevents nuclear localisation of ß-catenin. When Wnt ligands bind to cell-surface Frizzled receptors, Dishevelled proteins are activated which inhibit the ß-catenin degradation complex, leading to increased ß-catenin signalling. This signalling pathway is therefore

known as the Wnt pathway, of which APC is a key regulatory protein. Germ-line mutations in the APC gene result in familial adenomatous polyposis (FAP).

p53 mutations

Mutations in the TP53 gene occur in approximately 50% of CRC. The p53 protein mediates cell cycle arrest, activates DNA repair enzymes and can initiate apoptosis when DNA damage has been detected by the cell. Inactivation of both TP53 alleles often coincides with transition from adenoma to adenocarcinoma (5).

MAPK signalling

KRAS is mutated in approximately 30% of CRC and is a key component of the MAPK (mitogen-activated protein kinase) signalling pathway. Binding of epidermal growth factor to its receptor (EGFR) leads to activation of KRAS, a G-protein, which subsequently binds and activates BRAF (see Figure 1-2). BRAF mutations are found in approximately 5% of CRC. BRAF phosphorylates and activates MEK, MEK phosphorylates and activates MAPK and MAPK alters the activation and levels of many transcription factors controlling transcription of important genes involved in the cell cycle (6). BRAF, MEK and MAPK are all serine/threonine kinases. Mutations in KRAS and BRAF in CRC lead to constitutive activation of these proteins and uncontrolled cell cycle signalling. KRAS and BRAF mutations are profiled in CRC tissue to predict the response to therapies that act on the MAPK pathway. Cetuximab and panitumumab are monoclonal antibodies that block the EGFR receptor to prevent signalling through the MAPK pathway but are ineffective in the presence of RAS or BRAF mutations (7).

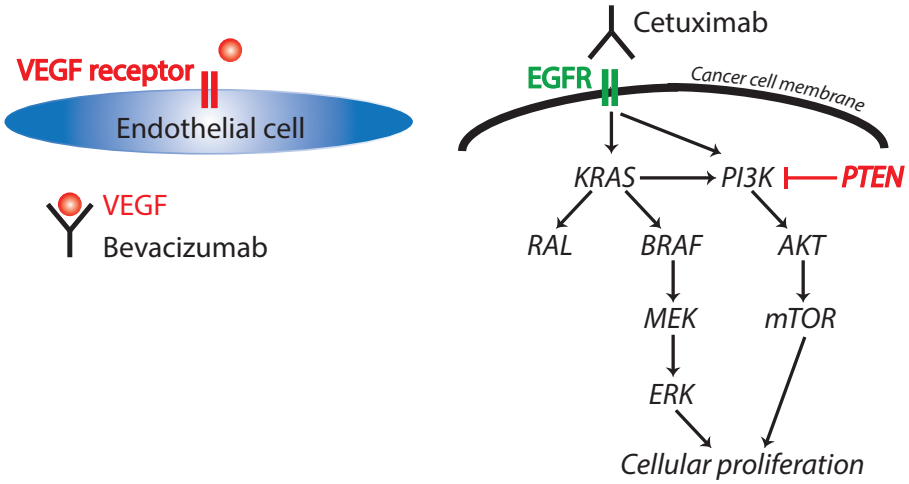

Figure 1-2: The VEGF, MAPK and PI3K signalling pathways. VEGF and EGFR are targeted by monoclonal antibodies. Figure adapted from Bass et al (6).

VEGF

VEGF is known to mediate tumour angiogenesis and in the context of CRC, is associated with aggressive disease (8). The monoclonal antibody, bevacizumab, targets VEGF and has proven efficacy in the treatment of metastatic CRC (9).

PI3K signalling

Growth factor signalling activates PI3K directly or indirectly, via KRAS activation (see Figure 1-2). Akt is a serine/threonine kinase and the main effector of the PI3K-Akt signalling pathway, becoming directly activated in response to PI3K (11). Mutations in PI3K signalling occur in 10-15% CRC. Akt activation leads to increased cellular growth and survival and the most important downstream effector is mTOR. PTEN is a tumour suppressor gene encoding a phosphatase that negatively regulates Akt signalling. Loss of PTEN expression is a poor prognostic marker in CRC (12).

TGF-ß signalling

Mutations in the TGF-ßR2 receptor occur in 30% of CRC and in 80% of microsatellite unstable tumours (10). TGF-ß binds to TGF-ßR2 which then attracts and phosphorylates TGF-ßR1. The activated TGF-ßR1 receptor then phosphorylates Smad2 and Smad3 to allow them to form a complex with Smad4. Loss of Smad4 expression has been reported in >50% of CRC and is associated with lymph node metastasis (11). Smad4 is located on the long arm of chromosome 18 which is an area commonly deleted in CRC. The Smad2/3/4 complex can translocate to the nucleus where it alters gene expression, including the induction of p21, leading to growth arrest. Mutations in the TGF-ß pathway occur in the later stages of the adenoma-carcinoma sequence. The DCC (deleted in colorectal cancer) gene is also sited on the long arm of chromosome 18 and is frequently deleted in CRC. The gene encodes a receptor for the neuronal protein, netrin-1. It is a dependence receptor, in that the absence of netrin-1 signalling leads to apoptosis. Deletion of DCC is a late event in the adenoma-carcinoma sequence although epigenetic silencing of the remaining copy occurs early.

Mismatch repair genes

In the microsatellite instability (MSI) pathway, microsatellites (repeated nucleotide sequences) gain substitution, insertion or deletion mutations that result from inactivation of mismatch repair genes. The hMSH2 or hMLH1 mismatch repair genes are usually affected. A germline mutation results in hereditary non-polyposis colorectal cancer syndrome (HNPCC). Sporadic cases of microsatellite instability result from transcriptional silencing of hMLH1 by promoter methylation and are associated both with carcinoma development from sessile serrated adenomas (as opposed to tubular and tubulo-villous adenomata) and mutations in the BRAF oncogene (11). MSI tumours

are more commonly right-sided, carry a better prognosis and are associated with dense lymphocyte infiltration.

HNPCC or Lynch syndrome is usually caused by inherited mutations of hMSH2 or hMLH1 but can also be due to mutations in other mismatch repair enzymes: MSH6, PMS2. The condition is inherited in an autosomal dominant pattern. Approximately 3% of CRC is due to HNPCC and the condition is characterised by early-onset CRC with a predisposition for the proximal colon. There is an increased risk of synchronous and metachronous tumours and half of affected females will develop endometrial cancer. There is an additional risk of extra-colonic cancers: ovary, stomach, small bowel, pancreas, hepatobiliary tract, upper uroepithelial tract, brain (Turcot variant) and sebaceous adenomas/carcinomas (Muir-Torre variant).

DNA methylation

Both DNA hypomethylation and hypermethylation of gene promoters lead to epigenetic instability in CRC. DNA hypomethylation is associated with chromosomal instability. Hypermethylation occurs in promoter regions that contain CpG islands leading to a CpG island methylator phenotype (CIMP). There is an association between CIMP and BRAF mutations and most sporadic MSI tumours are CIMP positive. CIMP is more frequent in proximal tumours of the colon, an effect independent of MSI status (12).

CRC risk factors

Family history is a risk factor for the development of CRC. The relative risk when there is one first-degree relative with CRC is 2.3 (2.4 for colonic alone, 1.9 for rectal alone). When there is one first-degree relative with CRC diagnosed under the age of 45 years,

the relative risk is 4.0 (13). HNPCC carries an 80% lifetime risk of CRC while the development of CRC in FAP is almost inevitable.

A diet rich in red and processed meats and low in vegetables and fibre has been shown to increase the risk of CRC (14). These were the findings of the EPIC study which has investigated the diets of 400,000 men and women over 9 European countries. Obesity is a risk factor for CRC: BMI (body mass index) is associated with an increased risk of colon cancer in both men and women but an increased risk of rectal cancer in men only (15). Physical activity reduces the risk of CRC and a recent meta-analysis has shown an association between physical activity and the prevalence of colonic adenomas (16).

Both alcohol intake and smoking are risk factors for CRC as well as many other cancers (17). Non-steroidal anti-inflammatory drugs (NSAIDs) have been shown to reduce the risk of developing CRC. Furthermore, NSAIDs can induce regression of pre-existing adenomas and prevent the formation of new polyps. This effect has also been demonstrated in patients at high risk of sporadic CRC (18).

Patients with ulcerative colitis (UC) and Crohns colitis have a higher risk of CRC than the general population, with recent data suggesting a risk of 7.5% after 30 years of disease. The British Society of Gastroenterology (BSG) therefore recommends surveillance colonoscopy at intervals based on risk criteria (19). Patients with extensive colitis, early onset of disease and UC-associated primary sclerosing cholangitis are at particularly high risk.

Polyposis syndromes

Polyposis syndromes are hereditary conditions that are associated with an increased CRC risk. FAP is classically inherited as an autosomal-dominant disease due to a germline mutation of the APC gene. Adenomatous polyps develop as the remaining normal copy of the APC gene becomes inactivated. Progression to malignancy occurs at an average age of 35-40 years (20). Gardner syndrome is a variant of FAP in which the extra-intestinal manifestations of the disease are particularly prominent: osteomas, dental anomalies, epidermal cysts and desmoid tumours. Other extra-intestinal manifestations include periampullary adenomas, papillary carcinoma of the thyroid, hepatoblastoma, osteomas of the mandible and skull and congenital hypertrophy of the retinal pigment epithelium (CHRPE). Turcot syndrome is the association of colorectal polyposis (either FAP or HNPCC) with central nervous system tumours such as glioblastoma multiforme and medulloblastoma. MYH-associated polyposis is another FAP variant that is autosomal recessive due to a mutation in the hMYH gene that codes for a mismatch repair enzyme.

Peutz-Jeghers syndrome is characterised by hamartomatous polyps throughout the gastrointestinal tract and is inherited in an autosomal dominant manner. The gene responsible in most cases is STK11, a serine/threonine kinase. Mucocutaneous pigmentation is an almost universal feature and there is in increased risk of developing CRC, oesophago-gastric cancer and pancreatic cancer.

Familial juvenile polyposis is inherited in an autosomal dominant manner and the majority of cases are due to either mutations in the BMPR1A or SMAD4 genes.

Hamartomatous polyps form from a young age in the stomach, small intestine and colorectum, increasing the risk of CRC.

Cowden disease, also known as the multiple hamartoma syndrome, is an autosomal dominant condition due to a mutation in the PTEN gene. Hamartomatous lesions are present in the skin and mucous membranes and lead to an increased risk of many cancers, including CRC.

Presentation

Patients with CRC may or may not be symptomatic. CRC can give rise to rectal bleeding, a change in bowel habit, abdominal pain, tenesmus, or an abdominal or rectal mass. The presence of CRC can lead to iron-deficient anaemia, diagnosed through blood testing. Symptoms may be noticed by patients who are then referred for further investigation by their doctor. Alternatively, patients may be referred for further investigation following the results of screening tests. Bowel cancer screening in England is currently offered in the form of 2 yearly faecal occult blood (FOB) tests to patients over the age of 50 years. Patients may also present for screening or surveillance investigations based on an increased risk of CRC.

Investigations include endoscopic examination of the colon and rectum (flexible sigmoidoscopy, colonoscopy) and imaging of the abdomen and pelvis (computerised tomography, magnetic resonance imaging, virtual colonoscopy).

The majority of CRC develops from pre-existing polyps, according to the adenoma-carcinoma sequence (21). Polyps identified during endoscopic procedures are thus removed (polypectomy) to histologically assess for foci of malignancy and to prevent

progression along the sequence. Indeed, the incidence of CRC has been shown to decrease within a long-term screening programme involving colonoscopy and polypectomy. The majority of CRC is sited in the left-side of the colon. An audit of all CRC treated at the Queen Elizabeth Hospital Birmingham (QEHB) from April 2006 to July 2010 evaluating the tumour position is in keeping with the published literature (see Figure 1-3).

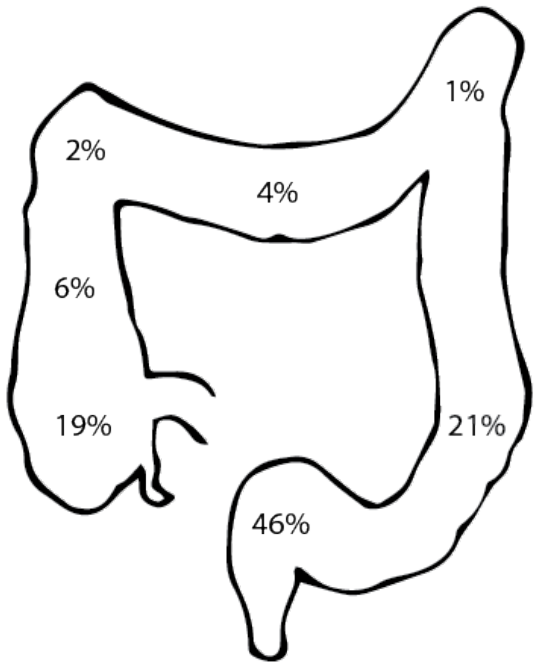

Figure 1-3: CRC frequency by location, based on data from the QEHB, April 2006 to July 2010.

Treatment

The treatment of CRC depends on the disease stage i.e. the extent that the disease has spread. There are two staging systems in common use in the UK.

TNM Classification of malignant tumours

This system is maintained by the International Union Against Cancer (UICC) and the American Joint Committee on Cancer (AJCC). *T* describes the size of the tumour, *N* describes the regional lymph node involvement and *M* describes distant metastasis (22). Specifically, T1 requires the tumour to invade the submucosa. T2 requires the tumour to have invaded the muscularis propria. T3 denotes that the tumour has invaded the serosa layer and T4 requires that the tumour has invaded adjacent organs or perforated the visceral peritoneum (see Figure 1-4). Regarding N staging, N0 means that no regional lymph nodes are involved. N1 denotes that 1-3 regional lymph nodes are involved while N2 means that 4 or more lymph nodes are involved. M0 and M1 denote the absence and presence of distant metastasis respectively, usually to the liver or lungs.

T1 N0 and T2 N0 tumours are also known as AJCC Stage I. T3 N0 and T4 N0 tumours are AJCC Stage II. Lymph node involvement without metastasis is AJCC Stage III and the presence of metastasis is AJCC Stage IV.

The Dukes staging classification predates the TNM staging system but is still often cited both clinically and in the literature. Dukes A tumours are confined to the bowel wall and do not invade into the muscularis propria (T1 N0). Dukes B tumours invade at least into the muscularis propria and possibly beyond and are therefore equivalent to T2/T3/T4 N0 tumours. Dukes C tumours have involved regional lymph nodes (C2 means the apical lymph node is involved and C1 means that the apical lymph node is not involved). The Dukes C classification is equivalent to T1-4 N1-2 M0. Dukes D denotes distant metastasis and is equivalent to T1-4 N0-2 M1.

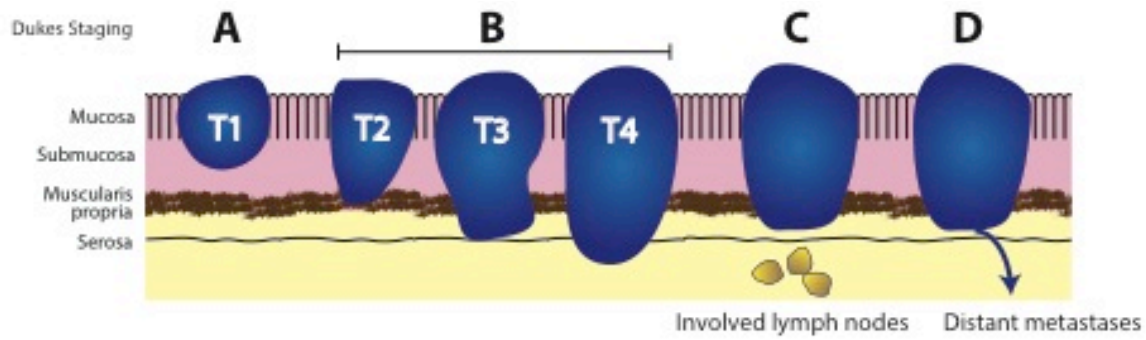

Figure 1-4: TNM and Dukes Staging Systems.

Surgery

Resection of the segment of bowel containing the primary tumour is the mainstay treatment for CRC with the aim to provide cure. The segment of bowel is resected along with its vascular pedicle and associated lymphatics. For colonic tumours, the choice is essentially between a right hemicolectomy or a left hemicolectomy. Right hemicolectomy involves division of the ileocolic and right colic arteries at their origins from the superior mesenteric artery while a left hemicolectomy involves division of the interior mesenteric artery at its origin from the aorta. The ends of the remaining colon are then anastomosed.

Rectal cancers are resected either by anterior resection or abdomino-perineal resection of the rectum. Anterior resection is so-named for historical reasons due to the anatomical anterior approach taken to resect the rectum. The rectal stump is anastomosed to proximal colon and a defunctioning stoma may be performed to protect this anastomosis. In an abdomino-perineal resection, the anal canal is also excised and the patient is left with a permanent end-colostomy. The choice between an anterior resection and abdomino-perineal resection is primarily dependent on the height of the tumour above the anal verge.

Resection of CRC is the primary treatment of the disease provided that a patient is fit for surgery. If a patient has advanced disseminated disease, bowel resection may also be indicated to provide local disease control, but patients will also require treatment of their metastases. In the context of advanced disseminated disease, bowel resection or surgical bypass procedures may also provide palliation of bowel symptoms. In the case of locally advanced tumours, a cure may still be possible with the resection of adjacent viscera.

Chemotherapy

In the UK, approximately one quarter of patients diagnosed with CRC have lymph node involvement (AJCC Stage III, Dukes C, TNM N1+). Such stages carry a 50-60% risk of recurrent disease following surgery. 5-Fluorouracil based chemotherapy is used as an adjuvant treatment in such patients and increases the disease-free survival at 5 years from 42% to 58% when compared to surgery alone (23). More recently, the combination of oxaliplatin with 5-FU regimes has been shown to further improve disease-free survival rates at the expense of increased toxicity (24).

Stage II CRC (Dukes B, T3+ N0) only has a recurrence rate of 20% at 5 years post-surgery and therefore very large studies are required to ascertain any benefit from chemotherapy. In an RCT conducted on such patients, the absolute survival benefit at 5 years has been estimated to be 3.6% (25). However, within this group of stage II patients, exists a subgroup who are more likely to experience disease recurrence and are therefore thought to benefit from adjuvant chemotherapy more than other stage II subgroups.

Radiotherapy

The colon is mobile within the peritoneal cavity, which it shares with other organs including (the very mobile) small bowel. It is therefore difficult to accurately target colonic tumours and the use of radiotherapy is limited to the treatment of rectal cancer. Neoadjuvant radiotherapy, given as a *short-course* of 25Gy in 5 fractions, has been shown to reduce the risk of local recurrence. This is obviously of benefit to the patient but comes at a cost of sterility, increased risk of sexual dysfunction and impaired bowel function. NICE guidelines suggest reserving neoadjuvant short-course radiotherapy for patients with extramural vascular invasion, lymph nodes suspicious of malignant involvement on imaging, or T3b staging (i.e. satellite deposits in the pericolorectal tissues).

So-called *long-course* radiotherapy of 40-50Gy over 5-6 weeks is used to shrink locally advanced rectal cancer. This may enable successful complete surgical resection or permit anterior resection in place of abdomino-perineal resection for rectal cancer.

The immunology of colorectal cancer

There is evidence from both animal models and humans that the immune system is activated in response to primary tumours in an attempt to control or eliminate them (26). Evidence for this comes from studies in mice and humans, showing that immunodeficiency increases the incidence and severity of CRC. Firstly, immunodeficient mice are more susceptible than wildtypes to chemically-induced and spontaneous tumours and patients with primary, and particularly secondary immunodeficiency in response to immunosuppressive treatment in organ

transplantation, have an increased risk of solid non-viral tumours, including CRC, compared with the general population (27). Secondly, it is established that cancer patients can develop adaptive immune responses as seen by the formation of antibodies and T cells which recognise tumour antigens (26,28). Thirdly, the degree of tumour lymphocytic infiltration correlates with survival. Lymphocytic infiltration in CRC is independently associated both with improved overall survival and recurrence-free survival (29). Fifteen per cent of CRC exhibits MSI which carries an improved prognosis compared with microsatellite stable disease (30) and is associated with dense tumour lymphocyte infiltration.

Further analysis of lymphocyte phenotype has shown that the numbers of $CD8^+$ and $CD45RO^+$ (a marker of memory cells) T cells are independently associated with remission rates and survival and may be better predictors of disease outcome than the AJCC TNM Staging system (31). Densities of $CD8^+$ and $CD45RO^+$ cells are determined in the tumour core and invasive margin to derive an *immunoscore*. The challenges of standardising this score, so that it may be used in different laboratories and therefore introduced as a prognostic marker, is a focus of active research (32). There is no proven association between $CD8^+$ and $CD45RO^+$ cell counts in CRC liver metastases and patient survival and this has been highlighted as evidence supporting the immunoediting theory that cancer metastases have formed from cancer cells that have escaped immune control.

The process by which the immune system regulates cancer development is known as immunoediting. Three phases of this process have been defined: Elimination, equilibrium and escape (26). In the elimination phase, the immune system mounts an

inflammatory response to the tumour, involving the generation of tumour-specific $CD4^+$ and $CD8^+$ cells which home to the site of the tumour. The adaptive immune response leads to the killing of antigen-positive tumour cells. However, tumour cell variants bearing different antigens arise. The equilibrium phase represents a balance between tumour cell killing and the selective growth of tumour cell variants. Finally, in the escape phase, tumour cell variants are able to grow despite an intact host immune system. Thus, the development of variant antigens by tumour cells, or the downregulation of MHC antigens, allows the tumour to escape immunosurveillance. Other mechanisms exist to allow the tumour to escape the host's anti-tumour immune response. One such mechanism is infiltration of the tumour by immunosuppressive regulatory T cells (Treg).

Regulatory T cells (Treg)

Treg were originally identified by their ability to maintain self-tolerance, thereby preventing autoimmune disease (33). They are characterised by the expression of CD4, high levels of the IL-2 receptor CD25 and low levels of the IL-7 receptor CD127 on the cell surface and the expression of the Foxp3 transcription factor (34). Whereas conventional T cells (Tconv) become activated and proliferate in response to recognition of their cognate antigen together with appropriate co-stimulation, Treg act to suppress T cell activation and proliferation (see Figure 1-5).

Treg-mediated suppression occurs by a variety of different mechanisms and the predominant in vivo mechanism is unknown, perhaps depending on the target cell and immune microenvironment (35). Treg can both transfer cAMP to other T cells and mediate immunosuppression via the generation of adenosine. Treg consume IL-2,

effectively scavenging it from other T cells, and generate immunosuppressive cytokines such as IL-10, IL-35 and TGF-ß. Direct T cell killing by Treg, mediated by granzyme and perforin has been described (36), whilst indirect suppression is possible via the downregulation of co-stimulatory molecules on APC, mediated by CTLA-4 signalling, or by a novel mechanism in which CTLA-4 removes co-stimulatory molecules from the APC surface (37).

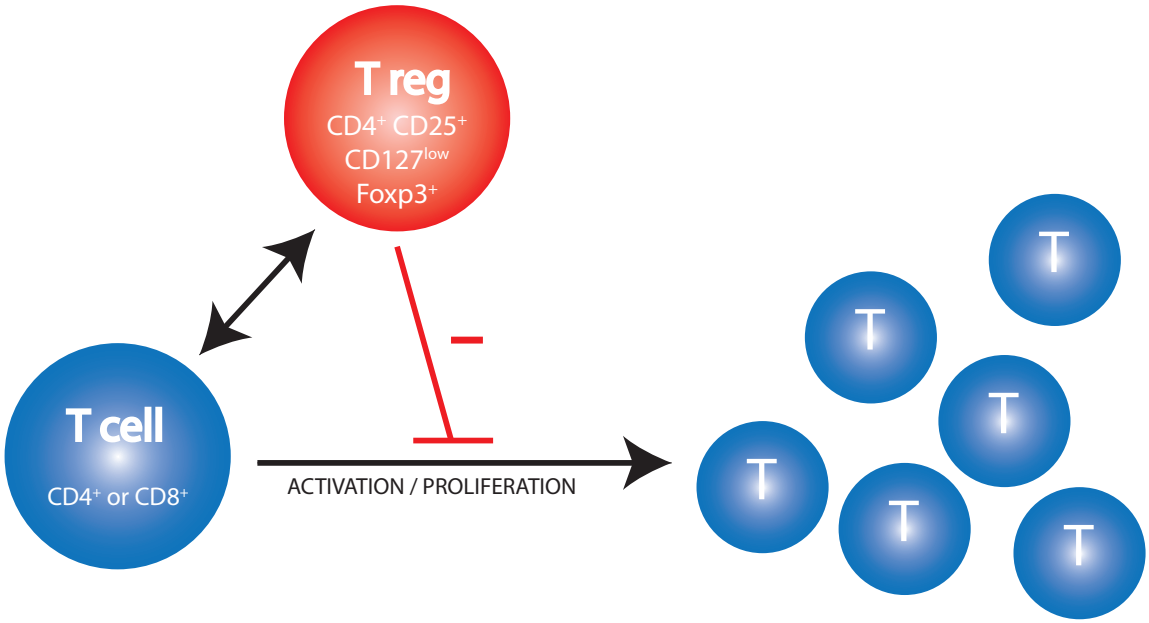

Figure 1-5: Treg act to suppress the antigen-induced activation and proliferation of Tconv.

Cell surface CD25 expression was first reported as a marker for suppressive T cells by Sakaguchi et al. They demonstrated that depletion of these cells in mice resulted in autoimmunity that subsequently disappeared upon reinfusion (33). CD25 can be used to efficiently isolate Treg for use in T cell suppression assays. The combined use of low cell surface expression of CD127 together with CD25 expression as a more elaborate

Treg signature is a more recent development, allowing for the exclusion of activated T cells, which express CD25 and CD127 (38).

Evidence that Foxp3 is the master regulator of Treg differentiation comes from studies showing high amounts of Foxp3 mRNA and protein in $CD4^+CD25^+$ suppressive T cells and loss-of-function mutations in Foxp3 were shown to be responsible for the multi-organ autoimmune disorder, IPEX (in the human) and scurfy (in the mouse). Similarly, forced expression of Foxp3 in $CD4^+CD25^-$ cells leads to a Treg phenotype and suppressor function (39).

Naturally-occurring versus induced Treg

Two populations of Treg exist. Naturally-occurring (nTreg) are generated in the thymus and are present from 13 weeks of gestation in the human (40). In the mouse, nTreg develop in the neonatal thymus. Treg may also be induced from both murine and human $CD4^+CD25^-$ cells in vitro by culture with TGF-ß (41). These are known as induced Treg (iTreg). Both nTreg and iTreg express the canonical Treg markers: CD25, Foxp3 and CTLA-4 and it has therefore proven difficult to distinguish the two subsets (42). Helios is a transcription factor that can reportedly be used as a marker for nTreg (43). Thymic Treg emigrants express Helios, while peripherally induced Treg do not (44). The stability of Foxp3 expression is a hallmark of nTreg: iTreg lose expression of Foxp3 on re-stimulation in the absence of TGF-ß. The stability of nTreg Foxp3 expression has been linked to demethylation of CpG motifs in a highly-conserved element of the Foxp3 locus known as the Treg-specific determining region (TSDR) (45). Thus, it is possible to identify nTreg by assessment of the methylation status of the TSDR.

Other suppressive T cell populations

Other populations of suppressive T cells exist but further study of their role in disease is difficult due to a lack of consensus regarding specific identification markers (46). Type-1 regulatory T cells (Tr1) can be induced from naïve T cells and characteristically express high levels of IL-10 in the absence of foxp3 expression. Th3 cells are also induced from naive T cells, mediate suppression via TGF-ß and express low levels of IL-10 and intermediate levels of Foxp3 (47). A population of suppressive $CD8^+$ cells have been described in CRC, which express CD25 and Foxp3, and are likely induced from other $CD8^+$ cells (48).

Treg and cancer

There have been a number of studies that have demonstrated tumour Treg enrichment relative to other compartments in various cancer-bearing mouse models, with promotion of anti-tumour immunity through Treg depletion (49). This is the basis of the Treg-mediated tumour immune escape hypothesis. According to this hypothesis, T cells infiltrating a tumour attempt to mount an anti-tumour immune response that is hampered by the presence of Treg. Certainly, Treg have been shown to inhibit reactivity of tumour-specific T cells in CRC patients. Treg depletion results in the proliferation of a tumour-reactive T cell population from the peripheral blood of CRC patients in vitro (50). Accordingly, increased numbers of Treg in human CRC tissues have been demonstrated along with many other solid and haematological malignancies. A recent study has demonstrated that the proportion of Treg in peripheral blood was increased in CRC patients compared with controls, and returned to normal levels following bowel resection. $CD4^+$ T cell responses were identified to CRC antigens in the majority of patients and some of these responses were suppressed by Treg.

Interestingly, the existence of Treg-mediated suppressed T cell responses was linked to disease recurrence at one year (51).

Given the hypothesis of Treg-mediated suppression of the anti-tumour immune response, it might be expected that Treg density increases with advancing tumour stage, thereby enhancing tumour escape and allowing progression. One study has reported a positive correlation between Treg density and advancing disease stage although the relationship did not reach statistical significance (52). In contrast, larger studies have shown a statistically significant negative correlation between Treg density and advancing disease stage (53,54). The published literature is also conflicting with regard Treg infiltration of the tumour-draining lymph nodes (TDLN) in CRC, with one study reporting an association between higher Treg infiltration and improved survival (55) while another has reported a correlation between Treg infiltration and advancing tumour stage (56).

This reported decrease in Treg density with advancing disease stage is peculiar to a small number of solid tumours, notably CRC. Rather, a high density of Treg has been associated with poor outcomes in ovarian, pancreatic and hepatocellular carcinoma (57–59). The suppressive capacity of the Treg population is likely to be more relevant than Treg cell numbers, but more difficult to study.

Despite these reports of decreased Treg densities with advanced disease stage, a postulated tumour immune-evasive role for Treg is borne out from robust Treg depletion studies. Depletion of Treg in mouse models has been shown to result in rejection of CRC cell lines providing durable tumour immunity (60). There is now also

direct evidence that Treg depletion results in enhanced tumour vaccine activity in patients with CRC (61).

Lymphocyte trafficking

If Treg are to be effective, they must migrate to the correct tissue location to carry out their functions. Hence, it is important to study how they migrate and localise within the body. The concept of lymphocyte trafficking was first suggested by James Gowans in 1963 and then demonstrated in the late 1970s when T cells harvested from the sheep intestine were autologously transfused back into the animal and were found to home back to the intestine (62). Lymphocytes migrate into tissues via the endothelium lining blood vessels which acts to regulate where and when circulating cells are recruited. To cross the endothelium into tissues, cells must first interact with the vessel wall and be captured from flowing blood in a process of rolling interactions which allows the cells to be activated, leading to arrest and firm adhesion followed by transmigration (see Figure 1-6). These interactions are a process of sequential molecular steps mediated by adhesion molecules and chemokines. Some of these molecular players are generic and operate in many vascular beds but others have a restricted distribution and are able to regulate tissue-specific recruitment, bringing selectivity to the process of trafficking.

With regard intestinal lymphocyte trafficking, specialised dendritic cells (DCs) in the intestine sample antigen and then migrate to lymphoid tissues. Here the DCs interact with naïve T cells to generate primed effector lymphocytes. To ensure that these lymphocytes home to the small intestine where the antigen was encountered, they are programmed to express the chemokine receptor CCR9 and the integrin $\alpha_4\beta_7$. This is a retinoic acid-dependent process and the presence of the required retinal

dehydrogenase is largely restricted to intestinal DCs (63). CCL25, the ligand for CCR9, is expressed in the intestine and mediates activation along with the ligand for $\alpha_4\beta_7$, namely MAdCAM-1, allowing tissue-specific recruitment of primed lymphocytes to the small intestine. Following lymphocyte activation, $\alpha_4\beta_1$ binds to VCAM-1 in a process known as *firm adhesion*. However, it is not clear whether CCR9 is involved in lymphocyte trafficking to the colon. Although a quarter of lymphocytes isolated from the inflamed colon express CCR9, the normal colon does not express CCL25 and $CCR9^+$ T cells do not enter the colon in animal models (64).

Naïve T cells traffic to secondary lymphoid organs by first becoming tethered and rolling using T cell-expressed L-selectin interacting with its ligand, peripheral node addressin (PNAd). This allows CCR7 on the naïve T cells to be activated by its chemokine ligand CCL21 on high endothelial venules. This activation allows alteration of integrin binding affinities to form a firm adhesion interaction between $\alpha_L\beta_2$ and VCAM-1. CCL17 and its receptor, CCR4, are thought to be important in lymphocyte trafficking to the skin (65). Treg migrate from the skin to draining lymph nodes at steady-state in a mouse model and then migrate back to the skin from draining lymph nodes during induced dermatitis (66). Adoptively transferred Treg from CCR7 -/- mice fail to home to lymph nodes while CCR4 -/- Treg fail to home to the skin (67).

With regard to other tissues, populations of gut intra-epithelial lymphocytes expressing CCR10 are recruited to biliary epithelial cells after stimulation of the epithelium to express CCL28 by LPS and IL-1β. These recruited lymphocytes include a population of Treg which have demonstrable suppressive properties (68). Both CCR4 and CXCR3 are

expressed on Treg recruited to the inflamed liver. Flow-based assays have shown that CXCR3 plays the dominant role in recruiting these cells to the hepatic endothelium (69).

Cell Adhesion Molecules

Cell-surface proteins that are involved in binding to other cells or the extracellular matrix are known as cell adhesion molecules (CAMs). These can be classified as immunoglobulin-superfamily-CAMs, integrins, cadherins or selectins. The first two are calcium-independent proteins while the latter two are calcium-dependent.

Selectins

The selectins are a family of cation-dependent glycoproteins that bind cell-surface carbohydrates. The extra-cellular domain consists of a carbohydrate recognition motif, an epidermal growth factor-like motif and a varying length of repeated complement-regulatory protein-like motifs (70). The three family members are E-selectin, L-selectin and P-selectin. The first step of leukocyte trafficking is rolling of the circulating leukocyte along the endothelial wall and this is mediated by selectins (see Figure 1-6). L-selectin is expressed by most leukocytes while E- and P-selectin are expressed by inflamed endothelial cells (71). A ligand for all three selectins is P-selectin glycoprotein ligand 1 (PSGL-1). L-selectin also binds GlyCAM-1, MAdCAM-1 and PNAd. Secondary tethering can occur via interactions between L-selectin on one leukocyte and PSGL-1 on another in order to capture circulating leukocytes that do not express selectin ligands.

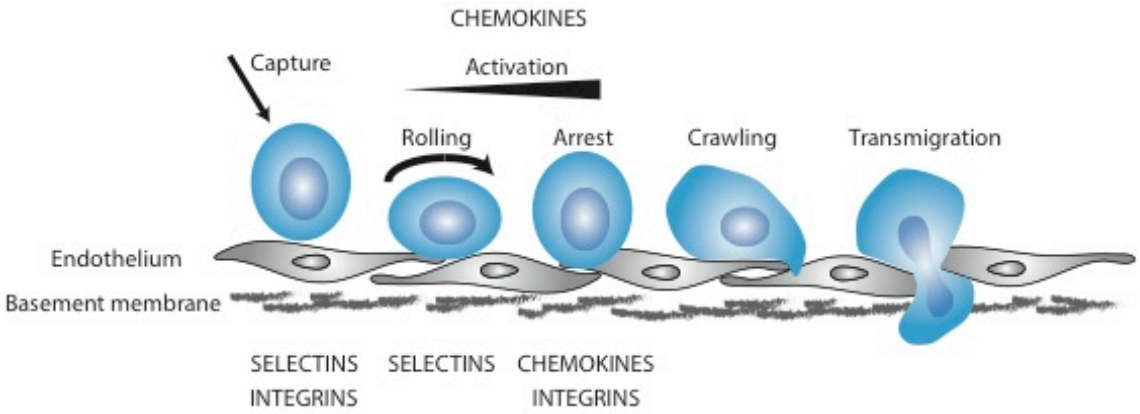

Figure 1-6: The steps involved in lymphocyte trafficking. Lymphocyte capture is mediated by selectins and integrins. Rolling along the endothelium is mediated by selectins. Lymphocytes become activated and arrest, mediated by chemokines and integrins, before crawling and transmigrating through the endothelium. Adapted from Ley et al (71).

There is evidence that E-selectin may be exploited by tumour cells to facilitate metastasis. Metastatic CRC cells can roll and adhere to endothelial cell monolayers expressing E-selectin and highly metastatic tumour cells bind more avidly than their less metastatic counterparts (72).

L-selectin is thought to be critically important for lymphocyte recruitment to secondary lymphoid tissues via high endothelial venules and is found on naïve T cells. L-selectin is expressed by Treg and it has been reported that only L-selectin expressing-Treg protect against the development of lethal colitis in a murine bone marrow transplant model (73).

Integrins

The integrins are molecules composed of α and β subunits that bind to cell-surface or soluble ligands and extracellular matrix proteins. Fourteen members of the integrin

family are known to be expressed by immune cells and the β1 and β_2 integrins are leukocyte-specific (74). Their ligands include fibronectin, vitronectin, collagen, laminin and members of the Ig-superfamily CAMs. Integrins contribute to intercellular adhesion, anchorage-dependent cell survival and regulate intracellular events via transmission of outside-in signals (75).

Epithelial cells, including those in colonic tissue, strongly express β_1 integrins whereas β_2 integrins are restricted to leukocytes (76). Variable expression of integrins is seen in CRC tissue. $\alpha_v\beta_6$ has been studied in relation to CRC metastasis (77) where it is involved in the degradation of the extracellular matrix during cancer progression. The β_1 integrin has been implicated in binding of CRC cells to hepatocytes during metastasis (78).

The $\alpha_4\beta_7$ integrin is expressed by memory gut-homing lymphocytes allowing them to bind to MAdCAM-1. Lymphocytes homing to non-mucosal tissues lack $\alpha_4\beta_7$ and express $\alpha_4\beta_1$, allowing binding to VCAM-1 (79). The integrin $\alpha_4\beta_7$ is expressed by the majority of intestinal intra-epithelial lymphocytes and only a minority of circulating and lamina proprial lymphocytes (80). $\alpha_E\beta_7$ is upregulated by T cells after entering the intestinal epithelium and allows binding to E-cadherin on the epithelial cell surface, promoting tissue lymphocyte retention.

MAdCAM-1 is expressed constitutively on endothelial cells throughout the small intestine and colon and can be upregulated at numerous other sites during inflammation. Aberrant expression of MAdCAM-1 on hepatic endothelium in ulcerative colitis promotes recruitment of gut-trophic lymphocytes resulting in chronic hepatitis

(63). In a murine model of colitis knockout of β_7 on Treg led to a reduction in colonic Treg infiltration (81). Treg subsets have been characterised by virtue of their integrin profile: $\alpha_4\beta_7^+$ Treg induce IL-10-secreting Tr1 lymphocytes (Type 1 regulatory cell) while $\alpha_4\beta_1$+ Treg induce TGF-ß-producing Th3 lymphocytes (T helper 3 cell) (82). Similarly, expression of $\alpha_E\beta_7$ identifies a population of Treg which produce small amounts of cytokines, yet are potently suppressive (83).

Integrins can mediate not only arrest and firm adhesion but also the rolling process as part of leukocyte recruitment. Both $\alpha_4\beta_7$—MAdCAM-1 and $\alpha_4\beta_1$—VCAM-1 interactions can mediate rolling in addition to the aforementioned selectin interactions (71). Lymphocyte arrest during the rolling process is triggered by chemokines and mediated by binding of integrins on lymphocytes to immunoglobulin superfamily members expressed by endothelial cells, for example $\alpha_4\beta_1$ with VCAM-1 and $\alpha_L\beta_2$ with ICAM-1 (84).

Soluble forms of VCAM-1 and ICAM-1 exist, their upregulation by endothelial cells mediated by cytokines derived from the tumour epithelium (85). Serum levels of VCAM-1, ICAM-1 and E-selectin are significant prognostic factors in CRC, perhaps reflecting their role in tumour progression and metastasis (86).

The integrin subunit α_E (CD103) is thought to mediate lymphocyte retention in epithelial tissues via interaction with its ligand, E-cadherin, expressed by epithelial cells (87). In a study analysing Treg in four different murine cancer models, almost all Treg expressed CD103 (88). The integrin sub-unit did not, however, appear to be involved in either homing or retention of Treg in relation to the tumour tissue. CD103 can be

induced on tumour-specific T cells by TCR engagement and local TGF-β. Interaction between CD103 on T cells with E-cadherin on tumour cells has been shown to recruit CCR5 to the immunological synapse. This has the effect of reducing the sensitivity of T cells to CCR5 ligands and provides an indirect means of lymphocyte retention in tumour tissues (89).

Chemokines and chemokine receptors

Chemokine receptors are a sub-family of G-protein-coupled receptors that are found predominantly on the surface of leukocytes and have a seven-transmembrane structure. On binding cognate ligand, receptor signalling leads to a range of cell activities including cell migration, differentiation and effector functions (90). In cancer biology, chemokine-chemokine receptor interactions are known to be a major determinant of macrophage, natural killer-cell and lymphocytic infiltration in human carcinomas (91). Chemokine receptors expressed on the cell surface may, however, not be functional (92,93). Most chemokine receptors recognise more than one chemokine i.e. they are promiscuous, but only rarely can chemokine and receptor interactions span receptor subclasses. Similarly, many chemokines can bind to multiple receptors. See Table 1-1 for a list of chemokine receptors and their ligands. Classification is based on molecular structure according to the number and spacing of conserved cysteine residues. There are four groups denoted by CXCR, CCR, CR and CX_3CR where C relates to a cysteine residue, X an intervening amino acid and R signifies a receptor as opposed to a ligand (L). There are eleven members of the CC group, seven of the CXC group and only one each of both the CX_3C and C groups.

The RNA profile of an array of chemokines and chemokine receptors was analysed in paired samples of CRC and distal colon from eight patients undergoing colonic resection (94). CCR1 and CCR5 together with their ligands CCL4 and CCL5 were found to be strongly overexpressed in the tumour tissue compared with the colon. The pro-angiogenic chemokines, CXCL1 and CXCL8, were also overexpressed with their receptor, CXCL2.

Table 1-1: List of chemokine receptors with their ligands

Receptor	**Ligands**
CCR1	CCL3,CCL5,CCL7,CCL13,CCL14,CCL15,CCL16,CCL23
CCR2	CCL2,CCL7,CCL8,CCL13,CCL16
CCR3	CCL5,CCL7,CCL8,CCL11,CCL13,CCL15,CCL16,CCL24,CCL26,CCL28
CCR4	CCL17,CCL22
CCR5	CCL3,CCL4,CCL5,CCL8,CCL11,CCL14,CCL16
CCR6	CCL20
CCR7	CCL19,CCL21
CCR8	CCL1
CCR9	CCL25
CCR10	CCL27,CCL28
CXCR1	CXCL6,CXCL7,CXCL8
CXCR2	CXCL1,CXCL2,CXCL3,CXCL5,CXCL6,CXCL7,CXCL8
CXCR3	CXCL9,CXCL10,CXCL11, CXCL4 (B isotype)
CXCR4	CXCL12
CXCR5	CXCL13
CXCR6	CXCL16
CXCR7	CXCL12
XCR1	XCL1,XCL2
CX3CR1	CX3CL1
CCX-CKR	CCL19,CCL21,CCL25
D6	CCL2,CCL3L1,CCL4,CCL5,CCL7,CCL8,CCL11,CCL13,CCL14,CCL17, CCL22
DARC	CCL2,CCL7,CCL8,CCL11,CCL13,CCL14,CCL16,CCL17,CXCL1,CXCL5, CXCL6, CXCL7, CXCL8, CXCL9, CXCL11, CXCL13

A brief overview of the role of individual chemokine receptors in relation to cancer immune cell recruitment will now be presented. Chemokine receptors are detected on

tumour-infiltrating leukocytes but are also found with a more restricted distribution on tumour cells and tumour-associated stroma. I will focus on the expression on infiltrating leukocytes:

CCR1 has been found on tumour-infiltrating leukocytes in a mouse model of breast cancer. The tumour infiltrate was reduced by treatment with a CCR1 antagonist (95). There are however no reports of CCR1-expressing lymphocytes in human CRC. Immature myeloid cells expressing CCR1 were recruited to tumours in a mouse model of CRC and liver metastases. Blockade of CCR1 in this model led to reduced metastasis and improved survival (96).

Lymphocytes infiltrating CRC liver metastases express low levels of CCR3, yet tumours express high levels of CCL24 (97). High levels of CCL24 may not lead to $CCR3^+$ T cell enrichment as the CXCR3 ligands, which are also secreted by CRC metastases, can inhibit CCR3-mediated functional responses (98).

Approximately 75% of Treg isolated from human peripheral blood express CCR4 (99). Injection of an adenoviral vector encoding an array of different chemokines found that CCL17 transduction induced tumour regression in a murine model of CRC, associated with $CD8^+$ cell infiltration (100). In a study on gastric cancer, tumour Treg infiltration was found to be positively correlated with CCL17+ or CCL22+ cell infiltration (101). In human ovarian cancer, tumour tissue and tumour-associated macrophages express CCL22 which can support the recruitment of $CCR4^+$ Treg into the tumour (57).

$CCR5^+$ T cells have been demonstrated in CRC by immunohistochemistry (102) and flow cytometry (103). The main ligands for CCR5 are CCL3, CCL4 and CCL5 which are all

expressed by CRC (102). In a murine model of pancreatic cancer, CCR5 expression was demonstrated on tumour-infiltrating Treg (104). Reduction of tumour CCL5 expression by shRNA was associated with smaller tumours and reduced tumour Treg infiltration.

Human CRC cells express CCL20 and CCR6 in a non-polarised manner and both molecules are upregulated compared with the colonic mucosa (105). A $CCR6^+$ Treg population is found in human breast cancer and their frequency is associated with a poor prognosis (106).

There is little evidence for CCR7-dependent T-cell recruitment to CRC. In fact, there is less expression of the CCR7 ligand, CCL21, in CRC compared with the colon (107). Peripheral blood Treg do however express high levels of CCR7, especially following Treg expansion (108). This probably directs their migration to lymphoid tissues rather than to sites of inflammation, or to tumours.

Peripheral blood T cells, including Treg express CCR8 (109). Blockade of the CCR8 ligand, CCL1, reduces the number of tumour-infiltrating Treg by inhibition of Treg induction as well as effects of recruitment (110).

CCR9 is expressed by memory and effector lymphocytes homing to the small bowel. Its ligand, CCL25, is selectively expressed in the small intestine and thymus (111). CCR9 is also expressed by gut-homing tolerogenic plasmacytoid dendritic cells which are potent inducers of Treg (112). There is little evidence for CCR9 dependent T cell trafficking to the human colon. CCL25 is not expressed in the normal colon (113), although it has been detected in inflamed and non-inflamed colonic tissue in a murine model of colitis

(114). Our own data show the presence of $CCR9^+$ T cells associated with CCL25 expression in inflamed human colon.

CCL28 *is* expressed by the epithelium in human colon and to a lesser extent, in the small intestine (115). It is the ligand for CCR10 and its expression is reduced in CRC compared with the colon (116). A recent study has shown that CCL28 is upregulated in hypoxic ovarian tumours, correlating with HIF-1α levels. This, in turn, leads to increased tumour $CCR10^+$ Treg infiltration (117). There is, as yet, no evidence for the existence of this pathway in CRC.

CXCR1 and CXCR2 are closely related chemokine receptors that recognise CXC chemokines possessing an E-L-R amino acid motif. CXCL8 (also known as IL-8) and CXCL6 bind chiefly to CXCR1 while the other E-L-R chemokines (CXCL1 to CXCL7) bind to CXCR2 only. Both CXCR1 and CXCR2 together with their ligand, CXCL8, are expressed by CRC cell lines with metastatic potential (118). CXCR1, CXCR2 and CXCL8 are expressed by the tumour epithelium in human CRC (119). Marked induction of CXCR1 and weak induction of CXCR2 on Treg has been demonstrated in response to IL-6 (120). However, there are no reports of CXCR1- or CXCR2- expressing Treg in CRC.

It is well established that activated $CD4^+$ cells express CXCR3, mediating T cell trafficking (121). CXCR3 expression has also been demonstrated by Treg in the inflamed human liver, enabling Treg to bind and transmigrate through the hepatic sinusoidal endothelium (122). $CXCR3^+$ Treg isolated from human peripheral blood are suppressive and migrate towards the ligand, CXCL10 (123). CXCR3 can also be upregulated by $CXCR3^-$ Treg following activation with anti-CD3 and anti-CD28 in the presence of IL-2. $CXCR3^+$ Treg have been identified in human CRC (124) and the

cognate ligands, CXCL9 and CXCL11, are overexpressed by CRC compared with the colon (94).

CXCR4 mRNA is expressed by Treg resident in malignant mesothelioma and the CXCR4 ligand, CXCL12, is expressed by the tumour tissue (125). Treg isolated from human peripheral blood were found to not migrate towards CXCL12 (126). However, on activation by monocyte-derived DCs, Treg upregulated CXCR4 and efficiently migrated towards its ligand.

CXCR5 was originally identified in Burkitt's lymphoma and subsequently found on B cells and on T cell subsets. Human tonsillar Treg express CXCR5 and it has been suggested that this may lead to migration to germinal centres (127). Human peripheral blood Treg express CXCR5 at relatively low levels (128).

Human peripheral blood Treg express little CXCR6 (128,129). CXCL16 is expressed by human CRC and there is a positive correlation between CXCL16 levels, lymphocytic infiltration and prognosis (130).

CXCR7, like CXCR4, binds to CXCL12. CXCR7 mediates chemotaxis of cancer cells towards CXCL12 in vitro but there are no reports of CXCR7 mediating tumour immune cell recruitment (131).

The ligand for CX3CR1, CX3CL1 (also known as fractalkine), is expressed by human CRC and CX3CL1 levels correlate with the degree of lymphocytic infiltration into the tumour and improved prognosis (132). CX3CR1 is expressed by tumour-resident NK cells and $CD8^+$ cells. There is however minimal expression of CX3CR1 on human peripheral blood Treg (133). Proliferation of Treg in the gut mucosa may be related to the

presence of CX3CR1^{+} APCs (134). In CX3CR1 -/- mice, gut Treg numbers and IL-10 production by gut macrophages was reduced. XCR1 expression by human peripheral blood Treg has been demonstrated (135). XCR1 is also expressed by human DCs, in particular intestinal DCs, which migrate towards the cognate ligand, XCL1 and extend projections through the colonic epithelium to sample the gut lumen (136).

Exploitation of chemokine signalling by cancers

Tumour cells may express a variety of chemokine receptors which have been implicated in promoting metastasis. Analysis of RNA and protein levels in primary and metastatic CRC have shown overexpression of CCR6 and CXCR4 in both primary and metastatic tumours compared to non-tumorous tissue (137). Highest tissue levels of CCL20 were found in the liver, the most common site for CRC metastasis. CXCR4-expressing tumour cells are enriched at the site of liver metastasis compared to the primary tumour and a CXCR4 inhibitor reduced the development of liver metastasis in a mouse model (138).

CXCR3 may be expressed by CRC tumour cells (139). In a mouse model, CXCR3 antagonism was found to reduce the incidence of lung but not liver metastases and this was associated with weaker expression of CXCL10 and CXCL11 in the liver compared to the lung.

CCR9 expression has been identified on melanoma cells that have metastasised to the small bowel, whereas CCR9 is rarely expressed by melanoma cells that have metastasised to other sites (140). This implicates the CCR9-CCL25 axis in the metastasis of melanoma to the small bowel.

Treg markers

GITR

GITR (glucocorticoid-induced TNFR-related protein) is a member of the TNFR superfamily and is expressed mainly by lymphocytes. Its ligand, GITRL, is expressed on APCs and acts as a co-stimulation signal for effector T cells (141). GITR is expressed by Treg under the control of Foxp3, yet its expression is not required for Treg to exhibit suppressive activity (142). GITR is not a specific marker for Treg as it is expressed at similar levels by activated $CD4^+$ and $CD8^+$ cells. Triggering of GITR may enhance or inhibit Treg suppression. In a murine model of CRC, Treg expressed increased levels of GITR compared with Treg isolated from the spleen (143).

CTLA-4

Binding of CD28 present on the surface of T cells, with CD80 or CD86 on APCs constitutes the second co-stimulatory signal, resulting in T cell activation. CTLA-4 is a cell surface receptor found on T cells that also binds CD80 or CD86, but provides an inhibitory signal (144). CTLA-4 is constitutively expressed by Treg, under the control of Foxp3 and deficiency of CTLA-4 results in impaired Treg suppressive capacity (145). Blockade of CTLA-4 both on Tconv and Treg has been shown to enhance the anti-tumour immune response (146).

CD27

CD27 is a member of the TNF receptor superfamily and part of a lymphocyte-specific subgroup comprised of CD30, CD40, 4-1BB and OX40. Its ligand is CD70, expressed on lymphocytes and dendritic cells. Lymphocytes upregulate CD27 following TCR engagement, thereby enhancing their survival. Effector T cells downregulate CD27,

suggesting that its co-stimulatory effects occur early on in the adaptive immune response (147). CD27 expression has also been used as a marker of naïve and memory lymphocytes while absence of expression is seen in effector populations (148).

In a murine model of CRC, the phenotype of Treg from the spleen was compared to that within the tumour (143). There were high levels of CD27 expression by Treg both in the tumour and spleen. As the tumour progressed, CD27 expression on tumour-infiltrating Treg diminished yet remained at stable levels in the spleen.

OX40 (CD134)

OX40 is a member of the TNF receptor superfamily. Knockout studies in mice have shown that OX40 plays an obligatory and non-redundant role in the generation of memory T cells via the upregulation of cell survival genes (149). Treg constitutively express OX40 but its use as a Treg marker is limited as OX40 is also expressed by activated effector T cells. Stimulation of OX40 in vivo can break tolerance to peptide antigens (150), highlighting the potential of OX40 as a target for therapy. Treg OX40 stimulation abrogates Treg suppressive function and inhibits induction of Treg from other T cells (151).

CD39 & CD73

CD39 is an ectonucleotidase that cleaves ATP to form AMP or ADP. Subsequently, AMP can be rapidly hydrolysed to from adenosine by CD73, another ectonucleotidase (see Figure 1-7). The catabolism of the triphosphate to the monophosphate by CD39 is the rate-limiting step for the formation of adenosine (152). CD39 is highly expressed by Treg in humans (153). Extra-cellular ATP promotes an inflammatory response via leukocyte recruitment and activation of the inflammasome. Activation of P2 receptors

leads to the production of inflammatory cytokines via NF-κB signalling. On the other hand, pericellular adenosine is immunosuppressive, an effect mediated at least partially through the A2A adenosine receptor. A2A receptor stimulation, on Treg and effector T cells, limits the production of lymphocyte-derived pro-inflammatory cytokines, independent of both TGF-ß and IL-10. Adoptive transfer of Treg in mice prevents the induction of colitis by effector T cells. However, Treg failed to control colitis when effector T cells lacked the A2A receptor (154). A2A receptor binding is associated with a rise in intracellular cAMP. It is possible that cAMP can be passed from Treg to effector T cells via gap junctions on close cell-to-cell contact (155). While Treg are well-known to suppress IFN-γ production by effector T cells, $CD39^+$ Treg but not $CD39^-$ Treg can suppress the production of IL-17 (156). Tumour-infiltrating IL-17 producing T cells (Th17s), are thought to carry a poor prognosis in CRC (157).

In murine models of metastatic CRC and melanoma, CD39 deletion in recipient mice inhibited hepatic growth of tumours (158). Furthermore, pharmacological inhibition of CD39 using polyoxometalates suppressed hepatic tumour growth in wild-type mice. Extracellular ATP has been shown to directly inhibit cancer cell proliferation and promote cancer cell death, an effect mediated largely through the P2X(7) receptor (159). CD39 expression therefore promotes tumour growth by scavenging extracellular ATP.

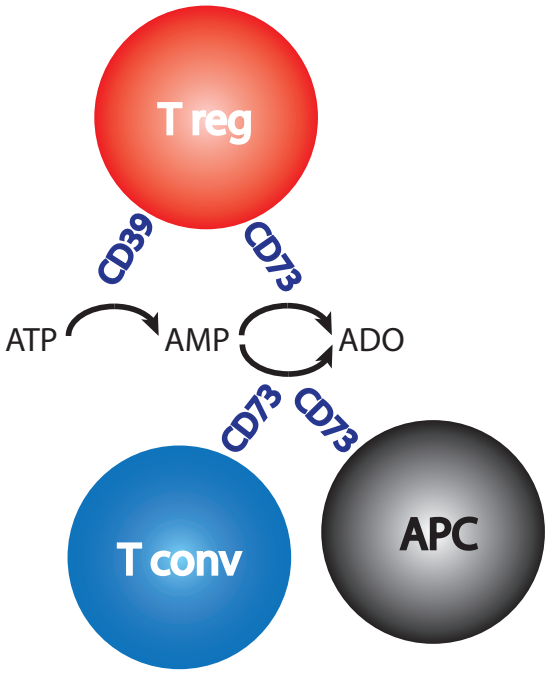

Figure 1-7: Extra-cellular adenosine is generated by cell surface CD39 and CD73 on Treg, Tconv and APC. Adapted from Ernst et al (155).

CD73 is expressed by 59% of the human peripheral blood Treg population, compared with 69% for CD39. On activation, CD73 is upregulated by all T cell subsets (160). Proliferation of human peripheral blood T cells is blunted by CD73 inhibition and in a murine model of gastritis, adoptive transfer of CD73-deficient Treg (but not wildtype Treg) fails to prevent gastric inflammation.

CD73 is also expressed by tumour cells, acting to suppress anti-tumour immunity and promote tumour cell metastasis (161). In a murine model of CRC, CD73-deficient mice, were resistant to tumour growth (162).

Summary

This chapter has provided an introduction to the molecular basis of CRC and how the immune system strives to control it. There is good evidence that the immune system mounts an anti-tumour immune response, the strength of which is associated with prognosis (31). Immunosuppressive Treg infiltrate CRC where they are enriched compared to other tissues and are thought to mediate an immune escape mechanism. This introduction has explained the processes involved in immune cell recruitment to tissues via chemokines and integrins – processes that apply to Treg and other lymphocytes. It is possible that these recruitment mechanisms could be manipulated to reduce tumour Treg infiltration and tip in the balance in favour of a robust anti-tumour immune response.

HYPOTHESIS

- The natural anti-tumour immune response against CRC is suppressed by Treg.
- Treg are actively recruited to the site of the tumour using a specific combination of chemokine receptors and integrins.
- Blockade of these receptors leads to a reduction in tumour Treg recruitment, thereby enhancing anti-tumour immunity and providing a novel therapy for CRC.

AIMS & OBJECTIVES

1. To quantify the degree of Treg infiltration in human CRC tissue at primary sites and within hepatic metastases compared with matched distal non-involved tissue.
2. To correlate Treg infiltration in human primary CRC with pathological factors, such as grade and stage, and with patient survival and disease recurrence.
3. To define the expression of chemokine receptors and adhesion molecules by Treg isolated from human primary and metastatic CRC and test their function. In parallel, to quantify the expression of the ligands for these receptors in tumour tissue.
4. To test the effects of inhibition of important chemokine receptors and adhesion molecules involved in recruiting Treg in vivo, using a murine model of CRC.

Chapter 2
MATERIALS & METHODS

Samples

Tissue samples of CRC and adjacent colon were obtained from patients undergoing a bowel resection as part of their treatment for CRC at the QEHB after consent and with approval from the local research and ethics committee (LREC South Birmingham 2003/242, renewed 2012). Peripheral blood samples were taken from some patients undergoing resection at the time of induction of anaesthesia. This was only possible after LREC renewal in 2012. Following bowel resection, the fresh specimen was assessed by the author and an experienced pathologist before samples of colonic mucosa and CRC tissue were taken. The pathologist was able to maximise the tissue yield that could be donated for research purposes whilst ensuring there was no interference with the clinical requirements for the specimen. In 2 cases colorectal polyp tissue was taken following resection. In the majority of such cases, the pathologist felt that there was no surplus polyp tissue for research purposes as the entire polyp was required to be pathologically assessed for foci of adenocarcinoma. To limit any cross-contamination between colon and CRC samples, pieces of colonic mucosa were taken from a macroscopically normal part of the colon, a minimum of 10cm distal to the tumour. In certain cases, it was possible to retrieve a TDLN from the mesentery of the resected tissue. TDLN were bisected and one piece was used for research purposes. The majority of the CRC, colon and TDLN tissue was placed in a Universal container containing RPMI 1640 medium (31870, Life Technologies Ltd, UK) with 1% foetal calf

serum (FCS, 10270-106, Life Technologies Ltd, UK), 5 mg Gentamicin–125 µg Amphotericin B (R-015-10, Life Technologies Ltd, UK) and 1% Glutamine–Penicillin–Streptomycin (GPS, 10378-016, Life Technologies Ltd, UK) in preparation for lymphocyte isolation. This medium will subsequently be referred to as complete medium (cRPMI). The final antibiotic concentrations were: penicillin 1 U/ml, streptomycin 1 µg/ml, gentamicin 10 µg/ml, amphotericin B 0.25 µg/ml. Smaller pieces of tissue were placed in Bijou sample containers, either dry or containing 10% formal saline (3036850, Adams Healthcare Ltd, UK). Dry containers were snap frozen in liquid nitrogen and stored at -80˚C. Formalised samples were paraffin-embedded and processed into blocks for use in immunohistochemistry experiments. Fresh samples in cRPMI were taken back to the laboratory and used immediately for the isolation of lymphocytes.

Tissue was also taken from patients who underwent a liver resection for CRC metastasis and had given consent. In this case, blocks of tissue were taken from the core of the liver metastasis and from the distal liver, at least 1 cm from the macroscopic edge of the metastasis. Anonymised clinical outcomes and pathology data were recorded allowing correlation of laboratory findings with patient and disease characteristics.

Approximately 2 g of colonic mucosa and 0.5 g tumour tissue was sufficient for flow cytometry experiments to quantify chemokine receptor expression on Treg.

Lymphocyte isolation from CRC, colon tissue and TDLN

Cell suspensions can be generated from tissue specimens by mechanical and/or enzymatic dissociation. The gentleMACS tissue dissociator (Miltenyi Biotec Ltd, UK) is a

benchtop instrument that automatically dissociates tissues in a standardised fashion. Published protocols exist for the mechanical dissociation of murine and human tissues (163). Protocols for dissociation of implanted murine and human tumours using the gentleMACS dissociator (164,165) involve enzymatic digestion steps but I avoided enzymatic digestion with collagenase and other enzymes that are known to remove lymphocyte surface molecules. Protease contaminations in enzyme preparations of DNase and collagenase have been shown to reduce expression of CD2, CD4, CD8, CD14, CD16, CD44 and CD56 on peripheral blood lymphocytes (166). A reduction in CD4, CD8, CD16 and CD56 expression by lymphocytes isolated from CRC occurs after only one hour of digestion with DNase and collagenase enzymes (167). Enzymatic isolation of liver-infiltrating lymphocytes using collagenase significantly reduces the expression of CXCR3 compared with mechanical isolation methods (168) and the use of dispase (a protease which cleaves fibronectin and collagens) reduces the expression of CD4 and CD25 by lymphocytes (169). Enzymatic digestion of tissues does however increase the lymphocyte yield compared to mechanical dissociation alone without affecting cell viability (170). Enzyme-based isolation methods are also associated with reduced proliferative capacity of lymphocytes compared with mechanical isolation. It is possible to conduct multi-colour flow cytometry experiments on as few as 2500 tumour-infiltrating lymphocytes (TIL) (171). Therefore, for phenotyping experiments, TIL were isolated by mechanical methods alone.

The classical method of lymphocyte isolation from the gut describes the separation and discrimination of intra-epithelial from lamina proprial lymphocytes (172). Diced colonic tissue is incubated in a 1 mM solution of dithiothreitol (DTT) to remove

adherent mucus followed by incubation in a 0.75 mM solution of ethylenediaminetetraacetic acid (EDTA) to dissociate the mucosal epithelium and liberate intra-epithelial lymphocytes. Lamina proprial lymphocytes are then isolated by collagenase digestion of the remaining tissue. Adherent mucus increases the viscosity of the sample and therefore interferes with washing and filtration steps. DTT was avoided as its use is associated with the downregulation of numerous cell surface receptors (173).

Once tissue samples had been taken to the laboratory, the cRPMI solution was discarded and the tissue placed in a shallow Petri dish, diced into 2-3 mm fragments and placed in C-tubes (130-096-334, Miltenyi Biotec Ltd, UK) for use with the gentleMACS dissociator. Each sample tube was run twice on the gentleMACS dissociator using the Mouse-Spleen-1 protocol and then washed through a fine mesh (NYL9087, John Staniar & Co Ltd, UK) with cRPMI. The filtrates from distal colon and CRC samples were then placed in three separate 50 ml centrifuge tubes each and made up to 50 ml per tube with cRPMI. The tubes were centrifuged at 300 x *g* for 5 minutes, the supernatant decanted and cells resuspended in 12 ml ice-cold cRPMI solution per sample.

Three 15 ml centrifuge tubes per sample were used for a discontinuous gradient separation step. Percoll solutions at 4˚C were used to create the gradient (17-0891-01, GE Healthcare Ltd, UK), with a 4 ml 30% solution carefully layered on top of a 4 ml 70% layer (see Figure 2-1). 4 ml cell suspension was then overlaid on the Percoll layers and centrifuged at 300 x *g* for 20 minutes with no brake.

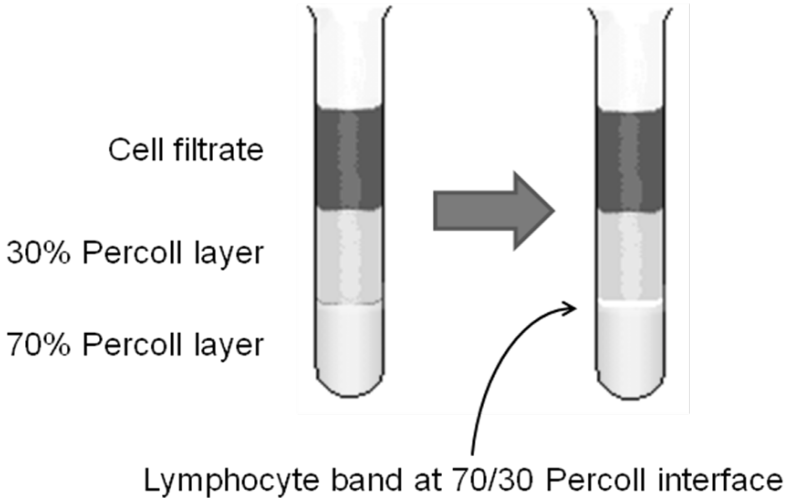

Figure 2-1: Discontinuous Percoll gradient.

The band at the 70/30 interface was aspirated from each 15 ml tube. The cells were then washed in a 50 ml centrifuge tube by making the volume up to 50 ml with ice-cold cRPMI and centrifuging at 300 x *g* for 5 minutes. The supernatant was discarded and the cells resuspended in 1 ml of ice-cold phosphate-buffered saline supplemented with 10% FCS and 1% GPS (cPBS) in preparation for downstream applications.

Selective use of enzymatic digestion

The lymphocyte yield for functional experiments such as suppression assays was more important than the preservation of cell surface markers. For these experiments, once the tissue had been diced into 2-3 mm fragments and transferred to C-tubes, 10 ml digestion buffer was added to each tube and the samples were spun on the gentleMACS machine, human-tumor-1 setting. The C-tubes were then agitated at 37˚C for 30 minutes. The samples were spun on the gentleMACS machine, human-tumor 2 setting,

then agitated again for 30 minutes at 37˚C. Finally, the samples were spun on the gentleMACS machine, human-tumor 3 setting before being washed through a fine mesh and layered on a Percoll gradient as before. This protocol is published by Miltenyi Biotec for use with their human tumor dissociation kit (130-095-929), a cocktail of enzymes designed to digest human tumour tissue optimised for a high yield of tumour cells and TILs while preserving cell surface epitopes. This kit was used twice and an exceptionally low level of CD25 expression was noted on the isolated TILs, an effect that has been reported for dispase (169). The reagents in the human tumor dissociation kit were therefore substituted with collagenase II (20 mg/ml, C2-22, VWR International Ltd, UK). The digestion buffer used was therefore RPMI, 1% GPS and 100µg/ml collagenase II. This buffer gave improved yields over mechanical digestion while preserving surface CD25.

Lymphocyte isolation from peripheral blood

Blood from patients undergoing venesection for haemochromatosis, from healthy donors or from CRC patients was used for phenotyping and in vitro experiments. All blood donors had given prior consent to donate for research purposes.

Blood was carefully layered over an equal volume of Lymphoprep™ (07801, Stem Cell Technologies Inc, Canada). The gradient was centrifuged at 300 x *g* for 30 minutes with no brake. Peripheral blood mononuclear cells (PBMCs) were aspirated from the plasma-Lymphoprep™ interface, washed with PBS and pelleted. The PBMCs were then resuspended in cRPMI.

Lymphocyte phenotyping

In order to identify viable lymphocytes isolated using the above methods, a live/dead fixable stain kit (L10119, Life Technologies Ltd, UK) was used. The fluorescent dye permeates necrotic cells and reacts with free intracellular amines, thereby labelling dead cells (174). The near-infra-red live/dead stain was used whose excitation and emission maxima are 750 and 775 nm respectively.

The number of live cells in the 1ml suspension was counted using a haemocytometer and the concentration of the cell suspension adjusted to 1 x 10^6 cells per ml cPBS. 1 µl per ml live/dead fixable stain was then added to the cell suspension together with 20 µl/ml of human FcR blocking reagent (130-059-901, Miltenyi Biotech Ltd, UK) and incubated in the dark at 4°C for 20 minutes. An equal volume of ice-cold cPBS was then added to wash off unbound fluorescent dye and the samples were pelleted and resuspended in a volume of cPBS to provide 100 µl cell suspension for each flow cytometry tube (5 ml polypropylene round-bottomed Falcon tubes, 352002, BD Biosciences).

Cell surface labelling was performed by incubating cells with antibodies listed in Table 2-1 in 100 µl cPBS for 30 minutes at 4°C in the dark on a rocker. One tube was incubated with the isotype-matched controls (IMC) for these antibodies at the same concentration. Some tubes contained cells labelled with single antibodies in order to perform colour compensation.

Table 2-1: Cell surface antibodies used for TIL phenotyping

Antigen	Clone	Fluorochrome	Isotype	Manufacturer	Code
CD3	UCHT1	Alexa-Fluor 750	Ms IgG1	Serotec	MCA463P750
CD4	RPA-T4	V500	Ms IgG1	BD	560768
CD25	M-A251	V450	Ms IgG1	BD	560355
CD127	HIL-7R-M21	FITC	Ms IgG1	BD	560549
CD127	eBioRDR5	APC	Ms IgG1	eBioscience	17-1278-42
CD8	RPA-T8	PE-CF594	Ms IgG1	BD	562282

In addition to the above antibody cocktail, each tube contained an antibody against various cell surface markers such as chemokine receptors or integrins conjugated to either APC or PE fluorochromes (see Appendix III). A cell surface marker could also be stained with an antibody conjugated to FITC if the CD127-FITC antibody was substituted with CD127-APC.

A typical experiment to quantify the cell surface expression of the chemokine receptors CCR5, CCR6 (both antibodies are of Mouse IgG1 isotype) and CCR7 (Mouse IgG2a isotype) on T cell subsets would require the following flow cytometry tubes and antibody combinations:

TUBE	Antibodies
1	Cells only
2	IMCs
3	CD3
4	CD4
5	CD25
6	CD127
7	CD 8
8	CD3/CD4/CD25/CD127/CD8/MsIgG1-APC/MsIgG1-PE
9	CD3/CD4/CD25/CD127/CD8/CCR5-APC/CCR6-PE
10	CD3/CD4/CD25/CD127/CD8/MsIgG2a-APC
11	CD3/CD4/CD25/CD127/CCR7

Following incubation with the cell surface antibodies, 1 ml ice-cold cPBS was added to each tube to wash off unbound antibody. The cells were pelleted and resuspended in 500 µl cPBS, ready for flow cytometric analysis.

Intra-cellular staining

In some experiments, the defined Treg population ($CD4^{+}CD25^{+}CD127^{low}$) was shown to express the transcription factor Foxp3 by performing intracellular staining. In other experiments, additional intracellular markers such as Ki67, CTLA-4 and Helios were labelled using the same technique.

Following cell surface staining, the cells were fixed and permeabilised by resuspending in formalin and saponin solutions for 5 minutes, part of the Foxp3 staining buffer kit (00-5523, eBioscience Ltd, UK) in place of cPBS. Cell were then washed, pelleted and

resuspended in 100 µl of saponin wash buffer. Cells were labelled with antibodies against various intra-cellular antigens or IMCs and incubated for 30 minutes at 4˚C in the dark on a rocker. Unbound antibody was washed off by adding 1 ml of wash buffer, pelleting and resuspending in 500µl cPBS, ready for flow cytometric analysis.

The following antibodies were used for intra-cellular staining together with their isotype-matched controls (see Table 2-2):

Table 2-2: Antibodies used for intra-cellular phenotyping of TILs

Antigen	Clone	Fluorochrome	Isotype	Manufacturer	Code
Foxp3	PCH101	PE	Rat IgG2a	eBioscience	12-4776-42
CTLA-4	BNI3	APC	Ms IgG2a	BD	560938
Helios	22F6	APC	Hamster IgG	Biolegend	137222
Ki67	35/Ki-67	FITC	Ms IgG1	BD	612472

Flow cytometry

The prepared samples were analysed using a CyAn ADP 3-laser, 9-colour flow cytometer (Beckman Coulter Inc, USA). The machine is equipped with 488nm, 405 nm and 642 nm solid-state lasers and is able to measure the following parameters:

Forward light scatter, Side light scatter

488 nm laser:-

FL1: FITC

FL2: PE

FL3: PE-TexasRed / PE-CF594

FL4: PE-Cy5 / PerCP

FL5: PE-Cy7 / Alexa Fluor 750

405 nm laser:-

FL6: V450, Pacific Blue

FL7: V500, Pacific Orange

635 nm laser:-

FL8: APC

FL9: APC-Cy7 / near-IR Live Dead dye

Data analysis was performed using Summit software version 4.3 (Dako, USA).

Samples containing cells only, cells labelled with IMCs and cells labelled with single colours were used to compensate for spectral overlap.

Gating strategy

The lymphocyte gate was based on cell size (forward and side light scatter) and on cell surface expression of CD3 in viable cells (absence of dead cell staining). Of this live lymphocyte population, the Treg population was defined by gating first on $CD127^{low}$ cells followed by gating on $CD4^+$ and $CD25^+$ cells (Live $CD3^+$ $CD4^+$ $CD25^+$ $CD127^{low}$). The expression of various cell surface and intra-cellular markers was defined by first setting the histogram regions for negative and positive populations. The regions were set so that the negative population included 98.5% of events using a sample stained with the full cocktail of different fluorochromes but replacing the fluorochrome-antibody to the marker of interest with a fluorochrome-conjugated isotype-matched control antibody. This is known as a Fluorescence-Minus-One (FMO) control.

The expression of cell surface and intra-cellular molecules by Treg was determined by application of the Treg gate to single-colour histograms, as demonstrated in relation to Foxp3 expression in Figure 2-2. The $CD127^{low}$ region was set to include 98.5% of the isotype-matched control population whilst the $CD25^-$ region was set to include 99.5% of the isotype-matched control population.

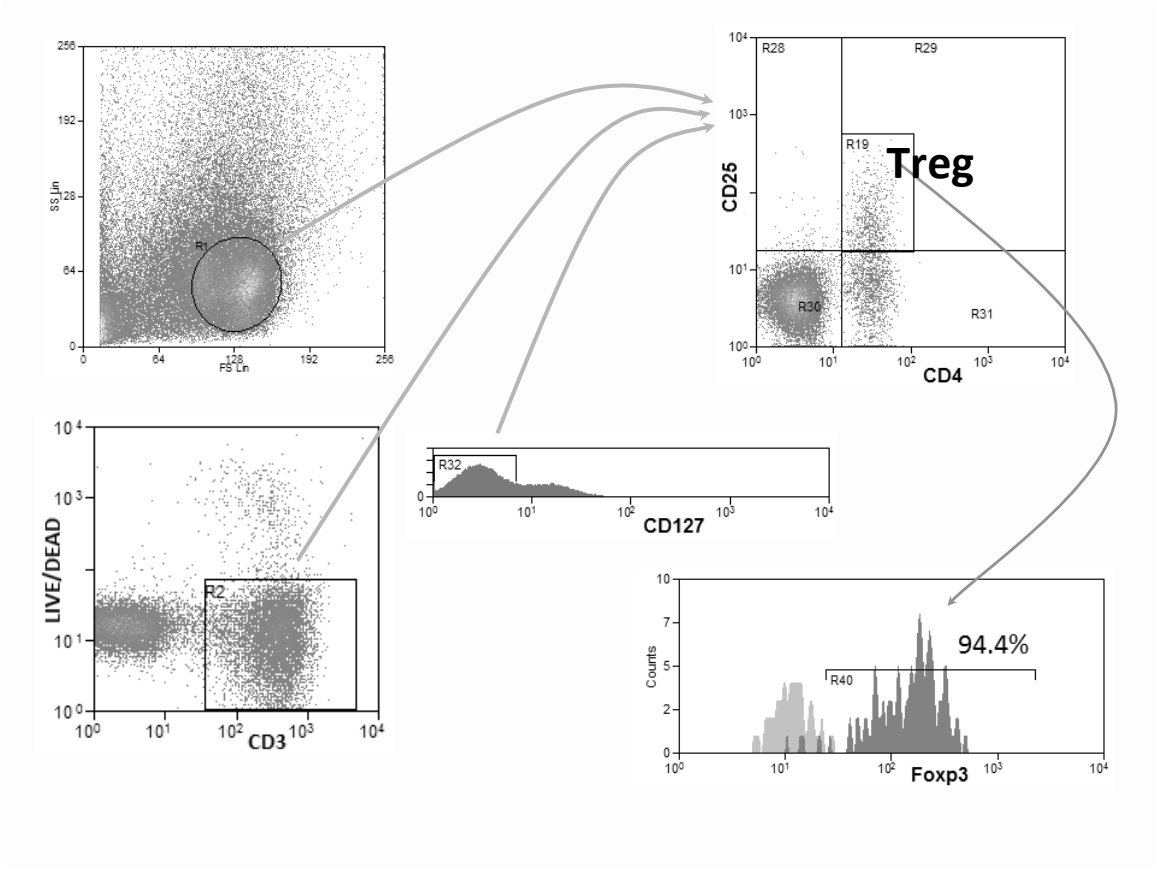

Figure 2-2: Defining the Treg population by flow cytometry: Forward and side light scatter and cell surface expression of CD3 with absence of dead cell staining defined live lymphocytes. Of this population, Treg were defined as $CD127^{low}$, $CD4^{+}$ and $CD25^{+}$.

Expression of cell surface and intra-cellular molecules by Treg was compared with Tconv ($CD4^{+}CD25^{-}$). These cells were defined using forward scatter-side scatter, CD3 expression and absence of dead cell staining as before, but also by expression of CD4 and absence of CD25 expression (see Figure 2-3).

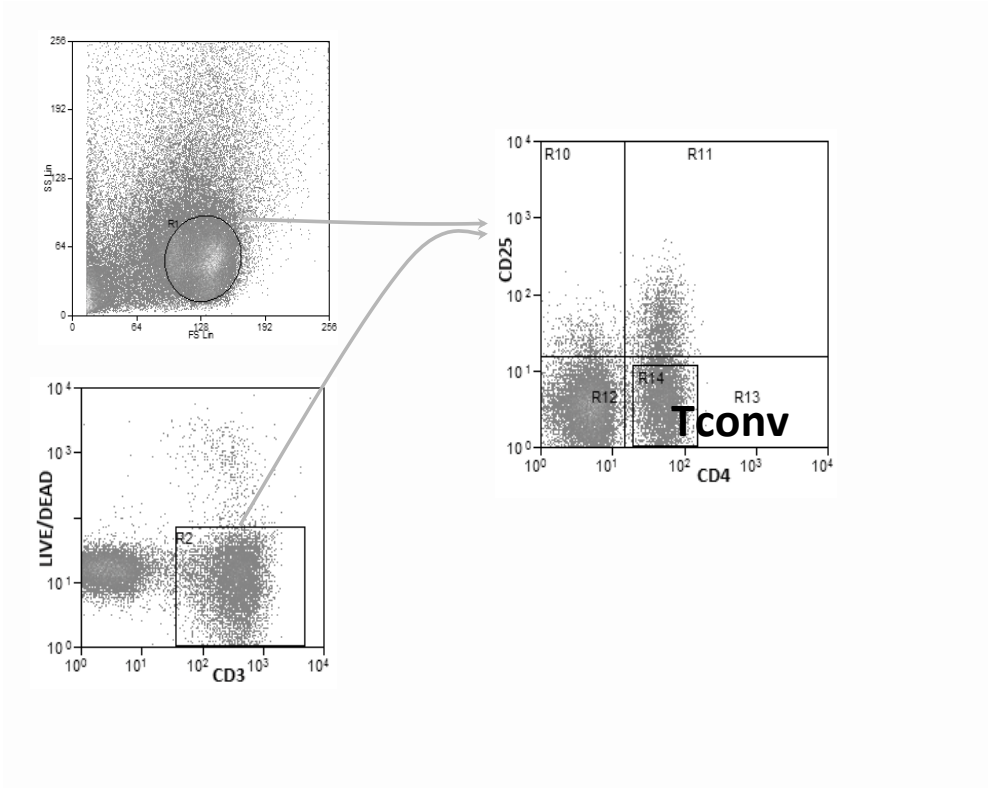

Figure 2-3: Defining Tconv ($CD4^{+}CD25^{-}$): Forward and side light scatter and cell surface expression of CD3 with absence of dead cell staining defined live lymphocytes. Of this population, Tconv were defined as $CD4^{+}$ and $CD25^{-}$.

Flow cytometric evaluation of the expression of cell surface and intra-cellular molecules by Treg and Tconv compared to IMCs was done on multiple matched samples of CRC and distal colon. The median expression of each molecule, in terms of both percentage expression and median fluorescence intensity (MFI), was calculated and comparisons between Treg versus Tconv and Treg in CRC versus distal colon were carried out. Differences in expression across matched samples were tested for statistical significance using the Wilcoxin signed-rank test.

Treg numbers

The proportion of $CD4^+$ cells with a Treg phenotype ($CD4^+CD25^+CD127low$) was calculated by dividing the cell count of the Treg defined region by the cell count of $CD4^+$ cells from the $CD4^+$ histogram, gated on live $CD3^+$ cells.

In some experiments, the absolute number of Treg was calculated through the addition of 20 µl of counting beads (AccuCheck PCB100, Life Technologies Ltd, UK) to the labelled cell suspension immediately prior to flow cytometry. The counting bead solution contains two different fluorospheres, to provide an internal standard, of known concentration. The beads are detected in the FL2 channel and can therefore be enumerated along with the number of cells in the Treg-defined region. The number of Treg per microlitre is obtained by relating the number of Treg counted to the total number of fluorescent bead events. The Treg number is then multiplied by the number of fluorospheres per unit volume. The two different fluorospheres (A and B) are in equal proportion and therefore assure the accuracy of the assay by verifying that an equal number of beads A and B are counted.

$$Final\ absolute\ Treg\ count = \frac{Number\ Treg\ counted}{Total\ number\ beads\ counted\ (A+B)}\ x\ Number\ beads\ per\ \mu l$$

Fluorescence-activated cell sorting (FACS)

TILs were isolated using digestion buffer as described in the section above (Selective use of enzymatic digestion) and sorted for use in downstream experiments such as suppression assays, proliferation assays and epigenetic analysis of the Foxp3 promoter. Prior to incubation with the live/dead marker, cells were labelled with the following antibodies (see Table 2-3):

Table 2-3: Antibodies used for cell surface labelling of cells to be sorted.

Antigen	Clone	Fluorochrome	Isotype	Manufacturer	Code
CD4	OKT4	PECy7	Ms IgG2b	Biolegend	317414
CD25	M-A251	APC	Ms IgG1	BD	555434
CD127	HIL-7R-M21	FITC	Ms IgG1	BD	560549
CCR5	CTC5	PE	Ms IgG1	R&D	FAB1802P

Cells were sorted using a MoFlo XDP High-Speed Cell Sorter (ML99030, Beckman Coulter Inc, USA). The MoFlo XDP is able to perform 4-way sorts at a rate of 70,000 sorts per second with 99% purity and can sort cells directly into a 96-well plate. The MoFlo XDP was equipped with 488 nm, 647 nm and 405 nm lasers and could therefore, in theory, detect 9 different colours exactly as described for the CyAn flow cytometer. However, the 405 nm violet laser gave poor resolution for highly expressed antigens, such as CD4. For this reason, CD4 and CD25 were not labelled with antibodies conjugated to fluorochromes detected with the violet 405 nm laser, namely V500 and V450, as for flow cytometric analysis. Rather, CD4 was labelled with a PECy7-conjugated antibody and CD25 was labelled with an APC-conjugated antibody, the fluorochromes of which are both excited by the red 647 nm laser. The 405 nm laser was able to resolve live and dead cells using the bright SYTOX® Blue dead cell stain (S34857, Life Technologies Ltd, UK).

5 minutes prior to running the sample on the cell sorter, SYTOX® Blue dead cell stain was added to the sample; this penetrates cells with compromised cell membranes, allowing dead cells to fluoresce bright blue (emission maxima at 480 nm) when excited by 405 nm violet laser light.

Gating strategy

The gating strategy for cell sorting was different from that used to identify Treg by flow cytometry, due to the absence of a CD3 label (see Figure 2-4). Cells were 3-way sorted in purity mode, either directly into a 96-well plate (for suppression and proliferation assays), or into 1.5 ml Eppendorfs for subsequent RNA or DNA extraction.

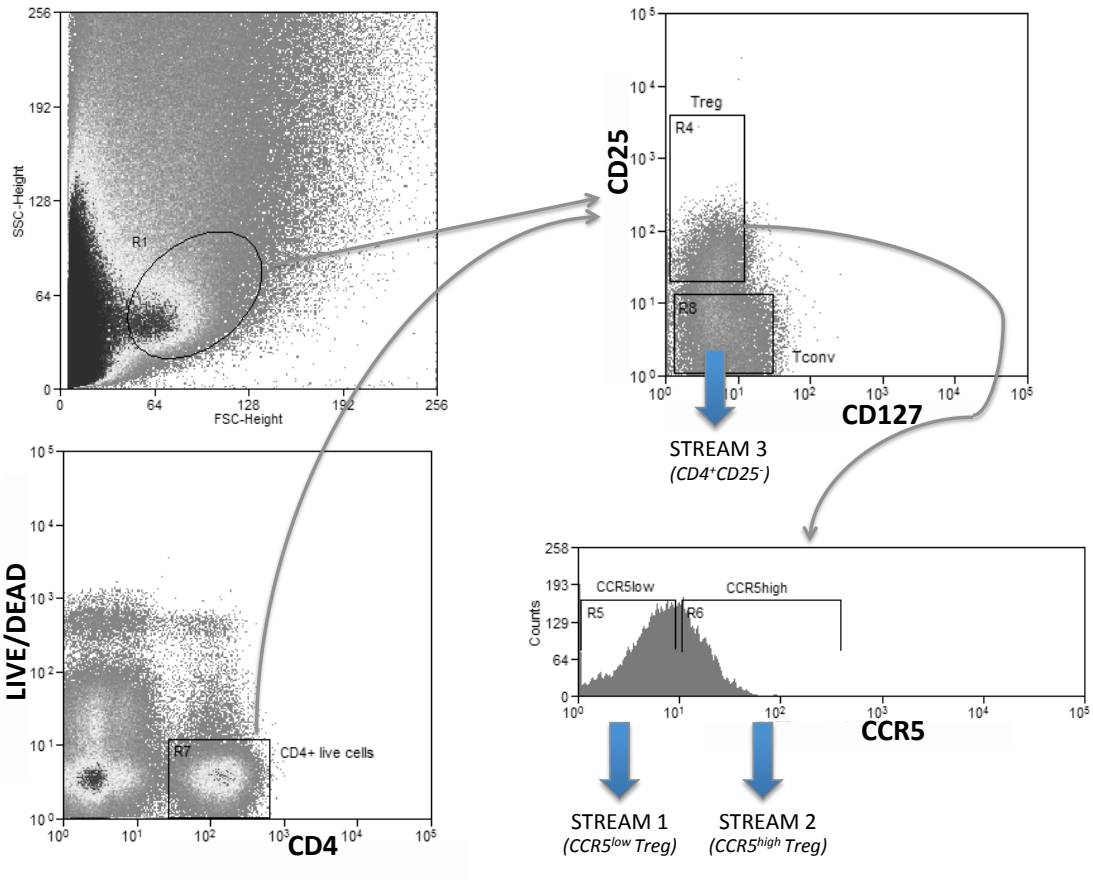

Figure 2-4: Lymphocytes based on forward scatter–side scatter were gated into a CD4–Live/Dead dot plot. $CD4^+$ live cells were then gated into a CD127–CD25 dot plot. This last dot plot was used to define Treg and Tconv cells. Treg were gated into a CCR5 histogram to define $CCR5^{low}$ and $CCR5^{high}$ Treg.

3-way sort

STREAM 1: $CD4^{+}CD127^{low}CD25^{high}CCR5^{low}$ (Live cells) *[$CCR5^{low}$ Treg]*

STREAM 2: $CD4^{+}CD127^{low}CD25^{high}CCR5^{high}$ (Live cells) *[$CCR5^{high}$ Treg]*

STREAM 3: $CD4^{+}CD25^{-}$ (Live cells) *[Tconv]*

The typical total yield of Treg was between 10,000 to 60,000 even for large samples of CRC weighing up to 5 g. For this reason, it was not possible to perform a post-sort purity check in all cases. Purity checks were performed for 2 samples only and demonstrated a mean Treg purity of 94.0% and a mean Tconv purity of 94.9% (see Figure 2-5). However, the purity of CCR5 expression on sorted Treg was less: A mean of 69.0% of $CCR5^{low}$ sorted Treg laid within the $CCR5^{low}$ region and 79.0% of $CCR5^{high}$ Treg laid within the $CCR5^{high}$ region.

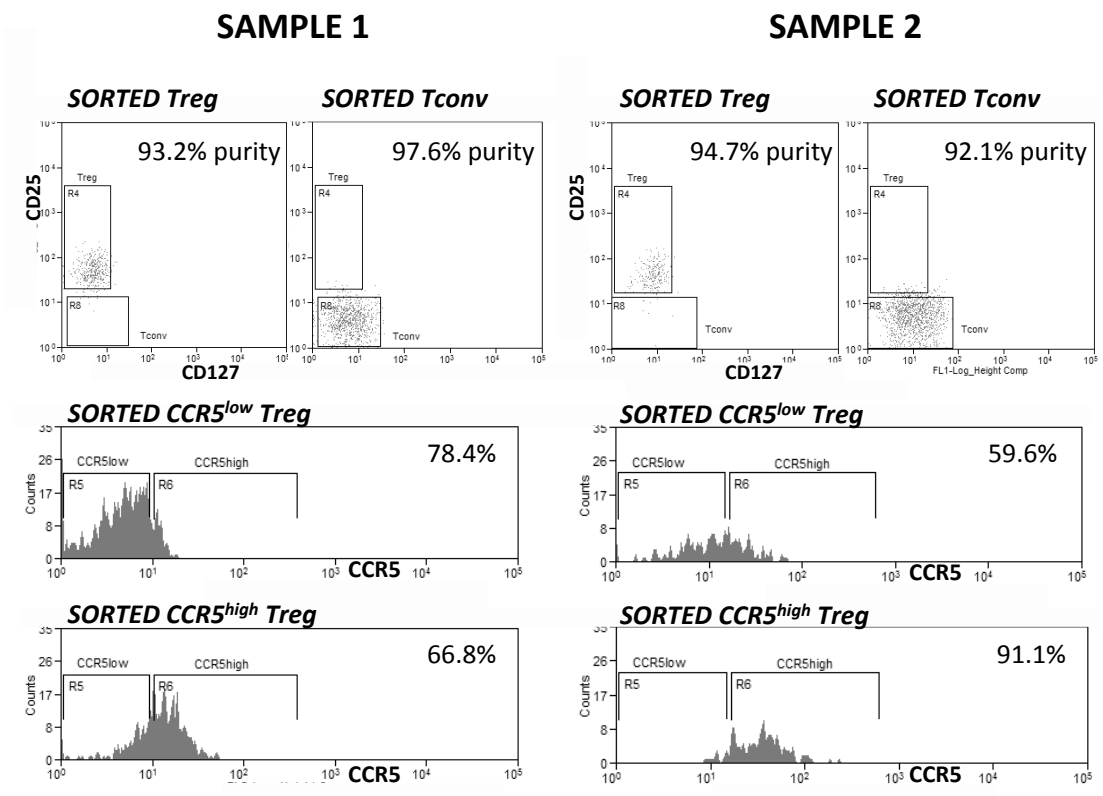

Figure 2-5: Purity check of sorted Treg and Tconv from two samples

Suppression assay

PBMCs, isolated from 10 ml of blood, were labelled with CellTrace Violet dye (C34557, Life Technologies Ltd, UK) by incubating the PBMC at a concentration of 2 x 10^6 / ml in RPMI with 1 µl / ml of 5 mM CellTrace Violet dye for 20 minutes at 37˚C. Unbound dye was quenched by adding 5 times the original staining volume of cRPMI then incubating the mixture for 5 minutes at 4˚C. The cells were then pelleted and resuspended in 100 µl of cPBS. The cells were incubated with CD4-PECy7 and CD25-APC antibodies (see Table 2-3) for 30 minutes at 4˚C, washed, pelleted and resuspended in 0.5 ml cPBS. CellTrace violet dye binds to intracellular amines which on cell proliferation, is detected at reducing fluorescent intensity in successive generations of cells. As such, $CD4^+CD25^-$ cells labelled with CellTrace Violet are referred to as responder T cells (Tresp).

Following preparation of antibody-labelled Tresp and TIL (as described in the previous section: Fluorescence-activated cell sorting (FACS)), target wells of a round-bottomed 96-well plate (3879, Corning Inc, USA) were filled with 150 µl cRPMI. An equal number of $CCR5^{low}$ Treg, $CCR5^{high}$ Treg and Tconv were 3-way sorted into different wells of the well plate. A specified number of Tresp were then plate-sorted into the same wells, yielding a well Treg : Tresp ratio of 1:1, 1:2 or 1:4. Tresp were also sorted into wells without Treg to act as positive and negative controls of a proliferative response (see Figure 2-6). A polyclonal stimulus for proliferation was provided by adding washed Human Treg Suppression Inspector beads (130-092-909, Miltenyi Biotec Ltd, UK) to each well at a bead : lymphocyte ratio of 1:2. The plate was incubated at 37˚C and 5% CO_2 for 3 days. The cells from each well were then transferred to FACS tubes and CellTrace violet dye wash-out was analysed on the CyAn flow cytometer. Results were

reported as percent suppression for each ratio of Treg to Tresp, as is common practice in the literature (175):

$$Percent\ suppression = 100 - \frac{Percentage\ of\ proliferating\ cells\ with\ Treg\ present}{Percentage\ of\ proliferating\ cells\ without\ Treg\ present}\ x\ 100$$

Differences in percent suppression between CRC-isolated Treg and $CD4^{+}CD25^{-}$ cells were tested for statistical significance using the Wilcoxin signed-rank test. According to the Treg Suppression Inspector manufacturer's protocol, the beads should be added at a bead : lymphocyte ratio of 1:1. However, after 3 suppression assays in which there was cell proliferation but no suppression, the ratio was changed to 1:2. This allowed both proliferation and suppression to be detected. The likely explanation for this relates to the absolute number of viable cells sorted into the plate. For example, the sorter is instructed to sort 10,000 Treg into a well followed by 10,000 Tresp. Following this sort, 20,000 beads would be added to the co-culture at a bead : lymphocyte ratio of 1:1. However, the sorter is only able to report sort *events* - the actual number of viable cells recovered is significantly less due to cell death occurring pre- or post-sort; adherence of cells to tube walls; precision of the flow cytometer. Typically, 50% recovery is obtained (176). Therefore, the actual bead : lymphocyte ratio is in the order of 2:1 and this polyclonal stimulus for proliferation may be too strong for the Treg to suppress.

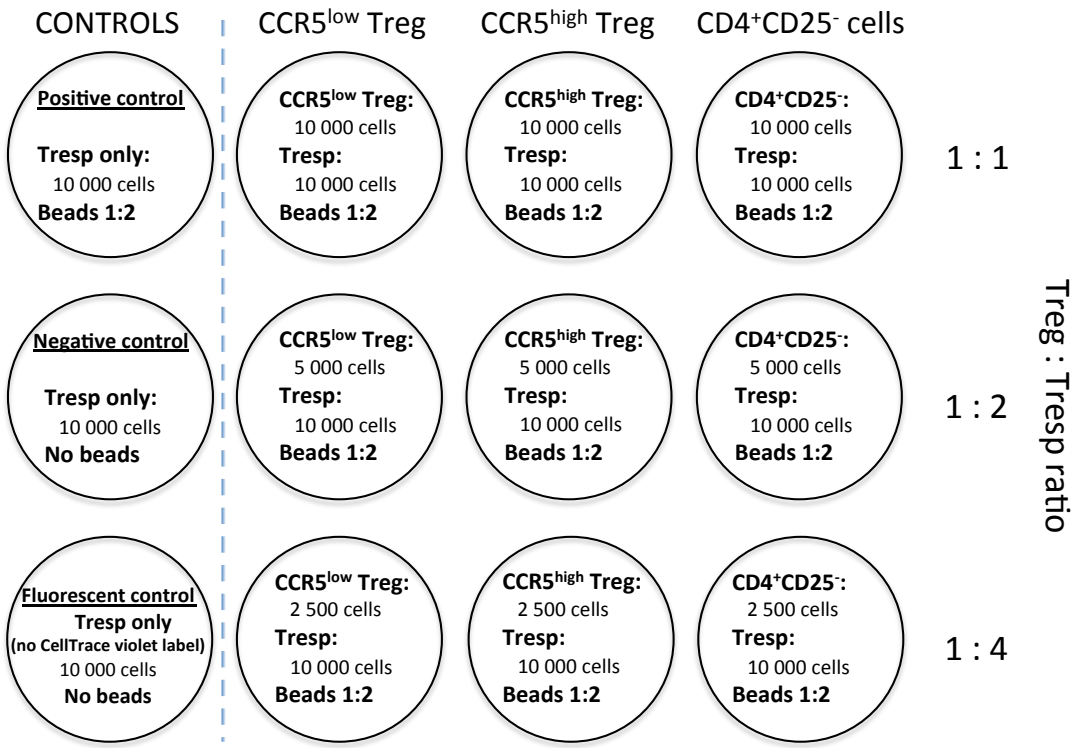

Figure 2-6: Typical 96-well plate set-up for a suppression assay using Treg and $CD4^+CD25^-$ cells isolated from CRC tissue co-cultured with Tresp isolated from allogeneic PBMC at different ratios and human Treg Suppression Inspector beads (bead : lymphocyte ratio 1:2).

Proliferation assay

TILs were isolated using digestion buffer as described in the section above (Selective use of enzymatic digestion) and then labelled with CellTrace Violet. TILs were then labelled with the near-infra-red live/dead fixable stain kit (L10119, Life Technologies Ltd, UK) for 20 minutes at 4˚C followed by the cell surface antibodies listed in Table 2-3 for 30 minutes at 4˚C.

An equal number of $CCR5^{low}$ Treg, $CCR5^{high}$ Treg and Tconv were 3-way sorted into different wells of a 96-well round-bottomed plate that had been filled with 150 µl cRPMI. A polyclonal stimulus for proliferation was provided by adding washed Human

Treg Suppression Inspector beads to each well at a bead : lymphocyte ratio of 1:2. The plate was incubated at 37˚C and 5% CO_2 for 3 days. The cells from each well were then transferred to FACS tubes and CellTrace violet dye wash-out was analysed on the CyAn flow cytometer. Results were reported as the percentage of cells proliferating for each well.

Cell migration assays

The functional relevance of chemokine receptors expressed by TILs was examined using transwell migration assays and by visualising real-time chemotaxis in microchambers.

Transwell migration assays

It was only possible to isolate small numbers of T cells from CRC samples and therefore, a 96-well transwell system was used (3387, Corning Inc, USA). The pore size was 5.0 μm to allow for lymphocyte migration from the upper to the lower compartment. The system allows access to both upper and lower compartments without disturbing the transwell insert: This enabled collection of migrated cells from the lower compartment and non-migrated cells from the upper compartment for subsequent analysis (see Figure 2-7).

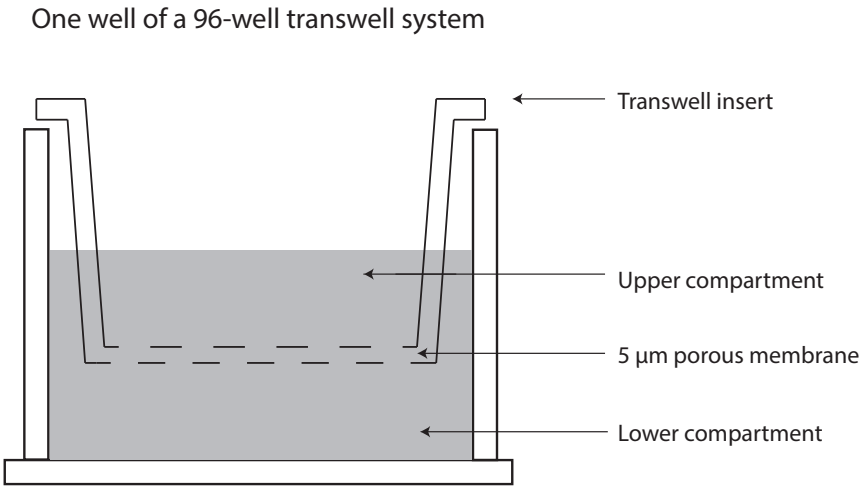

Figure 2-7: Transwell system to assess TIL migration to chemokines.

Lymphocyte isolation from CRC for use in transwell system

TILs were isolated using digestion buffer as described in the section above (Selective use of enzymatic digestion). M The number of cells present in the 1.1 ml suspension was counted using a haemocytometer. 250 µl, 750 µl and 100 µl of the cell suspension were placed in separate wells (A, B and C) of a 24-well plate and the volume in each well made up to 1 ml with RPMI + 0.1% BSA. 1 µl of a 1mM solution of Maraviroc was added to well A (final concentration of Maraviroc = 1 µM) and 1 µl of DMSO was added to well B. The cells in well C were untreated and used for flow cytometry analysis. The Maraviroc salt had been previously dissolved in DMSO, hence the use of DMSO as a vehicle control. The cells were left overnight to serum starve with or without the presence of Maraviroc. The cells were then transferred to 15 ml tubes, 10 ml PBS was added to wash the cells and the cells were pelleted. The Maraviroc-treated cells were resuspended in 150 µl of RPMI + 0.1% BSA; the DMSO-treated cells were resuspended in 450 µl of RPMI + 0.1% BSA.

Transwell set-up

Each condition was performed in duplicate. The transwell insert was removed. In column 1, 75 µl of DMSO-treated cell suspension was placed in the lower chamber of each of 2 wells. This served as the input control. In column 2, 235 µl of RPMI + 0.1% BSA solution was placed in the lower compartments of each of 2 wells. In columns 3 and 4, 235 µl of CCL4 solution (20 ng recombinant CCL4 per 1 ml RPMI + 0.1% BSA) was placed in each well (see Figure 2-8). This concentration had been used previously in published chemotaxis assays using human T cells and is physiological (177,178). Recombinant CCL4 was obtained from Peprotech Inc, USA (300-09). CCL4 was chosen over other CCR5 ligands as CCL4 has specificity for CCR5, while CCL3 and CCL5 bind to multiple chemokine receptors. The transwell insert was then replaced and 75 µl of DMSO-treated cell suspension was placed into the upper compartment of 2 wells in columns 2 and 3. 75 µl of Maraviroc-treated cell suspension was placed in the upper compartments of 2 wells in column 4.

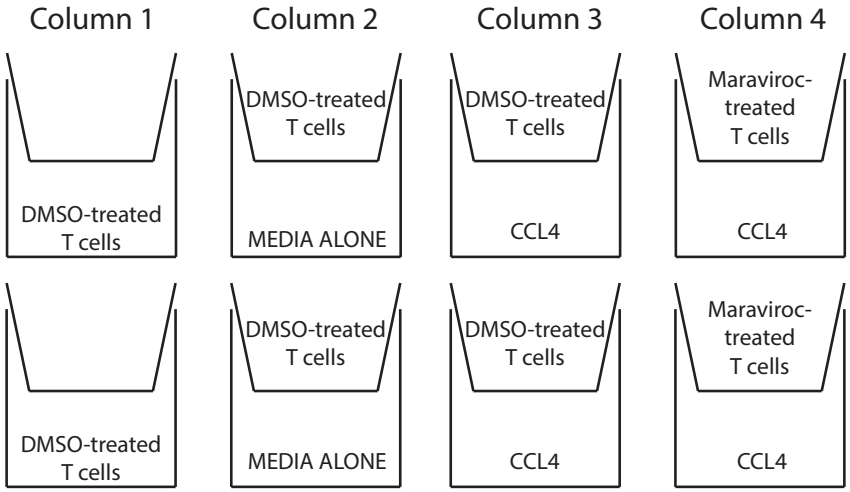

Figure 2-8: Schematic of transwell experiments.

The transwell plate was incubated at 37˚C 5% CO_2 for 4 hours. The contents of the lower chamber (containing migrated cells) and the upper chamber (containing non-migrated cells) were then aspirated and placed in flow cytometry tubes. The following antibody cocktail was added to each tube: 5 µl of anti-CD4-PE (555347, BD), 5 µl anti-CD25-APC (555434, BD), 5 µl anti-CD127-FITC (560549, BD) and 2.5 µl anti-CD8-Pacific Blue (344718, Biolegend). Cell suspension held back prior to DMSO or Maraviroc treatment was incubated with single antibodies from this cocktail for colour compensation. Cells were incubated with antibodies for 30 minutes at 4˚C then directly analysed by flow cytometry after the addition of 20 µl of counting beads.

Results were expressed as a chemotactic index, defined as:

$$\textit{Chemotactic index} = \frac{\textit{The absolute number (or percentage) of a lymphocyte subset that migrated in response to chemokine}}{\textit{The absolute number (or percentage) of the subset that migrated to media alone}}$$

The chemotactic index for all lymphocyte subsets migrating to media alone was therefore 1, by definition. Differences in the absolute numbers and percentage of cells across different conditions were tested for statistical significance using the Wilcoxin signed-rank test.

Fixation and staining of transwell inserts

Following the transwell experiment described above, the 5 μm porous membranes were washed by submerging the insert for 5 minutes in a new 96-well plate with each well containing 235 μl PBS. The cells remaining on the membranes were fixed by submerging the insert for 5 minutes into wells containing 4% paraformaldehyde. The membranes were washed twice by submerging in PBS for 5 minutes. Cells were permeabilised by submerging the insert into wells containing PBS + 0.3% Triton x100 for 5 minutes. The insert was then submerged into wells containing anti-Foxp3 antibody solution (Ab20034, Abcam plc UK, Dilution=1:100 in PBS) for 1 hour at room temperature. The insert was submerged twice into PBS 0.3% Triton x100 for 5 minutes. Cells were incubated in secondary antibody solution (anti-mouse IgG1-Alexa Fluor 488, A21121, Life Technologies Ltd, UK, 4 μg/ml in PBS) for 20 minutes at room temperature then washed twice for 5 minutes in PBS 0.3% Triton x100. The insert was submerged in DAPI solution for 5 minutes and washed once more in PBS 0.3% Triton x100. The membranes were punched out from the transwell inserts and mounted on microscope slides in Mowiol (81381, Sigma-Aldrich Ltd, UK). Foxp3-expressing cells on the membranes were visualised using a LSM510 confocal microscope (Zeiss) and the manufacturer's software.

Chemotaxis chambers

Lymphocytes were suspended in a collagen gel and seeded into the observation area of a microslide (µ-Slide Chemotaxis 3D, 80326, Ibidi). The gel was formed by mixing 150 µl of bovine collagen I solution (3mg/ml, C4243, Sigma-Aldrich Ltd, UK) with 20 µl of 10X MEM (M0275, Sigma-Aldrich Ltd, UK) then neutralising with 10 µl 7.5% sodium bicarbonate solution (S8761, Sigma-Aldrich Ltd, UK) on ice. 90 µl cell suspension was added to the gel and 6 µl of the gel/cell suspension mixture was placed in the observation area of each chamber of the microslide. The microslide was incubated at 37˚C for at least 1 hour until the gel had set. A chemokine solution was prepared by adding recombinant chemokine to RPMI + 0.1% BSA and warming to 37˚C. Once the gel had set, the right-hand reservoir of each chamber was filled with RPMI + 0.1% BSA. The left-hand reservoir was filled with chemokine solution and the observation area was imaged every 3 minutes using the CellIQ imaging system (CM Technologies, Finland).

PBMC activation and co-culture with tumour supernatant

PBMC were isolated as described in the above section: Lymphocyte isolation from peripheral blood. 1.6 x 10^5 cells were placed in each well of a flat-bottomed 96-well plate and the well volume was made up to 90 µl with cRPMI containing 20 IU/ml of recombinant IL-2 (PHC0023, Life Technologies Ltd, UK). 10 µl of RPMI + 0.1% BSA or 10 µl of CRC/colon supernatant was then added. 12 µl of washed Human T-Activator CD3/CD28 Dynabeads® (11161D, Life Technologies Ltd, UK) were added to each well, giving a bead to cell ratio of 3:1. CRC/colon supernatants had been previously prepared by incubating 0.5 g of CRC and 0.5 g matched distal colon tissue in 5 ml RPMI + 0.1% BSA + 1% GPS for 24 hours at 37˚C 5% CO_2. The supernatants were then aspirated,

passed through a 0.22 μm sterile syringe filter (SLGP033RS, Merck Millipore Ltd, UK), divided into aliquots and stored at -80˚C ready for future use.

After 48 hours of co-culture of PBMCs with beads ± supernatant, the beads were removed using a magnet and the cells were washed and resuspended in 90 μl cRPMI containing 20 IU/ml of recombinant IL-2. 10 μl of RPMI + 0.1% BSA or 10 μl of CRC/colon supernatant was again added to the wells. Following a further 48 hours of culture of PBMCs ± supernatant, the cells were washed and incubated with the following antibodies: Anti-CD3-AlexaFluor750 (MCA463P750, Serotec), anti-CD4-FITC (555346, BD Biosciences), anti-CCR5-APC (FAB1802A, R&D Systems) and a live/dead marker. Intra-cellular staining used the anti-Foxp3-PE (12-4776-42, eBioscience) antibody. Flow cytometric analysis of CCR5 expression by Tconv ($CD3^+CD4^+Foxp3^-$) and Treg ($CD3^+CD4^+Foxp3^+$) was performed.

In subsequent experiments, Treg and Tconv were isolated from PBMC by immunomagnetic separation and co-cultured separately with beads and supernatant. Treg (defined as $CD4^+CD25^+$ for these experiments) and Tconv ($CD4^+CD25^-$) were isolated from PBMC using the Dynabeads® Regulatory CD4+/CD25+ T Cell Kit (11363D, Life Technologies). 1.6 x 10^5 Tconv and 1.6 x 10^5 Treg were placed in separate wells and the volume made up to 90 μl with cRPMI containing 20 IU/ml of recombinant IL-2. CD3/CD28 beads and supernatant were added as before. 200 μl of culture supernatant was harvested at the end of the experiment (day 4) from wells in which Treg and Tconv had been cultured in media with and without activation beads. The concentrations of CCL3, CCL4 and CCL5 in the culture supernatant samples were measured using a Mix-N-Match ELISArray Kit (336111, SABiosciences), according to

manufacturer's instructions. Standard curves were not derived for each chemokine and absorbance was therefore the read-out in this semi-quantitative assay.

In certain experiments, neutralising antibodies or the small molecular CCR5 antagonist (UK-484900) were added to the culture supernatant to determine the effects on CCR5 expression and function by Treg and Tconv. UK-484900 was a gift from Pfizer Inc, USA and was used at a concentration of 2 μg/ml. The neutralising antibodies used were anti-IL-1Ra (MAB280, R&D Systems, used at 50 μg/ml), anti-TGF-ß1 (Ab10518, Abcam, used at 50 ng/ml) and anti-VEGF (AB-293-NA, R&D Systems, used at 6 μg/ml). Differences in CCR5 expression were tested for statistical significance using the Wilcoxin signed-rank test.

Immunohistochemistry and immunofluorescence

Immunohistochemical staining was carried out on both formal saline fixed paraffin-embedded (FFPE) tissue and tissue which had been snap frozen in liquid nitrogen. Immunohistochemistry for target antigens preferably use FFPE sections, as the morphology is better preserved than that for frozen sections. No staining was observed for target chemokines using FFPE sections and in these cases, frozen sections were preferred.

FFPE sections

5 μm sections were cut from FFPE tissue blocks. Sections were deparaffinised and rehydrated by passing the sections through fresh solutions of Clearene (3803600, Leica GmBH, Germany) and graduated alcohols. Sections were incubated with 0.3% hydrogen peroxide solution in methanol for 20 minutes at room temperature to block

endogenous peroxidase. Sections were then washed twice with Tris-buffered saline (TBS, 0.5M Tris Base, 9% sodium chloride, pH adjusted to 8.4 using hydrochloric acid) for 5 minutes. Antigen retrieval was performed by microwaving in pre-heated EDTA buffer (0.37 g EDTA in 1 l distilled water, pH adjusted to 8.0 using 1N sodium hydroxide, 0.05% Tween 20) for 15 minutes.

Frozen sections

5 µm sections were cut from frozen tissue blocks using a cryostat. Sections were allowed to thaw for 10 minutes, fixed by placing in acetone for 5 minutes and allowed to air dry for 30 minutes. Endogenous peroxidase was blocked by incubating sections with Peroxidase-Blocking Solution (S202386-2, Dako Ltd, UK) for 10 minutes followed by washing in TBS twice for 5 minutes.

Common immunohistochemistry protocol

The remainder of the protocol was universal to both FFPE and frozen sections. Endogenous Fc receptors were blocked by incubating sections in 10% casein solution (SP-5020, Vector Labs Inc, USA) for 30 minutes. Sections were then incubated in a primary antibody solution to the target antigen (see Table 2-4) at a pre-determined dilution or an IMC solution at equal concentration for 1 hour at room temperature. In prior experiments, serial sections were incubated with different primary antibody dilutions to determine the optimum dilution to maximise the sensitivity and specificity of the target antigen staining. The sections were washed twice in TBS containing 0.1% Tween-20 for 5 minutes and then incubated in an HRP-conjugated development solution (Vector ImmPress, MP-7500, Vector Labs Inc, USA) for 20 minutes at room temperature. Following a final wash in TBS + 0.1% Tween-20, sections were visualised

using either ImmPACT NovaRED (SK-4805, Vector Labs Inc, USA) or ImmPACT DAB (SK-4105, Vector Labs Inc, USA) with or without the addition of nickel to blacken the stain. Sections were counter-stained with Meyer's haematoxylin (S3309, Dako Ltd, UK) for 1 minute and blued in warm tap water for 1 minute. Sections were dehydrated by passing through graduated alcohol solutions then cleared by passing through fresh solutions of Clearene before mounting in DPX (3808600ED, Leica GmBH, Germany). Tissue expression was visualised using a Leica DM6000 (chromogenic) microscope and the manufacturer's software.

Table 2-4: Primary antibodies used for immunohistochemistry

Antigen	Clone	Isotype	Manufacturer	Code	Working concentration
Foxp3	236A/E7	Ms IgG1	Abcam	Ab20034	10 µg/ml
CD3	SP7	Rabbit IgG	Thermo Scientific	RM-9107	
CD4	1F6	Ms IgG1	Thermo Scientific	MA1-80223	
CD8	SP16	Rabbit IgG	Thermo Scientific	MA5-16345	
CCR5	45531	Ms IgG2b	R&D Systems	MAB182	10 µg/ml
VAP-1	Polyclonal	Rabbit	Sigma-Aldrich	HPA000980	2 µg/ml
CCL3	Polyclonal	Goat	R&D Systems	AF-270-NA	10 µg/ml
CCL4	Polyclonal	Goat	R&D Systems	AF-271-NA	10 µg/ml
CCL5	Polyclonal	Goat	R&D Systems	AF-278-NA	10 µg/ml
CCL20	Polyclonal	Goat	R&D Systems	AF-360	10 µg/ml
IMC		Ms IgG1	Dako	X0931	
IMC		Ms IgG2b	Dako	X0944	
IMC		Rabbit	Dako	M0737	

Double immunohistochemistry

Following visualisation of Foxp3 with DAB-nickel and before counter-staining with haematoxylin, sections were blocked for a second time in 10% casein solution for 30 minutes. Sections were then incubated in a second primary antibody solution – in this case, CCR5 for 1 hour at room temperature. Sections were washed then incubated with the Vector ImmPress system as before. CCR5 staining was visualised using ImmPACT NovaRED. No haematoxylin counter-stain was performed and sections were dehydrated, cleared and mounted as described above.

Double immunofluorescence

Sections were incubated with a mixture of different primary antibodies simultaneously for 1 hour at room temperature. The primary antibodies used together were of different isotypes. Sections were washed and then incubated with a mixture of secondary antibodies of different species conjugated to fluorochromes (see Table 2-5, all obtained from Life Technologies) for 20 minutes at room temperature. Sections were counter-stained with DAPI (Life Technologies, D1306) and mounted in Mowiol (Sigma-Aldrich, 81381). Tissue expression was visualised using a LSM510 confocal microscope (Zeiss) and the manufacturer's software.

Table 2-5: Secondary antibodies used for immunofluorescence

Host	Reactivity	Isotype	Fluorochrome	Code	Working concentration
Chicken	Goat	IgG	Alexa Fluor 488	A-21467	4 µg/ml
Donkey	Rabbit	IgG	Alexa Fluor 546	A-10040	4 µg/ml
Goat	Rabbit	IgG	Alexa Fluor 633	A-21070	4 µg/ml
Goat	Mouse	IgG1	Alexa Fluor 546	A-21123	4 µg/ml
Goat	Mouse	IgG2b	Alexa Fluor 633	A-21146	4 µg/ml

Chemokine capture and immunocytochemistry

Endothelial cells were isolated from enzymatically-digested matched CRC and distal colon samples (using techniques developed in our lab by Elizabeth Hepburn). In brief, tissue samples were diced and enzymatically digested as described in the above section (Selective use of enzymatic digestion). Endothelial cells were positively isolated by first labelling cells with CD31 microbeads (130-091-935, Miltenyi Biotec Ltd, UK) and then passing labelled cells twice through a magnetic column (130-042-401, Miltenyi Biotec Ltd, UK). Isolated $CD31^+$ cells were cultured in EBM-2 endothelial cell medium (CC-3156, Lonza Ltd, UK).

All chambers of a 6-chamber microslide (IB-80606, Ibidi GmBH, Germany) were coated with rat-tail collagen I (C3867, Sigma-Aldrich Ltd, UK) and left to dry overnight at room temperature. The chambers were washed with PBS and 1 x 10^5 passage 4 endothelial cells in EBM-2 media from either normal colon (NEC) or tumour (TEC) were seeded into each chamber. The slide was left for 48 hours for the endothelial cells to become confluent. The media was changed 4 hours after seeding and on a further 4 occasions

within a 48-hour period. Recombinant chemokine or PBS was added to each chamber for 30 minutes then washed out by 3 changes of PBS.

The endothelial cells were fixed by aspirating the media then adding 100 µl 4% paraformaldehyde to each chamber for 10 minutes at room temperature. The paraformaldehyde solution was washed from the chambers by adding 100 µl PBS to one side of the chamber and aspirating from the other 3 times. Endogenous Fc receptors were blocked by adding 100 µl of 2.5% normal horse serum to each chamber for 20 minutes at room temperature. The horse serum was then aspirated and solutions of primary antibody against CCL3, CCL4 and CCL5 or IMC in PBS were added to each chamber at a concentration given in Table 2-4. The fixed endothelial cells were incubated in primary antibody solution for 1 hour at room temperature. The chambers were then washed 3 times with PBS + 0.1% Tween-20 solution followed by the addition of 100 µl of Alexa Fluor 488-labelled anti-goat secondary antibody in PBS for 20 minutes at room temperature at the concentration given in Table 2-5. The chambers were washed three times with PBS + 0.1% Tween-20 solution, then filled with 100 µl PBS prior to visualisation using a LSM510 confocal microscope (Zeiss) and the manufacturer's software.

Real-time PCR

Gene expression by real-time PCR was performed using snap frozen samples of CRC and matched distal colon and the LightCycler 480 (Roche Ltd, UK). mRNA levels were expressed relative to reference genes as calculated by the $2(-\Delta\Delta Ct)$ method (relative quantification).

RNA extraction and cDNA synthesis

RNA was extracted from snap-frozen tissue samples using the Qiagen RNeasy minikit (74104, Qiagen GmBH, Germany) as per manufacturer's instructions. The RNA concentration was adjusted to 100 μg/ml by addition of RNase-free water following assessment of RNA quantity and quality by UV absorbance at 260/280 nm using a nanophotometer (P300, Implen GmBH, Germany). RNA was reverse transcribed from 3 μg RNA using the iScript kit (170-8891, Biorad Inc, USA) and stored at -80˚C until required.

Real-time PCR probes and primers

Primers and probes were designed using the RealTime Ready software (Roche Ltd, UK) for various chemokines and VAP-1. Intron-spanning primers were selected in all cases. Probes were obtained from Roche and reverse-phase purified primers were manufactured by Altabioscience (Birmingham, UK). The details of primers and probes used for gene expression analysis are shown in Table 2-6. Primers and probes for a panel of 10 different human reference genes were obtained from Roche (05046114001).

Table 2-6: Primers and probes designed with RealTime Ready software (Roche)

Gene	Accession number	Primer		UPL Probe
CCL3	ENST00000225245.5| ENSG00000006075.9	LEFT RIGHT	AATCTGCCGGGAGGTGTA TGCAACCAGTTCTCTGCATC	40
CCL4	ENST00000250151.3| ENSG00000129277.7	LEFT RIGHT	CCCAGCCAGCTGTGGTAT CTGAAGACTTCCTGTCTCTGAGC	85
CCL5	ENST00000366113.3| ENSG00000161570.3	LEFT RIGHT	CCTCATTGCTACTGCCCTCT GGTGTGGTGTCCGAGGAATA	16
CCL17	ENST00000219244.4| ENSG00000102970.5	LEFT RIGHT	GGCTTCTCTGCAGCACATC GGAATGGCTCCCTTGAAGTA	27
CCL17	ENST00000219244.4| ENSG00000102970.5	LEFT RIGHT	GCACACAGAGACTCCCTCCT AGTACTCCAGGCAGCACTCC	81
CCL19	ENST00000311925.2| ENSG00000172724.7	LEFT RIGHT	GCCTGCTGGTTCTCTGGAC GGATGGGTTTCTGGGTCAC	27
CCL20	ENST00000409189.3| ENSG00000115009.7	LEFT RIGHT	GCTGCTTTGATGTCAGTGCT GAAGAATACGGTCTGTGTATCCAA	39
CCL21	ENST00000259607.2| ENSG00000137077.3	LEFT RIGHT	TCCATCCCAGCTATCCTGTT AGCTCCTTTGGGTCTGCAC	13
CCL22	ENST00000219235.4| ENSG00000102962.4	LEFT RIGHT	CGTGGTGAAACACTTCTACTGG CCTTATCCCTGAAGGTTAGCAA	51
CCL22	ENST00000219235.4| ENSG00000102962.4	LEFT RIGHT	TTCTACTGGACCTCAGACTCCTG TGGCTCAGCTTATTGAGAATCA	37
CXCL9	ENST00000264888.4| ENSG00000138755.4	LEFT RIGHT	CCTTAAACAATTTGCCCCAAG TTGAACTCCATTCTTCAGTGTAGC	4
CXCL10	NM_001565.2	LEFT RIGHT	GAAAGCAGTTAGCAAGGAAAGGT GACATATACTCCATGTAGGGAAGTGA	34
CXCL11	ENST00000306621.3| ENSG00000169248.3	LEFT RIGHT	AGTGTGAAGGGCATGGCTA TCTTTTGAACATGGGGAAGC	76
IPO8	ENST00000256079.4|	LEFT	ACAGCACTGCAGGAGGTGTA	87

	ENSG00000133704.4	RIGHT	GCCTCCCTGTTGTTCAATCT	
VAP-1	ENST00000308423.1| ENSG00000131471.1	LEFT RIGHT	CAATGAGACCATTGCTGGAA TGTCCTCTGCATGTGGGATA	49

An amplicon was not detected using primers designed by the RealTime Ready software for CCL17, CCL22 and CXCL11. This was despite using 2 different designs for CCL17 and CCL22 and alteration of the annealing temperature. Furthermore, the amplification curves for CCL3, CCL4 and CCL5 appeared only after 50 cycles. In these cases, pre-designed primers and probes were purchased from Applied Biosystems Inc, USA (see Table 2-7). The primers and probes were provided as a gene expression assay mix.

Table 2-7: Gene expression assay mix (primers and probes) obtained from Applied Biosystems Inc, USA.

Gene	Accession number	Assay ID
CCL3	NM_002983.2	Hs00234142_m1
CCL4	AY312578.1	Hs01031494_m1
CCL5	NM_002985.2	Hs00174575_m1
CCL17	NM_002987.2	Hs00171074_m1
CCL22	NM_002990.4	Hs01574247_m1
CCR5	NM_000579.3	Hs99999149_s1
CXCR3	NM_001142797.1	Hs01847760_s1
S1PR1	NM_001400.4	Hs00173499_m1
BCL2	NM_000633.2	Hs00608023_m1
KLF2	NM_016270.2	Hs00360439_g1
GAPDH	NM_002046.3	Hs03929097_g1
18S	HSRRN18S	Hs03003631_g1

Real-time PCR procedure

The template cDNA was added to a mixture of primers, probes and master mix (LightCycler 480 Probes Master, 04 707494 001, Roche) with the following volumes per well (of a 96-well PCR plate):

Master mix	10 µl		
Left primer	1 µl	}	
Right primer	1 µl	}	or 1 µl Applied Biosystems primer-probe mix
UPL probe	1 µl	}	with 7 µl PCR water.
PCR water	5 µl	}	
Template cDNA	2 µl		

To provide negative controls, template cDNA was replaced with PCR water and a –RT (minus reverse transcriptase) control where reverse transcriptase was omitted from the cDNA synthesis reaction.

The following programme was run using the LightCycler 480:

Pre-incubation:	1 cycle	
		95˚C for 10 minutes
Amplification:	55 cycles	
		95˚C for 10 seconds
		59˚C for 30 seconds
		72˚C for 1 second
Cooling:	1 cycle	
		40˚C for 10 seconds

Selection of reference genes

Reference genes were used to normalise the mRNA fraction of different samples. It is important that the expression of chosen reference genes do not vary between tissue samples. It has been shown that traditional choices of reference genes can vary considerably between CRC and matched colon (179–182). The MIQE guidelines

(Minimum Information for Publication of Quantitative Real-Time PCR Experiments) state that normalisation against a single reference gene is unacceptable unless there is clear evidence for its invariant expression. The number and choice of reference genes must be experimentally determined (183). For this reason, absolute quantification of a panel of 10 different human reference genes (G6PD, PPIA, GAPD, TBP, ß2M, GUSB, PBGD, HPRT, ACTB, PGK1) was performed for cDNA synthesised from 3 µg of RNA from 8 samples of CRC with matched colon. Absolute quantification was performed in triplicate for each sample and differences in absolute expression between matched samples were compared using the Wilcoxin-signed rank test. It has been shown that both the data range and outlying values can have a profound effect on such analyses and therefore, a stability measure algorithm has been developed based on the principle that the expression ratio of two control genes should be identical in all samples for stable genes (184). The algorithm is known as geNorm and forms part of commercially available software (qbase+, Biogazelle, Belgium). This software calculated the most stable reference gene using the absolute quantification data from the above panel of different reference genes. Raw absolute quantification Ct (cycle threshold) values were converted into relative values by subtracting the highest Ct value from all other Ct values for each gene measured before inputting into the geNorm software. The data were also fed into other popular algorithms, namely Normfinder (185) and Bestkeeper (186). There is currently no consensus as to whether one algorithm is superior to the others.

Relative quantification

cDNA synthesised from 3 µg of RNA from 8 different CRC and matched distal colon samples was analysed for differences in expression of various targets (see Table 2-6 and Table 2-7) relative to chosen housekeeping genes, calculated by the 2(-ΔΔCt) method. Each reaction was performed in duplicate.

Gene expression by sorted Treg and Tconv

Treg ($CD4^+CD127^{low}CD25^{high}$) and Tconv ($CD4^+CD25^-$) were two-way sorted into 1.5 ml Eppendorfs containing 350 µl RLT buffer (79216, Qiagen GmBH, Germany), using methods as described above (Fluorescence-activated cell sorting (FACS)). RNA was extracted from a minimum number of 10,000 sorted cells using the RNeasy micro kit according to manufacturer's instructions (74004, Qiagen GmBH, Germany). Total RNA was reverse transcribed into cDNA using the iScript kit. Gene expression of Foxp3, CCR5, S1P1R, BCL2 and various transcription factors were compared between Treg and Tconv relative to GAPDH, calculated by the 2(-ΔΔCt) method. Each reaction was performed in duplicate.

Determination of methylation at the Foxp3 locus

To measure the percentage unmethylation at the TSDR, DNA was isolated from Treg and Tconv, followed by bisulfite treatment of the DNA then quantitative analysis of methylated alleles (QAMA) by real-time PCR.

DNA extraction from sorted Treg and Tconv

10000 to 20000 $CCR5^{low}$ Treg, $CCR5^{high}$ Treg and Tconv ($CD4^+CD25^-$) were isolated from 3 different CRC samples by FACS 3-way sorting into 1.5ml Eppendorfs containing PBS,

as described above (Fluorescence-activated cell sorting (FACS)). The cell suspensions were pelleted by centrifugation for 10 minutes at 300 *x g* in a microfuge, then resuspended in 200 µl PBS. DNA was extracted from the cell suspensions using the DNeasy Blood & Tissue Kit (69504, Qiagen GmBH, Germany) according to manufacturer's instructions.

Bisulfite conversion of extracted DNA

Treatment of DNA with sodium bisulfite deaminates unmethylated cytosine to uracil while methylated cytosines are not deaminated (187). This reaction is the basis for the downstream identification of DNA methylation. DNA samples were bisulfite treated using the Epitect Bisulfite kit (59104, Qiagen GmBH, Germany) according to manufacturer's instructions. The quantity and quality of recovered bisulfite-treated DNA was assessed by measurement of UV absorbance at 260/280 nm.

QAMA analysis

The bisulfite-treated TSDR region was amplified using primers as detailed in Table 2-8. The primers were designed so that the TSDR region was amplified irrespective of its methylation status. A Taqman® probe labelled with 6-carboxyfluorescein (FAM) was designed to specifically bind to an unmethylated sequence while another Taqman® probe labelled with 4,7,2'-trichloro-7'phenyl-6-carboxyfluorescein (VIC) was designed to specifically bind to a methylated sequence (see Table 2-8). To achieve maximum specificity, each probe was designed to span 3 CpGs within the TSDR. The primers, probes and method have been previously published (188). Primers and probes were obtained from Applied Biosystems Inc, USA.

Table 2-8: Primers and probes used for methylation analysis at the TSDR

Primer / probe	Sequence	Label	Concentration
Forward primer	GAAATTTGTGGGGTGGGGTATTTGTTTT	-	1 µM
Reverse primer	ATCTACATCTAAACCCTATTATCACAACCCCC	-	1 µM
Methylated probe	TCGGCGTATTCGG	VIC	166 nM
Unmethylated probe	AGTTTGGTGTATTTGGT	FAM	166 nM

The template bisulfite-treated DNA was added to a mixture of primers, probes and master mix (LightCycler 480 Probes Master, 04 707494 001, Roche Ltd, UK) with the following volumes per well (of a 96-well PCR plate):

Master mix	10 µl	
Forward primer	1 µl	(20 µM stock solution)
Reverse primer	1 µl	(20 µM stock solution)
VIC-labelled probe	1 µl	(3.32 µM stock solution)
FAM-labelled probe	1 µl	(3.32 µM stock solution)
Bisulfite-treated DNA	6 µl	

A negative control was provided by substitution of DNA with PCR water. Treg DNA was placed in a reaction omitting the VIC-labelled probe and Tconv DNA was placed in a reaction omitting the FAM-labelled probe to provide single colour controls required for colour compensation. All samples and controls were performed in duplicate. Roche recommends performing quintuplicate repeats for the purpose of colour compensation but there was insufficient DNA from the sorted cells to achieve this. Therefore cDNA derived from human colonic tissue was mixed either with 18S-VIC- or 18S-FAM-labelled probes with associated primers, master mix and PCR water as described above (Real-time PCR procedure) in quintuplicates.

The following programme was run using the LightCycler 480:

Pre-incubation:	1 cycle
	95˚C for 10 minutes
Amplification:	55 cycles
	95˚C for 15 seconds
	60˚C for 60 seconds
Colour compensation:	1 cycle
	95˚C for 10 seconds
	40˚C for 30 seconds
	85˚C, continuous acquisition mode with 5 acquisitions per 1˚C
Cooling:	1 cycle
	40˚C for 10 seconds

VIC and FAM were colour-compensated using the LightCycler 480 software followed by absolute quantification of unmethylated and methylated target expression. The average methylated Ct was subtracted from the average unmethylated Ct to yield a ∂Ct value. The percentage of unmethylated DNA was estimated by plotting the ∂Ct value on a published standard curve (188).

Protein detection by Western blotting

Specific proteins were detected and semi-quantified by Western blotting, using protein lysates from snap frozen samples of CRC and matched distal colon.

Protein extraction from snap frozen samples

Protein was extracted from 20-30 mg snap-frozen tissue by incubation in ice-cold lysis buffer (CellLytic MT, 20 µl/mg tissue, Sigma-Aldrich Ltd, UK) containing one tablet of Proteinase Inhibitor Cocktail per 10 ml of lysis buffer (04693159, Roche Ltd, UK). The tissue was mechanically dissociated in the buffer solution using the GentleMACS tissue dissociator, Programme RNA-01 (Miltenyi Biotec Ltd, UK). Samples were pelleted at 3000 x *g* with maximum brake and the supernatant collected and placed in 1.5 ml Eppendorfs. The samples were then further agitated for 1 hour at 4˚C, pelleted in a

microfuge at 15000 rpm for 30 minutes at 4˚C and the supernatant collected. The supernatants (protein lysates) were kept on ice.

Protein concentration determination

The protein concentrations of the protein lysates were determined against a BSA standard using a bicinchoninic acid (BCA) assay. For each lysate, a 1:5 and 1:10 dilution was made by adding 10 µl of lysate to 40 µl of lysis buffer, or 5 µl of lysate to 45 µl of lysis buffer, respectively. The 50 µl volume of each dilution was enough to perform the assay for the lysate samples in duplicate. The BCA working solution was prepared by adding 50 parts of BCA solution (B9643, Sigma-Aldrich Ltd, UK) to 1 part copper (II) sulphate pentahydrate 4% solution (C2284, Sigma-Aldrich Ltd, UK). 200 µl of BCA working solution was required for each replicate. A BSA solution of 1000 µg/ml (P0914, Sigma-Aldrich Ltd, UK) was diluted in lysis buffer to provide concentrations of 0, 200, 400, 600, 800 and 1000 µg/ml. 200 µl of BCA working solution was placed in each well of a standard flat-bottomed 96-well plate using a multi-channel pipette. 25 µl of the different BSA protein standard concentrations were added to separate wells in duplicate. 25 µl of the different protein lysate dilutions were then added to separate wells in duplicate. The plate was incubated for 30 minutes at 37˚C. Absorbance from each well was then read at 562 nm. A standard curve was created by plotting the net absorbance at 562 nm against the BSA standard concentration in µg/ml. The standard curve was used to establish the protein concentrations of each protein lysate sample. The dilution (1:5 or 1:10) which yielded absorbances along the plotted linear portion of the standard curve was selected to calculate protein concentrations. Protein lysates were then diluted in cell lysis buffer to normalise the protein concentration to 2 mg/ml.

Western blot technique

Gel casting

SDS-PAGE (sodium dodecyl sulphate polyacrylamide gel electrophoresis) was performed to separate proteins in the protein lysate samples using the Mini-PROTEAN® Tetra Cell system (Biorad Inc, USA). A stacking gel (5% acrylamide) was layered over a polymerised resolving gel (12% acrylamide) between 2 glass plates to cast a 1.5 mm gel. The resolving gel was made by mixing 3.4 ml deionized water with 4.0 ml Protogel 30% (EC-890, National Diagnostics Ltd, UK), 2.5 ml resolving buffer (1.5 M Tris, pH 8.8) and 0.1 ml 10% SDS. 60 µl 10% ammonium persulphate solution (A3678, Sigma-Aldrich Ltd, UK) and 60 µl of N,N,N',N'-tetramethylethylenediamine (TEMED, T9281, Sigma-Aldrich Ltd, UK) was added to the mixture to initiate polymerisation. The gel was poured between the 2 glass plates, leaving enough space from the top of the plates for a stacking gel and comb, and 30 µl industrial methylated spirits (IMS) was placed on top of the gel. The resolving gel was then left for 10 minutes to set. The stacking gel was made by mixing 5.7 ml deionized water with 1.7 ml Protogel 30%, 2.5 ml stacking buffer (0.5 M Tris, pH 6.8) and 0.1 ml 10% SDS. 60 µl 10% ammonium persulphate solution and 60 µl of TEMED was added to the stacking gel mixture which was then layered on top of the resolving gel. A 10-well comb was inserted into the stacking gel which was then removed after the gel had set.

Sample preparation

5 µl of 5X SDS-PAGE sample buffer (200 mM Tris pH 6.8, 20% glycerol, 10% SDS, 0.05% bromophenol blue and 10 mM ß-mercaptoethanol) was added to 20 µl of each 2 mg/ml protein lysate samples in a 1.5 ml Eppendorf. The samples were heated for 2 minutes at

100˚C then pelleted at maximum speed in a microfuge for 1 minute. The casted gels were assembled in the electrophoresis apparatus and submerged in 1X running buffer (10X running buffer = 30.3 g Tris, 144 g glycine, 10 g SDS in 1 litre distilled water). 20 µl sample was added to each lane in the stacking gel, with one lane reserved for a protein ladder (10 µl PageRuler Prestained Protein Ladder, 26616, Thermo Scientific Inc, USA) and one lane for a negative (distilled water) or positive (recombinant chemokine) control. Electrophoresis was performed for approximately 30 minutes at 200 V. In some instances, it was found that chemokine protein was self-associating, leading to multiple bands on developed blots. Therefore 8M urea was added to the sample buffer to act as a chaotrope, thereby destabilising hydrophobic bonds and increasing the protein solubility (189).

Blot development

The resolving gel was removed from the electrophoresis apparatus and placed on a piece of filter paper soaked in transfer buffer (28.8 g glycine, 6.0 g Tris, 400 ml methanol, 1 g SDS in 2 litres of distilled water). A nitrocellulose membrane (RPN2020D, Amersham Hybond-ECL, GE Healthcare Ltd, UK) was then placed directly onto the gel. Another transfer buffer-soaked filter paper was placed on top of the membrane and the filter paper sandwich was placed between 2 Scotch pads in the transfer apparatus. The apparatus was placed in the electrophoresis tank, submerged in transfer buffer. A flea was placed in the bottom of the tank and an ice-block was inserted to the back of the tank. Electrophoresis was performed for 1 hour at 100 V with continuous stirring.

The apparatus was disassembled and the membrane was removed and covered in Ponceau S solution (P7170, Sigma-Aldrich Ltd, UK) and incubated on a rocker for 5

minutes. The solution was then rinsed off the membrane to ensure that protein had transferred. The membrane was blocked by incubation with 25 ml 5% non-fat milk (5 g non-fat milk powder in PBS + 0.02% Tween 20) for 1 hour at room temperature on a rocker. 12.5 ml milk solution was removed and stored at 4˚C and primary antibody against the protein of interest was added to the remaining 12.5 ml of milk solution and incubated overnight at 4˚C on a rocker. The primary antibodies used to probe for proteins of interest are shown in Table 2-9.

Table 2-9: Primary antibodies used for Western blotting

Antigen	Clone	Isotype	Manufacturer	Code	Working concentration
CCL3	Polyclonal	Goat	R&D Systems	AF-270-NA	0.1 µg/ml
CCL4	Polyclonal	Goat	R&D Systems	AF-271-NA	0.1 µg/ml
CCL5	Polyclonal	Goat	R&D Systems	AF-278-NA	0.1 µg/ml
CCL20	Polyclonal	Goat	R&D Systems	AF-360	0.1 µg/ml
CXCL9	49106	Ms IgG1	R&D Systems	MAB392	1 µg/ml
CXCL10	Polyclonal	Goat	R&D Systems	AF-266-NA	0.1 µg/ml
CXCL11	Polyclonal	Chicken	Thermo Scientific	PA1-27877	1 in 2000
VAP-1	TK8-14	Ms IgG2a	Gift from David Smith at Biotie Therapies, Finland		2 µg/ml
GUSB	Polyclonal	Sheep IgG	R&D Systems	AF6144	1 µg/ml
GAPD	GAPDH-71.1	Ms IgM	Sigma-Aldrich	G8795	0.05 µg/ml

The milk solution containing primary antibody was poured off the membrane and the membrane was washed 3 times with 50 ml PBS + 0.02% Tween 20 for 5 minutes on an orbital shaker. The 12.5 ml milk solution stored at 4˚C was poured onto the membrane and secondary antibody conjugated to horseradish peroxidase (HRP) was added to the solution (see Table 2-10) and incubated for 1 hour at room temperature on a rocker.

The secondary antibody solution was discarded and the 3 washes with PBS + 0.02% Tween 20 repeated. The membrane was covered with enhanced-chemiluminescence substrate (PI-32109, Thermo Scientific Inc, USA) for 1 minute, before wicking off and covering the membrane in plastic wrap. Films (CL-XPosure 34088, Thermo Scientific Inc, USA) were placed inside cassettes with the covered membrane for a defined time period (30 seconds to 40 minutes) and were developed using the Compact X4 (Xograph Healthcare Ltd, UK).

Stripping of primary and secondary antibodies from the membrane allows the membrane to be re-probed for a different protein of interest, a technique that may prove useful when evaluating multiple targets (190). However, probing for GAPD in CRC protein lysate samples, using a membrane that had been stripped, resulted in weak or absent bands. Therefore, all Western blot experiments involved transferring protein to a new membrane for probing of one protein at a time.

Table 2-10: HRP-labelled secondary antibodies used for Western blotting.

Host	Reactivity	Isotype	Manufacturer	Code	Working concentration
Rabbit	Mouse	Polyclonal	Dako	P0161	0.28 µg/ml
Rabbit	Goat	Polyclonal	Dako	P0160	0.28 µg/ml
Donkey	Sheep	Polyclonal	R&D Systems	HAF016	1 in 1000
Rabbit	Chicken	Polyclonal	Invitrogen	61-3120	0.4 µg/ml

Band densitometry

The density of the developed Western blot bands is proportional to the protein concentration. Measurement of band density is therefore *semi-quantitative*, in that there is no standard curve to enable absolute protein concentrations to be calculated.

Band density was calculated using ImageJ (Version 1.46r, NIH, USA) which has built-in gel image analysis functions. Differences in band densities between CRC and matched colon samples were tested for statistical significance using the Wilcoxin signed-rank test.

Graphical presentation and statistical analysis

Data was presented in graphical format using Prism version 5.0f (GraphPad Software Inc, USA) or R version 2.15.2 (The R Foundation for Statistical Computing, Austria). Statistical analysis was performed using R or SPSS Statistics version 20 (IBM Corporation, USA). Advice on the statistical methods and testing used in this thesis was obtained from Professor Mohammed Mohammed (School of Health Studies, University of Bradford – previously at Primary Care Clinical Sciences, University of Birmingham). P values were given to 2 significant figures.

In general, differences between unrelated groups were tested for statistical significance using the Mann-Whitney U test while differences between related groups were tested using the Wilcoxon signed-rank test. P values <0.05 were considered to be statistically significant. Asterisks were placed in figures to indicate statistically significant differences, using the following convention:

* ≤ 0.05

** ≤ 0.01

*** ≤ 0.001

Chapter 3
Phenotype of tumour-infiltrating Treg

Introduction

The expression of chemokine receptors and integrins by T cells will determine which cells are recruited to tumours. Enrichment of Treg has been reported in CRC by both immunohistochemical and flow cytometric methods (52–54,191–193). It is hypothesised that differences between Treg and Tconv in terms of chemokine receptor and integrin expression, explain why Treg are recruited to tumours in preference to Tconv, thereby leading to Treg enrichment.

In this thesis, the term Treg refers to lymphocytes expressing both CD4 and CD25 with low levels of CD127, i.e. $CD4^+CD25^+CD127^{low}$. Conventional T cells (Tconv) refers to lymphocytes expressing CD4 and low levels of CD25, i.e. $CD4^+CD25^-$.

This chapter presents evidence for Treg enrichment in CRC tissue compared to matched distal colon, TDLN and peripheral blood. I carried out a systematic and comparative analysis of the expression levels of chemokine receptors, Treg markers and integrins by Treg, Tconv and $CD8^+$ cells.

Findings

Treg enrichment in CRC compared with distal colon

Lymphocytes were isolated from CRC, colon, TDLN and peripheral blood as described in Chapter 2. There were a total of 70 samples of CRC from 70 patients, with matched

distal colon in 60 cases, matched TDLN in 8 cases and matched peripheral blood in 7 cases. There were also 2 polyps, both of which were reported as having moderate dysplasia. The proportion of $CD4^+$ cells with a Treg phenotype ($CD4^+CD25^+CD127^{low}$), referred to as the *Treg proportion*, was calculated for each sample and compared across tissue compartments (see Figure 3-1). Statistical significance was tested by the Wilcoxin signed-rank test when comparing differences between the matched tissues of CRC, distal colon and TDLN. Differences in the Treg proportion between tissue samples and unmatched blood samples were tested for statistical significance using the Mann-Whitney test. There was no significant difference in the Treg proportion of peripheral blood samples between control patients and patients with CRC (P=0.49, Mann-Whitney). However, differences in the Treg proportion between all other tissue compartments reached statistical significance.

The absolute number of Treg present in different tissue compartments was measured by flow cytometry using counting beads, adjusted for tissue weight. There was a statistically significant difference in the number of Treg per mg of tissue between CRC and matched distal colon (Wilcoxin signed-rank test) – see Figure 3-2a.

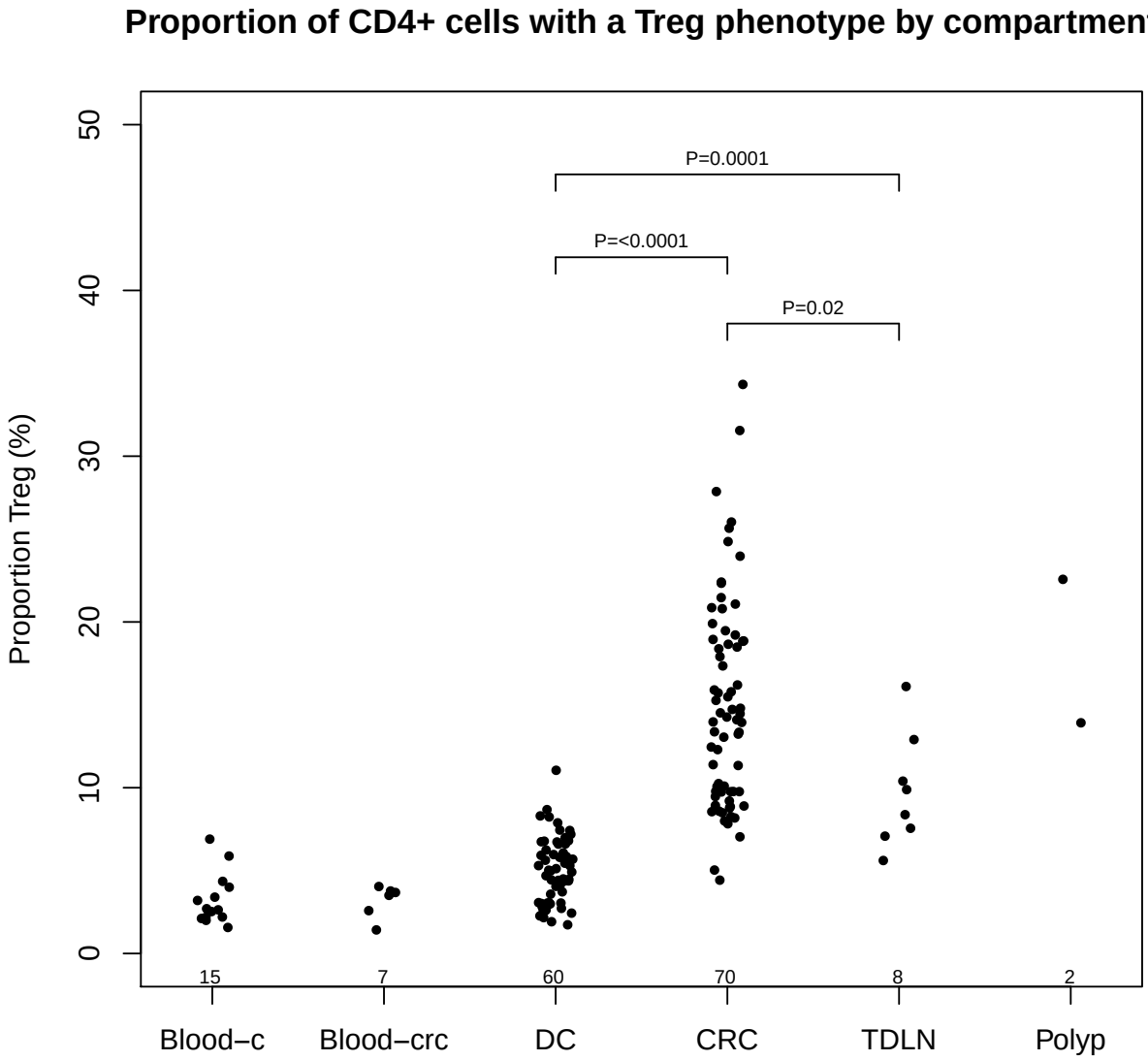

Figure 3-1: The proportion of $CD4^+$ cells with a Treg phenotype in different tissue compartments. 'Blood-c' = peripheral blood samples from healthy volunteers or HFE donors. 'Blood-crc' = peripheral blood from patients with CRC taken at induction of anaesthesia. DC = distal colon. Numbers in black along x-axis represent number of cases in each group. Capped lines indicate statistically significant differences between groups (Wilcoxin signed-rank test).

Live and apoptotic cells

The median proportion of dead lymphocytes ± interquartile range (IQR) differed significantly by sample type: 25.9% (12.8 – 41.6) for CRC versus 6.9% (2.8-10.6) for distal colon ($P<0.01$, Wilcoxin signed-rank test). Annexin-V staining was performed on one sample to quantify the proportion of early apoptotic cells. 9.9% of CRC-isolated Treg were positive for Annexin-V, which was comparable to the proportion for Tconv (9.0%) and $CD8^+$ cells (9.6%), suggesting that the isolation procedure did not result in a proportionately high level of Treg apoptosis.

CD8 : CD4 ratio

The ratio of CD8 to CD4 T cells was measured in different tissues (see Figure 3-2b). There was no difference between the proportion of CD8 : CD4 T cells in 34 samples of CRC with matched distal colon. The median CD8 : CD4 ratio was 0.45 (IQR: 0.32-0.75) in CRC and 0.50 (IQR: 0.34-0.82) in matched distal colon ($P=0.962$, Wilcoxin signed rank).

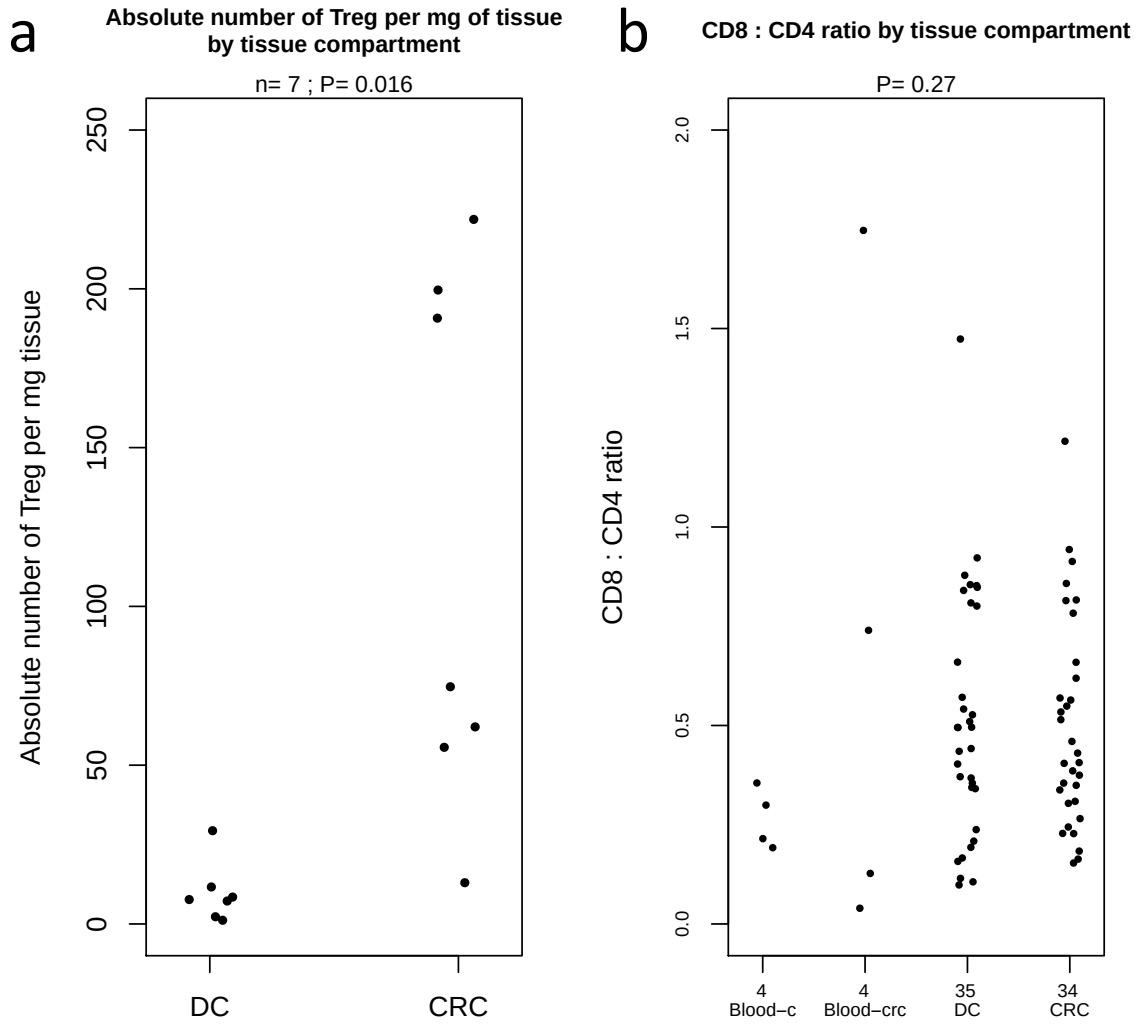

Figure 3-2: (a) Absolute number of Treg per mg of tissue by tissue compartment. (b) CD8 : CD4 ratio by tissue compartment. 'Blood-c' = peripheral blood samples from healthy volunteers or HFE donors. 'Blood-crc' = peripheral blood from patients with CRC taken at induction of anaesthesia. DC=distal colon. Numbers in black along x-axis represent number of cases in each group.

Treg expressed high levels of the transcription factor, Foxp3

The expression of the Treg master transcription factor Foxp3 by tumour-resident Treg, Tconv and $CD8^+$ cells was assessed by intracellular staining and flow cytometry (see Figure 3-3). The median percentage expression of Foxp3 was 93.5% (IQR: 92.0-96.2), 16.2% (IQR: 13.8-19.5) and 6.5% (IQR: 4.7-12.7) for Treg, Tconv and $CD8^+$ cells respectively. The difference in Foxp3 expression between Treg and Tconv was statistically significant ($P<0.01$, Wilcoxin-signed rank). Tconv expressing Foxp3 did so at lower levels than Treg, in terms of MFI. These may reflect a subset of activated T cells.

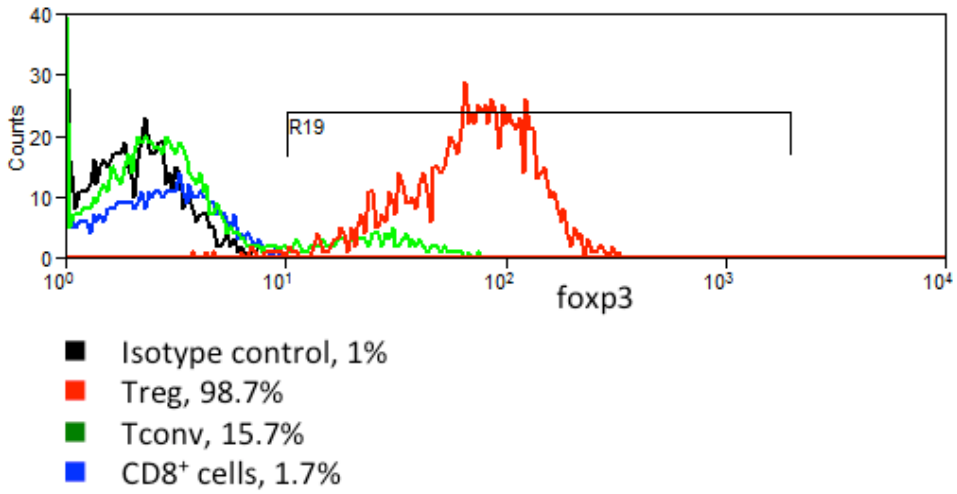

Figure 3-3: Foxp3 expression by Treg, Tconv and CD8+ cells isolated from CRC tissue. Data representative of 9 unique matched samples.

Factors associated with the CRC Treg proportion

Patient factors (age at operation, gender) and CRC factors were tested for association with the proportion of tumour-infiltrating Treg (see Table 3-1). The CRC factors tumour position, grade, stage, extramural vascular invasion (EMVI) and volume were

chosen as they form part of the standard dataset used for pathology reporting of CRC and were thus available from hospital pathology reports (194). Survival and disease recurrence data were obtained from hospital correspondence records. MSI and KRAS mutations were sought in selected cases by immunohistochemistry or PCR, respectively. The decision to perform testing for MSI and KRAS mutations was made by the pathologists. Patient age and tumour volume were continuous variables and were thus divided into quartiles in order to perform grouped analysis testing for association with the proportion of Treg. Associations were tested for statistical significance using the Mann-Whitney test or Kruskall-Wallis test for categories with two-groups or more than two groups, respectively. Scatterplots illustrating the relationship between patient age and tumour volume with the Treg proportion are shown in Figure 3-4.

Table 3-1: Association of patient and CRC factors with the proportion of tumour-infiltrating Treg

Factor	n	Median (%)	IQR (%)	P-value
Age:				
<62	20	15.1	(9.8-17.6)	0.21
62-69	15	13.2	(9.8-18.9)	
70-76	18	15.3	(13.6-20.6)	
>76	17	11.4	(8.2-17.9)	
Gender:				
Male	38	14.0	(9.8-17.9)	0.63
Female	32	14.9	(9.9-19.6)	
Position:				
Right-sided	25	13.9	(9.2-18.9)	0.81
Left-sided	21	14.1	(10.1-17.4)	
Rectum	24	15.6	(9.5-20.1)	
Grade:				

Moderate	58	13.7	(9.3-18.9)	0.45
Poor	12	15.0	(13.0-16.7)	
Stage:				
Dukes A	9	14.3	(9.8-15.8)	0.45
Dukes B	26	13.7	(9.3-18.9)	
Dukes C	28	14.6	(10.0-19.6)	
Dukes D	7	14.5	(11.9-17.5)	
EMVI				
Negative	39	13.4	(9.8-18.4)	0.42
Positive	29	14.7	(9.8-20.9)	
Unknown	2	11.5	(9.8-13.1)	
Mismatch repair mutations:				
No mutation	7	13.4	(9.3-15.1)	0.14
Mutation	6	15.3	(14.5-18.4)	
Unknown	57	14.0	(9.8-18.9)	
KRAS mutation:				
No mutation	26	15.3	(13.4-19.1)	0.01
Mutation	18	9.8	(9.0-14.0)	
Unknown	26	14.9	(9.8-18.9)	
Tumour volume ($x10^3$ mm^2):				
<1.05	18	15.0	(10.4-18.8)	0.48
1.05-21.7	15	15.7	(9.9-20.4)	
21.8-56.7	18	13.3	(9.3-14.7)	
>56.7	19	14.8	(9.6-19.3)	
All cause mortality:				
Alive	62	14.0	(9.5-18.6)	0.23
Deaths	8	16.7	(12.1-20.4)	
CRC-specific mortality:				
Alive/non-CRC deaths	64	14.0	(9.7-18.7)	0.23
CRC-specific deaths	6	16.8	(12.8-22.8)	

Local recurrence:				
False	66	14.0	(9.8-18.8)	0.11
True	4	19.2	(14.4-26.6)	
Distant recurrence:				
False	64	14.0	(9.8-18.7)	0.21
True	6	17.7	(14.5-23.2)	
Local or distant recurrence				
False	63	13.9	(9.8-18.7)	0.25
True	7	14.5	(14.3-22.4)	

The only patient or CRC-specific factor associated with the tumour Treg proportion was the presence of a KRAS mutation. There was no association between Treg proportion and either tumour grade or stage. Interestingly, there was a trend for a higher Treg proportion in patients who subsequently develop local or distant disease recurrence, although these differences did not reach statistical significance.

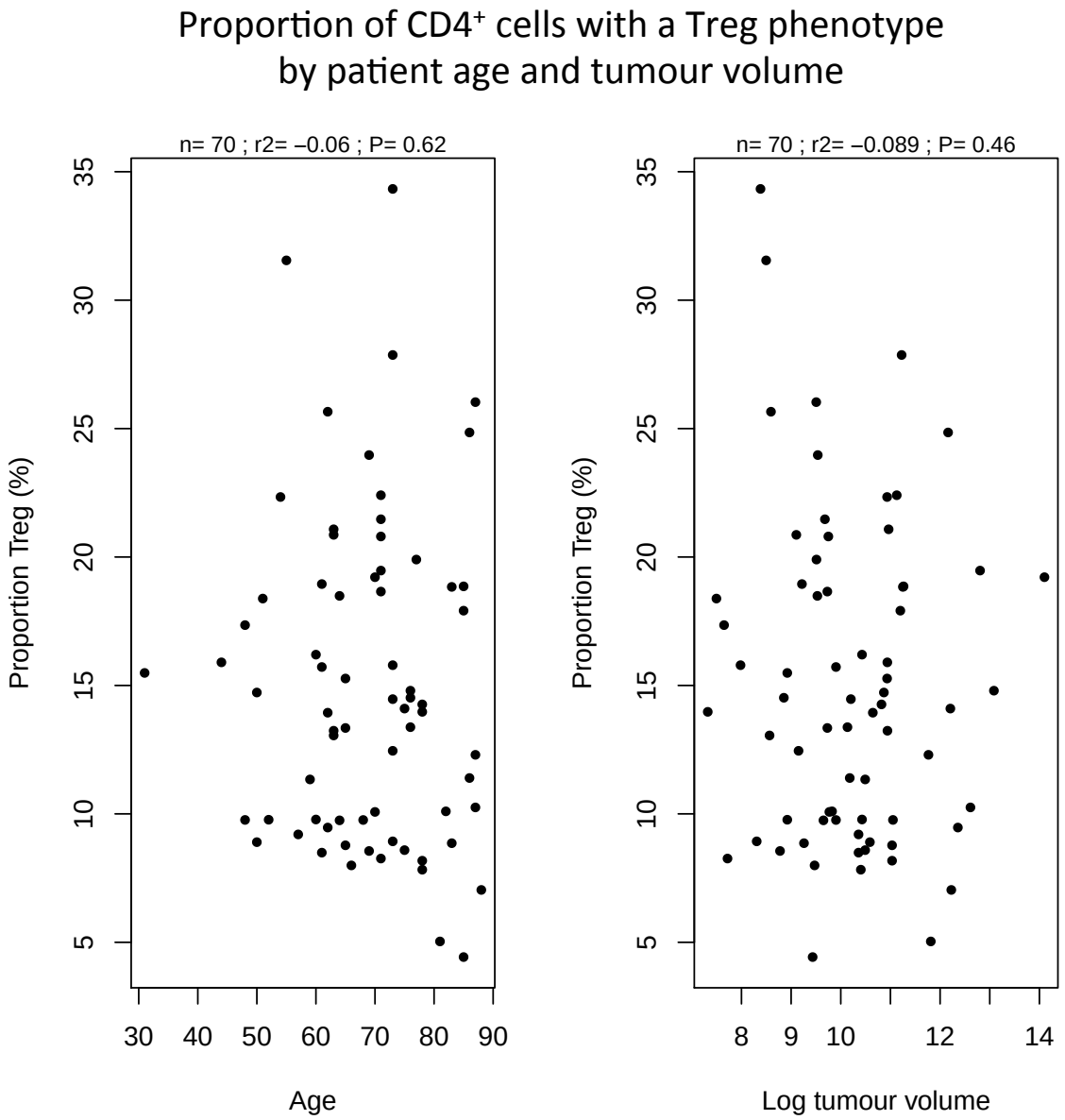

Figure 3-4: The proportion of tumour-infiltrating Treg by patient age and tumour volume. Note that tumour volume is plotted on a logarithmic scale.

Treg infiltration in CRC liver metastases

The Treg infiltration was measured in samples of CRC liver metastases and matched distal liver, using exactly the same methods as for primary CRC and colon tissue. Three matched tissue samples were assessed. The median Treg proportion was 3.7% (IQR: 3.0-4.5) for metastatic tissue and 1.9% (IQR: 1.1-2.3) for distal liver tissue. Two further

samples were processed but no live lymphocytes were isolated from the metastatic tissue. Given the problems with live lymphocyte yield and the small differences in Treg infiltration between metastatic and distal liver tissue, no further experiments were performed using CRC metastases. All further data presented in this chapter relate to primary CRC and colon tissue.

Chemokine receptor, integrin and Treg marker expression by TIL

The expression of different chemokine receptors, integrins and various Treg markers was compared between CRC-isolated Treg, Tconv and $CD8^+$ cells. Both percentage expression and MFI were compared. Positive expression was defined relative to a FMO control containing an IMC of the same isotype as the antibody against the antigen of interest. The FMO control region was set at <1.5% expression. Summary data from 64 separate flow cytometry experiments are presented. Statistical significance was assessed by Wilcoxin ranked-sign test and was adjusted for multiple comparisons using the Bonferroni method. Differences in chemokine receptor expression by cell type are shown in Figure 3-5. Treg expressed significantly more CCR4 and CCR5 compared with Tconv in terms of both percentage expression and MFI. Similarly, Treg expressed significantly more CCR5 compared with $CD8^+$ cells in terms of both percentage expression and MFI while $CD8^+$ cells expressed more CCR5 than Tconv by percentage expression only.

Significantly fewer Treg expressed CCR7 and CXCR4 compared with Tconv. Significantly more Treg expressed CCR6 compared with $CD8^+$ cells, with a trend for greater CCR6 percentage expression by Treg compared with Tconv.

The expression of various Treg markers by TIL is summarised in Figure 3-6.

As previously stated, there was significantly greater Foxp3 expression in terms of both percentage expression and MFI by Treg compared with Tconv. Differences in Foxp3 expression between $CD8^+$ cells and either Treg or Tconv did not reach statistical significance due to the small number of cases (n=3) in which Foxp3 expression was measured in $CD8^+$ cells. There was significantly greater CD39 expression, both in terms of percentage expression and MFI, by Treg compared with Tconv and significantly greater percentage expression of CD27 by Treg compared with Tconv.

The expression of different integrins by TIL is summarised in Figure 3-7.

Significantly more Treg expressed CD62L compared with Tconv, although the median percentage expression of CD62L was universally less than 20%. It should be noted that generally fewer experiments were performed analysing integrin expression on TIL compared to chemokine receptor expression. P-values were adjusted for multiple comparisons and it was therefore difficult to demonstrate statistically significant differences in the expression of antigens that were measured in only a small number of separate experiments. In relation to integrin expression, the unadjusted Wilcoxin-signed rank test reported a statistically significant reduction in the expression of the ß7 integrin between Treg and Tconv.

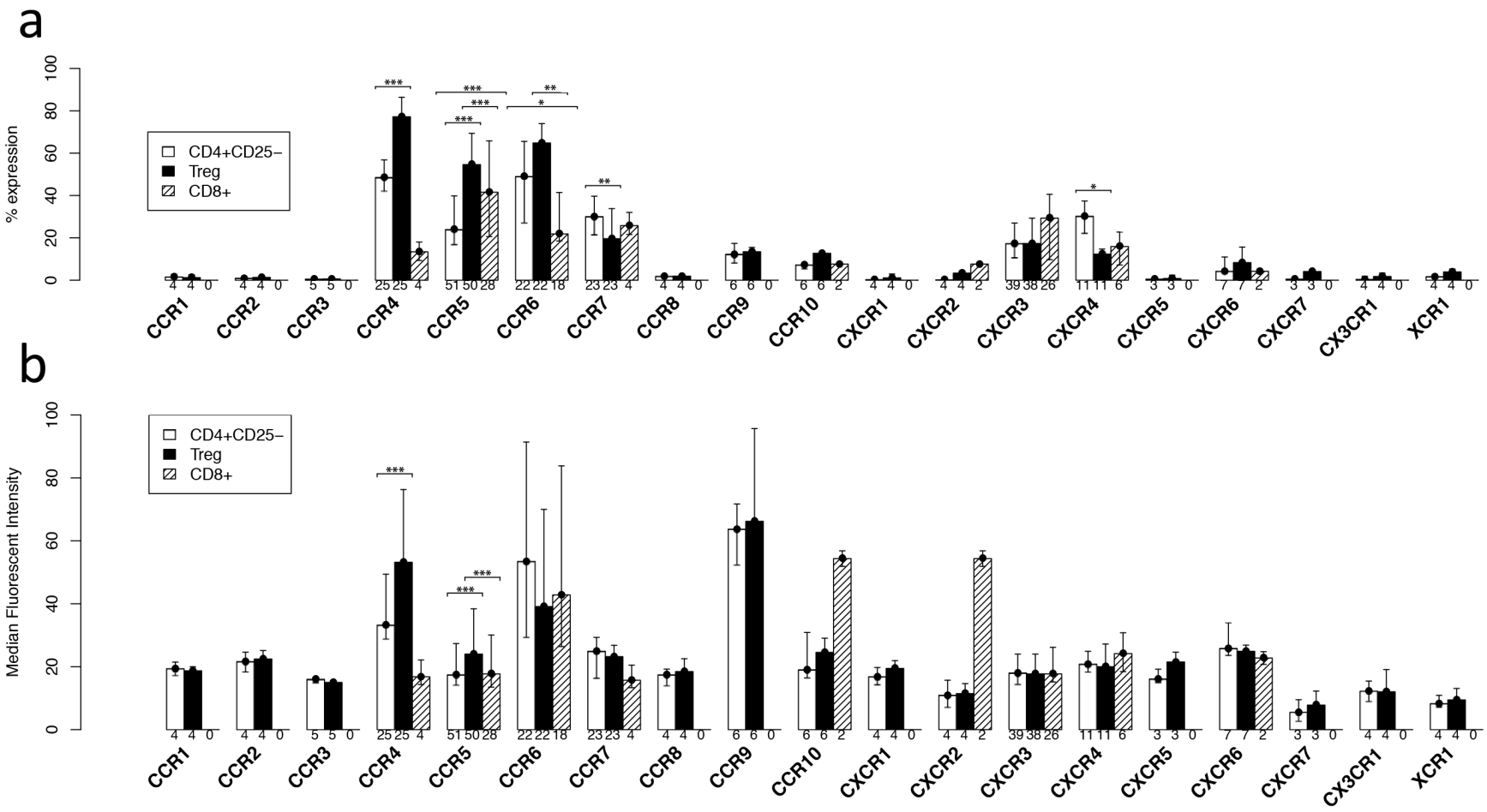

Figure 3-5: Chemokine receptor expression by TIL by cell type. (a) Median percentage expression. (b) Median MFI. Error bars represent the IQR about the median. Numbers along x-axis indicate the number of unique samples. Capped lines indicate statistically significant differences.

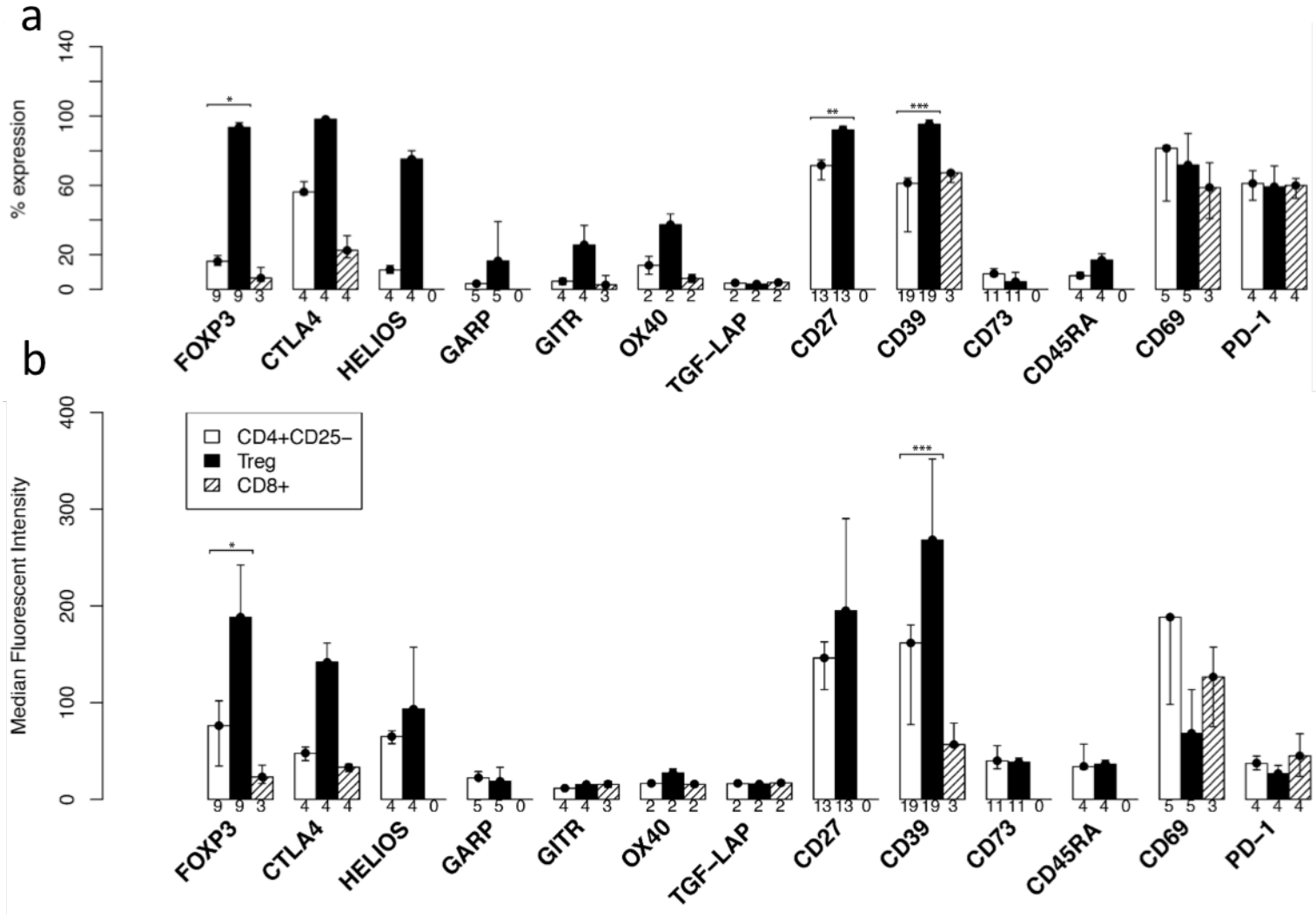

Figure 3-6: Treg marker expression by TIL by cell type. (a) Median percentage expression. (b) Median MFI. Error bars represent the IQR about the median. Numbers along x-axis indicate the number of unique samples. Capped lines indicate statistically significant differences.

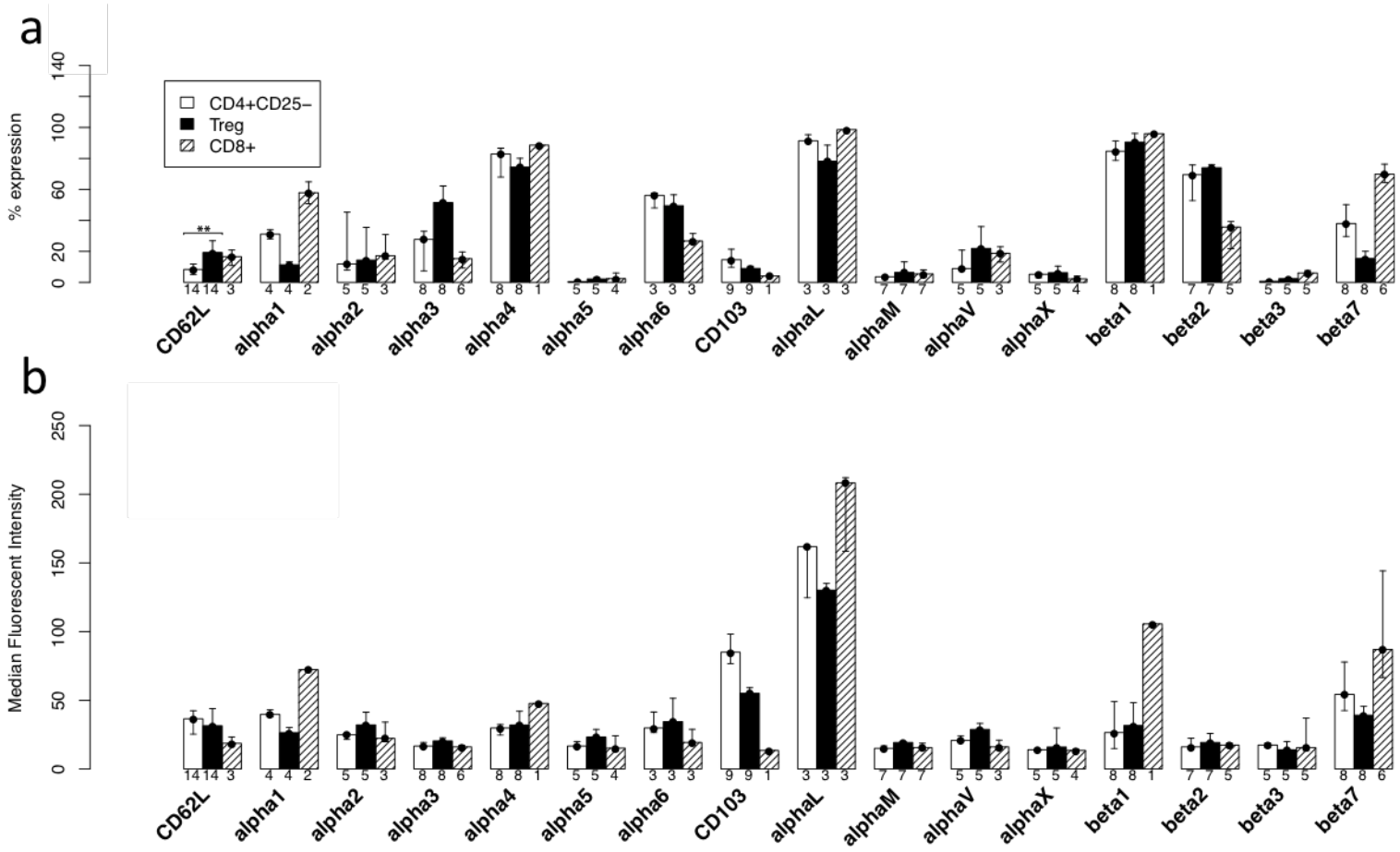

Figure 3-7: Integrin expression by TIL by cell type. (a) Median percentage expression. (b) Median MFI. Error bars represent the IQR about the median. Numbers along x-axis indicate the number of unique samples. Capped lines indicate statistically significant differences.

Comparison of chemokine receptor, integrin and Treg marker expression by Treg between CRC, matched distal colon and TDLN

The expression of chemokine receptors, integrins and Treg markers by CRC-isolated Treg was compared with Treg isolated from matched distal colon and TDLN. Statistical significance was assessed by Wilcoxin ranked-sign test and was adjusted for multiple comparisons using the Bonferroni method.

The summary data for chemokine receptor expression by Treg by tissue type is shown in Figure 3-8. Significantly more CRC-isolated Treg expressed CCR5 compared with Treg isolated from matched distal colon. There was no difference in CCR4 expression but a trend for increased CCR6 percentage expression by Treg isolated from CRC compared with Treg isolated from matched distal colon. There were no significant differences in Treg marker expression or integrin expression by Treg between CRC and matched distal colon or TDLN (see Figure 3-9 and Figure 3-10).

However, unadjusted P-values did demonstrate significantly less expression of ß7 and significantly more expression of ß1 by Treg isolated from CRC compared with distal colon. Similarly, unadjusted P-values demonstrated a significant difference between the percentage expression of CD39 by CRC-isolated Treg compared with Treg isolated from matched distal colon.

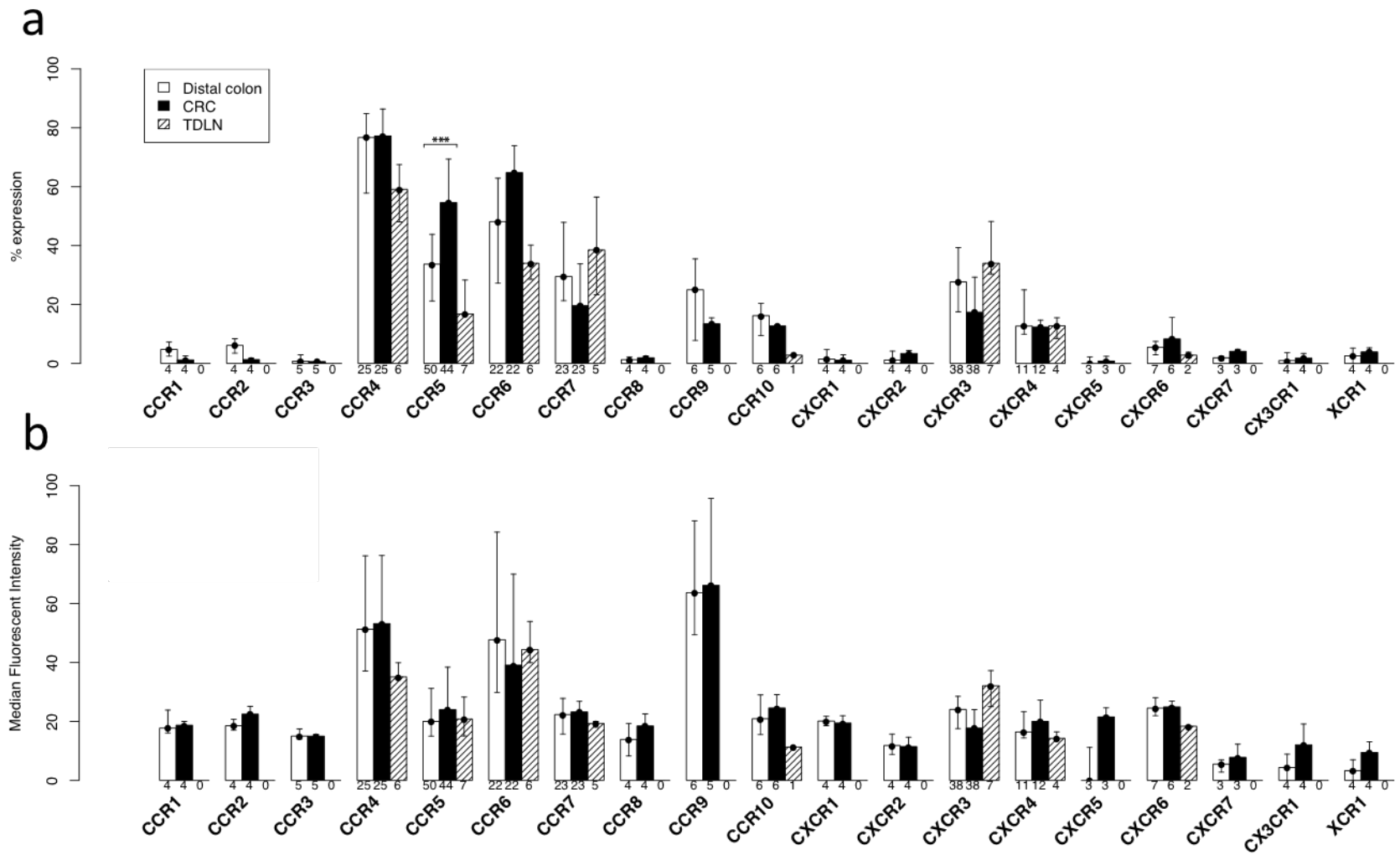

Figure 3-8: Chemokine receptor expression by Treg by tissue type. (a) Median percentage expression. (b) Median MFI. Error bars represent the IQR about the median. Numbers along x-axis indicate the number of unique samples. Capped lines indicate statistically significant differences.

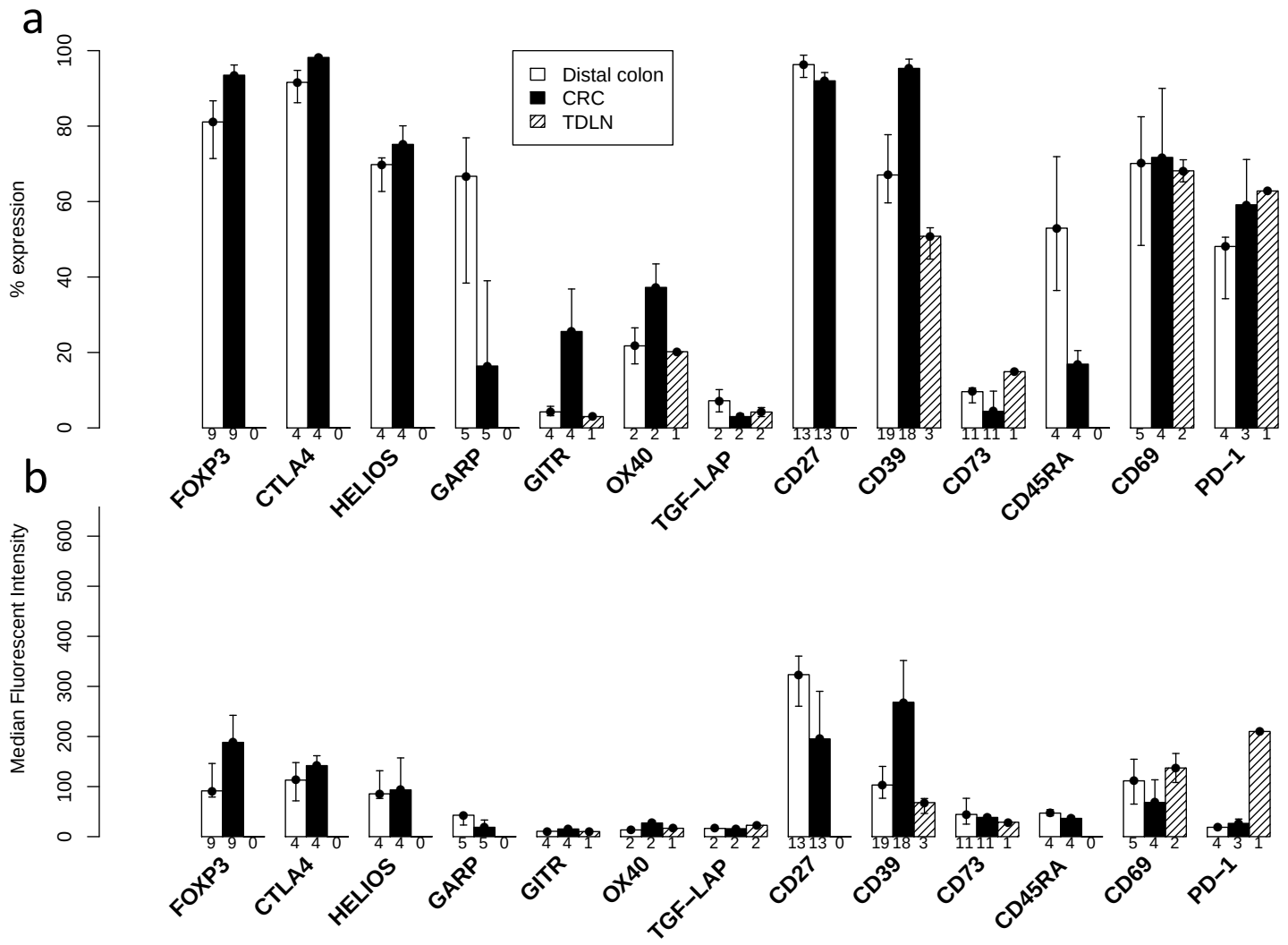

Figure 3-9: Treg marker expression by Treg by tissue type. (a) Median percentage expression. (b) Median MFI. Error bars represent the IQR about the median. Numbers along x-axis indicate the number of unique samples.

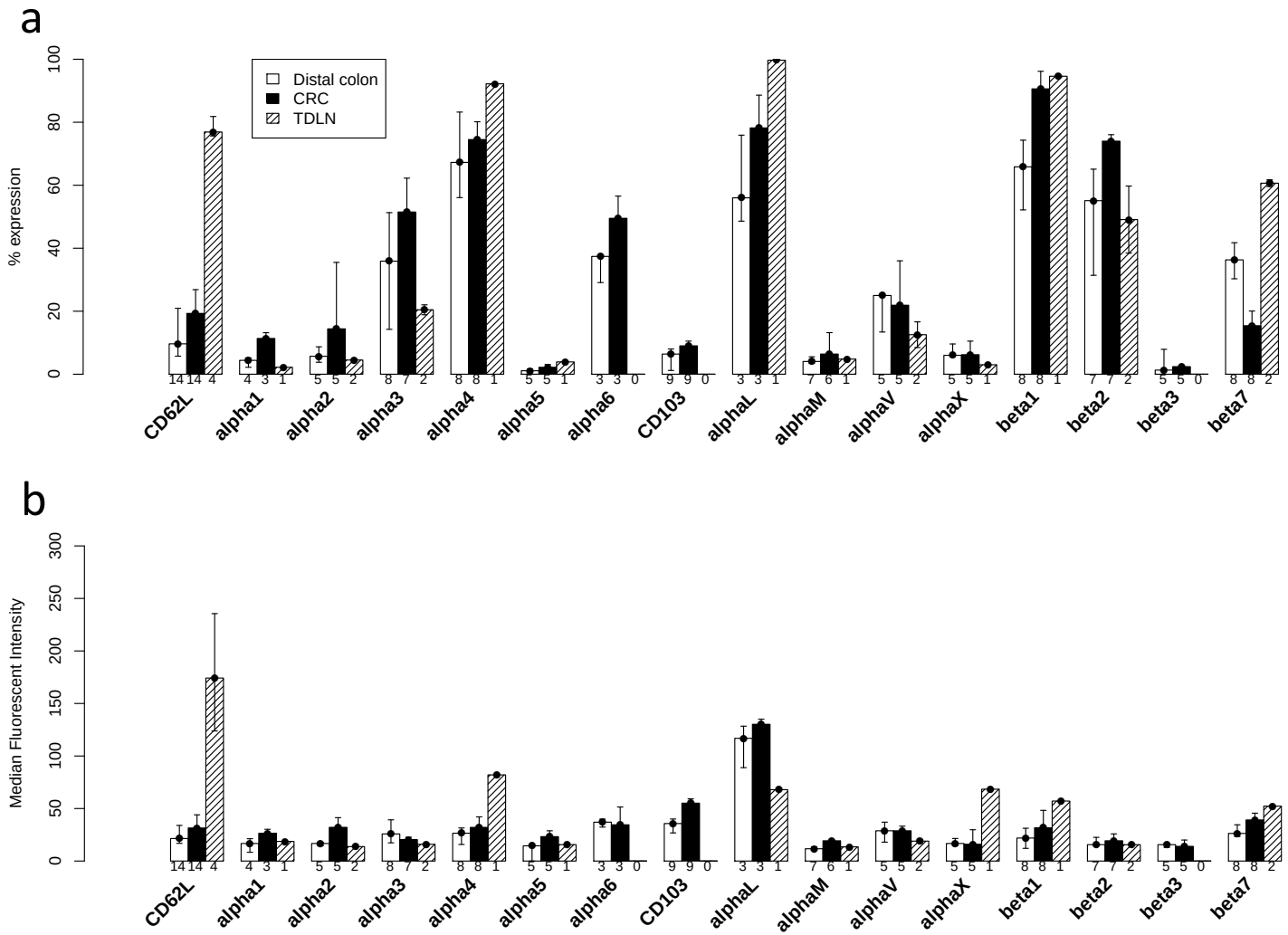

Figure 3-10: Integrin expression by Treg by tissue type. (a) Median percentage expression. (b) Median MFI. Error bars represent the IQR about the median. Numbers along x-axis indicate the number of unique samples.

The expression of chemokine receptors, Treg markers and integrins of interest by Treg isolated from the peripheral blood of patients with CRC was compared with the expression by Treg isolated from the peripheral blood of control subjects (either healthy volunteers or HFE patients) – see Figure 3-11. Statistical significance was assessed by the Mann-Whitney test and was adjusted for multiple comparisons using the Bonferroni method. Statistically significant differences in antigen expression between matched CRC, distal colon and TDLN are not represented in Figure 3-11 as these have been shown in previous figures. Statistically significant differences in antigen expression by CRC-isolated Treg compared with Treg isolated from the blood of either control subjects or patients with CRC are highlighted by capped lines.

There was significantly less percentage expression of CCR5 and CD39 by Treg isolated from blood than from Treg isolated from CRC tissue. There was significantly greater percentage expression of CCR7 and CD62L by Treg isolated from the blood of control subjects compared to Treg isolated from CRC tissue.

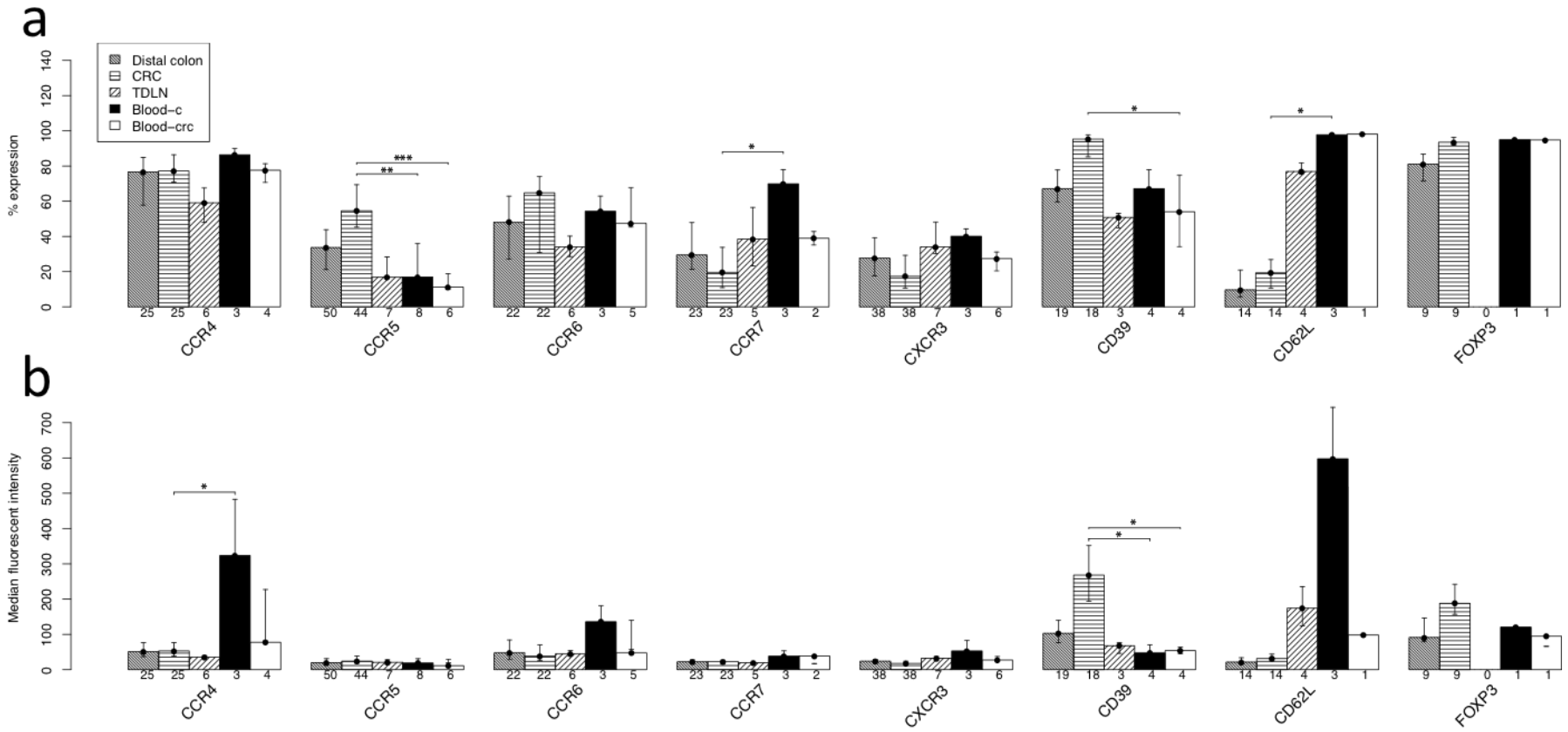

Figure 3-11: The expression of various markers by Treg isolated from the blood of control subjects and patients with CRC. (a) Median percentage expression. (b) Median MFI. Error bars represent IQR about the median. Numbers along x-axis indicate the number of unique samples. Capped lines indicate statistically significant differences between CRC-isolated Treg and Treg isolated from the blood of control subjects or patients with CRC. 'Blood-c' = blood samples from healthy volunteers or HFE donors. 'Blood-crc' = blood from patients with CRC taken at induction of anaesthesia.

One chemokine receptor that showed marked differences between cell type and tissue distribution, was CCR5. In the tumour, CCR5 was relatively overexpressed by Treg compared with both Tconv and $CD8^+$ cells, in terms of both percentage expression and MFI. Representative flow cytometry overlay histograms are shown in Figure 3-12. More Treg isolated from CRC expressed CCR5 than Treg isolated from distal colon or from peripheral blood. Other chemokine receptors, that were relatively overexpressed by CRC-isolated Treg compared with Tconv and CD8+ cells, were CCR4 and CCR6. However, there was no significant difference in the expression of these two chemokine receptors by Treg across different tissue types.

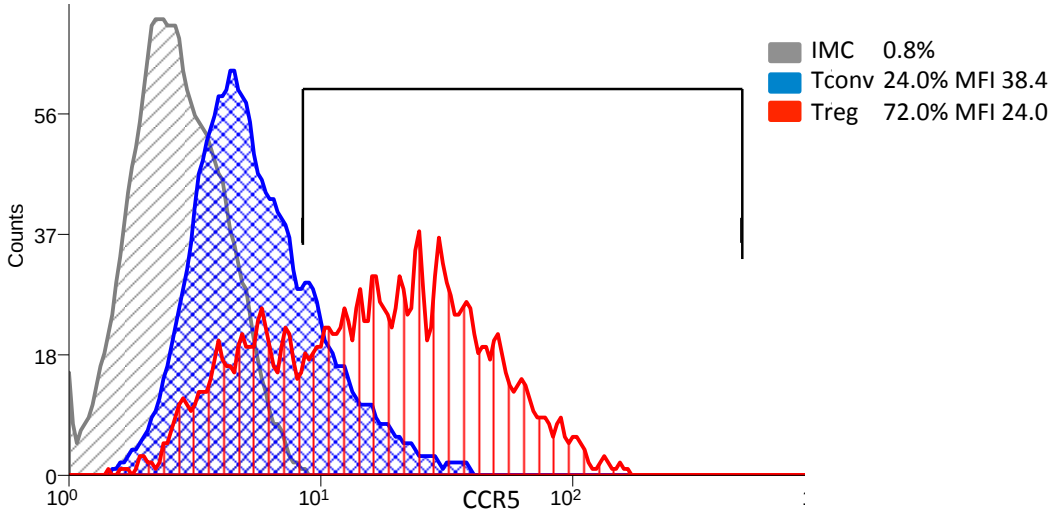

Figure 3-12: Flow cytometry data for CCR5 expression by CRC-isolated Treg compared with CRC-isolated Tconv and IMC for a single sample. Data representative of 51 unique samples.

Differences in CCR5 expression were dependent on antibody clone

In all 50 samples of matched CRC and distal colon, the percentage expression of CCR5 was higher by CRC-isolated Treg compared with Tconv. In all 50 samples, CCR5 percentage expression by CRC-isolated Treg was greater than the expression by Treg

isolated from distal colon. The clone of the anti-human CCR5 antibody used in these experiments was CTC5. In order to determine if the antibody clone had a bearing on the expression profile of CCR5 by Treg and Tconv, a different antibody clone (2D7-CCR5, BD Biosciences) was used in 3 separate experiments. Across the 3 experiments, the median CCR5 percentage expression by CRC-isolated Treg was 37.1% (IQR: 35.2-53.1) compared with 34.4% (IQR: 34-53.3) for Tconv. The median CCR5 percentage expression by Treg isolated from distal colon was 36.9% (IQR: 22.2-45.4). There was therefore no observed difference in the percentage expression of CCR5, as measured using the 2D7-CCR5 antibody clone, between Treg and Tconv within CRC tissue and between CRC-isolated and distal colon-isolated Treg.

CCR5 was overexpressed by Treg compared to Tconv at the mRNA level

In order to determine if there were differences in CCR5 gene expression between CRC-isolated Treg and Tconv, Treg and Tconv were isolated from CRC tissue by cell sorting. 10,000 to 20,000 Treg and Tconv were sorted from 4 separate CRC samples. RNA was isolated from the sorted cells, cDNA was synthesised and RT-PCR was performed. The expression of CCR5 mRNA and other target mRNAs were calculated relative to the expression of GAPDH mRNA. The fold change in target mRNA expression was expressed as a ratio of the target mRNA expression by Treg relative to GAPDH to the target mRNA expression by Tconv relative to GAPDH (see Figure 3-13). The mean fold change in Foxp3 mRNA expression by Treg relative to Tconv was 6.5 (SD=3.1), serving as an internal control for expected differences in gene expression between the two cell types. The mean fold change in CCR5 mRNA expression was 2.6 (SD=1.0), suggesting that the increased cell surface expression of CCR5 by Treg compared to Tconv is real

and may, at least in part, be explained by greater CCR5 gene expression by Treg compared with Tconv. Differences in the relative quantification of Foxp3, CCR5, KLF2 and CREB1 mRNA to GAPDH mRNA by Treg compared with matched Tconv were tested for statistical significance using the Wilcoxin signed-rank test.

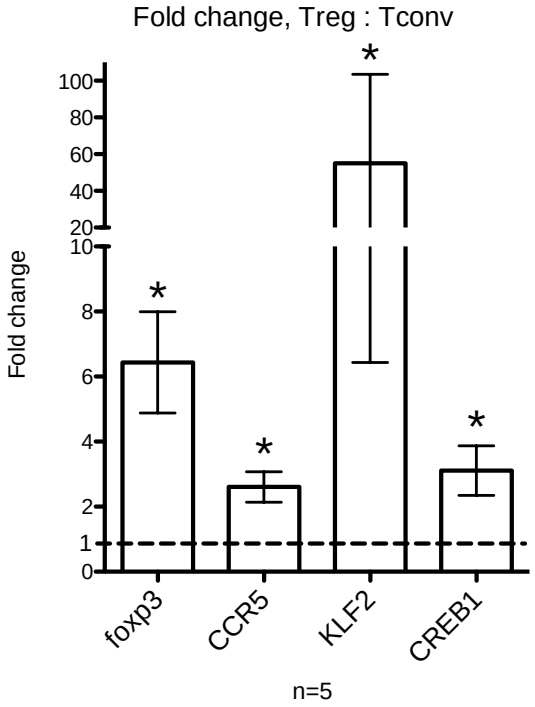

Figure 3-13: Mean fold change in mRNA expression by CRC-isolated Treg relative to CRC-isolated Tconv from 5 unique samples. Error bars represent standard error of the mean fold change. Asterisks represent statistically significant differences (Wilcoxin-signed rank test).

CCR5, Foxp3 double immunohistochemistry

In order to identify CCR5-expressing Treg in sections of CRC, double immunohistochemistry was performed. Foxp3 was visualised with DAB-nickel (antibody clone: 236A/E7), giving a black nuclear stain, and CCR5 with NovaRED™ (antibody clone: 45531), giving a brown/red cytoplasmic and cell surface stain (see Figure 3-14). No counter-stain was used. Double-labelled $CCR5^+$ $Foxp3^+$ cells were identified in the CRC stroma, although $CCR5^-Foxp3^+$ cells were also readily observed.

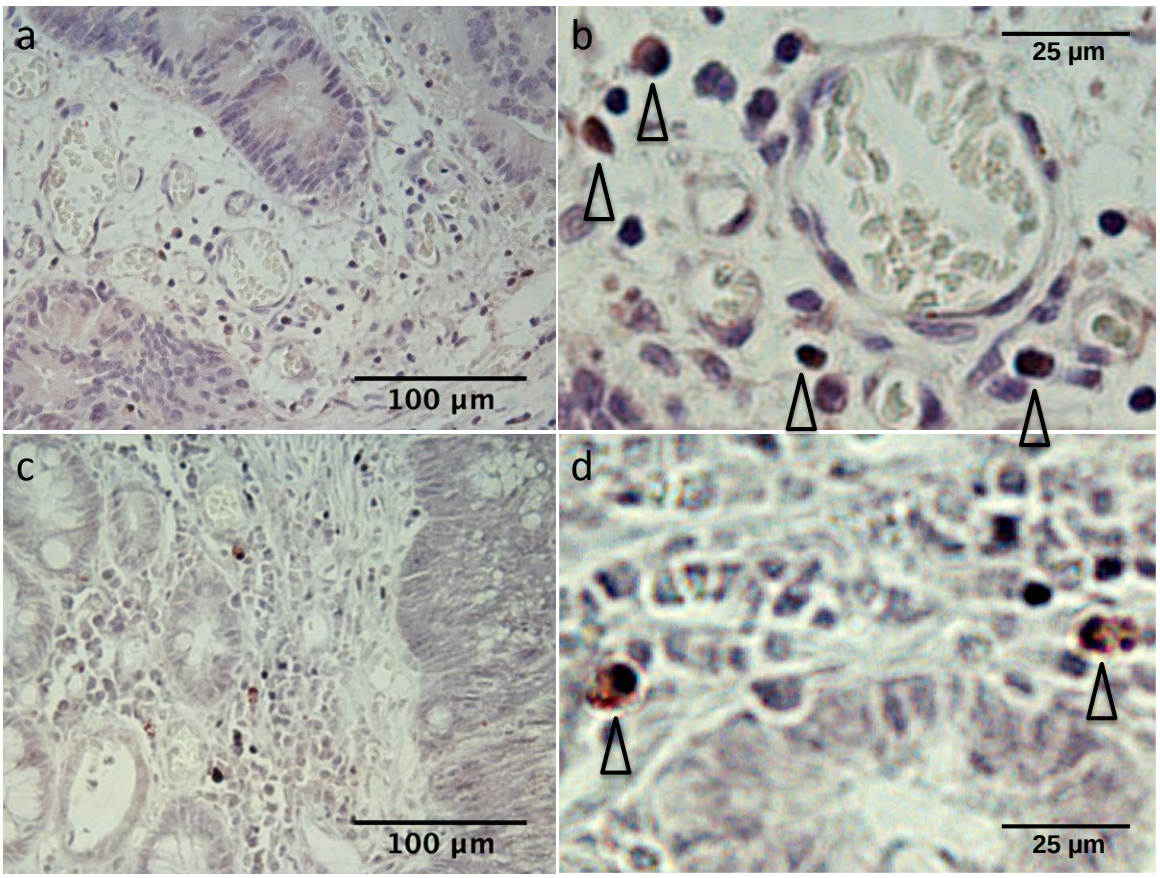

Figure 3-14: Double immunohistochemistry for CCR5 and Foxp3. (a+c) Sections from 2 different cases of CRC, x100 magnification, representative of 4 cases. (b+d) Same 2 cases, x400 magnification. Foxp3=black nuclear stain (DAB-nickel); CCR5=red/brown cytoplasmic and cell surface stain (NovaRED™). Open arrows point to dual-labelled ($CCR5^+$ $Foxp3^+$) cells.

Factors associated with CCR5 expression by CRC-isolated Treg

Patient factors and CRC factors were tested for association with the percentage expression of CCR5 (antibody clone: CTC5) by Treg isolated from CRC (see Table 3-2). Associations were tested for statistical significance using the Mann-Whitney test or Kruskall-Wallis test for categories with two-groups or more than two groups, respectively. There was no significant association between the percentage expression of CCR5 by Treg with any patient or CRC factors.

Table 3-2: Association of patient and CRC factors with the percentage expression of CCR5 by Treg isolated from CRC. EMVI = extramural vascular invasion.

Factor	n	Median (%)	IQR	P-value
Age:				
<62	17	52.5	(49.5-70.4)	0.81
62-69	10	62.8	(51.5-73.2)	
70-76	14	54.6	(38.2-63.0)	
>76	9	62.9	(48.5-62.9)	
Gender:				
Male	23	55.8	(39.2-74.3)	0.61
Female	27	53.4	(51.7-68.3)	
Position:				
Right-sided	16	53.0	(46.7-61.7)	0.23
Left-sided	15	61.9	(51.7-78.2)	
Rectum	19	56.9	(41.4-69.4)	
Grade:				
Moderate	42	64.7	(50.5-68.0)	0.65
Poor	8	53.0	(45.3-69.4)	
Stage:				
Dukes A	9	41.3	(37.1-55.8)	0.96
Dukes B	19	51.8	(45.0-69.7)	

Dukes C	17	62.9	(53.4-74.5)	
Dukes D	5	49.5	(44.2-64.3)	
EMVI				
Negative	26	57.4	(48.9-69.4)	0.94
Positive	23	53.4	(46.9-68.7)	
Unknown	1	37.1		
Mismatch repair mutations:				
No mutation	7	66.0	(55.2-80.5)	0.43
Mutation	5	55.2	(41.5-65.0)	
Unknown	38	52.9	(45.5-69.3)	
KRAS mutation:				
No mutation	26	51.7	(38.9-61.5)	0.09
Mutation	18	58.9	(51.7-73.5)	
Unknown	26	59.9	(51.4-69.3)	
Tumour volume ($x10^3$ mm^2):				
<1.05	14	58.6	(51.7-68.8)	0.30
1.05-21.7	11	56.9	(50.2-71.7)	
21.8-56.7	13	69.3	(41.5-74.5)	
>56.7	12	50.8	(40.8-54.1)	
All cause mortality:				
Alive	45	53.4	(41.5-70.1)	0.37
Deaths	5	64.3	(62.9-65.0)	
CRC-specific mortality:				
Alive/non-CRC deaths	45	53.4	(41.5-70.1)	0.37
CRC-specific deaths	5	64.3	(62.9-65.0)	
Local recurrence:				
False	46	53.4	(42.2-69.9)	0.58
True	4	60.6	(55.1-66.1)	
Distant recurrence:				
False	47	53.4	(42.9-69.7)	0.57

True	3	65.0	(58.4-67.2)	
Local or distant recurrence				
False	46	53.4	(42.2-69.9)	0.58
True	4	60.6	(55.1-66.1)	

Discussion

The data presented in this chapter have demonstrated that the Treg proportion was significantly increased in CRC compared with distal colon, TDLN and peripheral blood. 93.5% of Treg expressed the transcription factor Foxp3 compared to 14.2% of Tconv cells. The only CRC factor found to be associated with the CRC Treg proportion was the presence of KRAS mutations.

CCR4 and CCR5 were significantly overexpressed by Treg compared with Tconv, both in terms of percentage expression and MFI. The percentage expression of CCR5 was significantly greater by CRC-isolated Treg compared with Treg isolated from distal colon. CCR5 mRNA was significantly more highly expressed by CRC-isolated Treg compared with Tconv. KLF2 and CREB1 are genes involved in the regulation of CCR5 transcription and were also significantly more highly expressed by Treg compared with Tconv. There was a trend for lower levels of ß7 percentage expression by CRC-isolated Treg compared with Tconv and by CRC-isolated Treg compared with Treg isolated from distal colon. However, these differences did not reach statistical significance using P-values adjusted for multiple comparisons.

Treg enrichment in CRC

There have been numerous reports of increased numbers of Treg in the tumour tissue of various malignancies compared with healthy tissue and peripheral blood, when analysed by flow cytometric or immunohistochemical methods (see Table 3-3). There is also evidence for an increased frequency of Treg in the peripheral blood of cancer patients compared to healthy controls. With regard to CRC, immunohistochemical studies have demonstrated increased numbers of $Foxp3^+$ cells in CRC tissue compared

to healthy colon (54,191,195). Flow cytometry methods, which express Treg frequency as a proportion of $CD4^+$ cells, have shown a significantly increased Treg proportion in CRC compared with TDLN, in TDLN compared with peripheral blood and in CRC compared with matched colon (52,56). By RT-PCR, Foxp3 gene expression was increased in CRC compared with matched colon (196). This is entirely in keeping with the results presented in this chapter, demonstrating that the Treg proportion significantly increases in a step-wise fashion from peripheral blood, to distal colon, to TDLN, to CRC.

Table 3-3: Published literature providing evidence for Treg infiltration in solid tumours, assessed by flow cytometry and immunohistochemistry. CM=confocal microscopy; PB=peripheral blood; IHC=immunohistochemistry.

Tumour site	Compartments	Method	Definition	Findings	References
Ovarian	Tumour, blood	FC	$CD4^+CD25^+$	Increased frequency of Treg in tumour compared to PB.	(197)
	Tumour, ascites, TDLN	FC, CM	$CD3^+CD4^+CD25^+$	Increased frequency of Treg in tumour tissue compared to healthy ovarian tissue (CM).	(57)
Lung	Tumour, blood	FC	$CD4^+CD25^+$	Increased proportion of Treg in tumour compared to PB.	(197)
	Tumour	IHC	Foxp3	Increased Treg frequency associated with worse survival.	(198)
Breast	Tumour, blood	FC	$CD4^+CD25^+$	Increased frequency of Treg in breast cancer compared to normal PB.	(199)
	Tumour	IHC	Foxp3	Foxp3 staining intensity independently associated with survival.	(200)
Brain	Tumour, blood	FC	$CD4^+CD25^+$	Increased Treg frequency in glioma compared to normal brain tissue. Increased Treg frequency in cancer patient PB compared to controls.	(201)
Pancreas	Tumour	IHC	$CD4^+Foxp3^+$	Increased frequency of Treg in neoplastic lesions compared to inflammatory and healthy pancreatic tissue. High Treg frequency associated with cancer grade, stage and patient survival.	(58)
Head and neck	Tumour, blood	FC	CD4+CD25+	Increased frequency of Treg in tumours and PB of patients with tumours compared to PB of control subjects.	(202)

Oesophago-gastric	Tumour, blood Blood	FC FC	$CD4^+CD25$ $CD4^+CD25^+$	Increased Treg frequency in tumour compared to gastric mucosa and PB. Increased Treg frequency in cancer patient PB compared to PB of controls. Higher proportion of Treg in TIL from patients with late versus early stage disease. Increased Treg frequency in cancer patient PB compared to controls. Treg frequency decreased after resection and increased on recurrence.	(203) (204)
Liver	Tumour	IHC FC	Foxp3 $CD4^+CD25^+$	High numbers of intratumoral Treg inversely correlated with survival. Increased proportion of Treg in tumour compared to distal liver.	(59) (205)

Association of Treg enrichment with CRC factors

Given the hypothesis of Treg-mediated suppression of the anti-tumour response, it might be expected that tumour Treg density increases with advancing CRC stage. Indeed, there is some evidence that this is the case. In two immunohistochemistry studies involving 94 and 160 cases, low CD8/Foxp3 and CD3/Foxp3 ratios were found to be associated with shorter disease-free and overall survival in multivariate analyses (195,206). In a recent study of 76 cases specifically investigating the CD8/Foxp3 ratio in CRC, a high CD8/Foxp3 ratio was shown to be significantly associated with overall survival by univariate, but not multivariate, analysis (207). However, one small immunohistochemical study, n=57 (208), and two large studies of 967 and 1420 patients respectively (53,191) have demonstrated that high Treg frequencies in CRC are associated with improved survival. In the latter two studies, high Treg frequency was independently associated with improved survival in multivariate analyses (53,191). The relationship between Treg frequency and survival has been shown to be restricted to non-MSI cancers (53).

A smaller study of 40 cases, showed that Treg infiltration, measured by immunohistochemistry, was greater in early as opposed to late-stage disease, although there was no demonstrable association with survival (54). With regard MSI CRC, an investigation of T cell subsets in these cancers showed an association between high Foxp3 densities and early disease stage, absence of nodal invasion and absence of lymphovascular invasion (209). Studies that report an association between increased Treg frequency and improved survival highlight the beneficial role that Treg might play in suppressing a tumour-driven

inflammatory response that drives tumour progression. Support for this idea comes from the APC min/+ mouse model, where adoptive transfer of Treg led to regression of bowel tumours (210).

The absolute number of Treg may be misleading as the suppressive capacity of the population as a whole is more relevant than the number of Treg cells. Addressing the suppressive capacity of Treg in CRC, a study has demonstrated that Treg from CRC interact with mast cells, also present in CRC, resulting in downregulation of the suppressive cytokine, IL-10 (211). It has been suggested that gut bacterial infections in early life can protect against inflammation-associated malignancies such as CRC by modulating Treg function in the gut (210). CRC breaks down the normal mucosal barrier function of the gut resulting in increased exposure of the gastrointestinal immune system to microbiota (212). Increased Treg numbers in the tumour may be a reaction to this microbiota exposure rather than to an anti-tumour immune response. This association between high Treg frequency and favourable survival is not limited to CRC – similar relationships have been observed in lymphoma (213) and head and neck cancers (214).

There are therefore two sets of apparently contradictory immunohistochemistry studies: One set provides evidence that high Treg density is associated with worse prognosis (195,206,207), while the other set suggests the opposite (53,191,208). Further immunohistochemistry studies have failed to provide evidence of an association between Treg density and survival (54,215,216). One key difference between the two sets of immunohistochemistry studies is those demonstrating a worse prognosis in association with high Treg density reported

the ratio of Treg compared to other lymphocytes, either $CD3^+$ or $CD8^+$ cells, rather than reporting the absolute Treg count. It is possible that the ratio of Treg to non-Treg T cells may be of more importance given that high lymphocyte counts per se, are associated with a favourable prognosis in CRC (217). High Treg densities, measured by Foxp3 immunostaining, may therefore reflect dense lymphocytic infiltration, with proportionately high or low non-Treg / Treg ratios. In support of this notion, flow cytometric studies, which measure the Treg frequency as a proportion of $CD4^+$ cells, have shown no relationship between Treg frequency and prognosis (52,56). In fact, one of these studies described an increased Treg frequency in late-stage as opposed to early-stage CRC. One disadvantage of flow cytometric measurement of TILs in CRC is the dependence on fresh tissue which means that often, the exophytic portion of a tumour is retrieved for TIL isolation in order to avoid compromising pathological assessment and diagnosis. However, the exophytic portion may represent an adenomatous part of the tumour with no frank malignant tissue. Immunohistochemical studies, on the other hand, can make use of blocks from all portions of the tumour, including the invasive margin.

The marker chosen to define Treg also poses difficulties. Immunohistochemical studies use a Foxp3 nuclear stain to define Treg, although a few studies have used other markers such as CD25 (218). It has been shown that $CD4^+CD25^-$ T cells may express Foxp3 upon activation (219,220) and it is unclear whether Foxp3 immunohistochemistry identifies activated $CD4^+CD25^{dim}$, $CD4^+CD25^{high}$ cells as well as $CD4^+CD25^+CD127^{low}$ Treg. The data presented in this chapter have shown almost universal expression of Foxp3 by $CD4^+CD25^+CD127^{low}$ Treg

but also significant, albeit lower expression of Foxp3 by $CD4^{+}CD25^{-}$ cells. Foxp3 is also expressed by cells other than T cells, notable cancer epithelial cells (221), although it is relatively easy to distinguish these from T cells if manual counting is used.

An increase in Treg density with advancing disease stage does not preclude an important role for Treg in the establishment and progression of CRC. The frequency of Treg in tumours may be homeostatic in that the frequency is balanced according to the need for suppression of effector T cells. In this situation, the ratio of Treg to non-Treg T cells may be expected to remain relatively constant throughout disease progression. Several studies do indeed suggest that there is little alteration of Treg density by disease stage (54,56,215,216). The data presented in this chapter are consistent with this in that there was no difference in Treg proportion across different Dukes stages. There was also no association between Treg proportion with all-cause mortality, disease-specific mortality, or local or distant recurrent disease. A lack of association may reflect the low number of patients studied together with the low number of deaths and disease recurrences. Certainly, these numbers rendered a multivariate analysis inappropriate. The Treg proportion measured in the two moderately dysplastic polyps was comparable to that seen in CRC, suggesting that tumour Treg infiltration occurs early. This is consistent with another small study showing that Treg infiltration is an early event in the adenoma-adenocarcinoma pathway (222).

In our study, a significantly lower Treg proportion was seen in CRC with KRAS mutations compared with wildtype KRAS tumours (P=0.01, see Table 3-1). This

is consistent with a previous study which reported that the absolute number of $Foxp3^+$ cells was decreased in patients with KRAS mutations compared with wildtype KRAS while there was no difference in the absolute number of $CD3^+$ or $CD8^+$ cells (215). Differences in the ratios of $Foxp3^+$ cells to $CD3^+$ or $CD8^+$ cells were not analysed and the difference in $Foxp3^+$ cell number by KRAS status was not defined as statistically significant (P=0.036), as the P-value significance threshold was defined as ≤0.0009 – adjusted for multiple comparisons. Nevertheless, no such changes in $Foxp3^+$ cell number were observed for the other measured CRC molecular changes, namely CIMP status, BRAF mutations, PIK3CA mutations and LINE-1 hypomethylation. A recent study of 44 cases of CRC found no difference in the number of TILs, broken down into subsets including a $Foxp3^+$ group, by KRAS mutation (223). Again, the proportion of Treg relative to $CD3^+$ or $CD8^+$ cells was not analysed. There was also no difference in the overall TIL count between KRAS mutant and wildtype CRC in a larger study of 198 CRCs (224). It is unclear as to how a CRC KRAS mutation could result in a reduction in tumour Treg infiltration. It has been shown than KRAS mutant tumours undergo spontaneous apoptosis at a higher rate than wildtype tumours (224). It is therefore possible that apoptotic, as opposed to necrotic tumours may generate a weaker immune response, with an accompanying lower Treg infiltration. Against this idea is a report that Treg accumulate in vitro in a DC / T cell co-culture when the DCs are primed with apoptotic tumour cell supernatant (225), as opposed to necrotic tumour cell supernatant.

Others have demonstrated an increased Treg density in MSI CRC (215,226). The data presented in this chapter demonstrates no such increase in Treg density when reported relative to $CD4^+$ cells. This is consistent with other studies in which the ratio of $Foxp3^+$ cells to other lymphocytes is assessed (53,192,215). In contrast, an analysis of Foxp3 mRNA expression has shown that Foxp3 expression is decreased in MSI CRC compared with wildtype tumours (196).

CD8 : CD4 ratio

The median CD8 : CD4 ratio in CRC was 0.45 and was not significantly different from the ratio in the distal colon. These findings are consistent with some published studies (167,227,228). However, others have shown a decreased CD8 : CD4 ratio in CRC compared to colon tissue, brought about by an increase in the absolute number of $CD4^+$ cells in CRC relative to matched colon, while the absolute number of $CD8^+$ cells was similar across the two tissue types (229). Others have shown that the overall survival, adjusted for tumour stage and patient age, was greater for patients with higher tumour CD8 : CD4 ratios, highlighting the prognostic benefit of $CD8^+$ cell infiltration in CRC (227).

2D7 antibody blocks the ligand-binding site

The CTC5 anti-CCR5 monoclonal antibody, used to generate the phenotype data presented in this chapter, recognises an epitope at the CCR5 N-terminus (230). The 2D7 clone recognises an epitope positioned in the second extracellular loop and blocks binding of RANTES, MIP-1α and MIP-1ß (231). The binding characteristics of a panel of different monoclonal antibodies suggest that CCR5 exists in several different antigenic forms on the cell-surface of primary T cells (232). The heterogeneity of cell surface CCR5 is influenced by post-translational

modifications, G-protein coupling and the local lipid environment. The lack of expected differences in CCR5 expression between T cell subtypes using the 2D7 antibody may thus be due to the 2D7 clone not recognising the form of the CCR5 receptor when it is bound to one of its ligands. Overexpression of CCR5 by Treg compared with Tconv using the CTC5 clone may represent increased density of cell surface CCR5 bound to its ligand on Treg compared with Tconv. The affinity of different monoclonal antibodies against CCR5 has been studied and concluded that the use of 2D7 may underestimate total CCR5 surface expression under some conditions, while CTC5 exhibits high maximal binding levels and can detect different conformational states of the receptor (232).

Chemokine receptor expression by CRC-isolated Treg

The chemokine receptors CCR4 and CCR5 were overexpressed on CRC-isolated Treg compared with Tconv. Increased expression of CCR4 by tumour-isolated Treg compared to Tconv was originally reported in a study of TILs isolated from ovarian cancer (57). Indeed, CCR4 is known to be expressed by peripheral blood Treg to a greater extent than peripheral blood Tconv (99). Interestingly, $CCR4^+$ Treg appear to be primed to suppress autologous T cell proliferation, whereas $CCR4^-$ Treg first require activation in order to be suppressive. A study of chemokine receptors and integrins on T cell subsets isolated from CRC and distal colon has shown that CCR4 is expressed at high levels on Treg in CRC with significantly higher expression compared with Treg isolated from distal colon (193).

In a study of pancreatic cancer, T cells infiltrating human pancreatic cancer were found to express more CCR5 than T cells from the normal donor transplant

pancreatic tissue and the percentage of Treg expressing CCR5 was over twice that of non-regulatory T cells (104). In a pancreatic tumour mouse model, Treg again expressed more CCR5 than their non-regulatory counterparts (104). Similarly, CCR5 has been shown to be overexpressed on Treg compared with non-regulatory T cells in a murine model of CRC (233).

Increased expression of CCR5 by CRC-infiltrating Treg compared with Tconv has not been reported previously although high levels of CCR5 have been reported on TILs infiltrating human CRC compared with matched colon (102). CCR5 expression was higher on $CD8^+$ cells compared to $CD4^+$ cells - the Treg subset was not specifically assessed. By mRNA analysis, CCR5 expression was greater in CRC tissue compared to distal colon (234). A study in CRC, specifically assessing chemokine receptor expression by Treg, did not report any difference in CCR5 expression between Treg and Tconv compared across CRC and distal colon (193). The CCR5 antibody clone was not reported but as it was obtained from BD Biosciences, the clone must have been either 2D7 or 3A9. The different antibody clones could explain the differences observed in CCR5 expression between this study and the findings presented in this chapter. In support of this notion, a study assessing CCR5 expression by TIL in nasopharyngeal cancer using the 2D7 clone, demonstrated no significant difference in CCR5 expression between Treg and Tconv (235). A study in renal cell carcinoma showed that CCR5 was highly expressed on TIL (236). The study did not directly compare chemokine receptor expression between T cell subsets, but there was at least a trend to increased CCR5 MFI expression, by Treg compared with Tconv.

Other characteristic phenotypic differences between T cell subsets included higher cell surface levels of CCR6 on Treg, although the difference in percentage expression between Treg and Tconv did not reach statistical significance. $CCR6^+$ Treg have been identified in murine models of CRC (237) and in human malignancies (106). It has been suggested that $CCR6^+$ Treg represent a population of memory Treg which also express CD45RO and proliferate rapidly on re-stimulation in vitro (238). Twenty-two matched CRC / distal colon samples were used to analyse CCR6 expression on TIL compared to 50 for CCR5 expression. The differences in CCR6 expression between Treg and Tconv may therefore reach statistical significance with greater sample number. Nevertheless, the magnitude of the difference in CCR6 expression between Treg and Tconv is less than that observed for CCR5 and there is no accompanying difference in CCR6 expression in terms of MFI. In the case of integrins, there was a trend for reduced expression of $ß_7$ integrin by Treg isolated from CRC compared with Treg isolated from distal colon, which was statistically significant by unadjusted P-values. This is consistent with a recent study which used flow cytometry to demonstrate reduced expression of $\alpha_4ß_7$ integrin by CRC-Treg compared to colonic Treg (193). The investigators proceeded to measure the expression of the $\alpha_4ß_7$ ligand, MAdCAM-1, by RT-PCR and immunohistochemistry, demonstrating reduced expression of MAdCAM-1 by tumour tissue compared with matched colon.

Potential therapeutic benefit of CCR5 blockade

Little CCR5 is expressed by circulating lymphocytes, yet is expressed by lymphocytes isolated from a variety of different tissues (239). In particular,

CCR5 is highly expressed by T cells infiltrating inflamed joints and other inflamed tissues (240). As CCR5 is preferentially expressed by Treg in CRC, this receptor is a potential therapeutic target, particularly as CCR5 antagonists have a proven safety record in the treatment of other conditions, including HIV infection (241). Individuals with the CCR5Δ32 deletion mutation in the CCR5 gene are healthy, except perhaps for a weakened resistance to West Nile Virus infection (242). Interestingly, the CCR5Δ32 mutation is associated with reduced incidence of rheumatoid arthritis (243) and multiple sclerosis (244), is protective against systemic sclerosis (245) and is associated with increased renal transplant survival (246). The postulated explanation for the beneficial effects of the CCR5Δ32 mutation in these diseases is a reduction in immune cell recruitment to the affected tissues. The CCR5Δ32 mutation has been investigated in cancer: It has been shown that CCR5Δ32 is not associated with an increased susceptibility to breast cancer or CRC (247,248). The mutation is associated with a worse disease-free survival in breast cancer, although this is restricted to wild-type p53 cancers (247).

Chapter 4
Chemokine expression by CRC

Introduction

In Chapter 3, data were presented showing an increased expression of specific chemokine receptors by Treg compared with Tconv and $CD8^+$ cells. CCR4, CCR5 and to a lesser extent, CCR6, were expressed at higher levels by Treg than by Tconv and $CD8^+$ cells.

If these receptors are important for recruitment, their ligands must be expressed by the tumour tissue. This chapter presents an analysis of chemokine expression by CRC compared with matched distal colon by RT-PCR, Western blotting, ELISA, immunohistochemistry and flow cytometry.

Findings

CRC tissue chemokine expression by RT-PCR

RNA was isolated from 8 matched samples of CRC and distal colon and the RNA concentration was normalised to 100 µg/ml as described in Chapter 2 – Real-time PCR. All RNA samples had an acceptable purity, demonstrated by a 260/280 ratio of approximately 2.0 (range: 2.043-2.266).

Selection of reference genes

Absolute quantification of the expression of a panel of 10 different reference genes was performed using 8 matched CRC/colon samples in triplicate (see Figure 4-1). Simple

analysis for differences in reference gene expression between CRC and distal colon was performed using the Wilcoxon signed-rank test. This analysis demonstrated significant differences in gene expression between CRC and distal colon for the following genes: G6PD, GAPD, HPRT and PP1A. This suggests that these genes were unstably expressed across the two tissue types and would therefore be unsuitable reference genes. However, other algorithms are available to determine the most stably expressed genes. The absolute quantification data was fed into the geNorm algorithm (184) using the qbase+ software (Biogazelle, Belgium). GeNorm concluded that the 3 most stably expressed genes were IPO8, PP1A and GUS and recommended using two reference genes. The Bestkeeper software (186), concluded that the three most stable reference genes were G6PD, GUS and IPO8. The Normfinder software combines estimations of intragroup and intergroup variation to compute a stability value (185). The reference gene with the highest stability value was IPO8.

The genes GUS and IPO8 were reported as suitable choices for reference genes by more than one algorithm. In support of this combination, I found no significant difference in GUS and IPO8 expression between CRC and matched distal colon tissue (see Figure 4-1). These findings are consistent with published reports using GUS (249) and IPO8 (182) as reference genes in human CRC. It was thus decided that both GUS and IPO8 expression would be used as reference genes, in subsequent relative quantification RT-PCR experiments.

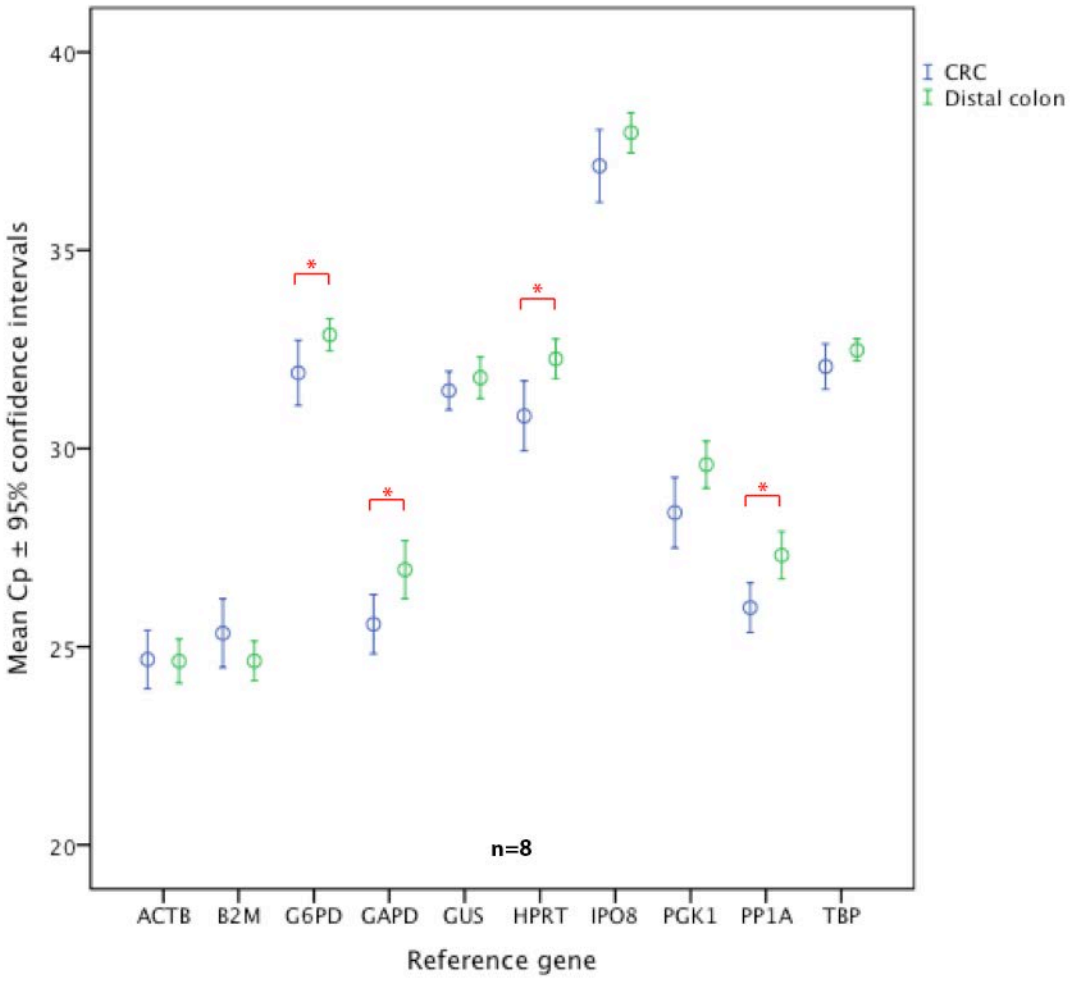

Figure 4-1: Absolute quantification (Cp) of reference genes by 8 matched CRC (blue) and distal colon (green) samples, performed in triplicate. Sample RNA concentration was normalised to 100 µg/ml. Red-capped lines indicate significant differences between matched samples (Wilcoxin-signed rank test).

Relative quantification of chemokine expression

Differences in the gene expression of various chemokines were analysed in duplicate relative to GUS and IPO8, calculated by the 2(-ΔΔCt) method. Initially, the probes and primers used were designed by RealTime Ready software (Roche), as described in Table 2-6. Amplicons were not detected using the primers and probes for the targets of CCL17, CCL22 and CXCL11. The annealing temperature was adjusted from 59˚C to 55˚C,

57˚C and 60˚C to no avail. For CCL17 and CCL22, a different RealTime Ready primer/probe design was selected, again without successful amplicon detection. Finally, a pre-designed primer-probe mix was purchased from Applied Biosystems Inc, USA, resulting in reliable amplicon detection for all 3 targets. The amplification curves appeared later than 50 cycles for the RealTime Ready designed probe and primers for the targets CCL3, CCL4 and CCL5. Again, the annealing temperature was adjusted to 55˚C, 57˚C and 60˚C with no associated improvement in the amplification curve profiles. Pre-designed primer/probe mixes for CCL3, CCL4 and CCL5 from Applied Biosystems resulted in curves below 40 cycles for all 3 targets.

Following testing of all the primer/probe designs, the designs selected for analysing chemokine gene expression assays are described in Table 2-6, for the following gene targets: CCL19, CCL20, CCL21, CXCL9, CXCL10, IPO8, VAP-1 (designed using the RealTime Ready software). Pre-designed primer/probe mix from Applied Biosystems was used for the following targets: CCL3, CCL4, CCL5, CCL17, CCL22, as described in Table 2-7.

The two ligands for the CCR4 chemokine receptor are CCL17 and CCL22. The gene expression of CCL17 and CCL22, relative to GUS and IPO8, for 8 samples of CRC with matched distal colon is shown in Figure 4-2. There was no significant difference in the gene expression of either of these two chemokines between CRC and matched distal colon.

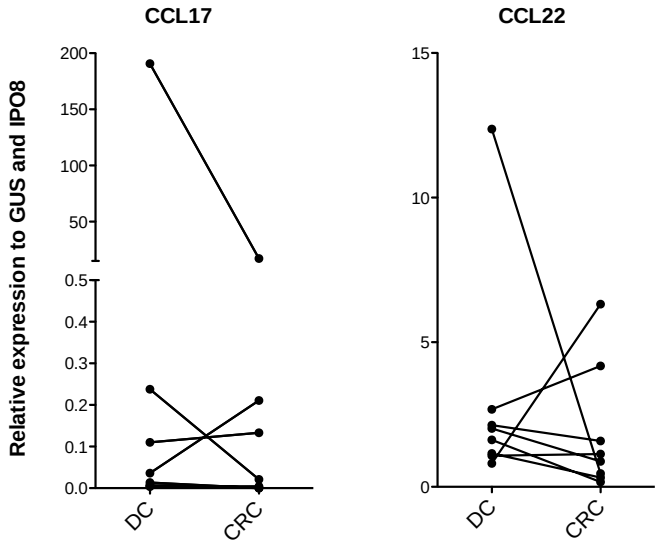

Figure 4-2: CCL17 and CCL22 gene expression relative to GUS and IPO8 for 8 samples of CRC with matched distal colon. Note different y-axis scales for the two graphs.

CCR5 has three main ligands: CCL3, CCL4 and CCL5 (250). The gene expression of these CCR5 ligands relative to GUS and IPO8 for 8 samples of CRC with matched distal colon is shown in Figure 4-3. There was increased gene expression of CCL3 and CCL4 in CRC tissue compared with matched distal colon, differences that reached statistical significance. There was no difference in CCL5 gene expression across tissue types.

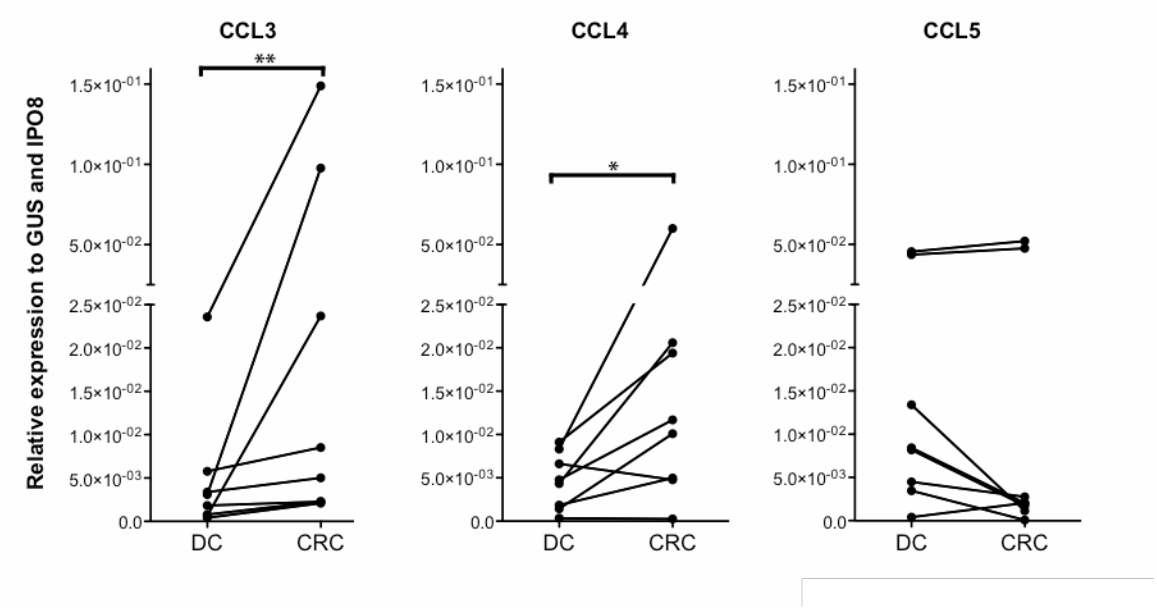

Figure 4-3: Gene expression of the CCR5 ligands (CCL3, CCL4 and CCL5) relative to GUS and IPO8 for 8 samples of CRC with matched distal colon. Note that the y-axis is split but identical for all 3 graphs. Capped lines indicate significant differences in gene expression between tissue types (Wilcoxin signed-rank test).

Significantly fewer CRC-isolated Treg expressed CCR7 compared with Tconv. There was also a trend for reduced CCR7 percentage expression by Treg isolated from CRC compared with Treg isolated from distal colon. For these reasons, the gene expression of the two CCR7 ligands (CCL19 and CCL21) was measured (see Figure 4-4). The trend was for reduced gene expression of the CCR7 ligands by CRC tissue compared with distal colon, but these differences did not reach statistical significance.

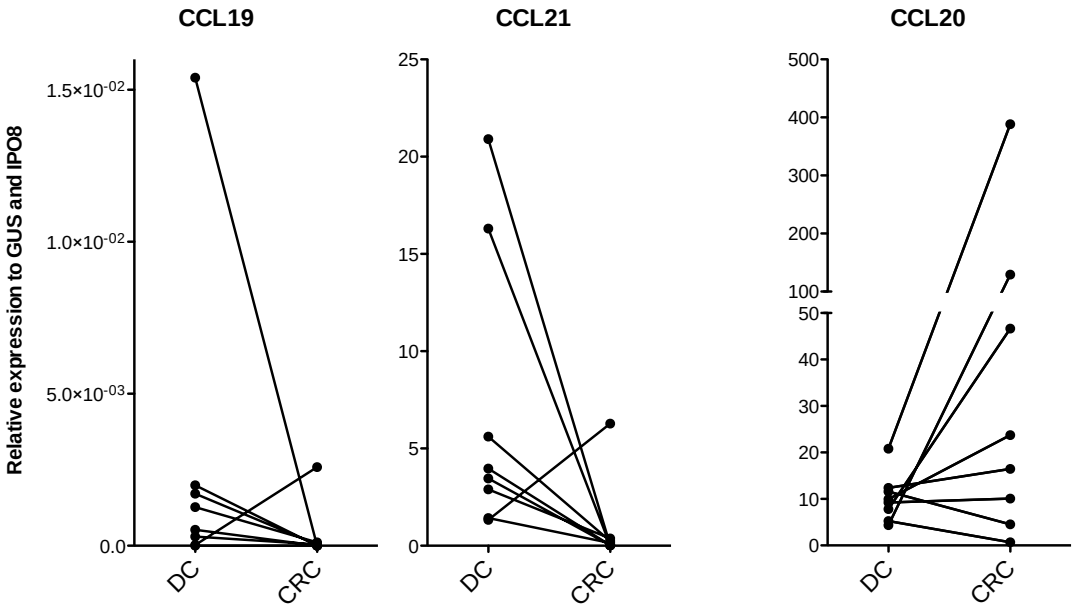

Figure 4-4: Gene expression of the CCR7 ligands (CCL19 and CCL21) and CCR6 ligand (CCL20) relative to GUS and IPO8 for 8 samples of CRC with matched distal colon. Note a different y-axis scale for each graph.

CCL20 is the only known cognate ligand for the CCR6 chemokine receptor (see Figure 4-4). There was no consistent difference in the gene expression of CCL20 across tissue types.

The chemokine receptor CXCR3 has 3 ligands (CXCL9, CXCL10 and CXCL11). There was no significant difference in CXCR3 expression between T cell subsets, nor between Treg isolated from CRC and distal colon. However, it has been reported by others that $CD4^+$ and $CD8^+$ CRC TILs express significantly less CXCR3 than lymphocytes isolated from matched colon tissue (193). For this reason, the gene expression of the CXCR3 ligands

was measured (see Figure 4-5). CXCL11 has also been shown to act as a natural antagonist of CCR5 in vitro (251).

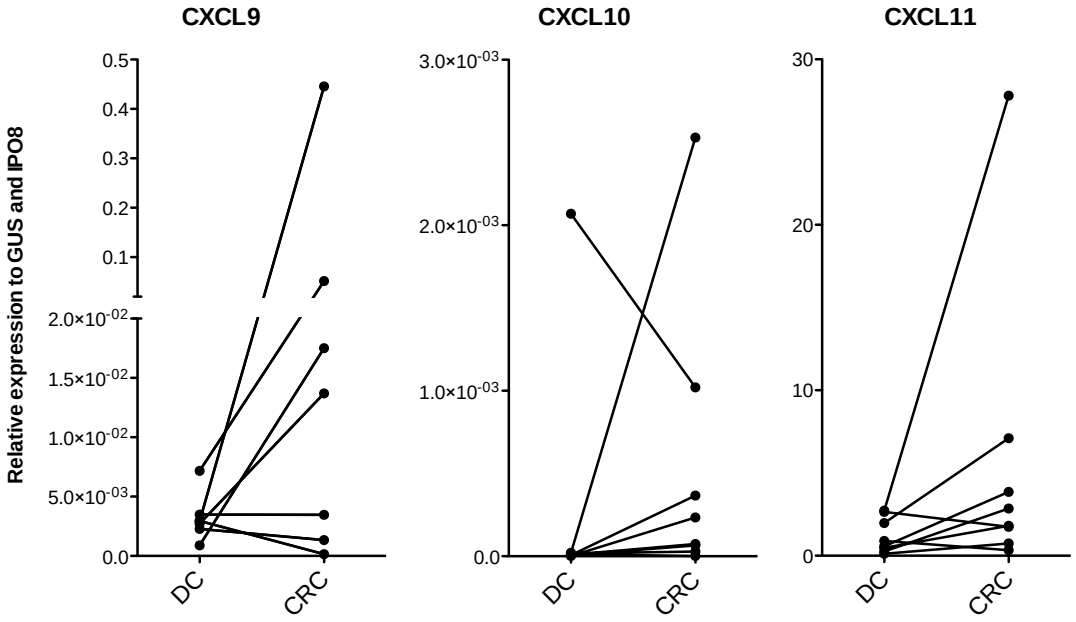

Figure 4-5: Gene expression of the CXCR3 ligands (CXCL9, CXCL10 and CXCL11) relative to GUS and IPO8 for 8 samples of CRC with matched distal colon. Note a different y-axis scale for each graph.

All three ligands were detectable in tumour tissue. In some patients, chemokines were expressed at higher levels in the tumour whereas in others, the levels were similar between involved and uninvolved tissue. Overall there were no consistent differences in the gene expression of CXCL9 between CRC tissue and matched distal colon. CXCL10 gene expression was detectable but present at low levels relative to GUS and IPO8. There was a trend for increased expression of CXCL11 by CRC compared with matched distal colon, but this difference did not reach statistical significance.

Chemokine expression at the protein level

The differences in chemokine expression described above relate to differences at the mRNA level which may not translate directly into differences in chemokine protein levels present in the tissue. Protein lysates were made from samples of CRC and matched distal colon. Total protein concentration of each sample was adjusted to 2 mg/ml. Western blots were performed, probing for CCL3, CCL4, CCL5, CCL20 and GUSB. GUSB was chosen as a control protein that was expected to have stable expression across CRC and distal colon samples, based on the investigation of suitable reference genes for RT-PCR experiments, described above.

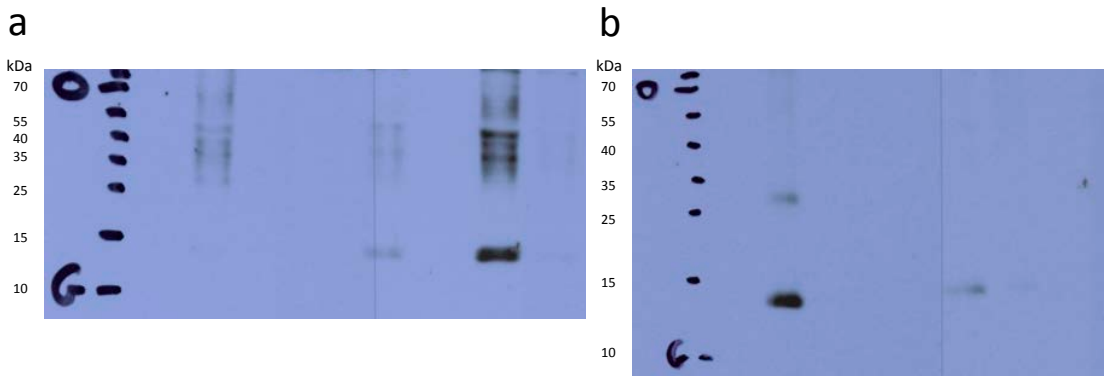

Figure 4-6: Western blots for chemokine in single CRC sample. Molecular weight of chemokine is approximately 12 kDa. (a) Standard sample buffer resulting in multiple bands; (b) Sample buffer containing 8M urea prevented self-association, yielding single band at correct molecular weight.

Two technical problems were encountered performing Western blotting for chemokines. Firstly, chemokines appeared to self-associate (see Figure 4-6), resulting in multiple bands. This meant that bands from chemokine multimers could not be

distinguished from non-specific protein bands. Semi-quantitative measurement of protein concentration was also impossible for chemokines in multimeric forms.

Secondly, for some batches of CRC samples with matched distal colon, no chemokine was detected. A summary of the Western blots performed for batches of samples yielding bands is shown in Figure 4-7. The bands for GUSB were seen at approximately 82 kDa and were of similar density for DC and CRC samples, as expected. CCL3, CCL4, CCL5 and CCL20 proteins are similar weights (9-15 kDa) and the bands were all seen at an appropriate position on the membrane. As can be seen in Figure 4-7, in general, CCL3 and CCL4 bands were denser for CRC samples compared to matched distal colon samples. However, some individual distal colon samples expressed a larger amount of chemokine than some individual CRC samples. Despite only 4 matched samples for CCL5 and CCL20, there was no consistent difference in band densities between CRC and matched distal colon for these two proteins.

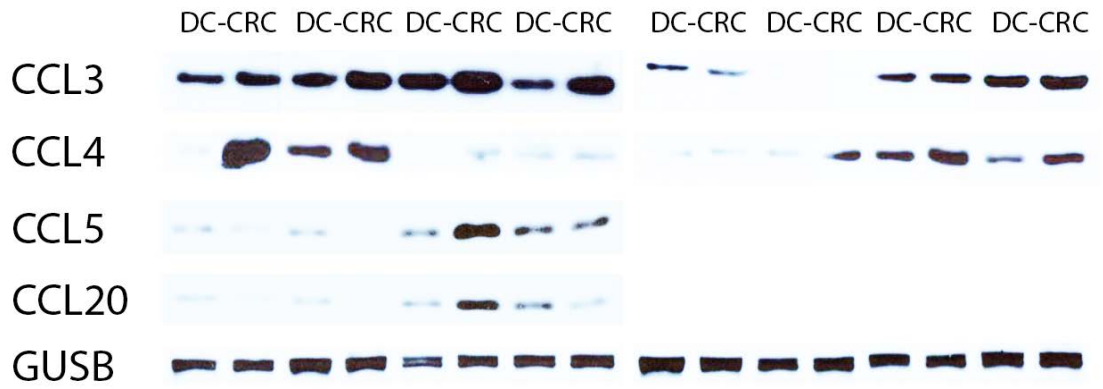

Figure 4-7: Summary of Western blots probing for CCL3, CCL4, CCL5, CCL20 and GUSB. Bands are presented left to right in pairs of matched distal colon and CRC. There were 8 matched samples for CCL3, CCL4 and GUSB, and 4 matched samples for CCL5 and CCL20.

Band densities were quantified using ImageJ, as described in Chapter 2, and differences between CRC and matched distal colon samples were tested for statistical significance using the Wilcoxin-signed rank test (see Figure 4-8). The increased expression of CCL3 and CCL4 by CRC compared with matched distal colon, as measured semi-quantitatively by Western blotting, reached statistical significance. There was no significant difference in the expression of GUSB by tissue type.

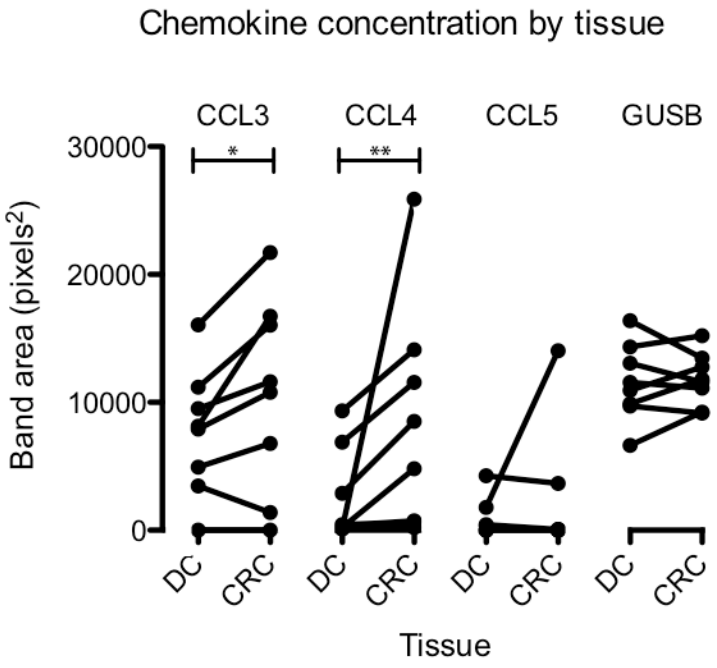

Figure 4-8: Band densities, as measured using ImageJ, representing semi-quantitative chemokine concentration by CRC and matched distal colon tissue. Eight matched samples for CCL3, CCL4 and GUSB. Four matched samples for CCL5. DC=distal colon. Capped lines indicate statistically significant differences (Wilcoxon signed-rank test).

Semi-quantitative measurement of chemokine concentrations by ELISA

Protein lysate concentrations of CCL3, CCL4 and CCL5 were measured using a Mix-N-Match ELISArray Kit (336111, SABiosciences), according to manufacturer's instructions. Standard curves were not derived for each chemokine and absorbance was therefore the read-out in this semi-quantitative assay. Confirming the Western blot findings, CCL3 and CCL4 levels were significantly higher in CRC samples compared with matched distal colon (see Figure 4-9), while there was no significant difference in CCL5 levels.

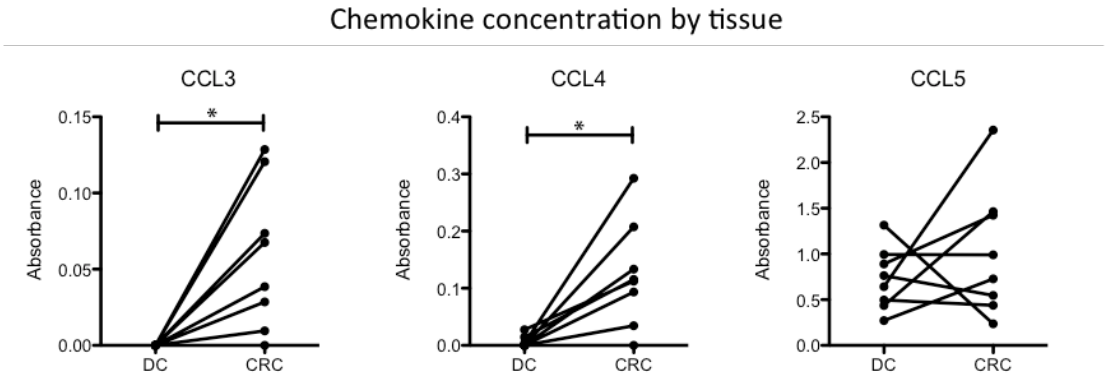

Figure 4-9: Semi-quantitative measurement of chemokine concentrations by tissue type, measured by ELISA. Data for 8 samples of CRC with matched distal colon is shown. Capped lines represent statistically significant differences (Wilcoxin signed-rank test).

Chemokine immunohistochemistry

Having established a significant increase in CCL3 and CCL4 in CRC compared with matched distal colon, at both the mRNA and protein level, the protein expression in tissue sections was localised by immunohistochemistry. Pieces of tissue from collected samples of CRC with matched distal colon had been processed into FFPE blocks or snap frozen and stored at -80˚C, in preparation for sectioning and use in immunohistochemistry experiments.

The methods and antibodies used for immunohistochemical staining are detailed in Chapter 2. Immunostaining for chemokines was first performed using FFPE tissue sections, which was unsuccessful. No significant positive staining was seen for CCL3, CCL4, CCL5 or CCL20. This was surprising as the antibodies had been tested on FFPE human tissue: CCL3 and CCL5 antibodies (AF-270-NA and AF-278-NA) on human tonsil; CCL4 antibody (AF-271-NA) on human brain; CCL20 (AF360) antibody on human skin.

Snap frozen tissue blocks were sectioned and stained with the same antibodies. Chemokine staining was compared to staining with control antibody of matched isotype and concentration. See Figure 4-10 (IMC), Figure 4-11 (CCL3), Figure 4-12 (CCL4), Figure 4-13 (CCL5) and Figure 4-14 (CCL20).

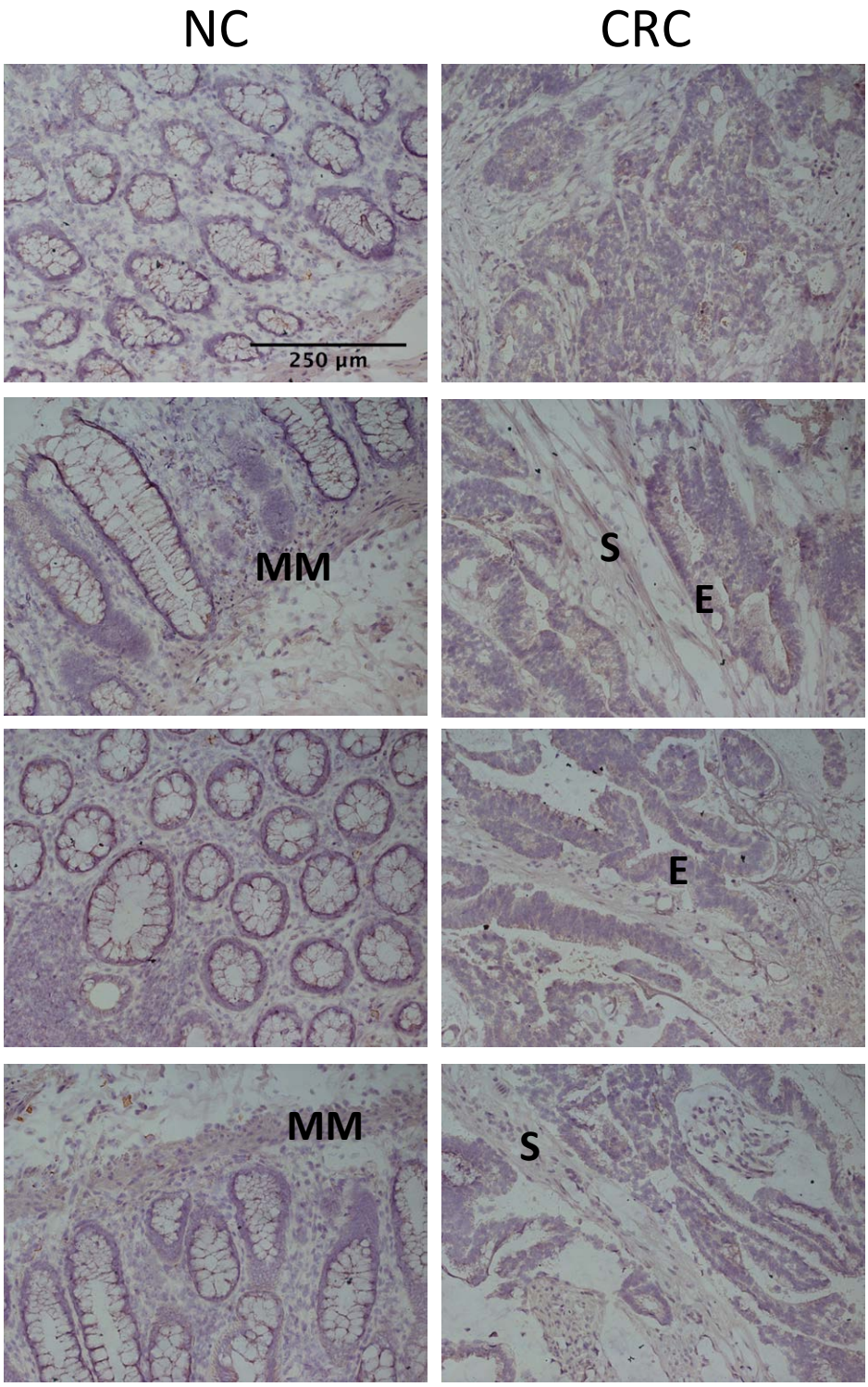

Figure 4-10: Immunohistochemistry of 4 sections of CRC (right) with matched distal colon (left) for IMC antibody at same concentration as target antibodies. Magnification x200. Background staining is seen in the stroma, epithelium and muscularis mucosae. S=stromal staining; E=epithelial cytoplasmic staining; MM=muscularis muscosae staining.

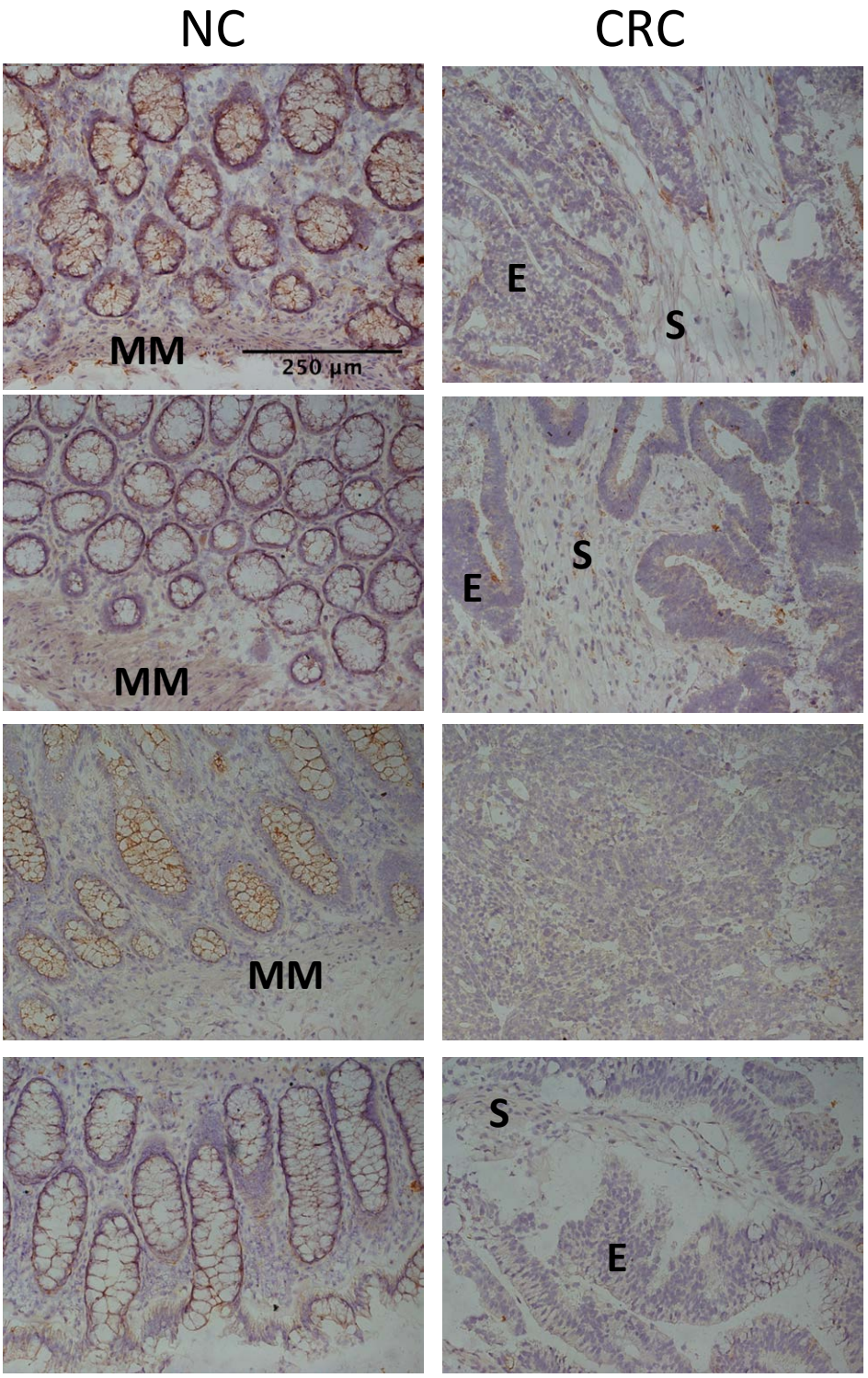

Figure 4-11: Immunohistochemistry of sections of CRC (right) with matched distal colon (left) for CCL3. Staining of 4 unique CRC samples with matched distal colon was performed. Magnification x200. S=stromal staining; E=epithelial cytoplasmic staining; MM=muscularis muscosae staining.

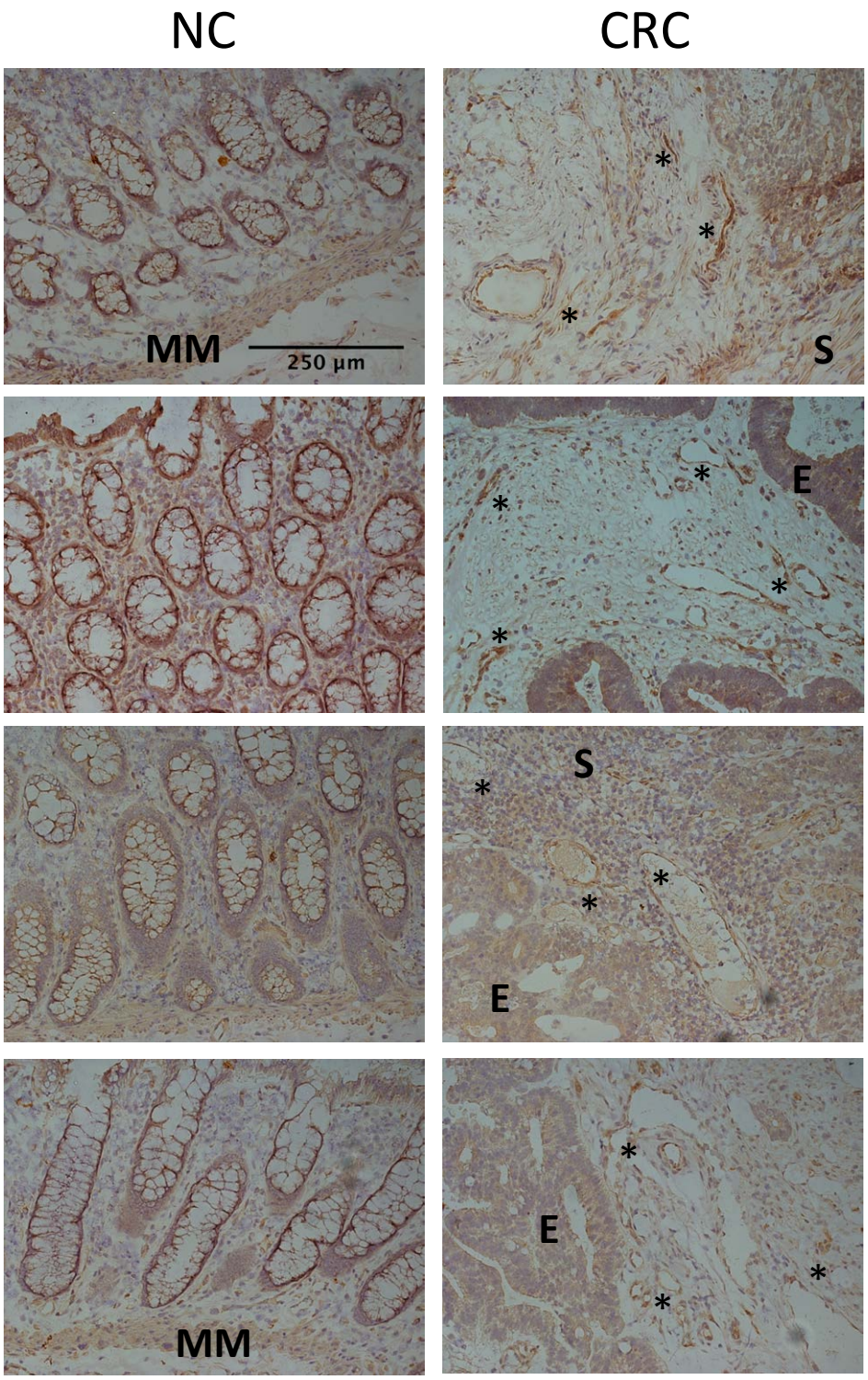

Figure 4-12: Immunohistochemistry of sections of CRC (right) with matched distal colon (left) for CCL4. Staining of 4 unique CRC samples with matched distal colon was performed. Magnification x200. S=stromal staining; E=epithelial cytoplasmic staining; MM=muscularis muscosae staining; Asterisks '*' CCL4 staining, localised to the endothelium.

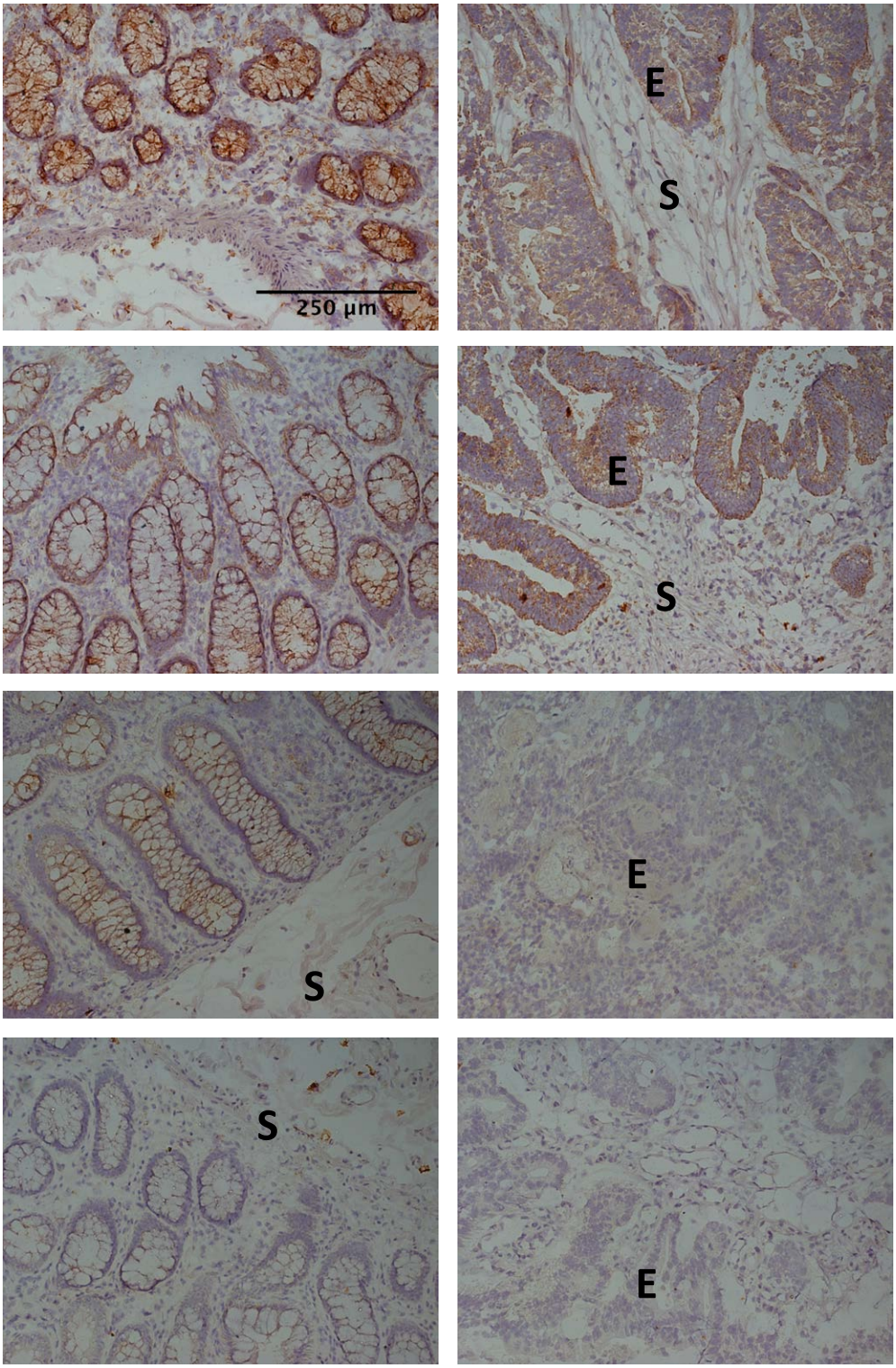

Figure 4-13: Immunohistochemistry of sections of CRC (right) with matched distal colon (left) for CCL5. Staining of 4 unique CRC samples with matched distal colon was performed. S=stromal staining; E=epithelial cytoplasmic staining.

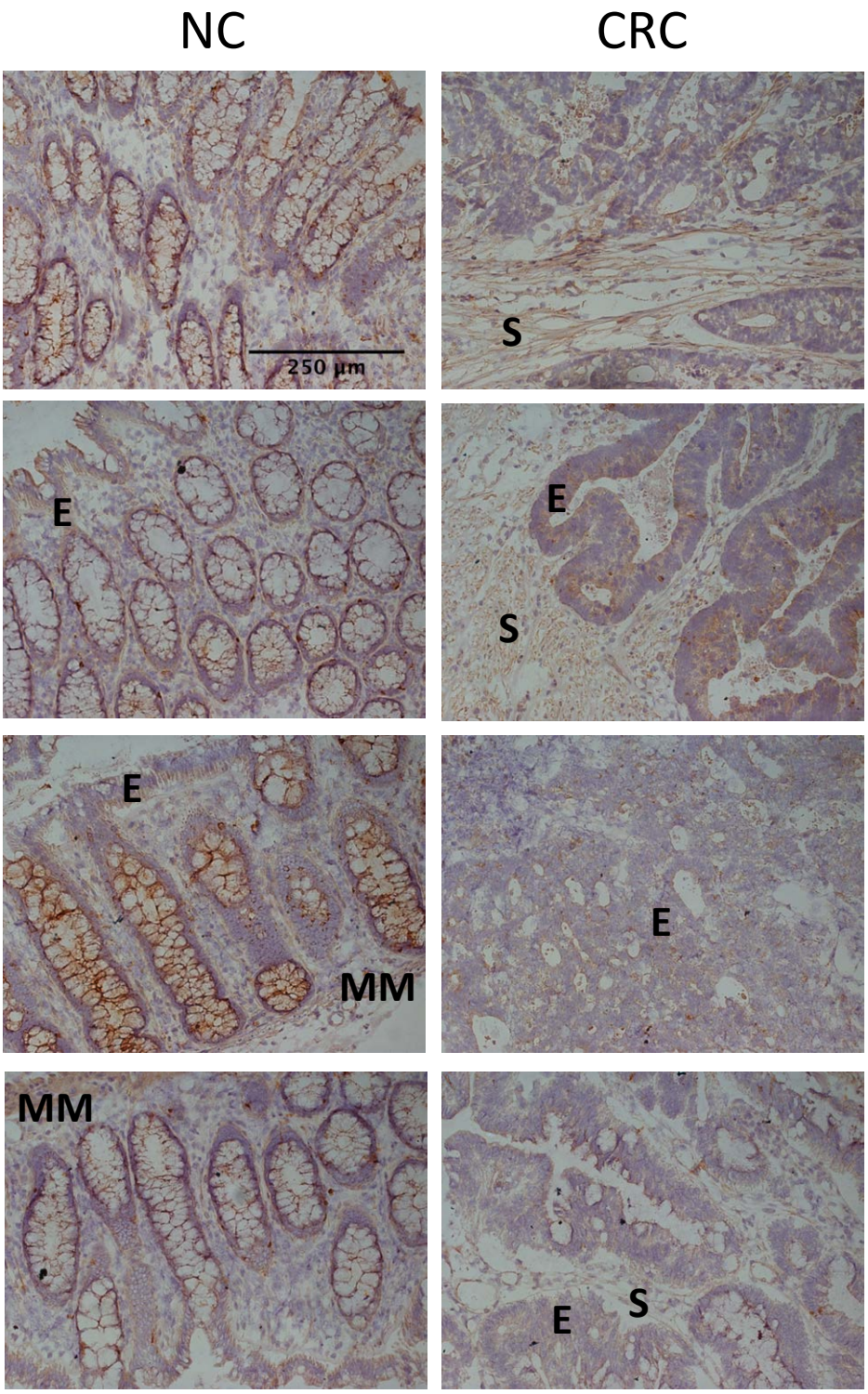

Figure 4-14: Immunohistochemistry of sections of CRC (right) with matched distal colon (left) for CCL20. Staining of 4 unique CRC samples with matched distal colon was performed.. S=stromal staining; E=epithelial cytoplasmic staining; MM=muscularis mucosae staining.

The stained sections were all reviewed by a senior pathologist with an interest in gastrointestinal pathology. The control sections demonstrated some background staining: marked background was related to mucous within the intestinal crypts but non-specific background staining was also present within the epithelial cell cytoplasm and in the stroma (see Figure 4-10). Generally, all 4 chemokines were detected within the epithelial cytoplasm of CRC tissue and absent from the epithelium of matched distal colon. However, given the background epithelial cytoplasmic staining observed with isotype-matched antibody, it was difficult to conclude that any epithelial cytoplasmic chemokine staining was specific.

One interesting finding from these immunohistochemistry experiments was that of positive staining for CCL4, localised to the endothelium in the stroma of CRC sections (see Figure 4-12). Such CCL4 staining was not observed in sections of distal colon. Further images demonstrating CCL4 staining of CRC endothelium at increased magnification are shown in Figure 4-15.

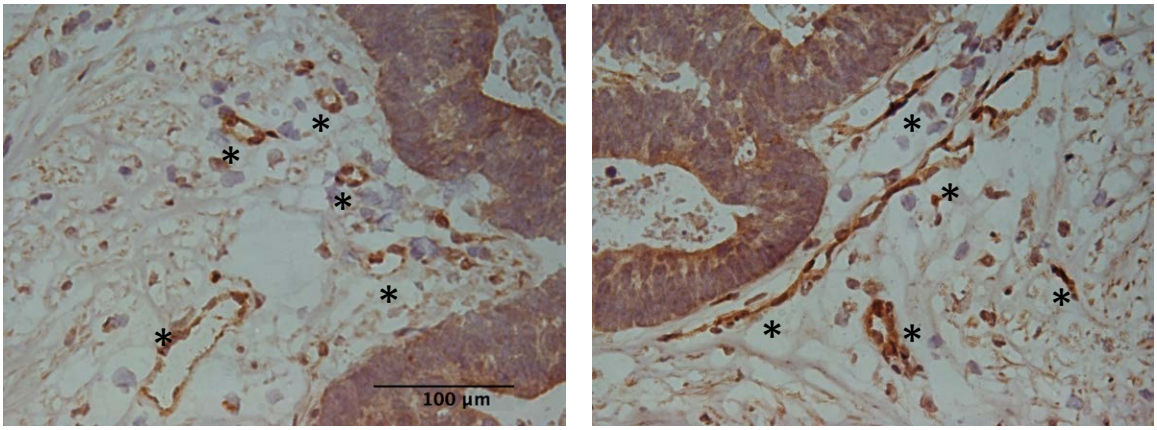

Figure 4-15: Immunohistochemistry of a single CRC section for CCL4, representative of 4 unique samples. Magnification x400. Asterisks '*' indicate areas of positive staining for CCL4, localised to the endothelium.

The endothelium has the ability to capture and present chemokines (252). Therefore, positive endothelial staining for CCL4 may represent capture of CCL4 produced not only by the endothelium but also by other cell types within the tumour tissue.

The CCR5 chemokine CCL4 can be captured by cultured endothelial cells

To determine whether tumour endothelium could indeed capture and present chemokines, endothelial cells were isolated from samples of CRC (CEC) and matched distal colon (NEC) and cultured. Passage 4 cells were seeded onto microslides and recombinant chemokine was added and washed off as described in Chapter 2: Chemokine capture and immunocytochemistry. Immunocytochemistry was then performed to detect recombinant chemokine that had been captured by the endothelium.

Positive CD31 staining was evident for both NEC and TEC while isotype-matched control antibody at the same concentration as the target antibodies resulted in no staining (see Figure 4-16). There was no constitutive positive staining observed for CCL4 without the prior addition of recombinant chemokine. However, following incubation with recombinant CCL4, positive staining for this chemokine was observed on both NEC and TEC monolayers. Thus, it appears that CCL4 can be captured by endothelial cells isolated from the colon and CRC.

The absence of positive staining for CCL3 and CCL5 by NEC and TEC may have been a result of problems with the experimental set-up, the chosen antibody specificity and concentration or the recombinant chemokines. The experiment was therefore repeated using cultured human umbilical vein endothelial cells (HUVEC), isolated from fresh human umbilical vein using CD31 magnetic beads. Immunocytochemistry for CCL3, CCL4 and CCL5 with and without prior incubation with recombinant chemokine was analysed (see Figure 4-17). The antibody concentration and staining procedures were identical for all experiments. Use of HUVEC resulted in a different chemokine capture profile to that of NEC and TEC. HUVEC expressed constitutive CCL3 and CCL4, but not CCL5, whereas NEC and TEC did not express any of the CCR5 chemokines (CCL3, CCL4, CCL5) constitutively. Following incubation with recombinant chemokines, no increase in CCL3 or CCL4 expression by HUVEC was detected, but there was marked capture of CCL5 by HUVEC, an effect that was not observed for NEC or TEC.

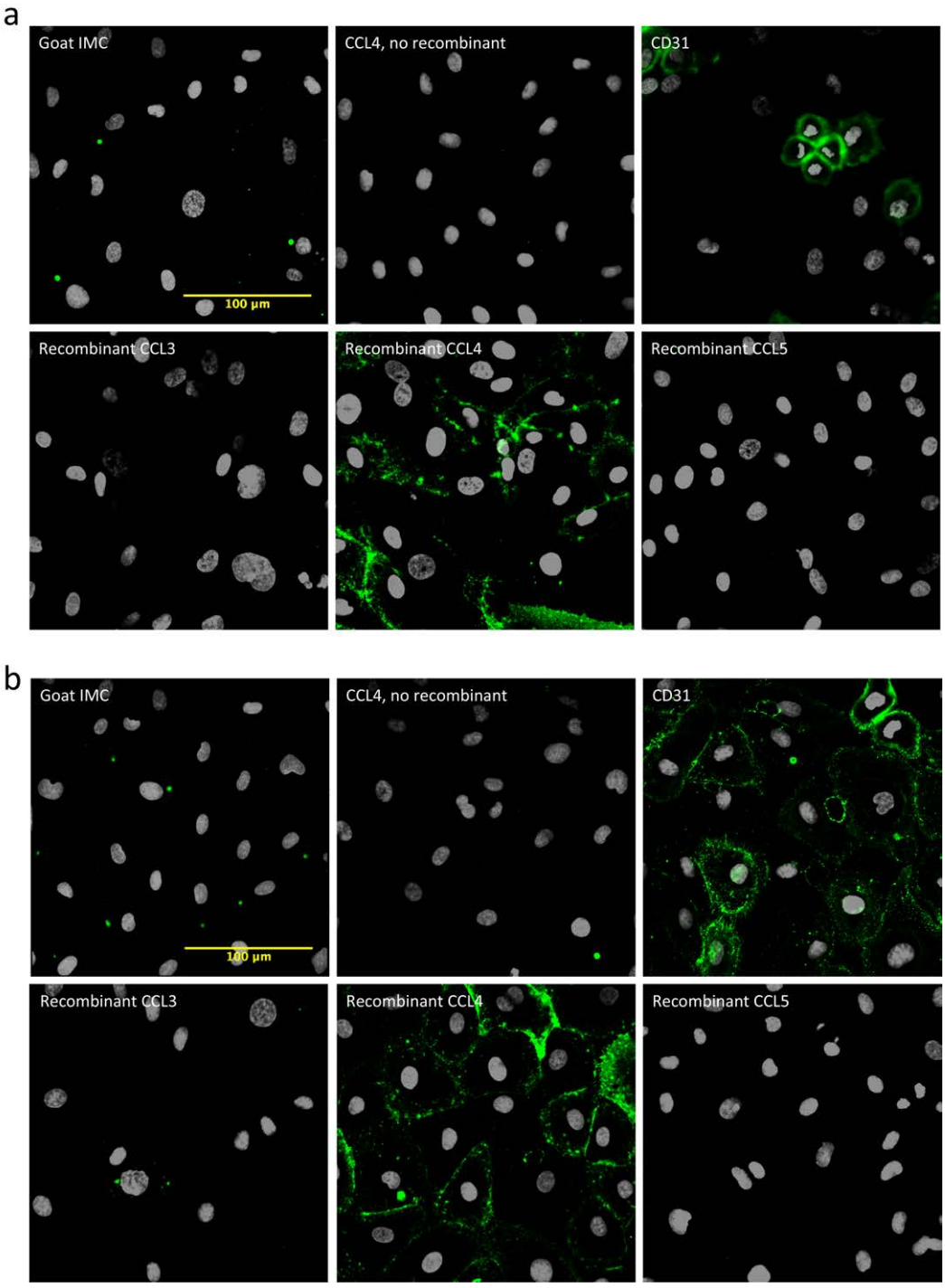

Figure 4-16: Immunocytochemistry of (a) NEC and (b) TEC for CCL3, CCL4 and CCL5 with and without prior incubation of recombinant chemokines. Top-left=IMC; Top-middle=immunocytochemistry for CCL4 without prior incubation with recombinant chemokine; Top right=CD31 (positive) control; Bottom-left=CCL3 immunocytochemistry post incubation with recombinant CCL3; Bottom-middle=CCL4 immunocytochemistry post incubation with recombinant CCL4; Bottom-right=CCL5 immunocytochemistry post incubation with recombinant CCL5. Images from a single experiment are shown.

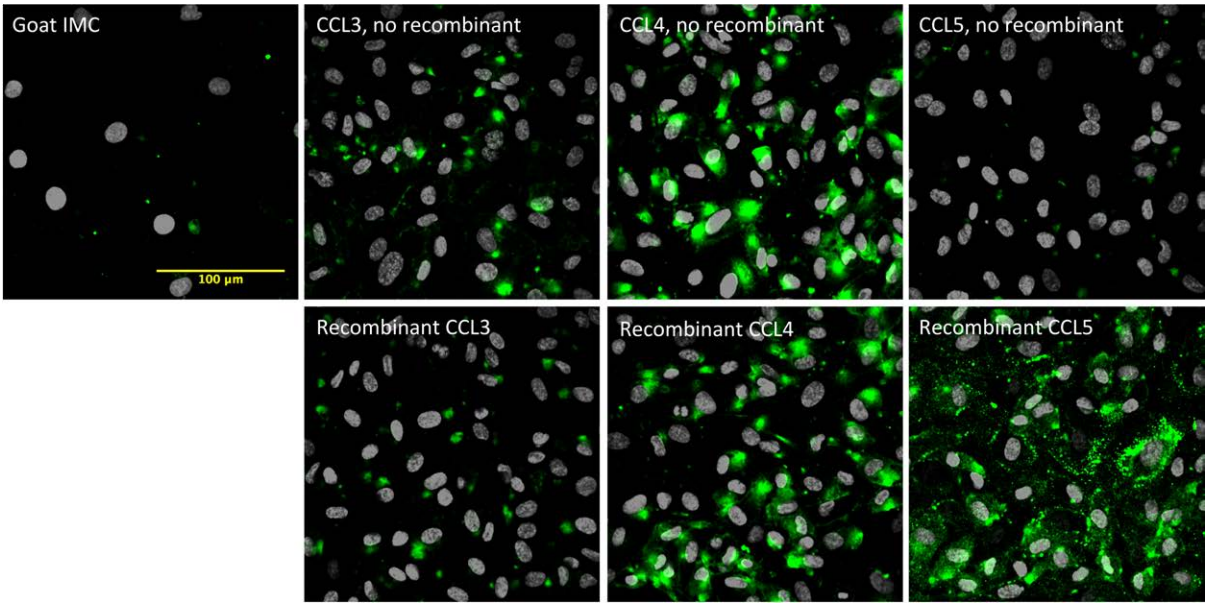

Figure 4-17: Immunocytochemistry of HUVEC for CCL3, CCL4 and CCL5 with (bottom row), and without (top row), prior incubation with recombinant chemokines. Images from a single experiment are shown.

In light of the above chemokine capture experiments, the positive CCL4 staining of the endothelium in CRC sections may indeed represent capture of CCL4 released by cells within the tumour.

Cellular source of CCR5 chemokines

The analytical method of choice for the detection of chemokines in defined cell subsets is flow cytometry. Published methodology evaluating chemokine expression by flow cytometry has distinguished *constitutive* expression (directly detectable) from *spontaneous* expression (detectable after culture with the protein transport inhibitor, brefeldin A) (253).

CRC and matched distal colon tissue were digested enzymatically as described in Chapter 2: Selective use of enzymatic digestion. Half of each sample was placed on ice while the other half was incubated with BD Golgiplug™, 1 µl per ml of cell suspension for 4 hours at 37˚C. BD Golgiplug™ contains brefeldin A. 1 µl per ml near infra-red live/dead fixable stain was then added to the cell suspension together with 20 µl/ml of human FcR blocking reagent and samples were incubated in the dark at 4°C for 20 minutes. Brefeldin-treated and untreated samples were then divided into equal volumes and placed in separate FACS tubes. The cell suspensions were incubated for 30 minutes at 4˚C with cell-surface directed conjugated antibodies to lymphoid and myeloid markers (CD3-PE, CD4-FITC, CD11b-PECy7), endothelial and fibroblast markers (CD31-FITC, CD90-PE) or an epithelial cell marker (EpCAM-PE). Samples were then washed, pelleted, fixed and permeabilised using the Foxp3 staining buffer kit, as described in Chapter 2. Intra-cellular staining was done by incubating the samples with 10 µl of conjugated antibody to CCL3, CCL4, CCL5 or isotype-matched control antibody for 30 minutes at 4˚C (see Table 4-1), followed by washing, pelleting and resuspending the samples in 500µl cPBS, ready for flow cytometric analysis.

Table 4-1: Conjugated antibodies used for intra-cellular chemokine staining.

Antigen	Clone	Fluorochrome	Isotype	Manufacturer	Code
CCL3	93342	APC	Ms IgG2b	R&D Systems	IC2701A
CCL4	24006	APC	Ms IgG2b	R&D Systems	IC271A
CCL5	21445	APC	Ms IgG1	R&D Systems	IC278A
Isotype control		APC	Ms IgG1	R&D Systems	IC002A
Isotype control		APC	Ms IgG2b	R&D Systems	IC0041A

The constitutive and spontaneous expression of chemokines by live lymphocytes ($CD3^+$), myeloid cells ($CD11b^+$), endothelial cells ($CD31^+$), fibroblasts ($CD90^+$) and epithelial cells ($EpCAM^+$) were evaluated by comparing chemokine antibody-labelled samples with those labelled with isotype-matched control antibody. Dot-plots were constructed with the cell subset marker (CD4, CD11b, CD31, CD90, EpCAM) on the y-axis and the chemokine on the x-axis (253). Data from one experiment is shown in Figure 4-18. All dot-plots were gated on live cells based on non-labelling with the live-dead marker and within a forward scatter-side scatter region appropriate to the cell type. The $CD4^+$ dot plot was also gated on $CD3^+$ cells. Positive expression of the chemokine of interest was defined by setting the negative region to include 97.5% of the IMC staining population.

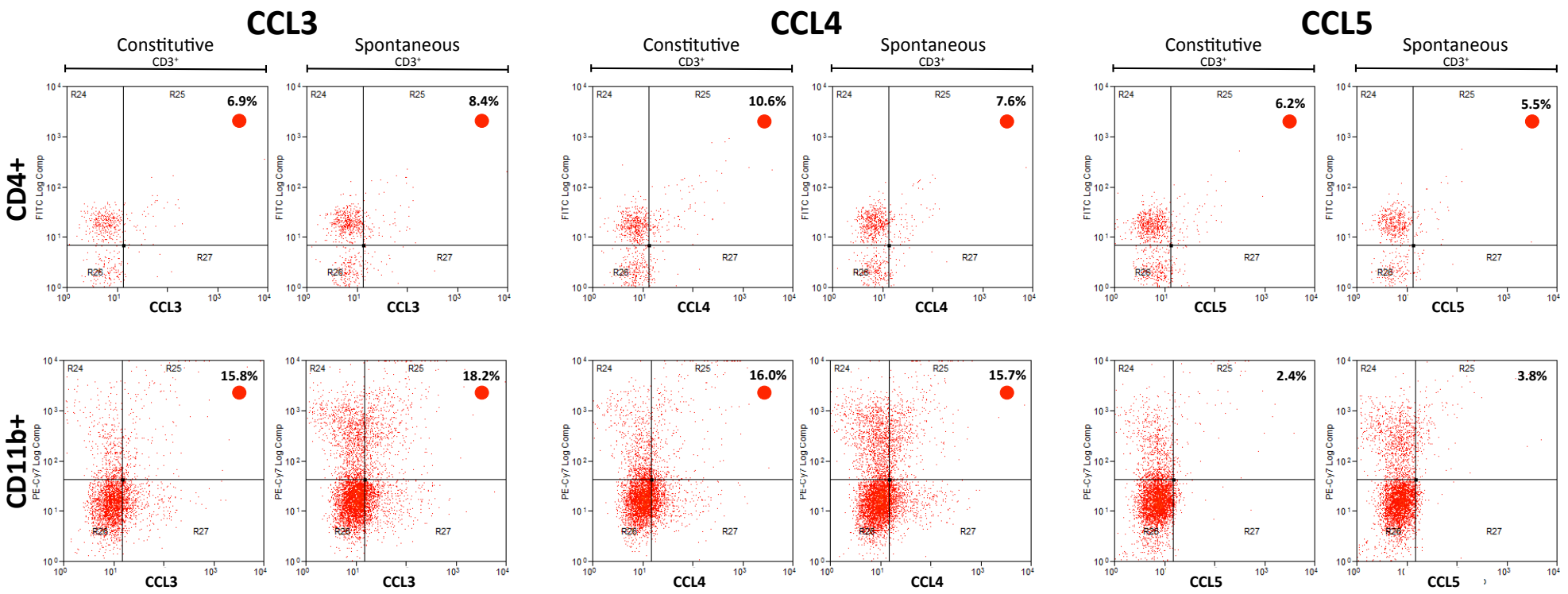

Figure 4-18: Cells isolated from CRC tissue were analysed for constitutive chemokine expression and after 4-hour culture with BD Golgiplug™ (spontaneous expression). Flow cytometry data from a single sample are shown, representative of experiments with 3 separate samples. All dot plots were gated on live cells based on non-labelling by a live-dead marker and on a forward scatter-side scatter region appropriate to the cell type. $CD4^+$ dot plots were also gated on $CD3^+$ cells. Red circles represent positive chemokine staining by the cell type of interest. Percentages represent percentage expression by given cell population. $CD4^+$ and $CD11b^+$ cells shown above, $CD31^+$, $CD90^+$ and $EpCAM^+$ cells shown on following page.

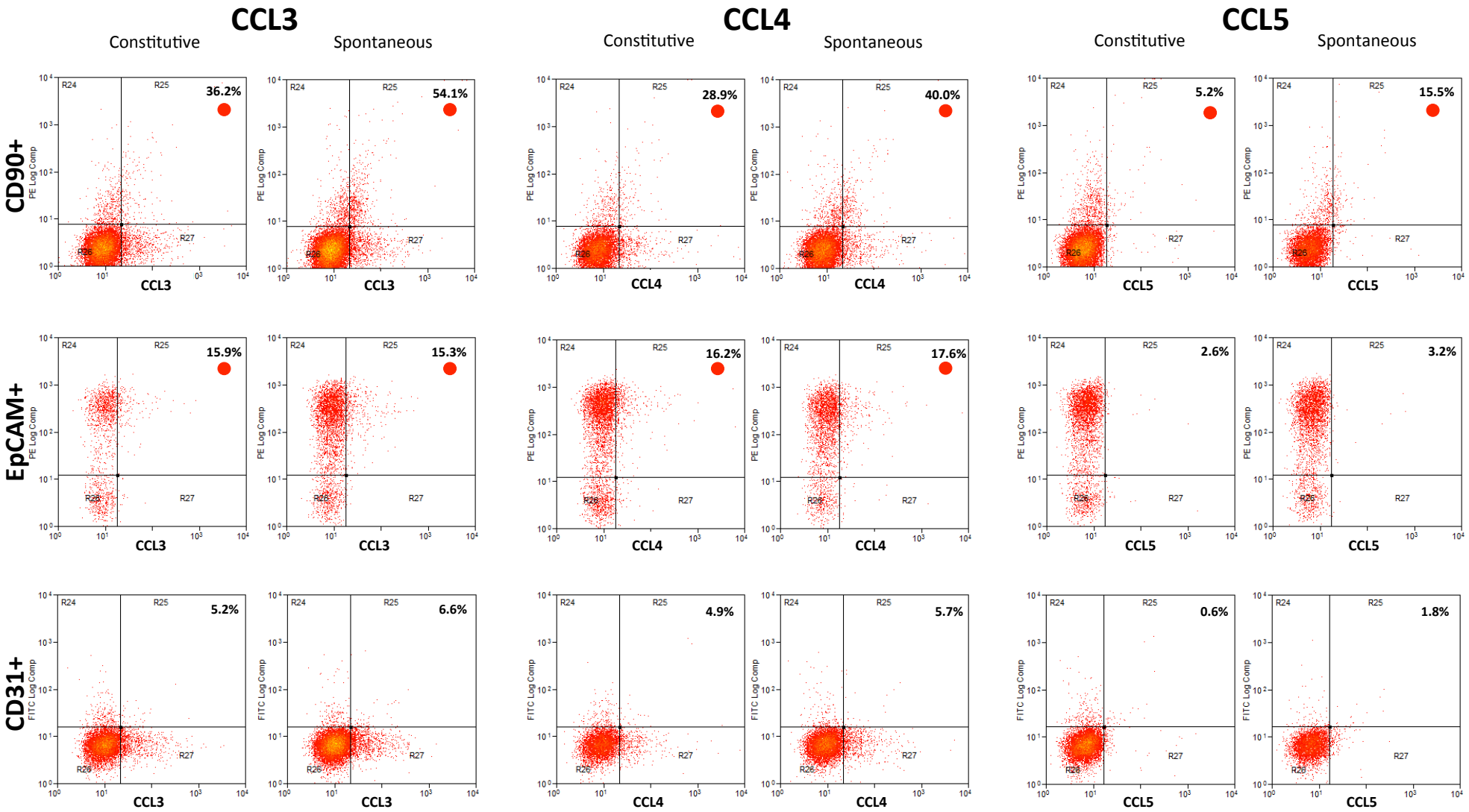
CCL3
Constitutive
Spontaneous
CCL4
Constitutive
Spontaneous
CCL5
Constitutive
Spontaneous
CD90+
EpCAM+
CD31+
36.2%
54.1%
28.9%
40.0%
5.2%
15.5%
15.9%
15.3%
16.2%
17.6%
2.6%
3.2%
5.2%
6.6%
4.9%
5.7%
0.6%
1.8%
R24
R25
R26
R27
PE Log Comp
FITC Log Comp

Surprisingly little constitutive or spontaneous chemokine expression was observed for any cell type and treatment with BD Golgiplug™ made only a small difference to chemokine expression. A summary of 3 identical experiments using different CRC tissue samples is shown in Figure 4-19). There was a small amount of CCL3, CCL4 and CCL5 expression by all cell types. The most notable chemokine expression was that of CCL3 and CCL4 by fibroblasts. Very little chemokine expression was observed with $CD31^+$ endothelial cells, although this may relate to a small sample yield of CD31-labelled cells, as can be seen in Figure 4-18.

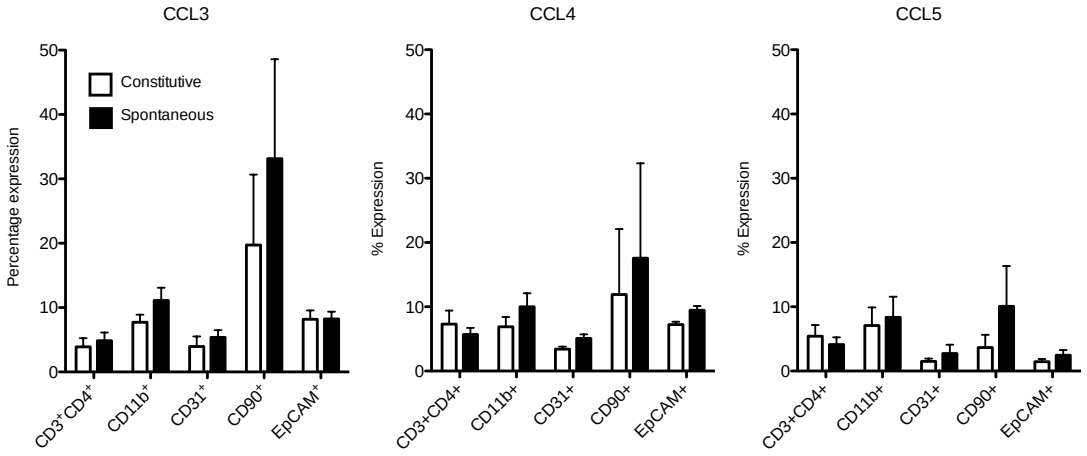

Figure 4-19: Summary of intracellular chemokine flow cytometry experiments from 3 unique samples. Median percentage expression of chemokine is shown for different cell types treated with (spontaneous), or without (constitutive), BD Golgiplug™. Error bars represent the IQR about the median. Note that positive expression of the chemokine of interest was defined by setting the negative region to include 97.5% of the IMC staining population.

Correlation between chemokine receptor and ligand expression

The expression of the CCR5 ligands (CCL3, CCL4 and CCL5) by CRC, measured by gene expression relative to GUS and IPO8, was compared to the expression of CCR5, measured on CRC-isolated Treg by flow cytometry. Data for both tissue ligand expression and Treg receptor expression were available for 12 samples (see Figure 4-20). A linear relationship between CCL3 and CCL4 tissue expression with Treg CCR5 percentage expression was observed. For each scatter plot, Pearson's correlation co-efficient (r^2) and P-values calculated from Pearson's product-moment correlation are quoted. There was no such correlation between CCR5 percentage expression by CRC-isolated Tconv and CRC ligand expression. The expression of the CCR5 ligands was then compared to the CRC Treg proportion, measured by flow cytometry (see Figure 4-21).

There was no correlation between the expression of the CCR5 chemokines by CRC tissue and the tumour Treg proportion. However, there was a significant correlation between CRC expression of the Treg transcription factor, foxp3, and tissue expression of CCL4. This correlation did not extend to the other chemokines, CCL3 and CCL5.

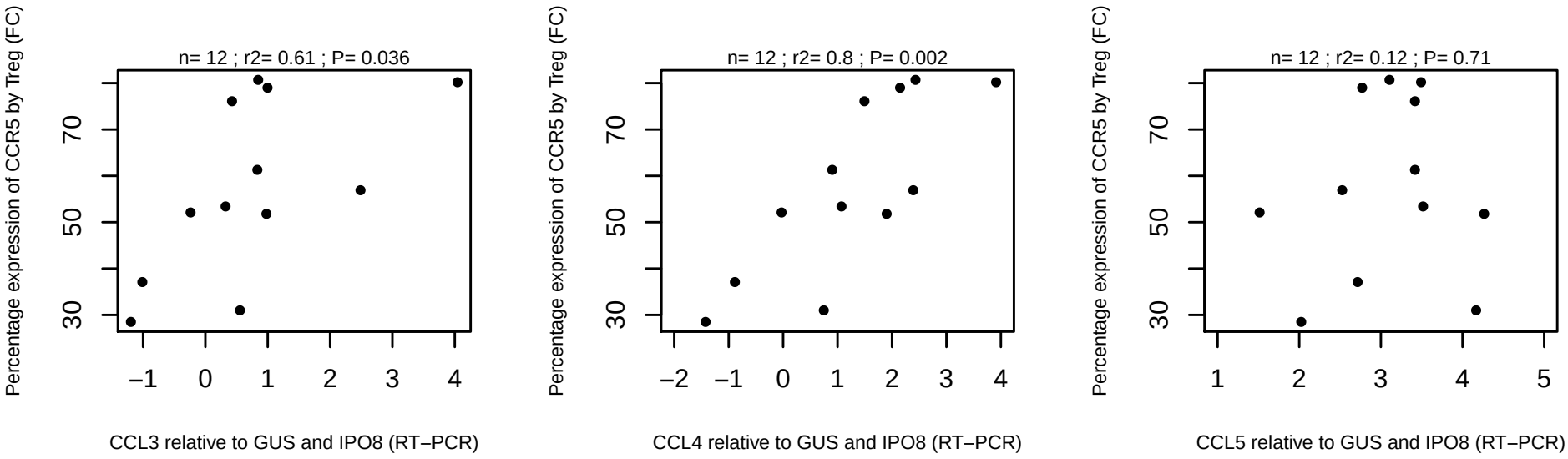

Figure 4-20: Scatter plots depicting percentage expression of CCR5 by CRC-isolated Treg against CRC tissue expression of chemokine ligands, measured by RT-PCR. FC=flow cytometry. r^2=Pearson's correlation co-efficient. P-values calculated from Pearson's product-moment correlation. Data from 12 separate samples are shown.

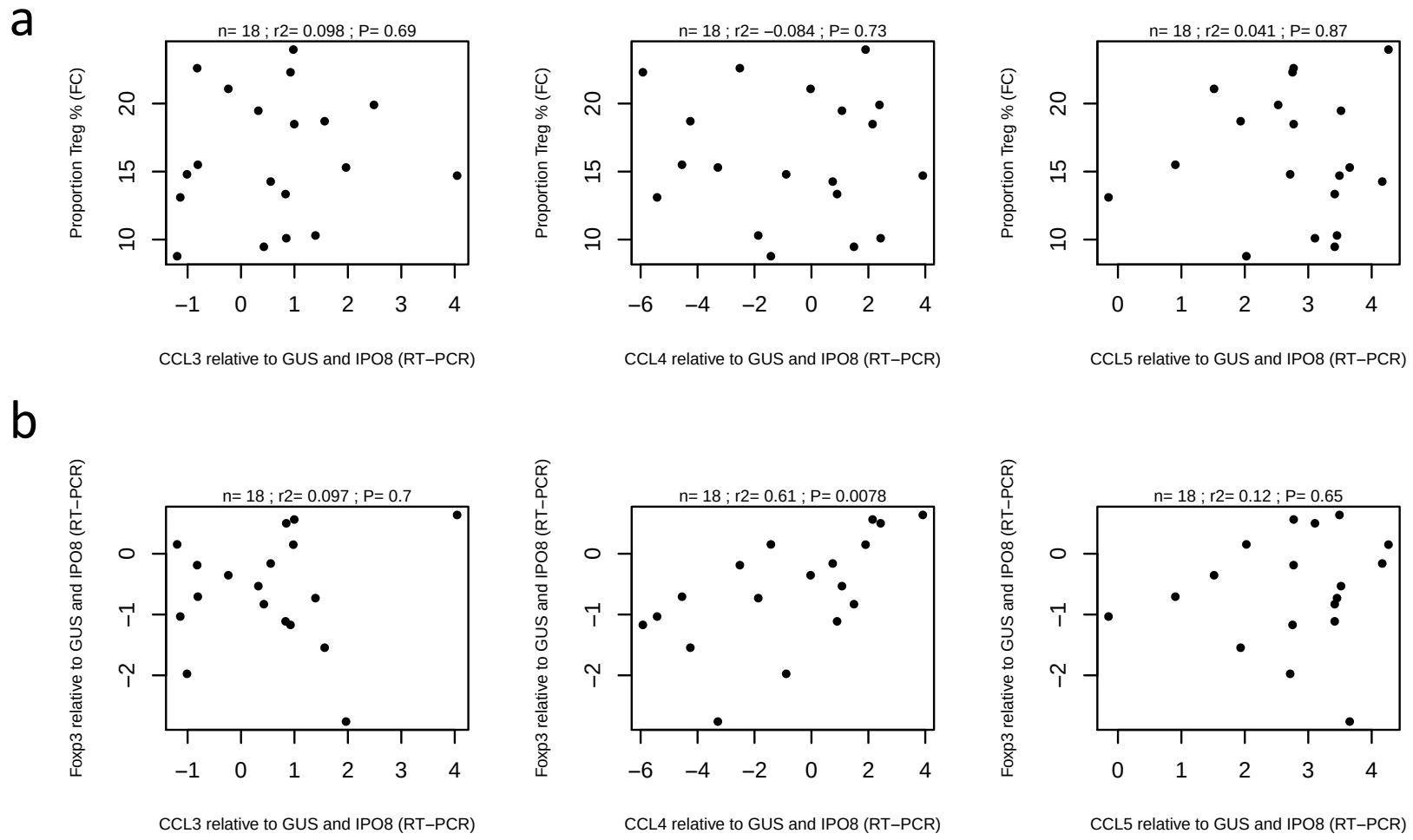

Figure 4-21: Scatter plots depicting (a) the proportion of CRC-infiltrating $CD4^+$ cells with a Treg phenotype (Treg proportion), measured by flow cytometry, and (b) CRC tissue expression of foxp3, measured by RT-PCR, against CRC tissue expression of chemokine ligands, measured by RT-PCR. FC=flow cytometry. r^2=Pearson's correlation co-efficient. P-values calculated from Pearson's product-moment correlation. Data from 18 separate samples are shown.

Discussion

The expression of different chemokines, notably the ligands for important chemokine receptors identified in Chapter 3 is reported in this chapter. Real-time PCR was performed using sample RNA of a standard concentration and measured quality, intron-spanning primers and reference genes of proven stable expression across CRC and colon tissues. CRC-isolated Treg express significantly more CCR4, CCR5 and to a lesser extent, CCR6 than Tconv. However, the ligands for CCR4 (CCL17 and CCL22) were not significantly overexpressed by CRC compared with distal colon at the mRNA level. An evaluation of CCR5 ligand gene expression demonstrated that CCL3 and CCL4, but not CCL5 were significantly overexpressed by CRC compared with distal colon. CCL3 and CCL4, but not CCL5 levels, as measured by RT-PCR, also correlated with CCR5 expression by CRC-isolated Treg and, for CCL4, also with CRC tissue expression of foxp3. The increased gene expression observed for CCL3 and CCL4 by CRC compared with distal colon was reflected at the protein level, as measured semi-quantitatively by Western blotting and ELISA. Immunohistochemistry demonstrated that endothelial cells in CRC stroma stained positively for CCL4, but not for CCL3 or CCL5.

It has long been known that cancers can secrete chemokines and this led to the hypothesis that tumours are directly responsible for the recruitment of different cell types from the blood, creating a tumour environment suitable for tumour growth and progression (254). CRC expression of specific chemokines, in conjunction with high levels of expression of the cognate receptor by specific immune cell subsets such as Treg, is evidence for a chemokine-driven recruitment pathway leading to the enrichment of Treg in the tumour.

CCR4 chemokines

In ovarian carcinoma, it was shown that CCR4-expressing Treg migrated to the tumour in response to the cognate chemokine CCL22, produced by tumour cells and macrophages (57). The presence of the CCR4 chemokine, CCL22, has been demonstrated in human colon by immunohistochemistry (255). The same study showed that the human colon adenocarcinoma cell line HT-29 expresses CCL22 at the mRNA level and that both CCL22 mRNA and protein was upregulated by stimulation with TNF-α or IL-1α. CCL22 gene expression by CRC tissue was demonstrated by PCR in 5 samples of CRC (102). The expression was weak compared to that of other measured chemokines and CCL22 gene expression was not increased in CRC compared with colon. There was also no demonstrable mRNA expression of CCL17. The findings presented in this chapter show detectable CCL17 and CCL22 mRNA in both CRC and unaffected colon with no significant difference between CRC and matched distal colon. Further analysis of the expression of CCR4 ligands in CRC was thus not performed. However, one previous study reported increased CCL22 protein expression by CRC compared with colon in 78 matched samples (256). Immunohistochemistry was said to detect both CCL17 and CCL22 within the epithelial compartment of the tumour.

Given these conflicting data with regard to CCL17 and CCL22 expression by CRC compared with matched colon tissue, a role for the CCR4 axis in the recruitment of Treg into CRC cannot be ruled out. CCL17 and CCL22 expression by $CD14^+$ myeloid cells has been reported in oesophageal (257) and gastric (258) cancers. Interestingly, in both studies, there was a significant correlation between the frequency of $CCL17^+$ or $CCL22^+$ $CD14^+$ cells and the frequency of Treg amongst TILs, suggesting that expression of the

CCR4 ligands led to migration of Treg into the tumour. However, there is also evidence that tumoral expression of CCL17 results in tumour regression associated with the infiltration of $CD8^+$ cells. Adenoviral vectors encoding CCL17 were injected into established subcutaneous murine CRC (100) and resulted in delayed tumour growth compared to control and led to tumour rejection in 3 out of 7 mice. These anti-tumour effects, were dependent on $CD8^+$ cells and injection of the CCL17-vector led to CD8+ cell recruitment into the tumour parenchyma. Tumour infiltration of Treg was not measured. However, the CCL17-vector anti-tumour effects were not abrogated by depletion of $CD4^+$ cells, suggesting that interruption of tumour Treg recruitment did not play a significant role in the observed anti-tumour effects.

CCR5 chemokines

Elevated levels of CCL3, CCL4 and CCL5 have been reported in a variety of different solid cancers and by a variety of different methods (see Table 4-2). The data presented in this chapter are consistent with this published literature, in that CCL3 and CCL4 were found to be elevated in CRC compared to matched distal colon at both the mRNA and protein level. CCL5 was not found to be consistently elevated in CRC compared to colon and this is supported by two studies measuring CCL5 levels by ELISA (259,260). The immunohistochemistry presented in this chapter shows positive staining for all 3 chemokines within the epithelial component of CRC as well as positive CRC endothelial staining for CCL4. Others have found increased staining for these chemokines in tumour compared to normal tissue for other cancers (see Table 4-2). With regard CCL4, the Human Protein Atlas has systematically profiled the expression of this chemokine in human tissues, including healthy colon and CRC (261). It should however be noted that

the reliability of the staining was defined as *uncertain* as only one antibody was used to create the profile. The majority of CRC samples in the atlas stained positively for CCL4 with membranous and cytoplasmic staining of the tumour epithelium. Weaker staining in the stroma was also noted, although specific staining of the endothelium was not described. Positive staining of CRC epithelium for CCL4 is consistent with the immunochemistry presented in Figure 4-12. The Human Protein Atlas has not yet profiled CCL3 or CCL5 expression.

Despite the lack of positive CCL4 staining of the CRC endothelium reported by the Human Protein Atlas, localisation of CCL4 to the endothelium has been clearly demonstrated in head and neck cancers (235). The flow cytometry data presented in this chapter supports the immunohistochemistry in that the CCR5 ligands are secreted by the tumour epithelium as well as cells in the stroma, the most important of which, are $CD90^{+}$ fibroblasts. The chemokine capture experiments also support the idea that CCL4 can be captured and presented by the CRC endothelium. It has previously been shown that endothelial cell lines of different origins have distinct binding patterns for different chemokines, independent of endothelial cell chemokine receptor expression (262). This effect has been explained by the differential composition of endothelial cell surface glycosaminoglycans by tissue origin. Chemokine binding to the endothelium was inhibited by the addition of soluble chondroitin sulphate and it has been shown that endothelial cells differ in their expression of glycosaminoglycans, in terms of length, charge density and the degree of sulphation (263). Endothelial cell surface glycosaminoglycan composition therefore results in a further degree of specificity for chemokine presentation, in addition to tissue-specific endothelial cell chemokine

receptor expression and native endothelial cell chemokine production. Endothelial cells may also express atypical chemokine receptors, acting as molecular decoys, which possess the ability to bind specific chemokines (264). Differences in endothelial cell chemokine receptor expression and cell surface glycosaminoglycan composition could account for the observed differences in chemokine capture by NEC, TEC and HUVEC. However, such differences in chemokine and glycosaminoglycan expression were not studied further. In summary, I have shown that CCR5 chemokines are expressed by CRC and CCL4 can be captured, in vitro at least, by the tumour endothelium. CCL4 presentation by the tumour endothelium places this chemokine in a position where it can engage circulating CCR5-expressing immune cells, potentially playing an important role in recruitment of such cells to the tumour.

When CCR5 was first characterised in the early 1990s, it was shown to be the cognate receptor for CCL3, CCL4 and CCL5 (250,265). It has since been shown that other chemokines can bind to CCR5 (266), namely CCL2, CCL7, CCL8, CCL11, CCL13. The expression of these other CCR5-binding chemokines was not evaluated.

A possible role for the recruitment of $CCR5^{+}$ Treg by tumours expressing CCR5 ligands has recently been demonstrated in murine tumour models (104,233). CCL5 production by the Pan02 and CT26 murine tumour cell lines, pancreatic and colorectal respectively, were disrupted using CCL5 small hairpin RNA (shRNA), giving rise to $Pan02^{low}$ and $CT26^{low}$ cells. In both studies, subcutaneously implanted tumours in immunocompetent mice grew more slowly following injection of $Pan02^{low}$ or $CT26^{low}$ cells compared with Pan02 or CT26 cells. When the mice were culled, the tumour lymphocyte infiltrate was analysed and showed a reduction of approximately 50% in the Treg proportion in

Pan02^{low} and CT26^{low} tumours compared with Pan02 and CT26 tumours. In a different study, inhibition of CCL5 in a CT26 subcutaneous tumour model was performed using an anti-CCL5 antibody given every 72 hours and starting 7 days after tumour cell implantation, and resulted in delayed tumour growth compared to control antibody (267). Tumour Treg infiltration was not measured.

Pan02^{low} and Pan02 tumours were implanted into Rag -/- mice to determine if there were any intrinsic differences in the growth kinetics of the two cell lines. The tumours grew at the same rate in these immunodeficient mice, suggesting that the differences observed in tumour growth and Treg infiltration between Pan02^{low} and Pan02 tumours implanted into immunocompetent mice, were dependent on a functioning immune system (104). Similarly, CT26^{low} and CT26 cells were implanted into nude mice, which the authors stated resulted in similar growth kinetics (233). However, it does appear that there is some separation of the growth curves, with slower growth for CT26^{low} compared to CT26 tumours, after 16 days. Nevertheless CT26^{low} tumours grew more slowly than CT26 tumours in immunocompetent mice with less Treg infiltration, again suggesting these differences required a functioning immune system. It is therefore likely that tumour-derived CCL5 interacts with the host immune system to result in delayed tumour growth and modulate Treg infiltration. However, as smaller differences in tumour growth between CT26^{low} and CT26 tumours were seen in immunodeficient mice, it is also likely that CCL5 has a direct effect on tumour growth. Supporting this idea, others have shown that CT26 cells proliferate in vitro in response to CCL5 (267). The proliferative response was maximal at a CCL5 concentration of 50 ng/ml with less proliferation seen at higher concentrations. The different roles that CCL5 may play in

terms of immune cell recruitment and direct effects on tumour growth are therefore complex and dependent on CCL5 concentration.

The three murine cancer models discussed above focus on the interaction between CCL5 and CCR5. To summarise, delayed tumour growth with an associated reduction in the tumour Treg proportion was observed in Pan02^{low} and CT26^{low} tumours compared with Pan02 and CT26 tumours in immunocompetent mice. However, an important role for CCL5 in modulating tumour growth directly in vivo cannot be ruled out. These studies only looked at the role of CCL5 in modulating tumour growth and immune cell infiltration, not other CCR5 ligands such as CCL3 and CCL4. Evidence has been presented in this chapter for elevated levels of CCL3 and CCL4 but not CCL5 in human CRC compared with other tissues, and the relative effect of blocking these chemokines alone, or in addition to CCL5 in similar murine tumour models to the ones described, have not been evaluated.

Table 4-2: Published literature describing chemokine measurements in tumours and normal tissues. IHC=immunohistochemistry; ISH=in-situ hybridisation; HCC=hepatocellular carcinoma.

Chemokine	Cancer site	Methods	Findings	References
CCL3	Colorectal	RT-PCR	Increased in CRC tissue compared to colon.	(234)(102)
	Glioma	IHC	CCL3 positive staining in glioma, increasing with tumour grade.	(268)
	Oral carcinoma	RT-PCR, IHC	Increased in oral carcinoma compared to healthy gingiva.	(269)
	Gastric	RT-PCR, ELISA	Increased expression in cancer compared to normal tissue.	(270)
	HCC	IHC	Increased in tumour compared to normal liver.	(271)
	Ovarian	ISH	CCL3 mRNA expression seen predominately in tumour stroma.	(272)
	Pancreas	RT-PCR	Increased in pancreatic cancer compared to normal pancreas.	(104)
CCL4	Colorectal	RT-PCR, ELISA	Increased in CRC tissue compared to colon.	(234)(102)(259)
	Breast	ISH	CCL4 mRNA expression confined to cells in stroma.	(273)
	Pancreas	RT-PCR	Increased in pancreatic cancer compared to normal pancreas.	(104)
	Gastric	IHC, RT-PCR, ELISA	Stronger CCL4 staining in cancer than normal epithelial cells. Increased mRNA and protein expression compared to normal tissue.	(274)(270)
	Head & neck	IHC	CCL4 detected on tumour endothelium.	(235)
	Lung	RT-PCR, IHC, ELISA	CCL4 expression in non-small cell tumours with a lymphocytic response compared to those without. CCL4 produced by tumour cells.	(275)
CCL5	Colorectal	RT-PCR	Increased in CRC tissue compared to colon.	(102)(267)
	Colorectal	ELISA	Reduced expression of CCL5 in CRC compared to colon.	(259)

	Head & neck	IHC	Produced by the majority of cancers, localised to tumour cells.	(235)
	Pancreas	RT-PCR	Increased in pancreatic cancer compared to normal pancreas.	(104)
	Breast	IHC, ELISA	Increased in cancer compared to normal breast tissue.	(276)(277)
	Cervical	ELISA	Increased in cancer compared to normal tissue.	(277)
	Lung	RT-PCR, IHC, ELISA	CCL5 expression higher in non-small cell tumours with a lymphocytic response compared to those without. CCL5 produced by tumour cells.	(275)
	Prostate	RT-PCR	Increased expression in cancer compared to benign hyperplasia.	(278)

Correlation of chemokines with Treg-CCR5 and Treg proportion

CCL3 and CCL4 levels, as measured by RT-PCR, significantly correlated with the percentage expression of CCR5 by CRC-isolated Treg, as measured by flow cytometry. There was no such correlation with CCL5 levels. A correlation between CCR5 expression by TILs with the expression of its ligands in CRC has not previously been reported. The correlation supports the hypothesis that high levels of CCL3 and CCL4 lead to the recruitment of $CCR5^+$ Treg. However, the Treg proportion was not found to correlate with CRC expression of CCL3 or CCL4. Therefore, these chemokines may indeed recruit $CCR5^+$ Treg, with the recruitment of $CCR5^-$ Treg being dependent on other recruitment pathways. The interactions between CCR5 and its ligands are complex and exposure to cognate chemokine leads to CCR5 internalisation (279). It may therefore be expected that $CCR5^+$ cells would internalise CCR5 after having migrated along a chemokine concentration gradient. In vitro experiments have shown reduced cell surface expression of CCR5 by migrated T cells compared to non-migrated cells in transwell experiments with CCL5 present in the bottom chamber (280). Despite this, the intensity of tumour CCL3 expression, measured by immunohistochemistry, was found to correlate with intra-tumoral CCR5 expression (281). In dry eye syndrome, lacrimal CCL3, CCL4 and CCL5 levels were measured by ELISA and found to correlate significantly with CCR5 expression by lacrimal T cells (282). In a mouse model of periodontitis, CCL3, CCL4 and CCL5 levels measured at multiple time points, significantly correlated with CCR5 expression by T cells (283).

It is intriguing that there was a significant correlation between CCL4 and foxp3 expression despite no correlation between CCL4 and the Treg proportion. Treg ($CD4^+CD25^+CD127^{low}$) highly express foxp3 (median percentage expression 93.5%, see Chapter 3). However, activated non-regulatory T cells can also express foxp3 (284) - the percentage expression of foxp3 by the Tconv population ($CD4^+CD25^-$) was 15% (see Chapter 3). Despite lower levels of foxp3 expression by Tconv, there are proportionately more Tconv than Treg infiltrating CRC, and Tconv may therefore make a more important contribution to the total tissue foxp3 expression. It has also been demonstrated that foxp3 is expressed by tumour cells (221,285).

CCR20 and other chemokines

The ligand for CCR6, CCL20, is reportedly elevated in CRC compared with colon tissue (286). In a murine subcutaneous CRC model, CCL20 was expressed by tumour cells and tumour-associated macrophages. Tumour-resident Treg were shown to express CCR6 and intra-tumoral injection of CCL20 led to increased tumour-infiltrating Treg compared to vehicle injection (237). However, as the results in this chapter show, there was no demonstrable increase in CCL20 by CRC compared to matched distal colon either at the mRNA or the protein level. For this reason, study of the function of the CCR6-CCL20 axis was not undertaken, although CCR6 blockade was performed in a mouse model (see Chapter 6). Immunohistochemistry did demonstrate positive staining for CCL20 in the epithelial component of the tumour. The ligands for CXCR3 (CXCL9, CXCL10 and CXCL11) were not found to be significantly overexpressed by CRC compared with matched distal colon by RT-PCR. Based on this finding, in

conjunction with the lack of CXCR3 expression by Treg as reported in Chapter 3, it was decided not to perform any further investigation of the expression of CXCR3 ligands.

This chapter has shown that CCR5 chemokines are expressed by CRC using a number of different techniques. This evidence, together with the preferential expression of CCR5 by tumour-infiltrating Treg suggests that the CCR5 axis is involved in the recruitment of Treg to CRC.

Chapter 5
Functional properties of Treg

Introduction

In order for chemokine-dependent migration of Treg to CRC to occur, chemokine receptors need to be expressed on the cell surface of Treg and the cognate ligands, by the tumour. The chemokine receptor signature of CRC-isolated Treg was therefore established and the presence of cognate chemokines within CRC was confirmed. This chapter presents data demonstrating that CCR5, present on CRC-isolated Treg, functions as a chemotactic receptor in vitro. CCR5 expression by Treg and Tconv was measured in co-culture experiments with tumour supernatant to determine if the tumour microenvironment may be responsible for the induction of cell surface CCR5 by resident T cells. It has been shown that T cell CCR5 expression correlates with T cell activation (287) and therefore, T cells were activated in the presence or absence of tumour supernatant. The suppressive capacity of the CRC-isolated Treg was then tested. Finally, TSDR analysis was performed on DNA obtained from $CCR5^{low}$ and $CCR5^{high}$ CRC-isolated Treg to determine if these Treg subsets were nTreg or iTreg.

Findings

Lymphocyte migration assays

The functional integrity of CCR5, expressed by CRC-isolated Treg, was tested in a transwell system. Lymphocytes were isolated from CRC by non-enzymatic methods followed by $CD3^{+}$ immunomagnetic separation as described in Chapter 2: Transwell

migration assays. T cells were either treated with Maraviroc or vehicle control (DMSO) then placed in the upper compartment of a transwell system. The T cells were allowed to migrate towards recombinant CCL4 at a concentration of 20 ng/ml, placed in the lower chamber. CCL4 was chosen over other CCR5 ligands because it is a specific for CCR5 and the concentration of 20 ng/ml because this is the optimal concentration for T cell migration responses. It has already been shown that CCL4, like CCL3, was significantly overexpressed by CRC compared with matched distal colon at the mRNA and protein level. Unlike CCL3, CCL4 was also found to localise to the tumour endothelium and correlated significantly with CCR5 expression by Treg.

The lymphocytes were allowed to migrate for 4 hours at 37˚C. The lymphocytes in the lower (OUTPUT) and upper (INPUT) chambers were then analysed by flow cytometry. A summary of 6 transwell experiments broken down by lymphocyte subset (Treg, Tconv, $CD8^+$) is shown in Figure 5-1. Differences in the absolute numbers and percentage of cells across different conditions were tested for statistical significance using the Wilcoxon signed-rank test.

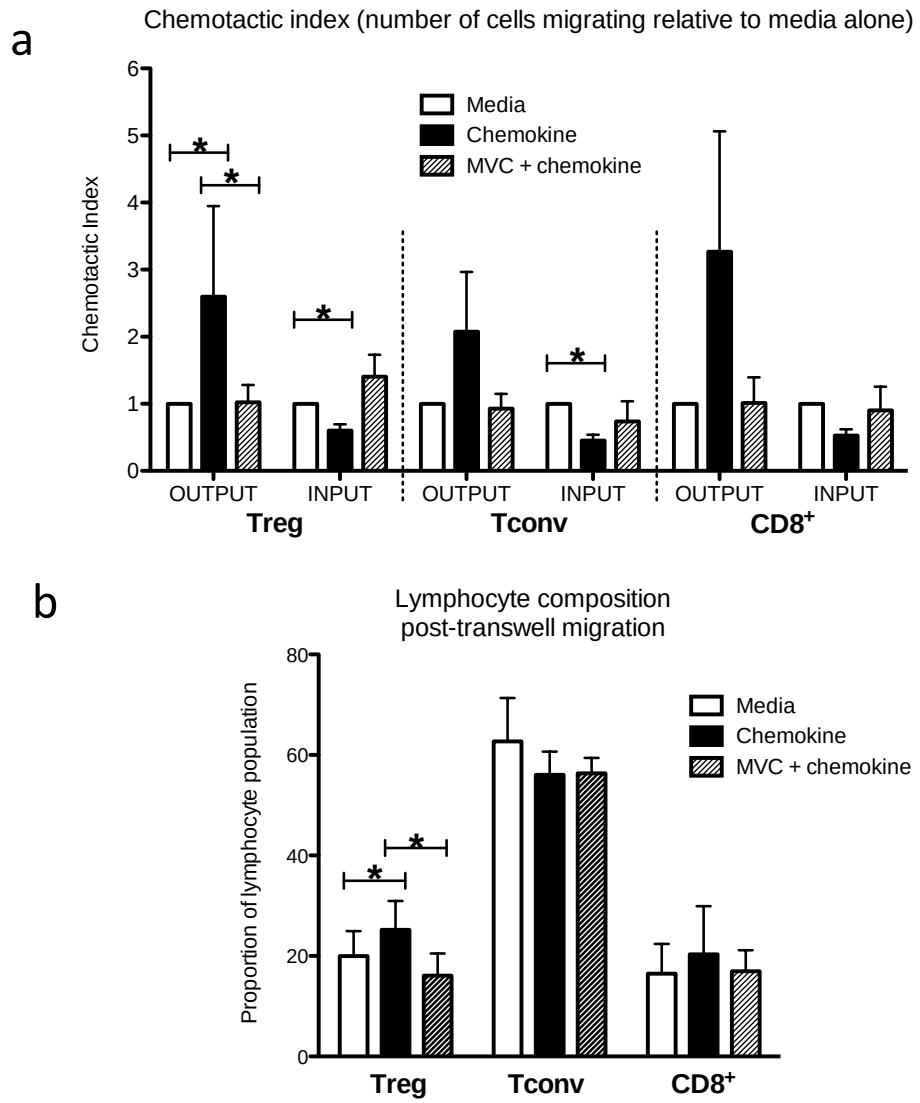

Figure 5-1: Summary of 6 transwell experiments. (a) Mean chemotactic index of the absolute number of Treg / Tconv / $CD8^+$ cells in the lower chamber (OUTPUT) and the upper chamber (INPUT) of the transwell apparatus. Conditions were DMSO-treated cells with media alone, DMSO-treated cells with chemokine (20 ng/ml CCL4) and Maraviroc (MVC) treated cells with chemokine. (b) Composition of migrated cells in the lower chamber of the transwell apparatus, given as mean proportion of all lymphocytes (%). Error bars represent standard error of the mean. Capped lines indicate statistically significant differences.

There was a trend for all lymphocyte subsets to migrate in response to chemokine, represented by the black OUTPUT bars being greater than 1. The difference between the number of Treg migrating in response to chemokine and in response to media alone reached statistical significance. Pre-treatment of lymphocytes with Maraviroc abolished the migration to chemokine and the difference between the number of DMSO-treated Treg to Maraviroc-treated Treg migrating to chemokine reached statistical significance. There was also a reciprocal, statistically significant, reduction in the number of Treg remaining in the upper INPUT chamber with chemokine compared with the number of Treg in the upper chamber with media alone. The Treg proportion was significantly increased in response to chemokine compared with media alone. The observation that migration of CRC-isolated $CD3^+$ lymphocytes towards CCL4 results in enrichment of Treg in the lower chamber confirms a preferential migration response. There was no difference in the proportion of migrated $CD3^+$ cells that were Tconv or $CD8^+$ in response to chemokine compared with media alone.

In addition to using flow cytometric analysis to determine the composition of the migrating cells through the transwell apparatus, in a single experiment the porous membranes of the transwell inserts were stained for Foxp3 and DAPI to determine the composition of the cells that migrated through and adhered to the membrane. Blue (DAPI) stained cells represent $CD3^+$ cells within the membrane. Dual blue and green (Foxp3) stained cells represent $CD3^+Foxp3^+$ cells within the membrane, indicative of Treg (see Figure 5-2).

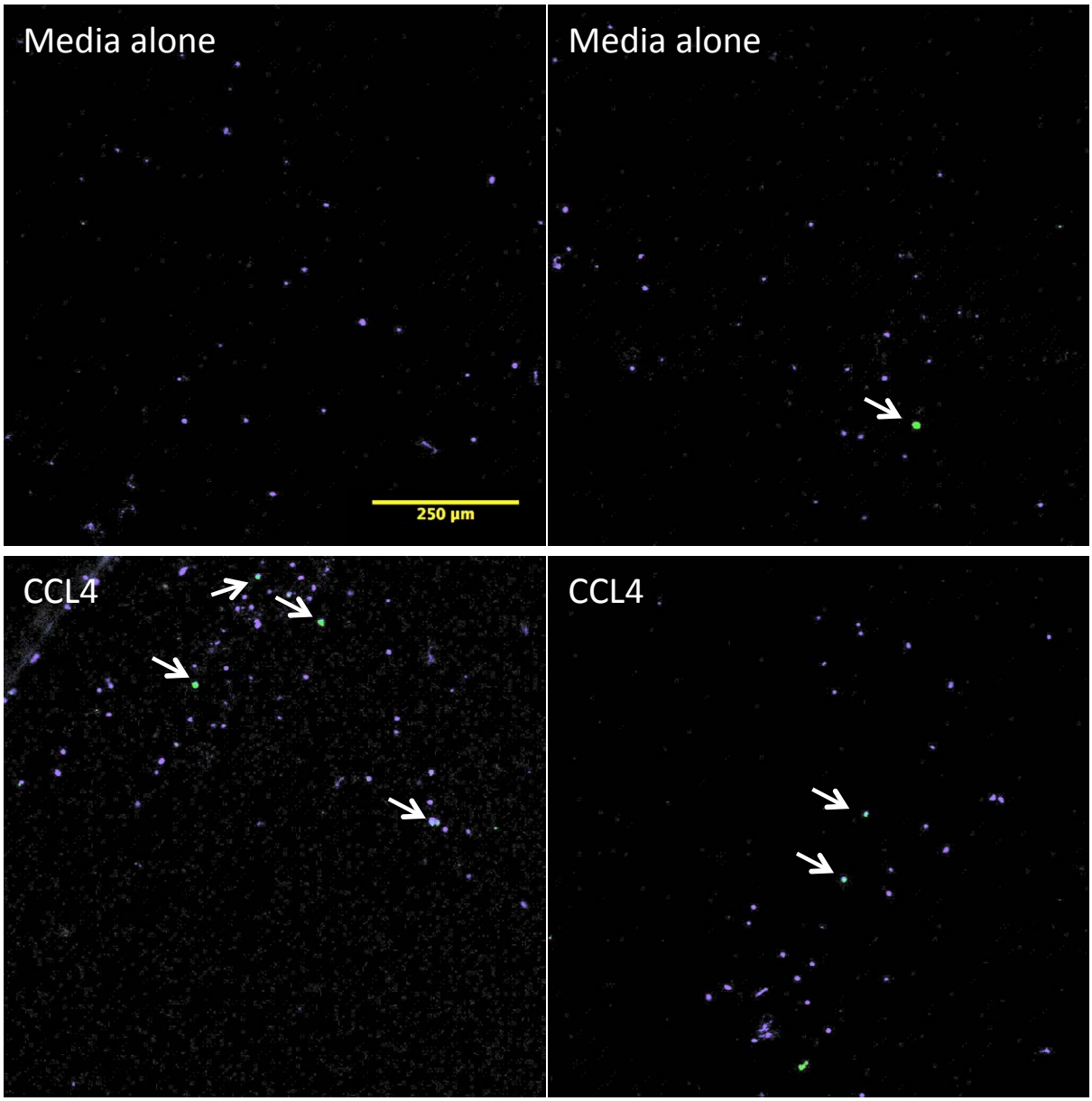

Figure 5-2: Immunofluorescent staining of transwell membranes from a single transwell experiment. Two representative fields of the transwell membrane from an experiment with media alone (top), or chemokine (bottom), in the lower chamber. X100 magnification. Blue staining = DAPI. Green staining = Foxp3. White arrows indicate dual DAPI and Foxp3 staining.

The presence of $DAPI^+$ cells was patchy within the membrane. The number of $DAPI^+$ cells and $DAPI^+Foxp3^+$ cells were enumerated over four x100 magnification fields for 3

separate experiments. The mean number was reported ± SD. The membranes from transwell experiments using DMSO-treated lymphocytes with media alone in the lower chamber, DMSO-treated lymphocytes with chemokine in the lower chamber and Maraviroc-treated lymphocytes with chemokine in the lower chamber were compared. There was no difference in the mean number of $DAPI^+$ cells over the three conditions (99.1 ± 70.1 versus 108.8 ± 83.0 versus 98.9 ± 66.2, P=0.94, Kruskall-Wallis test). The number of $DAPI^+Foxp3^+$ cells were not enumerated and compared across different conditions as the cells were too few in number (range 1-6 cells/field).

3D chemotaxis assay

An attempt was made to directly visualise chemotaxis of CRC-isolated lymphocytes to CCR5 ligands using a 3-dimensional microslide (288). The microslide, produced by Ibidi GmbH, Germany, allows for the suspension of lymphocytes in a collagen gel inside a narrow observation area that is connected to two separate lateral reservoirs. The observation area was filled with PBMC suspended in a gel, as described in Chapter 2: Chemotaxis Chambers. Seeding the required gel volume of 6 µl into the microslide, without forming any bubbles, was technically challenging. Gel spilt into the lateral reservoirs before setting. It was also difficult to establish a chemokine gradient without disturbing the gel. Chemotaxis of PBMCs towards CXCL12 was observed in one experiment but was not reproduced in a second experiment. It was estimated that 20,000 lymphocytes were needed per 6 µl of gel to give approximately 50 cells per field to track. Given the lymphocyte yields from some human CRC samples, the technique is attractive as chemotaxis may be analysed using small cell numbers. Given the technical difficulties encountered optimising the experiment to visualise PBMC chemotaxis, the use of the slides for CRC-isolated lymphocytes was not pursued.

CCR5 induction

Co-culture experiments

CRC-isolated Treg express more CCR5 than Tconv (see Figure 3-8) and is one line of supporting evidence for differential recruitment of Treg and Tconv to CRC. An alternative explanation for this finding would be that CCR5 expression by Treg is induced by the tumour microenvironment. T cell activation correlates with CCR5 expression (287) and indeed, TILs from CRC express activation and cytotoxic markers (229). PBMC were isolated, activated with CD3/CD28 beads and co-cultured with or without CRC/colon supernatant as described in Chapter 2: PBMC activation and co-culture with tumour supernatant. CCR5 expression by Tconv (defined as $CD3^{+}CD4^{+}Foxp3^{-}$) and Treg (defined as $CD3^{+}CD4^{+}Foxp3^{+}$) was measured by flow cytometry. CD25 expression was not used to define Treg in these experiments as it was found that all T cells expressed CD25 following bead activation. Summary data from 3 separate experiments using supernatant from one pair of CRC and distal colon samples are presented in Figure 5-3a. More Treg expressed CCR5 than Tconv, in terms of percentage expression, under all conditions. Bead activation increased percentage CCR5 expression by both Tconv and Treg. Addition of supernatant to the co-culture increased percentage CCR5 expression further, an effect observed more for CRC than distal colon supernatant. Differences were not tested for statistical significance as only 2 separate experiments were performed. Bead activation and supernatant co-culture made no difference to CCR5 expression in terms of MFI (data not shown).

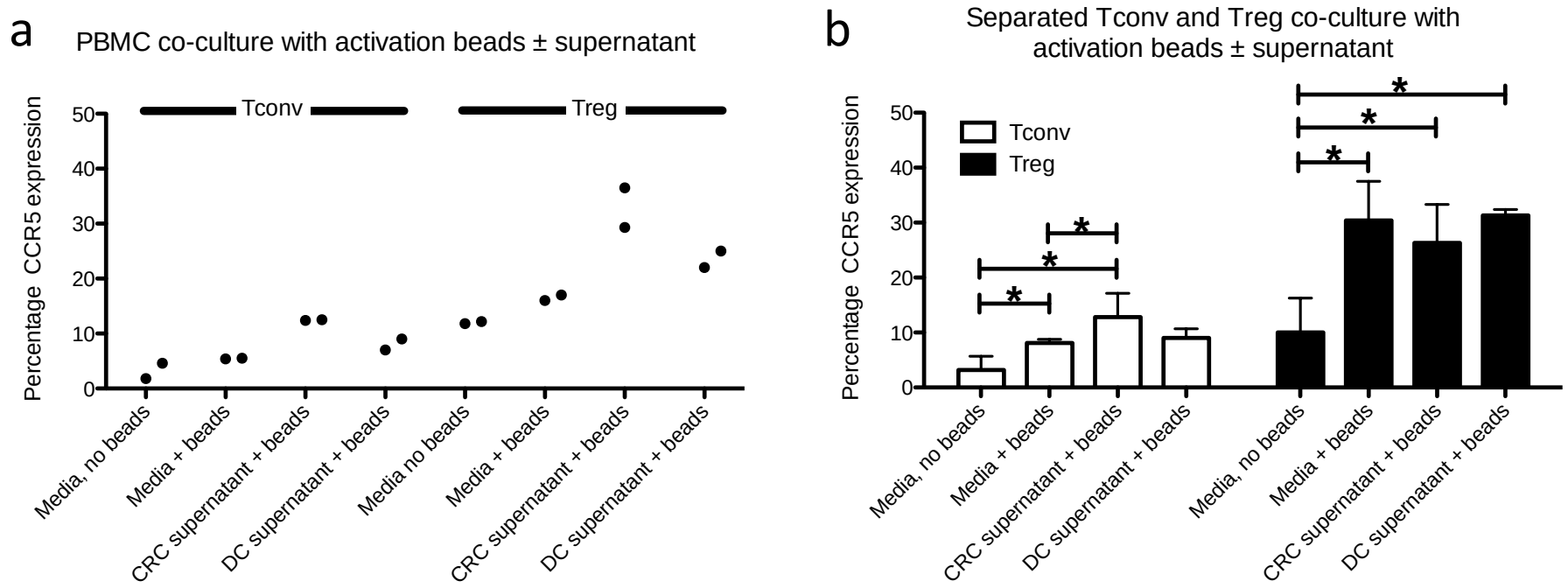

Figure 5-3: (a) Percentage CCR5 expression by Tconv and Treg following co-culture of PBMC with CD3/CD28 beads ± CRC/DC supernatant. Individual data points are shown from 2 separate experiments. (b) Median percentage CCR5 expression by Tconv and Treg cultured separately with CD3/CD28 beads ± supernatant. Data represents a summary of 5 experiments. DC = distal colon. Error bars represent the IQR about the median. Capped lines indicate statistically significant differences between groups.

It was clear that Foxp3 expression was upregulated by T cells post-activation with CD3/CD28 beads. Therefore, the Treg phenotype ($CD3^+CD4^+Foxp3^+$), although appropriate for lymphocytes not activated by beads, represents a different cell population post bead-activation (see Figure 5-4). The increased percentage expression of CCR5 by bead-activated Treg compared with bead-activated Tconv, cultured with or without supernatant, may represent increased CCR5 expression by activated compared with less activated T cells. For this reason, Tconv ($CD4^+CD25^-$) and Treg ($CD4^+CD25^+$) were isolated from PBMC using immunomagnetic separation methods. Following isolation of Tconv and Treg, the co-culture experiments were repeated under the same conditions but with Treg and Tconv in separate wells. This allowed for the effects of bead activation and co-culture with supernatants on Treg and Tconv to be assessed separately.

As before, there was increased percentage expression of CCR5 by Treg compared to Tconv for all conditions (see Figure 5-3b). There was significantly greater CCR5 percentage expression by bead-activated Treg, cultured with or without supernatant, than by Treg cultured without beads. There was no difference in percentage CCR5 expression between bead-activated Treg cultured with supernatant (from CRC or distal colon) compared with bead-activated Treg cultured without supernatant. There was a small but significant difference in percentage CCR5 expression by bead-activated Tconv compared with Tconv cultured without beads. Culture of Tconv with CRC, but not DC, supernatant significantly increased percentage CCR5 expression compared with bead-activated Tconv cultured in media alone. Bead activation and supernatant co-culture made no difference to CCR5 expression in terms of MFI (data not shown).

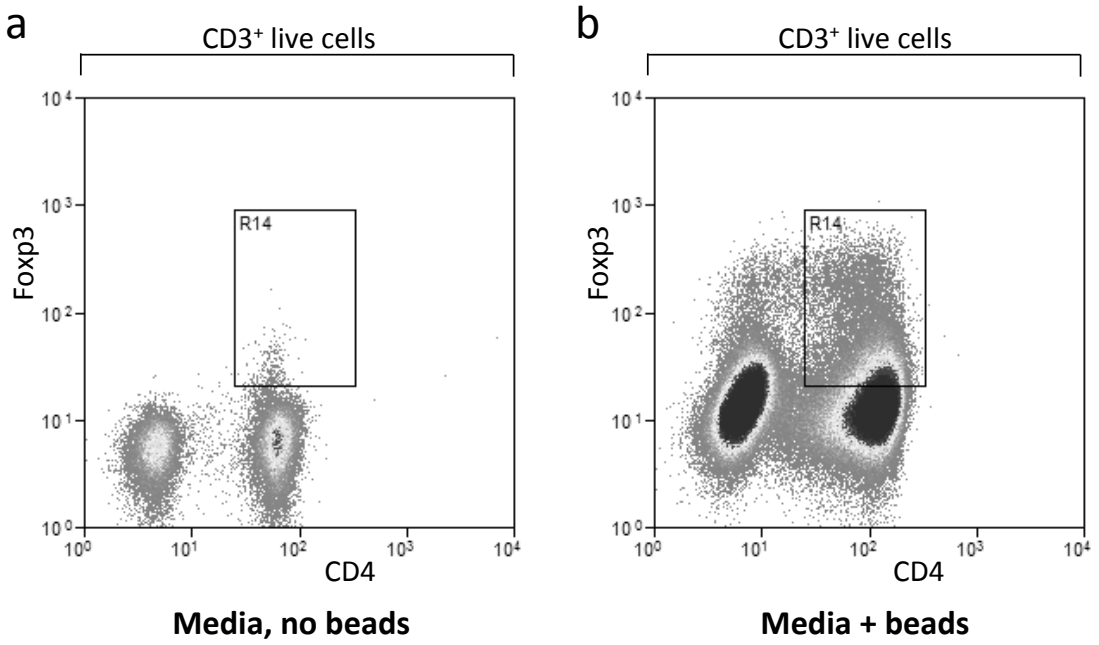

Figure 5-4: Foxp3 expression by $CD3^+CD4^+$ PBMCs: (a) cultured in media alone for 4 days and (b) post-culture with CD3/CD28 beads for 48 hours, followed by further 48 hour culture in media after beads have been removed. The region 'R14' is in the same position on both dot plots. Flow cytometry data is from a single experiment representative of 4 separate experiments.

Multiplex supernatant protein assays

CCR5 expression by Tconv was increased by the addition of CRC supernatant to the co-culture and an attempt was made to determine the supernatant cytokines responsible. Multiple cytokines were measured using the Proteome Profiler™ Cytokine Array Panel A and Angiogenesis Array (R&D Systems Inc, USA). The kit contained capture antibodies to various proteins, spotted on nitrocellulose membranes. Supernatants were mixed with a cocktail of biotinylated detection antibodies. The supernatant/antibody mixture was incubated with the membrane so that protein/antibody complexes were bound by its cognate immobilised capture antibody

on the membrane. Bound protein/antibody complexes were then visualised using Streptavidin-HRP and chemiluminescent detection reagents. The intensity of light produced at each spot on the membrane was proportional to the amount of bound protein. Semi-quantitative protein measurements were made by measuring the density of the spots using an ImageJ macro (see Appendix IV). Each kit contained 4 membranes allowing for duplicate semi-quantitative measurement of protein concentrations in 2 matched CRC/distal colon supernatants. Protein concentrations in CRC supernatants were compared with matched distal colon supernatants and differences were tested for statistical significance using the Wilcoxin signed-rank test for paired data. Unadjusted P-values are reported in Table 5-1.

Table 5-1: Median supernatant protein concentration (measured semi-quantitatively by densitometry) by tissue type. Median values represent 2 samples of CRC with matched distal colon supernatant with technical duplicates. P-values were calculated by the Wilcoxin signed-rank test, unadjusted for multiple comparisons. '*' represent significant differences at the <0.05 level. Blank entries represent no detectable protein and P-values were only calculated if protein was detected for both samples of CRC and distal colon supernatant.

Protein	CRC	DC	P-value	Protein	CRC	DC	P-value
Activin-A	11.7	6.1	* 0.02	IL-17		2.0	
ADAMTS-1	4.4	0.7	* 0.01	IL-17E	1.0	0.9	
Amphiregulin	48.5	29.8	0.31	IL-1Ra	75	24.7	* 0.044
ANG	107.6	68.7	* 0.001	IL-1ß	64.7	33.6	0.24
Ang-1	8.1	1.2	* 0.002	IL-1α	2.0	1.6	
Ang-2	3.4	1.6	0.067	IL-2	1.0	0.7	

Artemin	3.1	0.3	* 0.009	IL-23	2.1	2.3	0.35
C5/C5a	2.5	20.8	0.20	IL-27	2.3	0.8	0.086
CCL1		0.8		IL-32a		0.7	
CCL2	4.2	0.6	* 0.019	IL-4		0.6	
CCL3	3.0	0.8	0.054	IL-5		1.1	
CCL4				IL-6	100.5	90.2	0.29
CCL5	0.5	0.8		IL-8	110.9	98.9	0.26
CD40L				LAP (TGF-ß1)	9.2	6.1	0.08
CXCL1	52	9.8	0.19	Leptin	2.0	0.4	* 0.028
CXCL10	0.9	1.3		MIF	102.3	96.1	0.19
CXCL11		0.5		MMP-8	93.6	38.5	0.14
CXCL12		1.5		MMP-9	92.6	46	0.18
CXCL16	17.4	1	0.17	NRG1-ß1	17.2	6.8	0.11
CXCL4	75.6	36.5	0.16	PD-ECGF	7.3	2.2	0.064
DPPIV	25.2	14.2	0.27	PDGF-AA	6.5	0.7	0.12
EG-VEGF	6.2	2.7	0.05	PDGF-AB/BB	4.9	1.3	
EGF	2.5	0.3	* 0.026	Persephin	9.0	6.7	0.32
Endoglin	3.0	0.1		PIGF	4.2	0.7	* 0.015
Endostatin	64	30.3	0.17	Plasminogen	2.8	0.9	0.057
Endothelin-1	5.8	2.3	0.099	Prolactin	1.5	0.4	* 0.041
FGF-1	5.9	3.6	0.25	PTX3	8.5	5.7	0.35
FGF-2	63.2	10.9	* 0.022	Serpin-B5	14.9	1.0	0.18
FGF-4	2.2	0.2	* 0.021	Serpin-E1	110.7	76.3	0.17
FGF-7	2.9	0.3		Serpin-F1	56.2	59.5	0.14
G-CSF	22.1	23.1	0.49	SerpinE1	95.5	65	0.30
GDNF	1.7	0.1		sICAM1	35.8	22.5	0.31
GM-CSF	87.9	21.4	0.065	sTREM-1		0.3	

HB-EGF	6.1	1.7	0.11	TIMP-1	118.8	91.6	0.19
HGF	43.6	10.9	0.06	TIMP-4	2.3	0.3	* 0.013
IFNγ	1.6	0.9	0.28	TNFα	0.8		
IGFBP-1	7.9	5.4	0.34	TSP-1	71.2	50.3	
IGFBP-2	34.2	12.3	0.21	TSP-2	3.3	1	* 0.008
IGFBP-3	41.3	0.9	0.20	uPA	100.1	48.2	0.12
IL-10		1.6		Vasohibin	2.2	0.8	* 0.020
IL-12p70	2.6	0.7		VEGF	66.1	25.9	0.11
IL-13	0.3	0.9		VEGF-C	1.8	0.5	* 0.043
IL-16	12.5	4.3	0.22				

There were 15 proteins that were of significantly higher concentration in the CRC compared with the distal colon supernatant. These were IL-1Ra, Activin-A, ADAMTS-1, ANG, Ang-1, Artemin, EGF, FGF-2, FGF-4, leptin, MCP-1, PIGF, prolactin, TIMP-4, TSP-2, vasohibin and VEGF-C. These proteins were too many in number to study the effects of their inhibition in co-culture experiments. IL-1RA levels have been shown to be increased in melanoma tumours in CCR5 -/- mice compared with wildtypes (289) and there may therefore be an important association between IL-1RA levels and CCR5 expression. TGF-ß1 increases CCR5 expression on peripheral blood T cells (290). TGF-ß1 is also upregulated by Treg from wildtype mice following stimulation with CCL5, but by Treg from CCR5 -/- mice (291). In a murine wound healing model, CCR5 -/- mice displayed a reduction in TGF-ß1 and VEGF at wound sites compared to wildtype mice (292) and it is known that CCL5-mediated angiogenesis depends both on CCR5 and VEGF expression (293). TGF-ß1 and VEGF were expressed at higher levels in CRC than in distal colon supernatants, although the differences did not reach statistical

significance. However, based on the above cited literature and the supernatant protein levels, it was decided to study the effects of inhibition of IL-1Ra, TGF-ß1 and VEGF on cell surface CCR5 expression in the supernatant co-culture model.

Inhibition of supernatant proteins

Neutralising antibodies to IL-1Ra, TGF-ß1 and VEGF were added to wells containing separated Tconv and Treg with activating beads ± CRC supernatant. IMC antibodies were added to a control well with Tconv or Treg under the same conditions. There was no difference in CCR5 expression by activated cells cultured with CRC supernatant and the above neutralising antibodies to IL-1Ra, TGF-ß1 or VEGF compared with activated cells cultured with CRC supernatant and IMC antibodies (data not shown).

Culture supernatant chemokine concentrations

The concentrations of CCL3, CCL4 and CCL5 were measured in the culture supernatant, harvested at the end of the experiment (day 4) from wells in which Treg and Tconv had been cultured in media with and without activation beads (see Figure 5-5a). Chemokine levels were undetectable when Tconv and Treg had been cultured in the absence of activation beads. Cultured activated Tconv produced notably more CCL3, CCL4 and CCL5 than Treg. Culture of activated Tconv and Treg in the presence of the human CCR5 small molecular antagonist UK-484900 was performed to determine the importance of CCR5 internalisation in this CCR5 induction model. CCR5 inhibition resulted in a small increase in CCR5 expression by Tconv, in terms of both percentage expression and MFI (see Figure 5-5b+c).

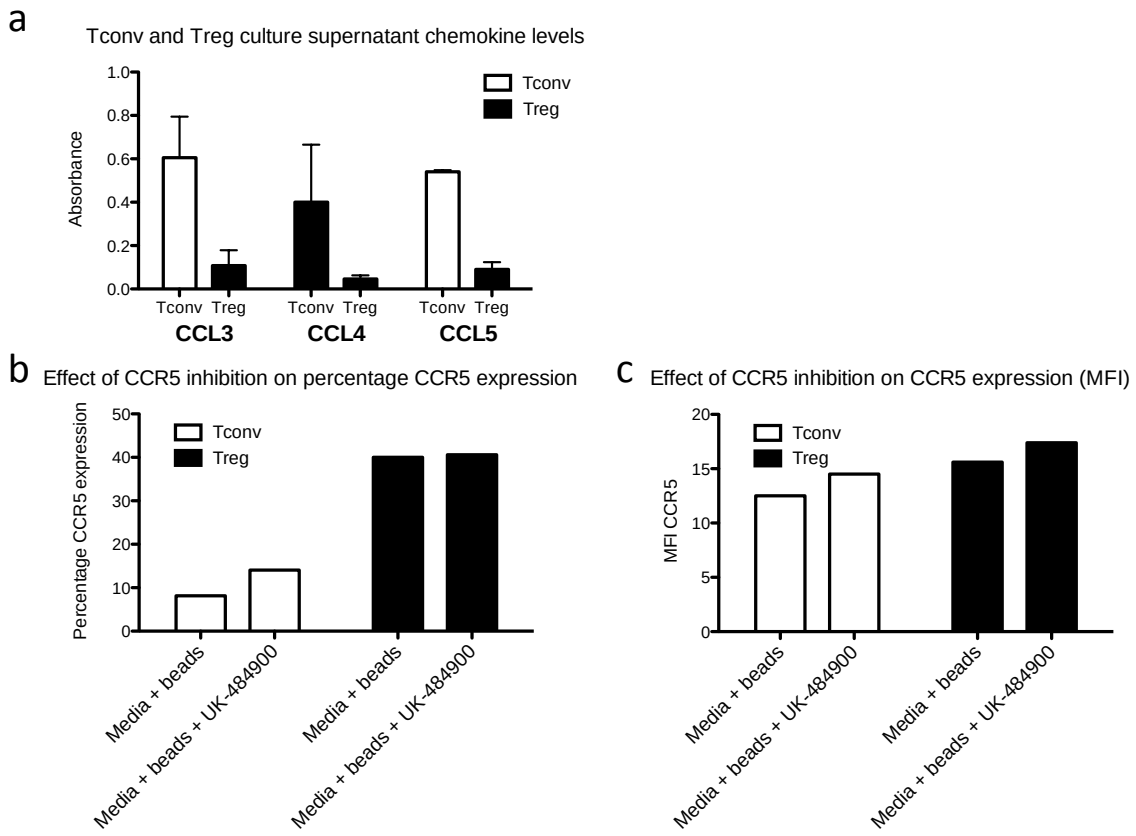

Figure 5-5: Tconv and Treg were cultured in separate wells with activation beads. (a) At the end of the experiment (day 4), culture supernatants were harvested and semi-quantitative measurement of CCL3, CCL4 and CCL5 concentrations were performed. Data represents the mean absorbance of 2 separate experiments with error bars showing the standard error of the mean. Tconv and Treg were cultured in the presence or absence of activation beads and UK-484900 (a CCR5 inhibitor) and CCR5 expression was measured by flow cytometry: (b) percentage CCR5 expression, (c) MFI. Data represents the findings from one experiment.

Treg suppressive capacity

I measured the levels of CD39, CTLA4 and Foxp3 on CCR5^{low} and CCR5^{high} Treg isolated from CRC. A summary of 4 flow cytometry experiments is shown in Figure 5-6. None of the differences reached statistical significance due to the small number of experiments. However, there was a clear trend for increased expression of Foxp3, CTLA-4 and CD39 by CCR5^{high} Treg compared with CCR5^{low} Treg, in terms of both percentage expression and median fluorescence intensity. It might therefore be expected that CCR5^{high} Treg would have an enhanced suppressive capacity compared with CCR5^{low} Treg.

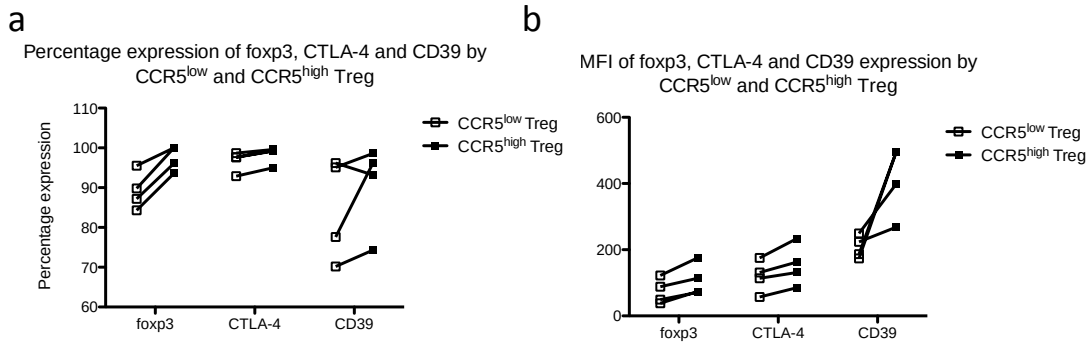

Figure 5-6: Expression of Foxp3, CTLA-4 and CD39, in terms of (a) percentage expression and (b) MFI, by CCR5low and CCR5high Treg, isolated from CRC. The data from 4 separate experiments are shown. MFI = median fluorescence intensity.

Suppression assays were used to assess the ability of Treg, isolated from CRC, to suppress the proliferation of allogeneic PBMC-isolated CD4^{+}CD25^{-} responder T cells (Tresp) was assessed. The methods are described in detail in Chapter 2: *Suppression assay*. Treg and Tconv were isolated from CRC by cell sorting with a purity of approximately 95%. CCR5^{low} Treg and CCR5^{high} Treg were isolated separately with lower purities of approximately 70% and 80% respectively (see Chapter 2:

Fluorescence-activated cell sorting (FACS). A total of 5 suppression assays were performed successfully. Representative results from one experiment, of which enough Treg were isolated to perform 3 different Treg : Tresp ratios, is shown in Figure 5-7. Following 72 hours of culture, 75% of Tresp proliferated in response to Treg Suppression Inspector beads alone. Both CRC-isolated $CCR5^{low}$ Treg and $CCR5^{high}$ Treg suppressed proliferation of Tresp in a dose-dependent manner while CRC-isolated Tconv did not. Ten experiments using Treg isolated from CRC and 4 experiments using Treg isolated from PBMCs were performed in the process of optimising the suppression assay before the assay could be performed successfully. The co-culture time was reduced from 5 days to 3 days to limit the proliferation of Tresp. Most importantly, the cell : bead ratio was changed from 1 : 1 to 2 : 1 to reduce the stimulus for proliferation of Tconv to a level at which proliferation can be suppressed.

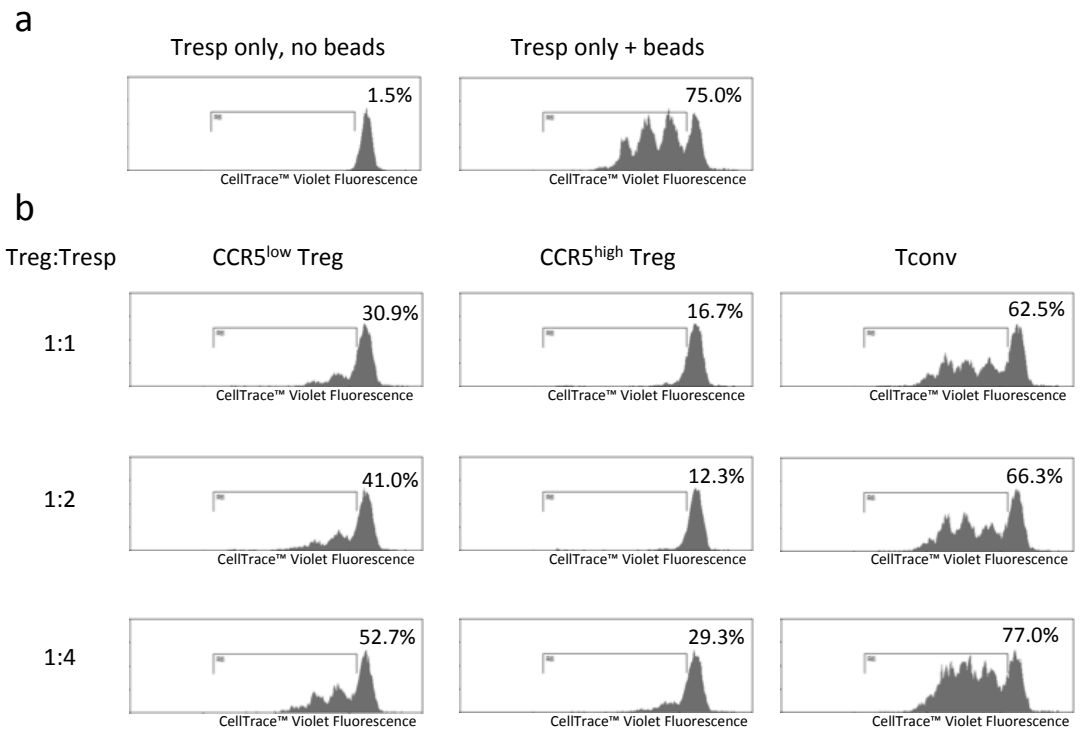

Figure 5-7: Suppression assay using CCR5^{low} and CCR5^{high} Treg isolated from one sample of CRC. Data is representative of 5 separate experiments. (a) Tresp proliferation following 72 hours of culture with or without Treg Suppression Inspector beads. (b) Tresp proliferation following 72 hours of culture with Treg Suppression Inspector beads and either CRC-isolated CCR5^{low} Treg, CCR5^{high} Treg or Tconv. Numbers at the top-right of each histogram indicates the percentage of proliferating cells.

Depending on the total number of Treg that were able to be isolated from the CRC sample, multiple different ratios of Treg to Tresp were used in the assay. A data summary from the 5 suppression assays is shown in Table 5-2. Certainly, at Treg : Tresp ratios of 1:1 and 1:2, Treg suppressed Tresp proliferation whereas Tconv did not. Only two assays at a Treg : Tresp ratio of 1:4 were performed, one of which did not show any suppression of Tresp proliferation by Treg. The differences in percent

suppression by CCR5^{low} Treg, CCR5^{high} Treg and Tconv were compared using pooled data for Treg : Tresp ratios of 1:1 and 1:2. Differences were tested for statistical significance using the Wilcoxon signed-rank test. Both CCR5^{low} Treg and CCR5^{high} Treg suppressed Tresp proliferation significantly more then Tconv, P=0.043 and P=0.018, respectively and CCR5^{high} Treg were significantly more potent suppressors of proliferation compared with CCR5^{low} Treg (P=0.018).

Table 5-2: Summary of 5 separate suppression assays. The percent suppression of Tresp proliferation is shown for CRC-isolated CCR5^{low} Treg, CCR5^{high} Treg and Tconv at different Treg : Tresp ratios. The number of Treg/Tconv represents the number of sort events given by the MoFlo XDP High-Speed Cell Sorter, rather than the absolute number of sorted viable cells.

			Percent suppression (%)		
Experiment	Ratio Treg:Tresp	Number Treg/Tconv	CCR5^{low} Treg	CCR5^{high} Treg	Tconv
A	1:1	10000	28.5	32.1	0.0
B	1:1	5000	75.1	81.4	-16.0
C	1:1	10000	58.8	83.6	16.7
D	1:1	10000	6.7	46.6	-1.3
C	1:2	5000	45.3	77.7	11.6
D	1:2	5000	8.7	34.3	16.8
E	1:2	5000	55.1	72.2	-0.7
C	1:4	2500	29.7	60.9	-2.7
D	1:4	2500	0.0	6.0	-9.4

In vitro proliferation of CRC-isolated Treg and Tconv

Treg are enriched in CRC compared to distal colon and peripheral blood (see Figure 3-11). Selective recruitment of Treg by CRC may explain this observed enrichment. However, at least two other possibilities exist: Treg may proliferate more than Tconv within the tumour; and Treg may be induced from Tconv. Regarding the former, Ki67 expression by CRC-isolated Treg and Tconv, was measured by flow cytometry (see Figure 5-8a+b). Ki67 protein is a marker of proliferation, expressed in all active phases of the cell cycle, but not by resting cells (294). There was a statistically significant increase in Ki67 percentage expression by Treg compared with Tconv, suggesting that Treg were proliferating more than Tconv within the tumour. Bcl2 mRNA expression was measured relative to GAPDH mRNA expression by Treg and Tconv, isolated from CRC by cell sorting (see Figure 5-8c). Bcl2 is an important anti-apoptosis gene (295) and was expressed at slightly higher levels by Treg than by Tconv, although this difference did not reach statistical significance.

To test whether CRC-isolated Treg proliferated more than Tconv, cells were labelled with CellTrace™ Violet then isolated from CRC and peripheral blood by cell sorting and a proliferation assay was performed as described in Chapter 2: Proliferation assay. $CD4^+CD25^-$ cells (Tresp) were isolated from the peripheral blood of a different donor to the CRC sample. 10 000 cells of each subtype were sorted and proliferation in response to Treg Suppression Inspector beads for 72 hours was measured by flow cytometry (see Figure 5-8d). Peripheral blood Tresp ($CD4^+CD25^-$) proliferated in response to Treg Suppression Inspector beads more than CRC-isolated Tconv ($CD4^+CD25^-$). Treg did not proliferate in response to beads at all.

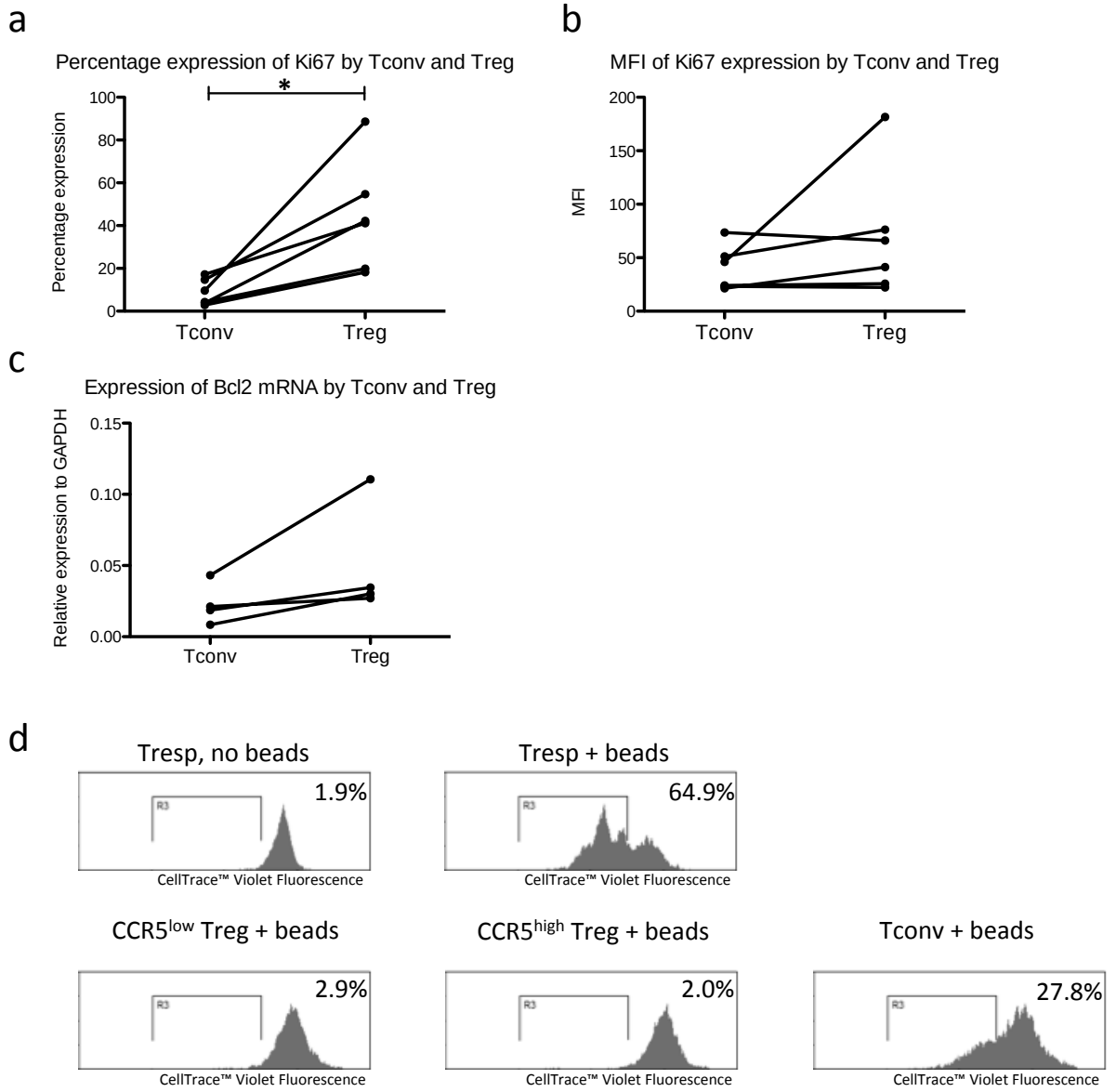

Figure 5-8: Ki67 expression in terms of (a) percentage expression and (b) MFI, by Treg and Tconv, isolated from CRC. Data from 7 experiments shown. (c) Relative expression of Bcl2 mRNA to GAPDH mRNA by Treg and Tconv, isolated from CRC. Data from 4 experiments are shown. (d) Proliferation assay comparing proliferation of peripheral blood $CD4^{+}CD25^{-}$ cells (Tresp) to $CCR5^{low}$ Treg, $CCR5^{high}$ Treg and Tconv, isolated from CRC. Numbers at the top-right of each histogram indicates the percentage proliferation. Data represents lymphocytes isolated from one sample of CRC and unmatched peripheral blood. Capped line indicates a significant difference (Wilcoxin signed-rank test). MFI = median fluorescence intensity.

Naturally-occurring versus induced Treg

Treg may be naturally-occurring thymic emigrants (nTreg) or induced from other T cells (iTreg). Treg enrichment in CRC may therefore represent induction of Treg from other T cells rather than active recruitment of nTreg into the tumour. Helios expression by CRC-isolated Treg and Tconv was measured by flow cytometry (see Figure 3-6 and Figure 5-9a+b). Median (IQR) percentage Helios expression by Treg was 75.2% (70.6-80.8) compared to 11.2% (9.2-14.9) by Tconv. This difference reached statistical significance. Analysis of the demethylation status at the TSDR for $CCR5^{low}$ Treg, $CCR5^{high}$ Treg and Tconv, isolated from 4 different CRC samples, revealed a significantly greater percentage of unmethylated DNA at the TSDR for both $CCR5^{low}$- and $CCR5^{high}$ Treg compared with Tconv (see Figure 5-9c).

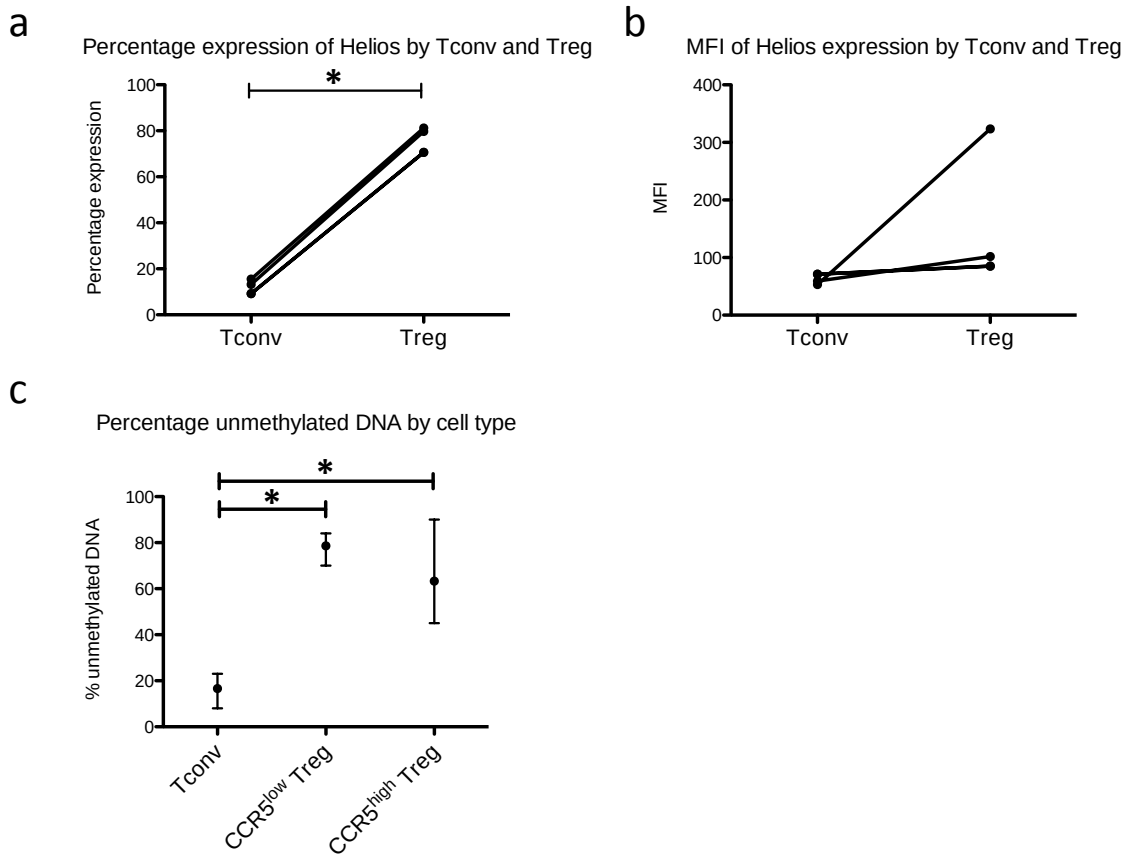

Figure 5-9: Helios expression by Tconv and Treg isolated from CRC, in terms of (a) percentage expression and (b) median fluorescence intensity. Data from 4 unique CRC samples are shown. (c) Percentage of unmethylated DNA at the TSDR by cell type. The mean percentage of unmethylated DNA is plotted for Tconv, CCR5^{low} Treg and CCR5^{high} Treg, isolated from 4 different CRC samples. Error bars represent the range of percentage of unmethylated DNA. Capped lines represent a statistically significant difference (Wilcoxon signed-rank test).

Discussion

The functional properties of CRC-isolated Treg, in terms of the ability to undergo chemotaxis in response to CCR5 ligands, suppressive capacity and proliferative capacity have been presented in this chapter. TSDR analysis supports the idea that CRC-resident Treg are nTreg, rather than iTreg. Finally, in vitro experiments using peripheral blood lymphocytes have demonstrated that surface CCR5 expression can be induced by culture with CD3/CD28 activation beads, an effect that can be modified by the addition of CRC or distal colon supernatant.

CRC-isolated Treg migrate towards CCL4

The proportion of migrated lymphocytes with a Treg phenotype increased significantly with chemokine compared with media alone. Reciprocally, there was a significant reduction in the proportion of non-migrated cells with a Treg phenotype with chemokine compared with media alone, and these effects were abolished by pre-incubation of the lymphocytes with Maraviroc. Thus Treg are preferentially recruited by CCL4, most likely as a consequence of their higher levels of expression of CCR5 than Tconv. Given that CCR5 is preferentially expressed by Treg than Tconv, and CRC expresses more CCL3 and CCL4 than matched colon tissue, it is likely preferential recruitment of Treg that accounts for their higher frequencies in CRC tissue in vivo. Tconv and $CD8^+$ cells showed similar migratory responses to CCL4, reflecting their comparable levels of CCR5 (see Figure 5-1).

Evidence from animal models suggests that $CCR5^+$ Treg migrate towards their ligands in vivo. Intravenous recombinant CCL5 administered to rats in a renal allograft model resulted in egress of $CCR5^+$ Treg and prompt graft rejection (296) and intra-tumoral

injection of recombinant CCL4 and CCL5 resulted in accumulation of $CCR5^+$ Treg in a mouse melanoma model (297). Patients treated with Maraviroc show reduced T cell chemotaxis and CCR5 internalisation in response to CCL5 in vitro and a reduced incidence of visceral graft-versus-host disease (298). It was postulated that these clinical outcomes are a consequence of reduced tissue recruitment of $CCR5^+$ Th1 effector T cells. The data presented in this chapter are consistent with the above study (298), in that Maraviroc was able to inhibit chemotaxis of $CCR5^+$ human T cells towards their cognate chemokines.

The cells expressing CCR5 in human CRC include lymphocytes and macrophages, supporting the hypothesis of CCL5-dependent recruitment of lymphocytes to tumours (267) and also the tumour epithelium (103).

The transwell assays were only performed using CCL4. The conclusions regarding migration-dependent Treg enrichment can therefore not be justified with regard to other CCR5 ligands, although there is no reason to suspect that other CCR5 ligands would not behave similarly. The lymphocyte yield from each CRC sample only provided enough lymphocytes to perform a transwell assay using one chemokine at one concentration. The summary of 6 transwell experiments shown in Figure 5-1 therefore required 6 separate CRC samples. Chemotaxis of human T cells towards CCL4 at concentrations of between 10-100 ng/ml has been previously reported (177,178,299). The chemotactic response is often biphasic with respect to chemokine concentration (300) and it was therefore fortunate that there was a consistent chemotactic response to the chosen concentration of 20 ng/ml. A more pronounced difference in the migration of Treg compared to Tconv may have been observed with a different

chemokine concentration, although this was not tested. Others have performed similar chemotaxis assays by allowing a pooled T cell population to migrate towards chemokines and then analysing the phenotypic differences of migrated cells (120,301). One possible explanation for an enrichment of Treg among migrated T cells would be T cell upregulation of CD25 by the process of migration. If this were the case however, CD25 expression would also be expected in those cells that migrated to media alone. Others have shown that enrichment of $CD25^+$ T cells in the migrated T cell fraction was only observed when chemokines were used, for which the cognate receptors were overexpressed by $CD4^+CD25^+$ T cells (301). This study of chemotaxis of peripheral blood lymphocytes demonstrated Treg enrichment through migration towards the ligands for CCR4 and CCR8. This was consistent with the greater expression of CCR4 and CCR8 by peripheral blood Treg compared with Tconv. No Treg enrichment was noted through migration towards CCR5 ligands but this is consistent with low CCR5 expression by peripheral blood Treg (see Figure 3-11).

Immunofluorescent staining of the transwell membrane was unsuccessful in that there were too few $Foxp3^+$ cells to enumerate. The transwell membrane was not designed to quantify migration in this manner but it was attempted to allow quantification of $Foxp3^+$ cells by immunofluorescence rather than $CD4^+CD25^+$ cells, as measured by flow cytometry. Staining of the transwell membrane is performed as part of the classical Boyden chamber assay in which migrated cells become trapped on the underside of the membrane, a valuable technique for low cell input numbers (302). Such Boyden chamber assays were not performed as they would not have permitted the identification of different lymphocyte subsets.

Induction of cell surface CCR5

Functional studies of $CCR5^+$ lymphocytes is hampered by the fact that peripheral blood T cells express a low level of CCR5 (303). Ten day culture of PBMC with IL-2 alone, stimulation with PHA (phytohaemagglutinin) and IL-2, and stimulation with CD3/CD28 beads are all described methods to induce CCR5 expression by T cells (304). CD3/CD28 bead stimulation leads to only a modest increase in CCR5 expression at the cell surface (303). However, this was the preferred method used for the experiments presented in this chapter due to its simplicity. Given that media required replacement every 2 days, CRC/colon supernatant was in too short supply to allow for 10-day culture. Stimulation with CD3/CD28 beads is more physiological than PHA stimulation (305) and PHA-stimulated T cells have been shown to be exhibit impaired function in terms of proliferative capacity and cytokine production (306). The results presented in this chapter demonstrated an upregulation of CCR5 by Treg, and to a lesser extent Tconv, following activation by CD3/CD28 beads. This is consistent with a study measuring CCR5 mRNA in cultures of Tconv and Treg pre- and post-activation with CD3 and IL-2 (307). The addition of CRC or distal colon supernatant to the co-culture resulted in increased expression of surface CCR5 by Tconv, but not by Treg. The supernatants contain many different cytokines and growth factors, only some of which were measured (see Table 5-1). Neutralisation of IL-1Ra, TGF-ß1 and VEGF did not have any obvious inhibitory effect on CCR5 induction by supernatant co-culture. Others have reported CCR5 induction by an array of different cytokines including: IL-2, IL-4, IL-10, IL-15 and IFN-γ (308). These were not readily detected in the CRC or distal colon supernatants and their inhibition was therefore not tested in the co-culture experiments.

Chemokine production by T cells (CCL3, CCL4, CCL5) directly downregulates CCR5 on the surface of T cells in an autocrine manner (309). Nevertheless it is possible for activated T cells, to express high levels of CCR5 whilst expressing increased levels of CCR5 ligands at the same time (310)(311). Freshly-isolated Treg from peripheral blood express CCR5 but rapidly downregulate the receptor on expansion ex vivo (312). Activated Tconv produced notably more CCL3, CCL4 and CCL5 than Treg (see Figure 5-5). It was therefore thought possible that lower CCR5 expression by Tconv compared with Treg may be a direct result of greater Tconv expression of cognate chemokines, acting in an autocrine fashion to internalise the CCR5 receptor. Culture of activated Tconv and Treg in the presence of the human CCR5 small molecular antagonist UK-484900 was performed to test this idea. CCR5 inhibition resulted in only a small increase in CCR5 expression by Tconv. If chemokine internalisation of CCR5 significantly contributed to the differences in CCR5 expression by Treg and Tconv, CCR5 inhibition ought to result in similar levels of CCR5 expression by the two cell subsets. It is therefore unlikely that differential expression of CCL3, CCL4 and CCL5 by Tconv and Treg can explain the associated differences in CCR5 expression.

Treg suppression and proliferation

The suppression assays presented in this chapter have demonstrated that Treg isolated from CRC can suppress the proliferation of allogeneic peripheral blood T cells. This is consistent with other studies that have isolated Treg from CRC tissue and assessed the ability of these cells to suppress proliferation of allogeneic T cells in vitro (48,52). It is important to note that Treg are known to be susceptible to apoptosis (313) and dead or dying cells may result in false suppression seen in suppression assays (175). Treg

sorted from CRC were selected by their absence of staining with a live/dead marker. However, their viability post-sorting and following co-culture with Tresp was not performed.

With regard the suppression assay data presented in this chapter, $CCR5^{high}$ Treg were significantly more effective at suppressing allogeneic T cell proliferation than $CCR5^{low}$ Treg. A study comparing the suppressive capacity of murine $CD103^{+}$- versus $CD103^{-}$ Treg in a model of CRC, demonstrated that $CD103^{+}$ Treg suppressed the in vivo anti-tumour function of $CD8^{+}$ cells more than $CD103^{-}$ Treg (314). This was the result of $CD103^{+}$ Treg expressing significantly more CCR5 than $CD103^{-}$ Treg, enabling these cells to migrate efficiently into the tumour tissue. There was no difference however in the *in vitro* suppressive capacity of $CD103^{+}$- and $CD103^{-}$ Treg, isolated from the spleens of tumour-bearing mice. The percentage expression of surface CCR5 was approximately 28% for the $CD103^{+}$ Treg and 5% for the $CD103^{-}$ Treg populations. The $CD103^{+}$ Treg population was therefore not highly enriched for $CCR5^{+}$ Treg. The suppressive capacity of Treg from CCR5 -/- mice was compared to that of Treg from wildtype mice (307). CCR5-/- Treg were as effective as wildtype Treg at suppressing wildtype Tresp proliferation. However, the cell surface expression of CCR5 by wildtype Treg was not measured. A similar study compared the suppressive capacity of Treg isolated from the spleens of CCR2-/-, CCR4-/-, CCR5-/- and CCR7-/- mice to Treg isolated from wildtype mice (315). There was no difference in the suppressive capacity between wildtype Treg and the Treg isolated from any of the knockout mice.

In a recent study investigating the role of Treg in psoriasis, peripheral blood $CCR5^{+}$ Treg and unsorted Treg from healthy volunteers were compared for differences in

phenotype and suppressive capacity (316). $CCR5^{+}$ Treg expressed higher levels of Foxp3, measured by both PCR and flow cytometry. More importantly, $CCR5^{+}$ Treg demonstrated a higher suppressive capacity than the unsorted Treg at all Treg : Tresp ratios examined (1:1, 1:2 and 1:4). The suppression assays presented in this chapter are entirely in keeping with the findings from this recent study. There are no other studies that have directly compared the suppressive capacity of Treg by CCR5 expression. $CCR5^{low}$ Treg are still capable of supressing T cell proliferation, just less than their $CCR5^{high}$ counterparts. It thus appears that $CCR5^{high}$ Treg represent a population of activated highly potent Treg. The reason that similar findings were not observed when comparing CCR5-/- Treg to wildtype Treg, probably results from the lack of $CCR5^{high}$ Treg in the wildtype Treg pool.

Live Treg isolated from CRC did not proliferate in vitro. This is consistent with the reports of others (48,52). In contrast, CRC-resident Treg were shown to express higher levels of Ki67 compared with Tconv, suggesting that tumour-resident Treg proliferate more than Tconv in vivo. It is indeed possible that Treg readily proliferate in vivo while displaying anergic behaviour in vitro (317). A study of TILs in an orthotopic murine brain tumour model demonstrated higher levels of Ki67 by Treg compared to Tconv (318). Tumour-resident Treg may receive stronger antigen signals than Tconv, given that Treg respond to self-antigens and Tconv do not (319). Tolerised DCs have also been shown to allow the selective expansion of Treg (320). Therefore, in spite of the lack of proliferation of CRC-isolated Treg in response to mitogens in vitro, it cannot be ruled out that Treg are highly proliferative within the tumour microenvironment in vivo.

CRC-isolated Treg are naturally-occurring Treg

Treg may be classified as naturally-occurring thymic emigrants (nTreg) or induced from other T cells (iTreg). It has been shown that nTreg express the transcription factor Helios while induced Treg do not (321), allowing Helios to be used as a marker for nTreg. The median percentage expression of Helios by Treg isolated from CRC was 75.2%, suggesting that this Treg population was mostly nTreg. However, it has since been shown that Helios can be expressed by activated and proliferating $CD4^+$ and $CD8^+$ cells (44) as well as by iTreg, induced by peptide presented by APCs (322). It is interesting to note that although this latter study found that all thymic Treg expressed Helios, the transcription factor was only expressed by 70% of Treg in the periphery – similar to the level expressed by CRC-isolated Treg.

An evolutionary conserved element within the Foxp3 locus, known as the TSDR, is selectively unmethylated in nTreg but not in Tconv or iTreg (45). Therefore, by bisulfite treatment of DNA isolated from T cells and RT-PCR, it was possible to assess TSDR unmethylation and hence, identify nTreg as opposed to iTreg (188). $CCR5^{low}$ Treg, $CCR5^{high}$ Treg and Tconv from 4 separate samples of CRC were analysed. Despite the small sample number, it does appear that both $CCR5^{low}$- and $CCR5^{high}$ Treg are nTreg. It has previously been reported that Treg isolated from CRC are nTreg by TSDR methylation analysis (193), but this study did not qualify Treg by CCR5 expression status. The idea that tumour-infiltrating Treg are nTreg is further supported by studies on the T cell receptor repertoire of both Treg and Tconv. It would be expected that if Treg were induced from Tconv in tumours, the T cell repertoire of both cell subsets would be similar. This has been tested in mouse tumour models, concluding that

tumour-infiltrating Treg are nTreg (323). A similar analysis has not been performed in human CRC.

The data presented in this chapter has shown that CCR5 expressed on CRC-isolated Treg is functional and has the potential to lead to Treg enrichment in CRC. Furthermore, CRC-resident Treg are naturally-occurring rather than induced by the microenvironment. To test whether CCR5 blockade leads to a reduction in tumour Treg recruitment, pharmacological inhibition of CCR5 was performed in murine models of CRC.

Chapter 6
Murine CRC models

Introduction

Evidence has so far been presented that naturally-occurring CCR5^{high} Treg exist in human CRC tissue and that these cells are suppressive and migrate towards their cognate chemokine in vitro. To test the hypothesis that this Treg population is specifically recruited to CRC, a murine model of CRC was used in conjunction with strategies to inhibit CCR5. A recent study has shown that intra-tumoral injection of the CCR6 ligand, CCL20, resulted in increased tumour Treg infiltration compared with controls (237). Therefore, in one experiment, CCR6 was inhibited and its effects on Treg recruitment assessed.

Different murine models of CRC

The ideal murine model of human CRC would replicate all aspects of human CRC including sequential development of genetic alterations with ensuing changes in cellular behaviour, leading to tumour progression and metastasis. Furthermore, the ideal model would replicate the host responses typically seen in the human and maintain sensitivity towards therapeutics (324). Practicalities require predictable and consistent tumour take within a narrow timeframe. With regard this latter point, chemically-induced cancer models would be inappropriate for CCR5 inhibition models due to the long timeframe and low incidence of cancer development. In terms of genetically modified mice, a popular murine CRC model is the APC min/+ model which has a dominant mutation in the APC gene (325). Unfortunately, the location of the

tumours in the majority of APC min/+ mouse variants is the small intestine rather than the colon and the tumours are adenomas rather than adenocarcinomas. The development of CRC in this model is not predictable and takes time to develop. This is the main reason why studies on drug efficacy in mouse models make use of allografts and xenografts (326). Subcutaneous (sc) implantation of murine carcinoma cells allows for rapid consistent tumour formation and is accessible to allow monitoring of tumour growth. However the sc microenvironment may differ from that of the colon, influencing the interaction with the host immune system, levels of cytokines and growth factors and response to therapeutic agents (327). To mimic the human CRC microenvironment, orthotopic models of CRC have been developed, injecting murine CRC cell lines into the caecal pole via laparotomy (328), colonic wall via colonoscopy (329) or into the rectal wall under direct visualisation (330). The experiments described in this chapter used an sc allograft model, principally to obtain comparable tumours in all grafted mice prior to treatment with CCR5 inhibitors. The sc allograft model was also chosen to enable easy monitoring of tumour growth and to facilitate recovery of whole tumour tissue for analysis at the end of the experiment.

Monitoring tumour growth

Traditionally, tumour growth in murine cancer models has been monitored by calliper measurements of the tumour axes (331). Bioluminescent imaging (BLI) of tumours has been shown to detect impalpable tumours containing as few as 10 000 cells at sc sites (332). The principal of tumour BLI is as follows: Tumour cells expressing the enzyme *luciferase*, convert a substrate known as *luciferin* into light via a chemiluminescent reaction (333). Photons from this reaction are then detected by an imaging system.

Tumour cell lines are modified to express luciferase prior to sc implantation in mice. Luciferin is given to mice, typically by intraperitoneal (ip) injection, prior to imaging. Imaging of the tumour can therefore be performed non-invasively at multiple time points. The technique is useful to allow imaging of impalpable tumours and detect metastasis (332,334). Measurements of tumour burden by BLI has also been shown to correlate well with calliper measurements (331).

Inhibition of CCR5

Studies investigating the role of CCR5 in mouse models of human disease are hampered by the fact that no selective antagonist of murine CCR5 currently exists (335). A neutralising antibody to murine CCR5 is also not available. In contrast, a human CCR5 small molecular antagonist, Maraviroc, has been approved for the treatment of patients with HIV infection, acting by inhibition of viral entry through the CCR5 receptor (336). The drug has an excellent safety profile, is highly selective for CCR5 and is administered orally (337). Maraviroc possesses no activity however against murine CCR5 (338).

Met-RANTES

Met-RANTES is a functional antagonist of CCR5. Essentially, met-RANTES is recombinant human RANTES (CCL5) with an additional methionine at the amino terminus (339). Met-RANTES has been shown to antagonise the chemotactic effects of the natural ligands for CCR5 as well as reducing the inflammatory infiltrate in a rat chronic allograft rejection model (340) and a murine breast cancer model (341). The drug acts by inhibiting passage of internalised CCR5 into recycling endosomes, preventing re-expression of the receptor at the cell surface (342). However, met-

RANTES is not a specific CCR5 antagonist, as it also binds and inhibits signalling through CCR1 and CCR3 (343).

TAK-779

TAK-779 is a small molecular weight non-peptide antagonist of human CCR5 that was developed for its activity against R5 HIV-1 virus replication (344). TAK-779 inhibits murine as well as human CCR5, but is not specific for this receptor. TAK-779 also antagonises murine CCR2, CCR5 and CXCR3 (345,346). TAK-779 has been used to antagonise murine CCR5 in a model of pancreatic cancer, whereby CCR5 blockade reduced the infiltration of Treg into sc tumours (104). The use of TAK-779 has resulted in reduced inflammatory cell infiltration over vehicle in colitis, transplant and autoimmune animal models (346–348).

Human CCR5 knock-in mouse

Given the lack of an antagonist specific for murine CCR5, yet the existence of a highly-specific human CCR5 antagonist approved for use in humans with HIV infection, a human CCR5 knock-in mouse (hCCR5 KI) was constructed by Pfizer Ltd, UK (335). The drug, UK-484900, is a selective and potent human CCR5 antagonist, equivalent to Maraviroc. Maraviroc undergoes extensive first-pass metabolism in the mouse whereas UK-484900 does not (349). A twice-daily dosing regime of UK-484900 in mice results in complete functional CCR5 blockade allowing the hCCR5 KI mouse together with UK-484900 to be used to study the effects of selective CCR5 antagonism. The model was validated by showing that human CCR5 is activated by murine chemokines with the same EC_{50} as for human chemokines (349). In the hCCR5 KI mouse, the murine CCR5 open-reading frame (ORF) was replaced by the human ORF, ensuring that CCR5

transcription was regulated by the same processes as for wildtype mice. The details of the construction of the hCCR5 KI vector are published (335). The targeting vector was electroporated into E14 129 ES cells. Heterozygous animals carrying the hCCR5 allele were bred to mice expressing Cre recombinase under the control of the E2A promoter. This removed the neomycin-resistance cassette of the vector. Animals were then bred to homozygosity.

Materials and methods

Cell lines

CT26 (a N-nitroso-N-methylurethrane induced undifferentiated colon carcinoma cell line, strain = BALB/c) and CMT93 (a methyl azoxymethanol acetate induced rectal carcinoma cell line, strain = C57BL/6) were purchased from the ATCC via LGC Standards, UK. CT26 and CMT93 cell lines were transduced to express luciferase, as detailed below. Luciferase-expressing B16-F10 cells (B16-F10-Luc, a melanoma cell line, strain = C57BL/6) was provided by Professor Antal Rot (University of Birmingham, UK).

Mice

BALB/c and C57BL/6 wildtype mice were purchased from Charles River, UK. Following a materials transfer agreement with Pfizer Inc, USA, hCCR5KI mice embryos were reconstituted and a mixture of homozygous hCCR5, heterozygous hCCR5 and wildtype offspring were shipped from Charles River, MA, USA to the University of Birmingham, UK. hCCR5 KI mice were bred, genotyped using an automated genotyping service

(Transnetyx Inc., USA) and homozygote offspring were used in subsequent experiments.

CCR5 inhibitors

Met-RANTES was a gift from Dr Amanda Proudfoot, Merck-Serono, Switzerland. TAK-779 (Repository reference: ARP968) was obtained from the Centre for AIDS Reagents, NIBSC and was donated by the AIDS Research and Reference Programme, Division of AIDS, NIAID, NIH. UK-484900 was a gift from Pfizer Inc, USA.

CCR6 inhibitor

CCR6 was inhibited using a rat anti-mouse CCR6 neutralising antibody (Clone: 140706, MAB590-100, R&D Systems). This antibody has been previously shown to neutralise murine CCR6, without resulting in cell depletion, in vivo. Following one antibody injection, its presence could be detected on the surface of $CD4^+$ cells, an effect that persisted for at least 8 days (350).

Luciferase transduction of murine CRC cell lines

A murine stem cell virus (MSCV) was used as a retroviral luciferase expression vector. Gag (packaging genes), pol (reverse transcriptase) and env (envelope genes) were removed and replaced by the insert gene. The viral vector still contained the long-terminal repeat required for insertion into the host genome, packaging signal (ϕ) and the transcription and processing elements i.e. the promoter associated with the insert gene. Gag, pol and env genes were integrated into the packaging cell line to minimise the chance of creating a replication-competent retrovirus. The insert gene contained luciferase and promoter RNA together with the PAC gene to convey resistance to

puromycin. The MSCV-luciferase puromycin-resistance plasmid was provided by Professor Antal Rot (University of Birmingham, UK).

Transfection of packaging cell line

The packaging cell line (Phoenix Ampho cells, ATCC, USA) was seeded into a 6-well plate at a density of $2x10^6$ cells per well in 4 ml DMEM and left overnight at 37˚C 5% CO_2. 10 µg plasmid DNA in 500 µl DMEM was mixed with 20 µl Lipofectamine® 2000 (11668, Life Technologies Ltd, UK) in 500 µl DMEM and left for 20 minutes at room temperature. The Phoenix Ampho cells were washed with 3 ml of DMEM and then 4 ml of DMEM + 1 ml DNA/Lipofectamine® mixture was added to each well. The cells were incubated overnight at 37˚C 5% CO_2. The medium in each well was replaced with 4 ml IMDM + 20% FCS and the cells were incubated for a further 24 hours, this time at 32˚C 5% CO_2. The viral supernatant was harvested every 24 hours for 5 days and replaced with fresh media. The viral supernatant was centrifuged for 10 minutes at 200 x *g* to remove cells, placed in 1 ml aliquots and stored at -80˚C.

Transduction of CT26 and CMT93 cells

CT26 or CMT93 cells were seeded into 4 wells of a 6-well plate at a density of $1x10^5$ cells per well in 4 ml DMEM + 10% FCS. Cells were cultured overnight so that they were 50% confluent. 1 ml viral supernatant was thawed and 4 µg Polybrene® (AL-118, Sigma-Aldrich Ltd, UK) was added. The media from each well was aspirated and replaced with 2 ml of DMEM 10% FCS supplemented with 4 µg/ml Polybrene®. The cells were incubated for 5 minutes at 37˚C. 2 ml of viral supernatant supplemented with Polybrene® was added to 3 of the 4 wells. A further 2 ml of DMEM + 10% FCS supplemented with 4µg/ml Polybrene® was added to the fourth *control* well. The well-

plate was centrifuged for 1 hour at 300 x *g* at room temperature. The supernatants were aspirated from each well and replaced with 4 ml DMEM + 10% FCS. The media was aspirated and replaced at 24 and 48 hours followed by puromycin selection.

Puromycin selection

At the same time as CT26 or CMT93 cells were seeded into a 6-well plate for transduction, 1 x 10^5 cells were seeded into 12 wells of a 24-well plate in preparation for a puromycin sensitivity assay. 1 ml of DMEM + 10% FCS was added to each well, supplemented with puromycin (A11138, Life Technologies Ltd, UK) at the following concentrations (μg/ml): 20, 15, 10, 7.5, 5, 2.5, 1.25, 0.63, 0.32, 0.16, 0. The cells were cultured for 72 hours in this media at 37˚C 5% CO_2. The cells were detached by trypsinisation and 100 μl of cell suspension from each well was placed in a separate well of a 96-well plate in triplicate. 10 μl of MTT reagent (V13154, Vybrant® MTT Cell Proliferation Assay Kit, Life Technologies Ltd, UK) was added to each well, mixed gently on an orbital shaker for 1 minute and then incubated at 37˚C for 4 hours. Dissolving solution was added and the absorbance from each well was read at 570 nm.

A puromycin concentration of 1.25 μg/ml effectively killed non-transduced CT26 cells, 0.32 μg/ml for non-transduced CMT93 cells. 3 of the 4 wells of the 6-well plate containing transduced CT26 (CT26-Luc) or CMT93 (CMT93-Luc) cells had puromycin added at the above concentration plus two higher concentrations. For example, for the CT26-Luc cells, one well had puromycin added at a concentration of 1.25 μg/ml, the second well at 2.5 μg/ml, the third well at 5 μg/ml and the fourth well had no puromycin added. The cells were cultured for a further 72 hours and live cells cultured in the highest puromycin concentration were harvested and further cultured in DMEM + 10% FCS. Stable luciferase expression was tested by splitting

the cells at 80% confluence, sampling into a 6-well plate with in DMEM + 10% FCS and then adding 200 µl luciferin immediately prior to BLI (see Figure 6-1).

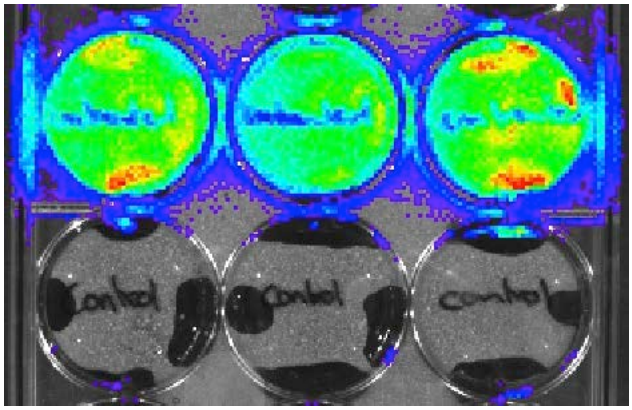

Figure 6-1: Luciferase-transduced CT26 cells (CT26-Luc). Control cells (bottom) did not express luciferase while expression was seen by CT26-Luc cells selected in puromycin (top).

Tumour cell in vitro proliferation assays

To test the effects of CCR5 inhibitors on tumour cell proliferation in vitro, 1 x 10^4 CT26-Luc, CMT93-Luc or B16-F10-Luc cells were seeded into wells of a 96-well plate in 200 µl of DMEM + 10% FCS. Met-RANTES, TAK-779, UK-484900 and PBS were added to wells at different drug concentrations in triplicate. The cells were then cultured for 24 hours at 37˚C 5% CO_2 at which point they had grown to 40-50% confluence. 20 µl of CellTiter 96® Aqueous One Solution (G3580, Promega Inc, USA), an MTT reagent, was added to each well using a multi-channel pipette. The well-plate was incubated at 37˚C for 3 hours and absorbance from each well was then read at 490 nm.

The murine pharmacokinetics of met-RANTES and TAK-779 are not known and it was not possible to assay drug levels in the serum or tissues. Individual doses of drug given to mice were 10 μg met-RANTES, 150 μg TAK-779 and 200 μg UK-484900, as has been used previously (104,297,341,347,349). Complete inhibition of radiolabelled CCL5 binding to CCR5 has been observed at 100 nM for both met-RANTES and TAK-779 (339,344), representing drug concentrations of 8 pg/ml and 53 pg/ml respectively. The pharmacokinetics of UK-484900 in the mouse has been studied (349) and a twice-daily sc dose of 200 μg leads to complete inhibition of CCR5 with a nadir serum concentration of 10 nM (equivalent to 6.5 ng/ml). The drug concentrations of met-RANTES, TAK-779 and UK-484900 used in the in vitro proliferation experiments were therefore likely to be higher than those found in the tissues in vivo.

Subcutaneous tumour models of CRC

Tumour cell suspensions were aspirated and expelled through a 25-gauge needle, then mixed with 0.4% Trypan blue solution (T8154, Sigma-Aldrich Ltd, UK). Cell viability was evaluated using a haemocytometer. All cell lines were 95% viable after passage through a 25-gauge needle and this gauge needle was therefore used for sc injection of tumour cells. At the start of the experiment, day 0, CT26-Luc cells were injected sc into the left flank of female BALB/c mice at a density of 5×10^5 cells in 100 μl of PBS. This density was shown in pilot experiments to produce a tumour less than 1.25 cm x 1.25 cm 10 days post-injection. CMT93-Luc were rejected by female mice in pilot experiments and by some male mice when injected in PBS. It was found that injection in extra-cellular matrix gel (ECM, E6909, from Engelbreth-Holm-Swarm murine sarcoma, Sigma-Aldrich Ltd, UK) resulted in viable tumours 10 days post-injection in

male mice. Therefore, CMT93-Luc cells were injected sc at day 0 into the left flank of male C57BL/6 mice at a density of 1 x 10^6 cells in 100 µl ECM gel. B16-F10-Luc cells were injected sc at day 0 into the left flank of hCCR5 KI mice at a density of 2.5 x 10^5 cells in 100 µl of PBS, as used previously by other investigators (351). All mice were weighed on day 0.

Tumours were barely palpable at day 7. Tumour engraftment was therefore ensured by BLI and was confirmed in all cases. Tumour growth was monitored by regular calliper measurements and BLI, according to the experiment schedule (see Figure 6-2). From day 7 up to and including day 17, mice were injected with either 10 µg met-RANTES ip once daily, 150 µg TAK-779 sc once daily or 200 µg UK-484900 sc twice daily. In some experiments, met-RANTES was delivered by an osmotic pump, in which case the daily total infusion was 10 µg. Mice were culled at day 17 following cardiac puncture. 200 µl blood was placed in a sterile Eppendorf. These blood samples were centrifuged at 350 x *g* for 10 minutes, the serum fraction was aspirated and stored at -80˚C. A further 500 µl blood was placed in a tube containing EDTA (Vacuette® 95057, Greiner Ltd, UK) on ice for lymphocyte isolation. Tumours and spleens were resected and placed in Bijous containing 10 ml cRPMI on ice. Bijous were weighed pre- and post-sampling to calculate the tumour weight.

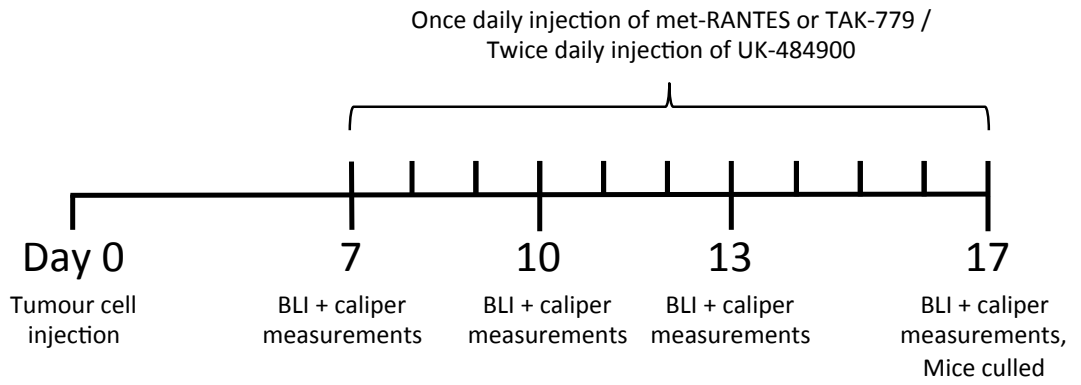

Figure 6-2: Subcutaneous (sc) tumour experiment schedule. BLI = bioluminescence imaging.

Sample preparation

In some cases, a small piece of tumour tissue was taken and placed in formal saline or snap frozen and stored at -80˚C, for later immunohistochemical or protein analysis, respectively. Whole tumour and spleen tissue in 10 ml cRPMI was transferred into C-tubes (Miltenyi Biotech) and spun on the gentleMACS dissociator using the Mouse-Spleen-1 protocol. Dissociated samples were then passed through a 70 µm cell strainer (08-771-2, Corning Inc, USA), pelleted and resuspended in 500 µl cRPMI. 500 µl blood samples were mixed with 5 ml red cell lysis buffer (R7757, Sigma-Aldrich Ltd, UK) and agitated for 5 minutes. The blood / lysis buffer mixture was then washed twice with 20 ml PBS and resuspended in 500 µl cRPMI. 0.5 µl of near-IR live/dead fixable stain (L10119, Life Technologies Ltd, UK) and 20 µl mouse serum (M5905, Sigma-Aldrich Ltd, UK) were added to tumour, spleen and blood samples. Samples were incubated for 20 minutes at 4˚C in the dark. 1 ml of ice-cold cRPMI was added to each sample and the samples were pelleted. Blood and tumour samples were resuspended in 500 µl cRPMI and spleen samples were resuspended in 2 ml of cRPMI. 1.5 ml of the spleen cell suspensions were discarded or used for single colour compensation controls. Cell

surface labelling was performed by incubating 500 µl of cell suspensions with the antibodies listed in Table 6-1 (excluding the anti-foxp3 antibody) for 45 minutes at 4˚C in the dark on the rocker. The hCCR5 antibody was used for experiments involving hCCR5 KI mice, otherwise the mCCR5 was used. Intra-cellular staining for foxp3 was performed as described in Chapter 2: Intra-cellular staining, using a rat anti-mouse foxp3 antibody as listed in Table 6-1.

Table 6-1: Cell surface and intra-cellular antibodies used for labelling of blood, spleen and tumour lymphocytes. mCCR5 = murine CCR5; hCCR5 = human CCR5.

Antigen	Clone	Fluorochrome	Isotype	Manufacturer	Code
CD3	145-2C11	PE-Cy7	Hamster IgG	Biolegend	100320
CD4	RM4-5	V500	Rat IgG2a	BD	560782
CD8	53-6.7	PE-CF594	Rat IgG2a	BD	562283
mCCR5	HM-CCR5	APC	Hamster IgG	Biolegend	107012
DX5	DX5	FITC	Rat IgM	Biolegend	108906
CXCR3	CXCR3-173	BV421	Hamster IgG	Biolegend	126521
hCCR5	CTC5	APC	Ms IgG1	R&D	FAB1802A
Foxp3	FJK-16s	PE	Rat IgG2a	eBioscience	12-5773

Flow cytometric analysis

Immediately prior to sample analysis, 20 µl of counting beads (AccuCheck PCB100, Life Technologies Ltd, UK) were added to the labelled cell suspension. Samples were analysed using the Cyan ADP flow cytometer and Summit 4.3 software (Beckman Coulter Inc, USA). Gating on lymphocytes was based on forward and side light scatter

followed by cell surface expression of CD3 and absence of dead cell staining. The Treg population was defined by gating on $CD4^+$ and $foxp3^+$ cells. The Tconv population was defined by gating on $CD4^+$ and $foxp3^-$ cells (see Figure 6-3).

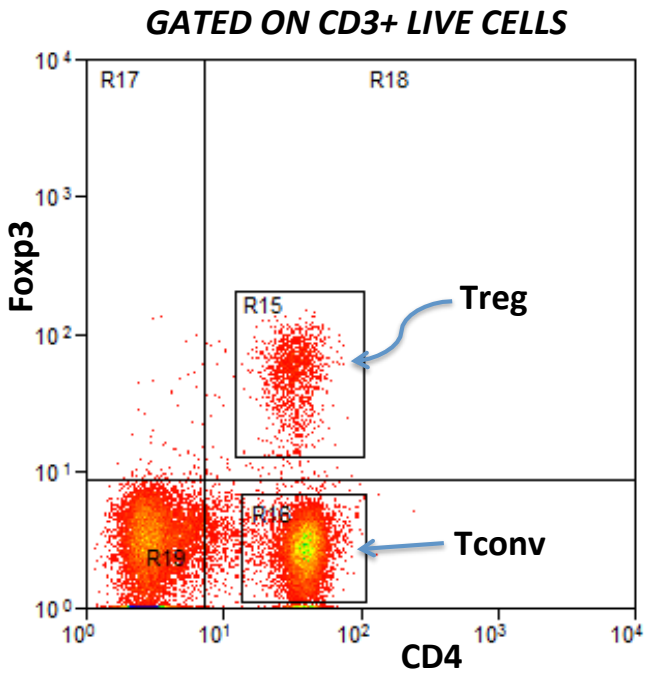

Figure 6-3: Gating strategy to define Treg and Tconv in blood, spleen and tumour samples by flow cytometry.

The proportion and absolute number of live $CD3^+$ cells that were $CD4^+$ or $CD8^+$ were evaluated. The proportion and absolute number of live $CD3^+$ $CD4^+$ cells that were Treg or Tconv were evaluated. CCR5 expression by different cell subsets was measured.

ELISA

Protein lysates were made from the tumour tissue samples as described in Chapter 2: Protein detection by Western blotting. Lysate total protein concentrations were

normalised to 300 μg/ml. Serum and tumour concentrations of CCL3, CCL4, CCL5 and VEGF were measured using a Mix-N-Match ELISArray Kit (336111, SABiosciences) and a mouse VEGF ELISA kit (MMV00, R&D Systems Inc, USA), according to manufacturer's instructions. Standard curves were not derived for each chemokine and absorbance was therefore the read-out in this semi-quantitative assay.

Immunohistochemistry

A tissue microarray was constructed from FFPE tumour samples. Sections were deparaffinised and rehydrated and immunohistochemistry was performed according to the methods described in Chapter 2: Common immunohistochemistry protocol. Sections were stained for CD31 (rabbit anti-mouse CD31, sc-28188, Santa Cruz Inc, USA, dilution 1/50) or isotype-control antibody at the same concentration.

Results

Chemokine receptor expression by tumour cell lines

Chemokine receptor expression by cultured tumour cell lines was assessed by flow cytometry (see Figure 6-4). Approximately one-third of CT26-Luc cells were found to express surface CCR5 and a smaller proportion expressed surface CCR6. B16-F10-Luc cells expressed both surface murine CCR5 and murine CCR1, but, as expected, not human CCR5. None of the cell lines expressed surface murine CXCR3.

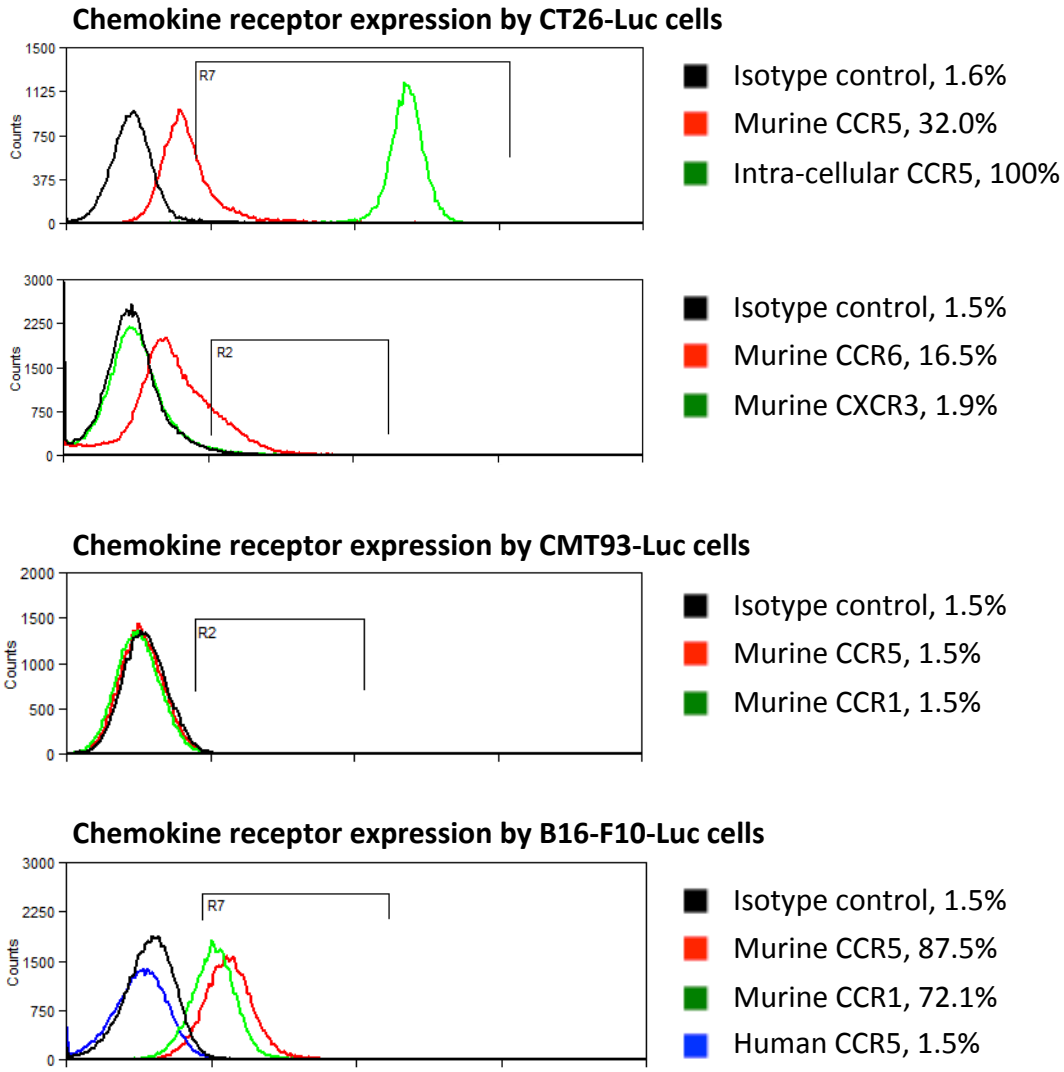

Figure 6-4: Chemokine receptor expression by tumour cell lines, as measured by flow cytometry. Quoted figures represent percentage chemokine receptor expression by cell line compared with isotype control antibody.

In vitro proliferation

The addition of met-RANTES to the culture media had no effect on CT26-Luc proliferation (see Figure 6-5). Similarly, UK-484900 had no effect on B16-F10-Luc or CMT93-Luc proliferation at doses of 250 µg/ml or less. There was some inhibition of

B16-F10-Luc proliferation at a dose of 500 µg/ml of UK-484900, although this difference did not reach statistical significance. TAK-779 significantly inhibited the proliferation of CT26-Luc cells at all studied doses.

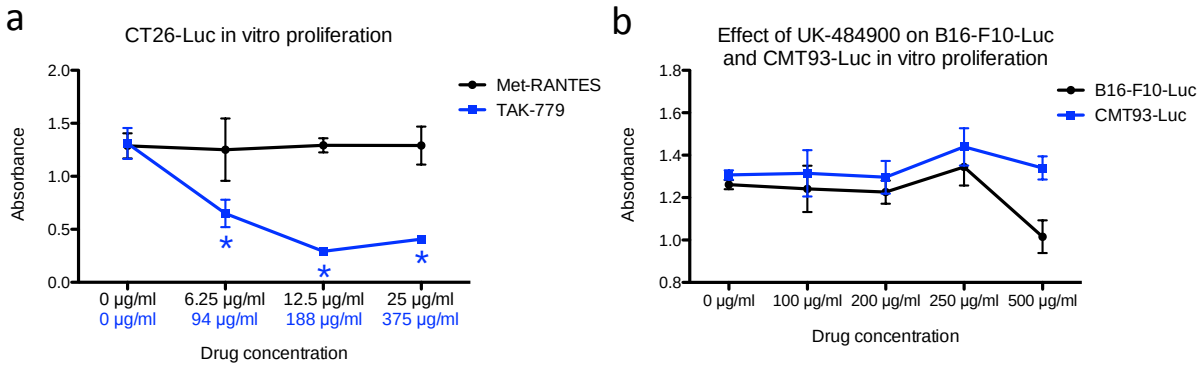

Figure 6-5: In vitro proliferation of tumour cell lines. (a) CT26-Luc proliferation in media containing different concentrations of met-RANTES (black) and TAK-779 (blue). Proliferation of B16-F10-Luc (black) and CMT93-Luc (blue) in media containing different concentrations of UK-484900. Data represent the mean absorbance of triplicate repeats. The error bars represent the standard error of the mean.

CCR5 expression by TILs

CCR5 expression by TILs isolated from control group tumours at day 17 were analysed by flow cytometry. Percentage and MFI expression by Treg was compared with expression by Tconv and $CD8^+$ TILs (see Figure 6-6a+b). Tumour Treg expressed significantly more CCR5, in terms of both percentage expression and MFI, than Tconv for all three cell lines. Treg also expressed significantly more CCR5 than $CD8^+$ cells with respect to B16-F10-Luc tumours. Tumour-isolated Treg expressed significantly more CCR5 than lymphocytes isolated from spleen and blood, in term of both percentage expression and MFI (see Figure 6-6c+d).

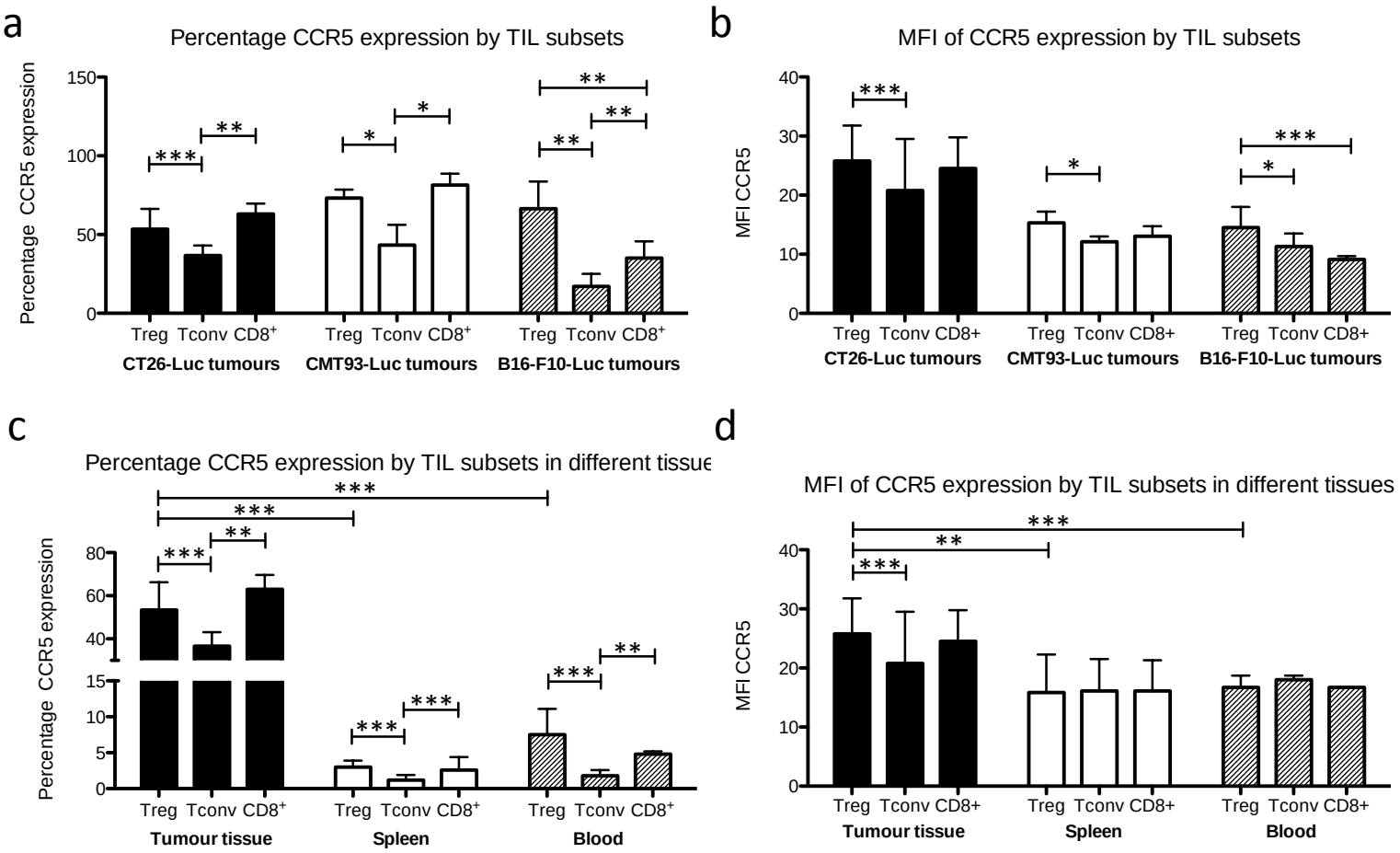

Figure 6-6: CCR5 expression by TILs isolated from control group tumours at day 17, in terms of (a) percentage expression and (b) MFI. Black bars = CT26-Luc tumours (16 unique tumours); White bars = CMT93-Luc tumours (6 unique tumours); Shaded bars = B16-F10-Luc tumours (11 unique tumours). CCR5 expression by lymphocytes isolated from 16 CT26-Luc control group tumours with matched spleen and blood: (c) percentage expression and (d) MFI. Black bars = tumour; White bars = spleen; Shaded bars = blood. Bars represent median expression; error bars represent the IQR. Capped lines indicate statistically significant differences (Wilcoxin signed-rank test).

CCR5 inhibition with met-RANTES by continuous infusion

The effect of met-RANTES on CT26-Luc tumour growth and Treg infiltration compared to control (PBS) injection in 10 8-week old female BALB/c wildtype mice was first evaluated by delivering met-RANTES or PBS via an ALZET® osmotic pump (Model 1004, Charles River, UK). The pump was placed in a surgically-created sc pouch in the inter-scapular area under general anaesthesia at day 7. The pump delivered a continuous sc infusion of met-RANTES at a rate of 10 μg / 24 hours (treatment group) or PBS (control group). One mouse in the control group died prior to implantation of the pump and another mouse from the control group was culled before the end of the experiment, as the pump insertion wound broke down. This left only 3 mice in the control group compared to 5 mice in the treatment group. The main results of tumour growth monitoring and flow cytometric analysis of TILs are shown in Figure 6-7. There were no differences in absolute numbers of tumour-infiltrating Treg or other TILs between treatment groups.

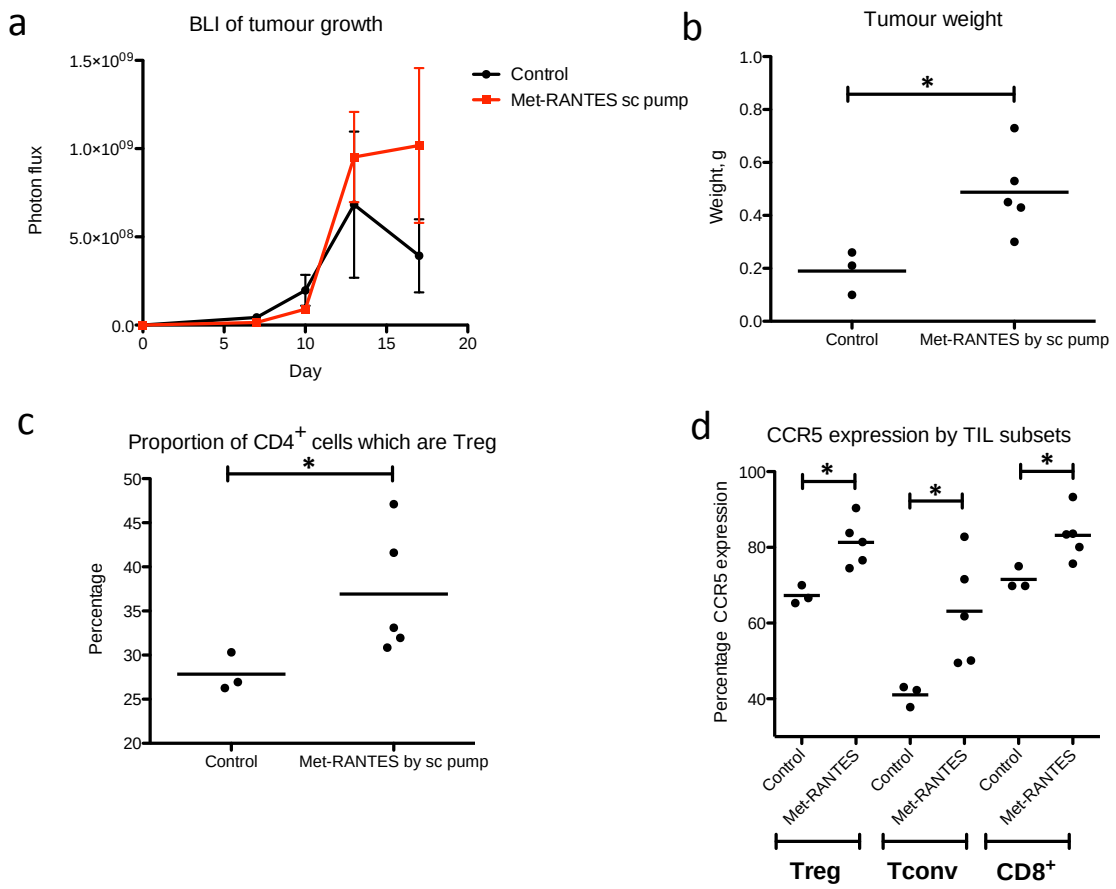

Figure 6-7: The effects of sc osmotic pump delivery of PBS (control group, n=3) or met-RANTES (treatment group, n=5) in CT26-Luc tumour-bearing BALB/c wildtype mice. Tumour growth was measured by (a) BLI and (b) tumour weight post-resection. Mean values are shown. Error bars represent the standard error of the mean. Capped lines indicate statistically significant differences (Mann-Whitney test). sc = subcutaneous.

It was surprising that tumours in the treatment group were larger than those in the control group. As met-RANTES has previously been reported to have partial agonist activity (352,353), it was hypothesised that met-RANTES may have exhibited a CCL5-like direct stimulation of CT26-Luc cell proliferation in this experiment. Therefore, the

experiment was repeated using ten 8-week old female BALB/c mice but on this occasion, met-RANTES was delivered by a continuous infusion of met-RANTES ip. This was achieved by performing laparotomies on all mice at day 7, then implanting osmotic pumps, containing either PBS or met-RANTES, into the peritoneal cavity. The main results from this experiment are shown in Figure 6-8. Again, met-RANTES treatment resulted in significantly larger tumours by BLI and calliper measurement compared to the control group, although this was not reflected in a significant increase in tumour weight post-resection.

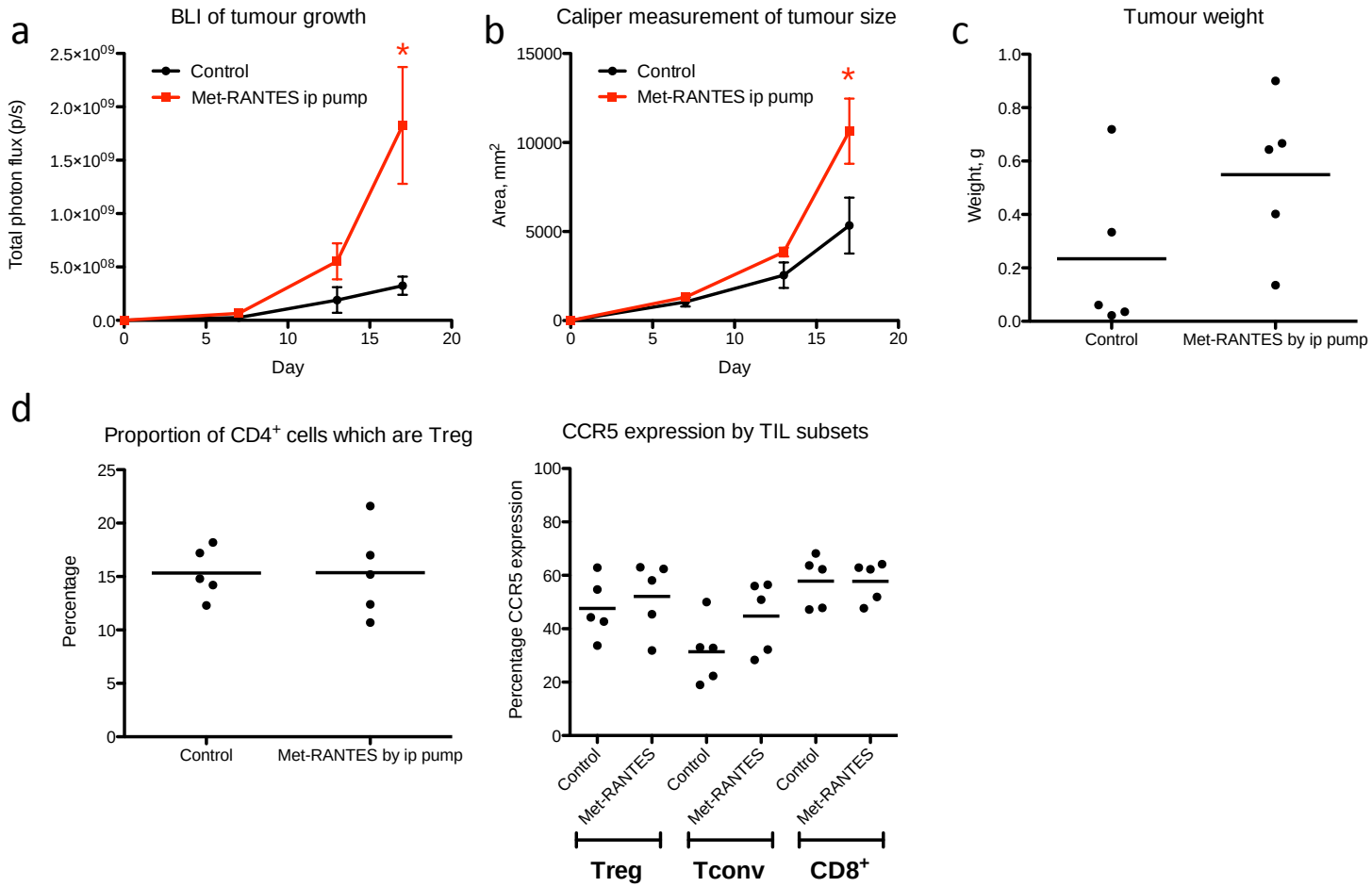

Figure 6-8: The effects of ip osmotic pump delivery of PBS (control group, n=5) or met-RANTES (treatment group, n=5) in CT26-Luc tumour-bearing BALB/c wildtype mice. Tumour growth was measured by (a) BLI, (b) calliper measurements and (c) tumour weight post resection. Mean values are shown. Error bars represent the standard error of the mean. Asterisks '*' indicate statistically significant differences in tumour growth at a given time point (Mann-Whitney test, $P<0.05$). ip = intra-peritoneal.

With delivery of met-RANTES by the ip route as opposed to the sc route, there was no difference in tumour Treg proportion and no difference in TIL CCR5 expression between the control and treatment groups.

CCR5 inhibition with met-RANTES and TAK-779 by repeated injection

It was hypothesised that delivery of met-RANTES by repeated injection might have different effects on tumour growth and Treg infiltration compared to delivery by continuous infusion. The experiment was therefore repeated using 27 8-week old female BALB/c mice (9 mice in each group), giving PBS (control group) or met-RANTES by once daily ip injection. A second treatment group received TAK-779 by once daily sc injection. The main results from this experiment are shown in Figure 6-9. Delivery of met-RANTES by once daily injection resulted in significantly delayed tumour growth by BLI, calliper measurement and tumour weight post-resection compared with controls. TAK-779 treatment also resulted in significantly delayed tumour growth. However, neither drug treatment was associated with a change in the tumour Treg proportion or a change in CCR5 expression by TIL subsets compared with controls. There were no differences in the absolute numbers of tumour-infiltrating Treg or other TILs between treatment groups.

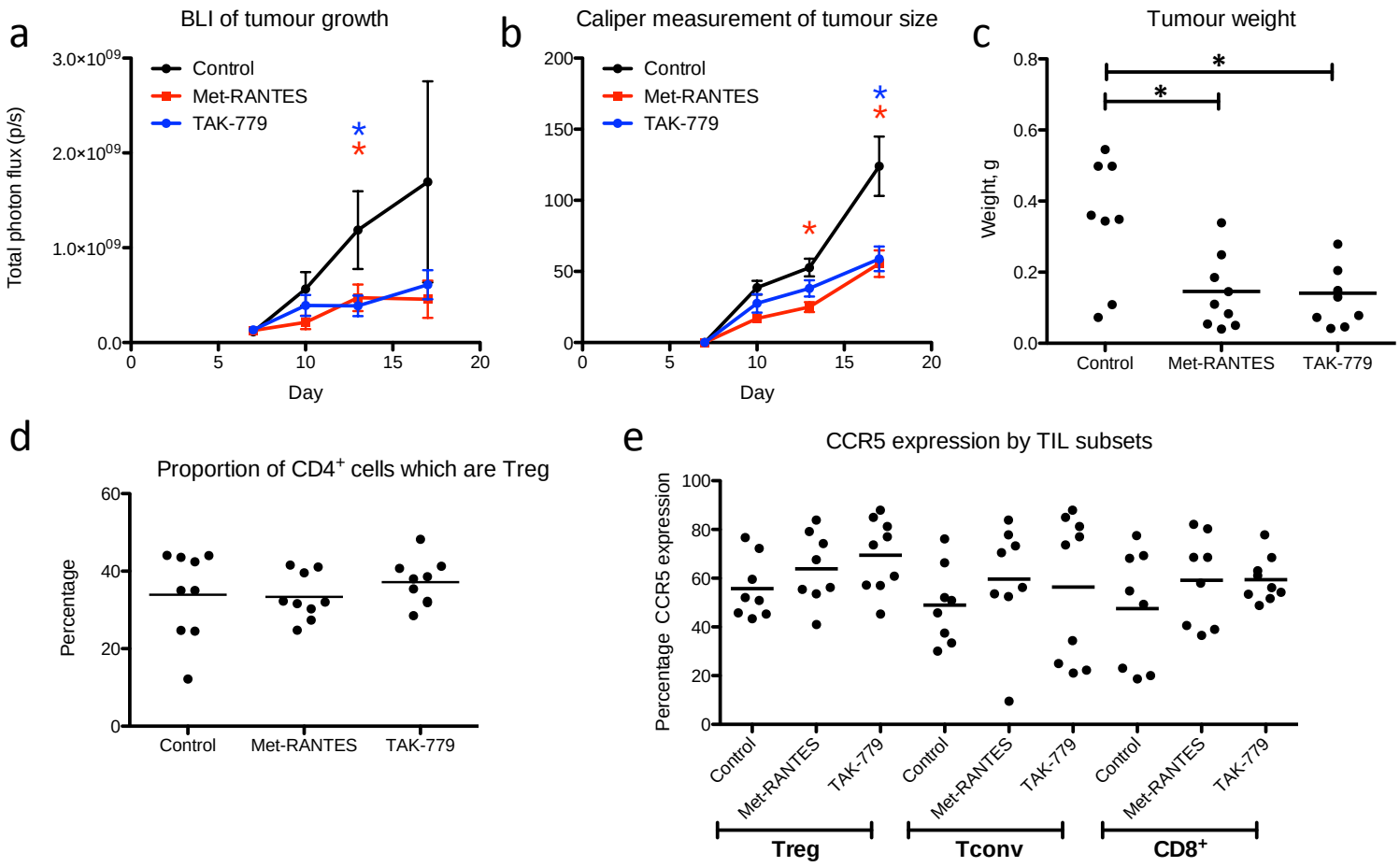

Figure 6-9: Once daily injection of PBS (control group, black, n=8), met-RANTES (red, n=9) or TAK-779 (blue, n=8) in CT26-Luc tumour-bearing BALB/c wildtype mice. Tumour growth was measured by (a) BLI, (b) calliper measurements and (c) tumour weight post resection. Mean values are shown. Error bars represent the standard error of the mean. Asterisks '*' indicate statistically significant differences in tumour growth at a given time point (Mann-Whitney test). Capped lines indicate statistically significant differences between groups (Mann-Whitney test).

CCR5 inhibition by UK-484900

Given the non-specific nature of CCR5 antagonism exhibited by met-RANTES and TAK-779, UK-484900 was used to specifically antagonise human CCR5 in hCCR5 KI mice. The same schedule as before was followed (see Figure 6-2), with mice receiving either twice daily sc PBS (control group) or twice daily sc UK-484900 (treatment group). hCCR5 KI mice are of a C57BL/6 background and therefore CMT93-Luc tumours were established as opposed to CT26-Luc. CMT93-Luc tumour cells were injected into 10 male mice, aged 7-9 weeks in ECM gel. The main results from this experiment are shown in Figure 6-10. There was no difference in tumour growth or the tumour Treg proportion in mice treated with UK-484900 compared with controls. However, tumours were rejected in 2 out of 8 mice in the control group and 3 out of 7 mice in the treatment group. There was also no progressive tumour growth between days 7 and 17, as was observed in the previous experiments. Problems with CMT93-Luc tumour establishment had previously been noted, as discussed in the above section: Subcutaneous tumour models of CRC. However, the use of male mice and injection of tumour cells in ECM gel had previously resulted in established tumours in 10 out of 10 C57BL/6 wildtype mice.

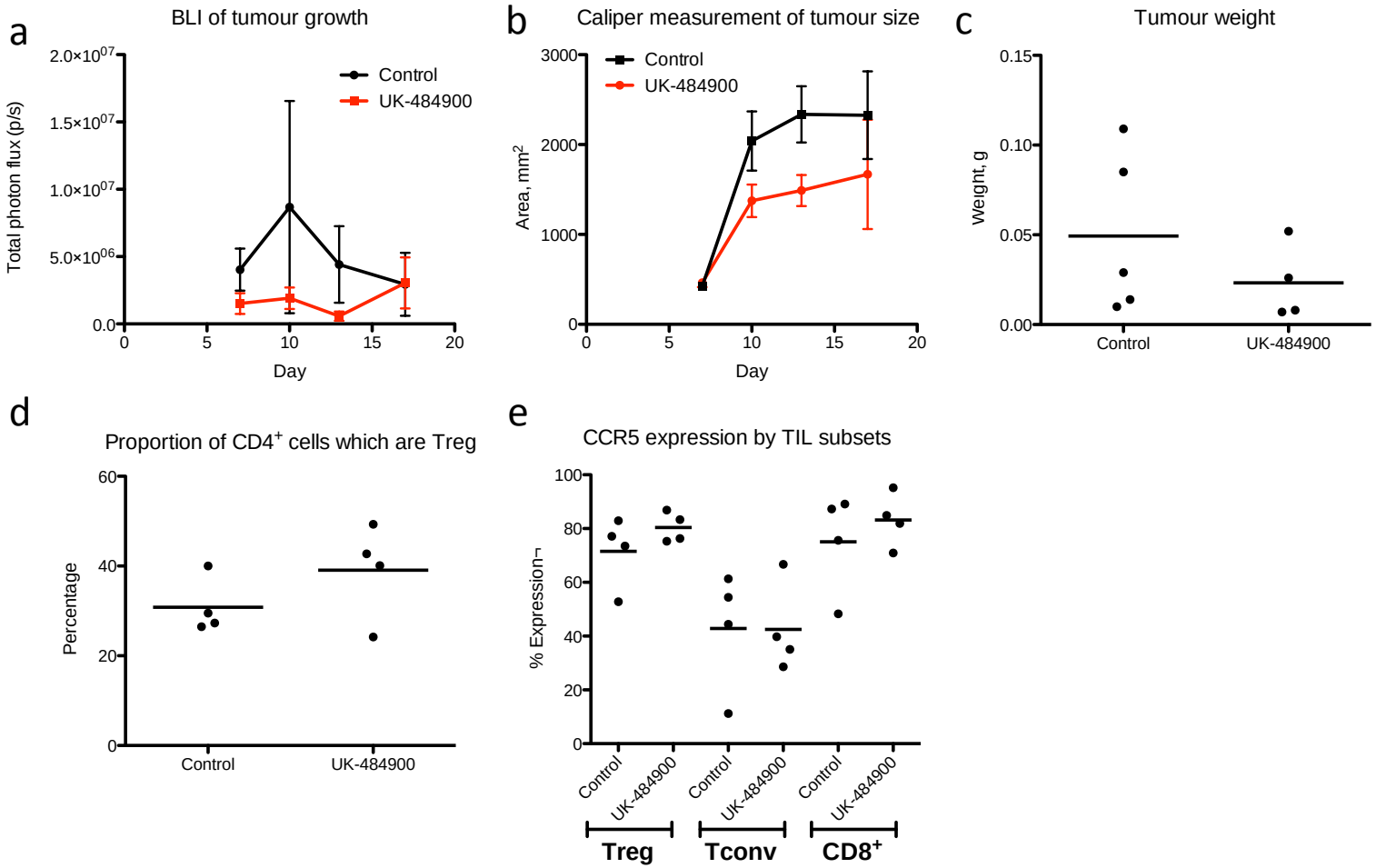

Figure 6-10: Twice daily injection of PBS (control group, n=5) or UK-484900 (red, n=4) in CMT93-Luc tumour-bearing hCCR5 KI mice. Tumour growth was measured by (a) BLI, (b) calliper measurements and (c) tumour weight post resection. Mean values are shown. Error bars represent the standard error of the mean.

A different cell line, B16-F10-Luc was therefore used to establish tumours in hCCR5 KI mice, which grew progressively in the time period of the experiment schedule and were not rejected. Despite B16-F10-Luc not being a CRC cell line, B16-F10-Luc tumours were enriched with Treg and the pattern of CCR5 expression by TIL subsets was similar to that seen in CT26-Luc and CMT-93 tumours (see Figure 6-6) as well as in human CRC (see Figure 3-5). B16-F10-Luc tumours were therefore established in 10 female hCCR5 KI mice, aged 7-9 weeks, and mice were then treated, as before, with either twice daily sc PBS (control group) or twice daily sc UK-484900 (treatment group). The results from this experiment are shown in Figure 6-11. Treatment with UK-484900 made no difference to the tumour growth or the tumour Treg proportion compared with controls. There was however significantly greater CCR5 percentage expression by tumour-infiltrating Treg in the treatment group compared with controls (Figure 6-11e) and a significantly greater CD8 : CD4 ratio in the treatment group compared with controls (see Figure 6-11f). There were no differences in the absolute numbers of tumour-infiltrating Treg or other TILs between treatment groups.

In spite of the tumour growth now being progressive with no observed tumour rejection, in conjunction with specific human CCR5 inhibition provided by UK-484900, the model did not demonstrate delayed tumour growth with associated reduced Treg infiltration as has been previously published in CCR5 -/- models (104,233).

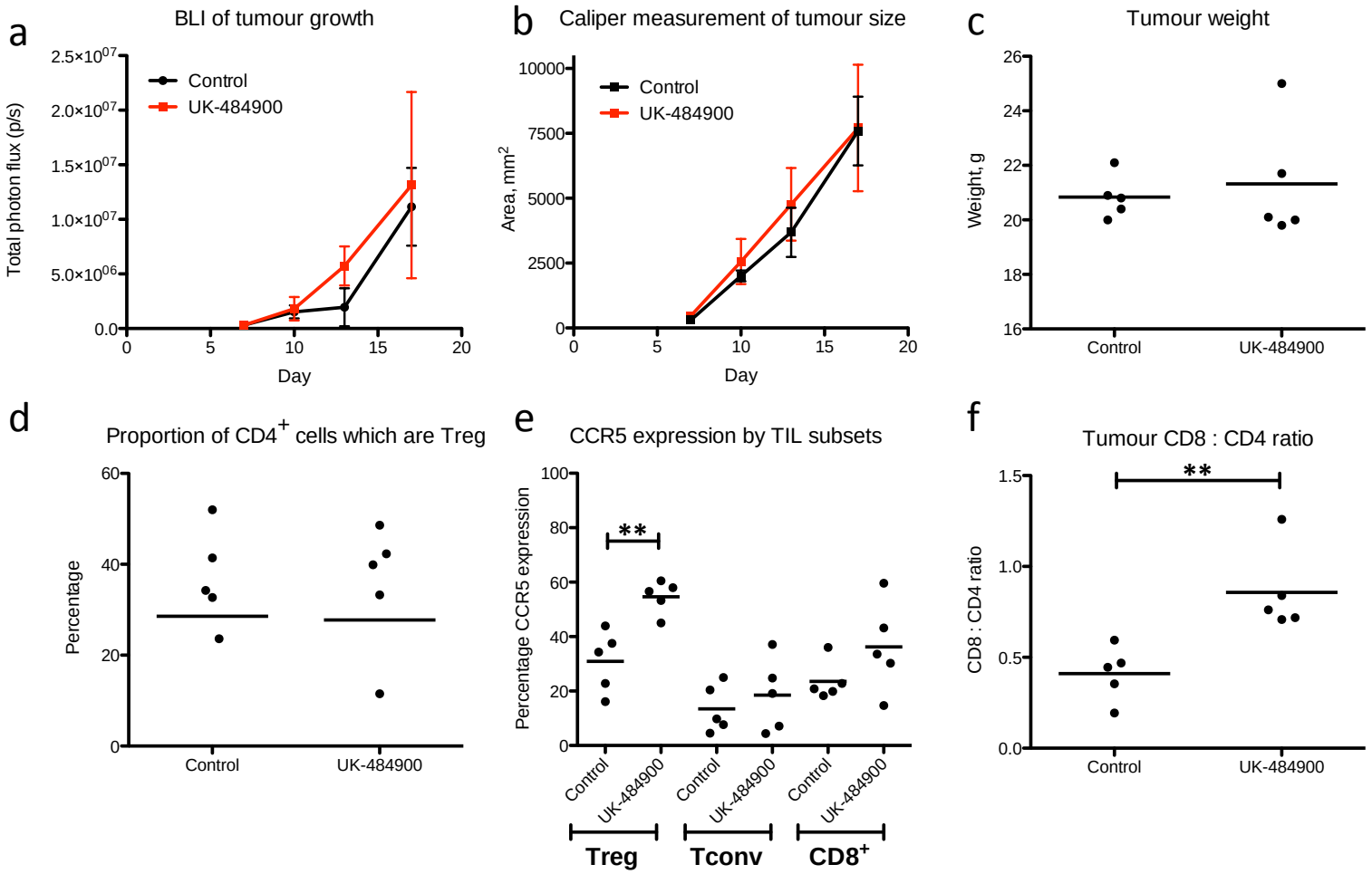

Figure 6-11: Twice daily injection of PBS (control group, n=5) or UK-484900 (red, n=5) in B16-F10-Luc tumour-bearing hCCR5 KI mice. Tumour growth was measured by (a) BLI, (b) calliper measurements and (c) tumour weight post resection. Mean values are shown. Error bars represent the standard error of the mean. Capped lines indicate statistically significant differences between groups (Mann-Whitney test).

In order to determine if CCR5 inhibition is required from the time of tumour cell injection to produce such effects, B16-F10-Luc tumours were established in 10 female hCCR5 KI mice, aged 7-9 weeks, and treatment with either twice daily sc PBS (control group) or twice daily sc UK-484900 (treatment group) was commenced from day 0. The duration of the experiment was 10 days, at which point mice were culled and blood, spleen and tumour tissue were analysed as before. The results from the experiment are shown in Figure 6-12.

Treatment of hCCR5 KI mice with UK-484900, commencing at the time of tumour cell injection, resulted in significantly delayed tumour growth compared with controls. There was no difference in the tumour Treg proportion between control and treatment groups. Unlike the previous experiment, where treatment was commenced 7 days post-tumour cell injection, there was neither a difference in CCR5 expression by tumour-isolated Treg nor in the tumour CD8 : CD4 ratio between control and treatment groups. There was also no difference in the proportion of live lymphocyte-gated cells that were $DX5^+$ (NK cells) or in the proportion of live $CD3^+$ cells that were $DX5^+$ (NKT cells) between control and treatment groups (data not shown).

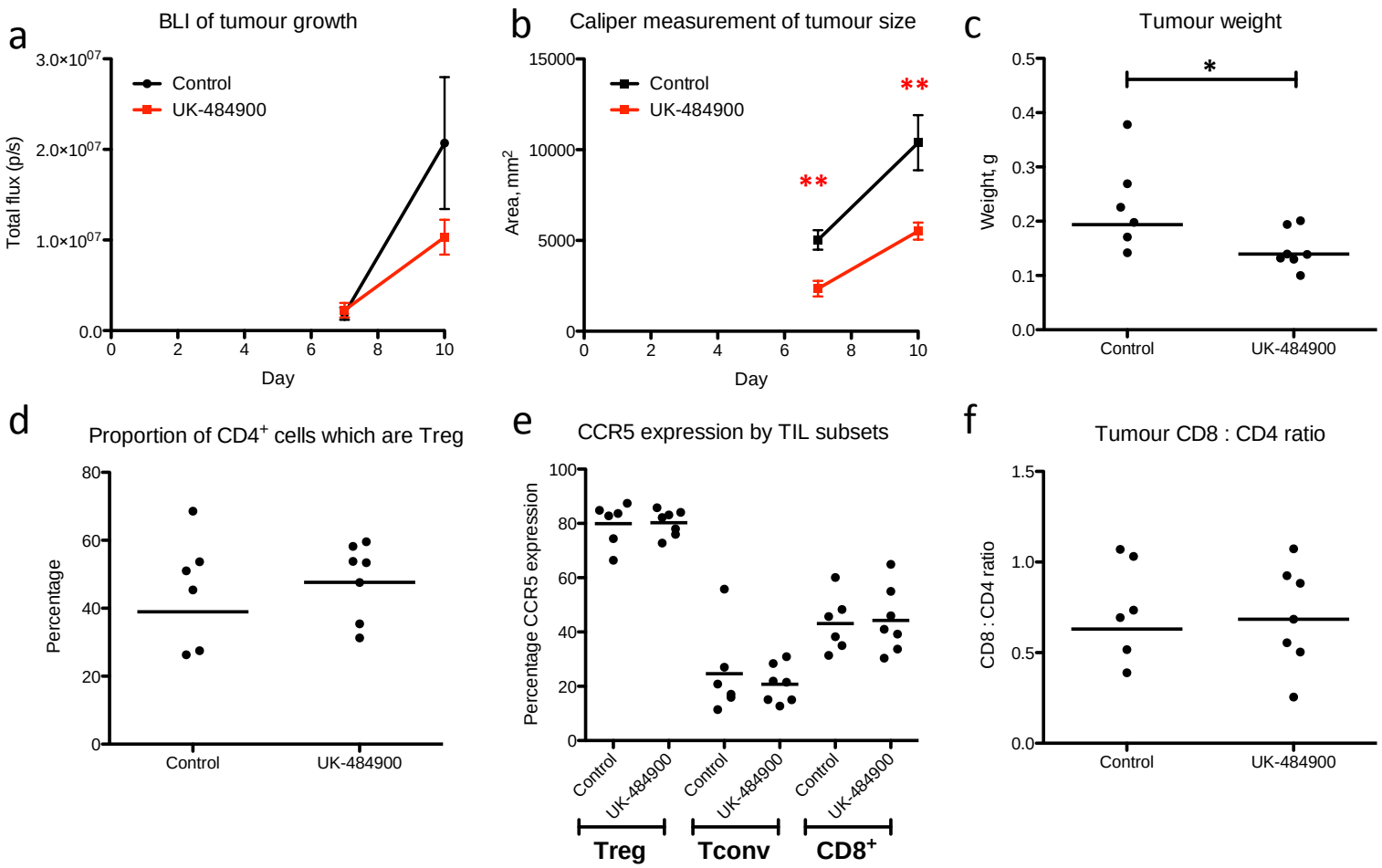

Figure 6-12: Twice daily injection of PBS (control group, n=6) or UK-484900 (red, n=7) in B16-F10-Luc tumour-bearing hCCR5 KI mice. Treatment was commenced at the time of tumour cell injection. Tumour growth was measured by (a) BLI, (b) calliper measurements and (c) tumour weight post-resection. Mean values are shown. Error bars represent the standard error of the mean. Asterisks '*' represent statistical significant differences in tumour growth at a specific time point (Mann-Whitney test). Capped lines indicate statistically significant differences between groups (Mann-Whitney test).

The absolute numbers of cells per gram of tumour tissue were calculated using counting beads (see Figure 6-13). There were no differences in the absolute numbers of cells between control and treatment groups.

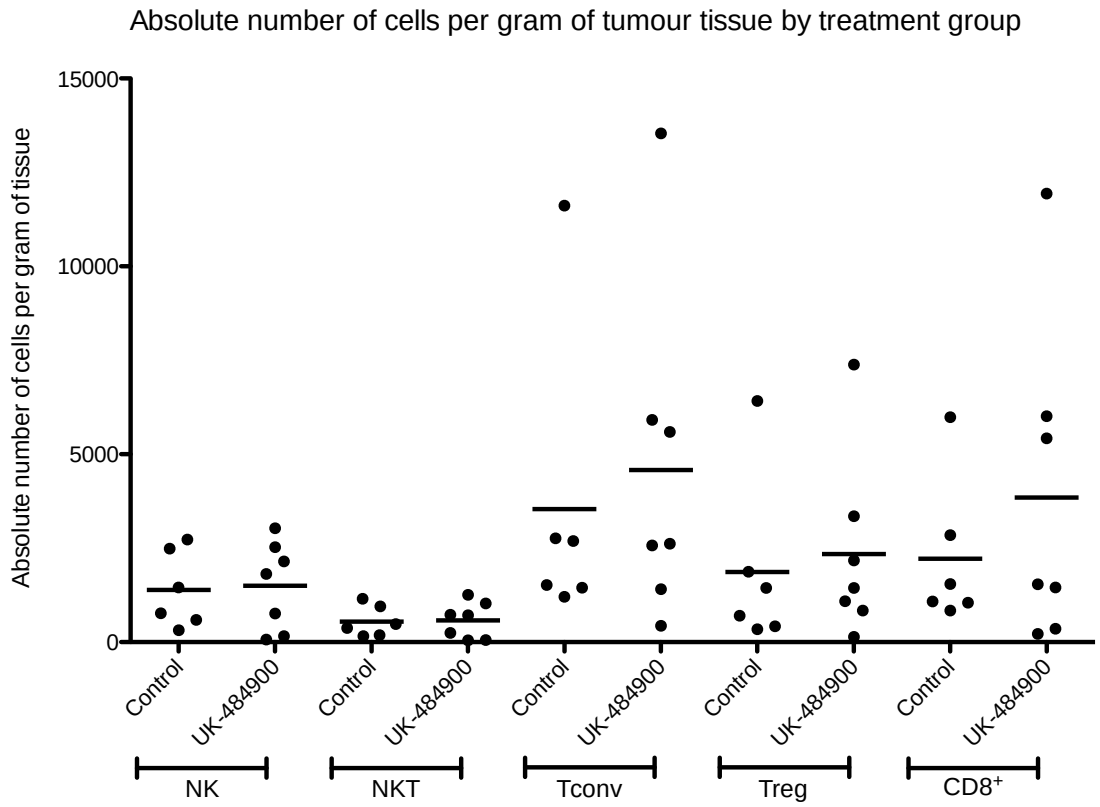

Figure 6-13: Absolute number per gram of tissue of different cell types infiltrating B16-F10-Luc tumours by treatment group.

CCR5 ligand concentrations in serum and tumour tissue

Small pieces of tumour tissue and serum were obtained from 4 control mice and 4 UK-484900-treated mice from the experiment described in the previous paragraph. Semi-quantitative measurements of CCL3, CCL4 and CCL5 concentrations in serum and tumour protein lysates were performed. There was a trend for higher levels of all

measured chemokines in the tumours of mice treated with UK-484900 compared with controls (see Figure 6-14), with the difference in CCL5 reaching statistical significance. Similarly, CCL5 levels were significantly higher in the serum of mice treated with UK-484900 compared with controls. Serum levels of CCL3 and CCL4 were undetectable.

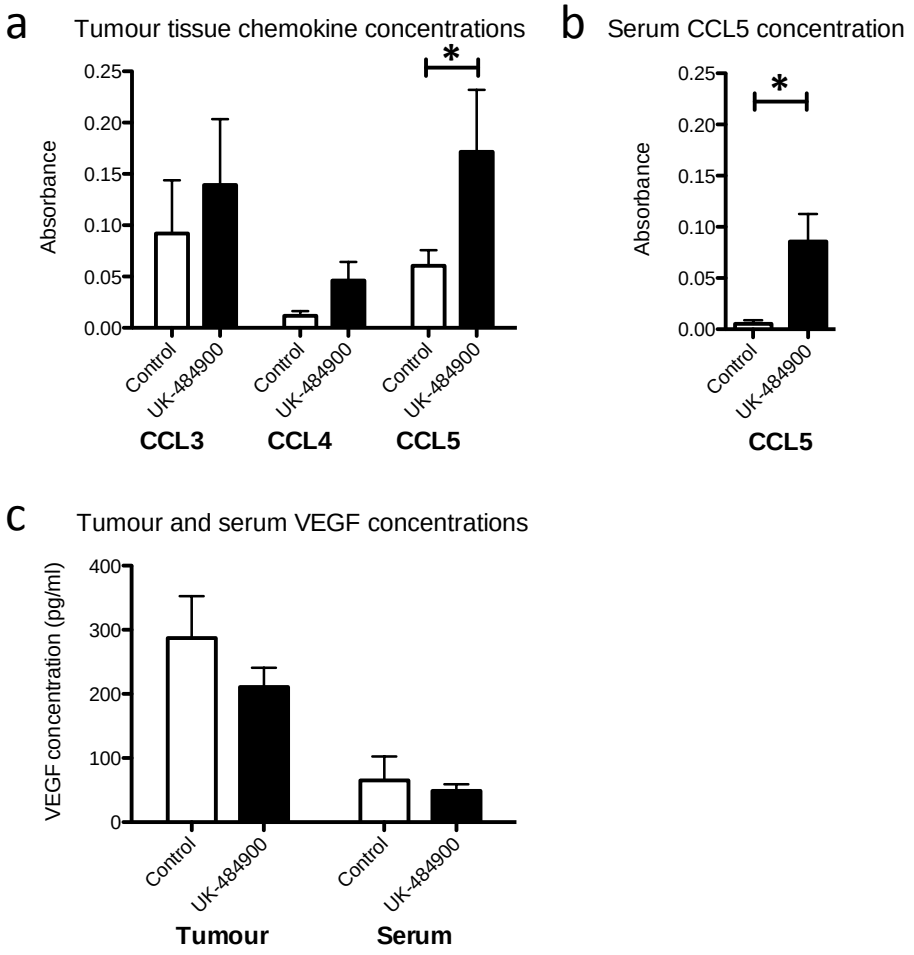

Figure 6-14: Tumour (a) and serum (b) levels of CCL3, CCL4 and CCL5 from hCCR5 KI mice treated with PBS (Controls, n=4) or UK-484900 (n=4) were measured semi-quantitatively. (c) Tumour and serum levels of VEGF from the same mice. Mean values are shown with error bars representing the standard error of the mean. Capped lines indicate statistically significant differences (Mann-Whitney test).

There was a trend for lower tumour and serum VEGF levels in UK-484900 treated mice compared with controls, although these differences did not reach statistical significance.

CD31 immunohistochemistry

A tissue microarray was constructed from FFPE tumour samples and stained for CD31 by immunohistochemistry. Unfortunately, there was scant $CD31^+$ endothelium observed within the small tissues samples, rendering a comparison of staining density between control and treatment groups impossible (see Figure 6-15).

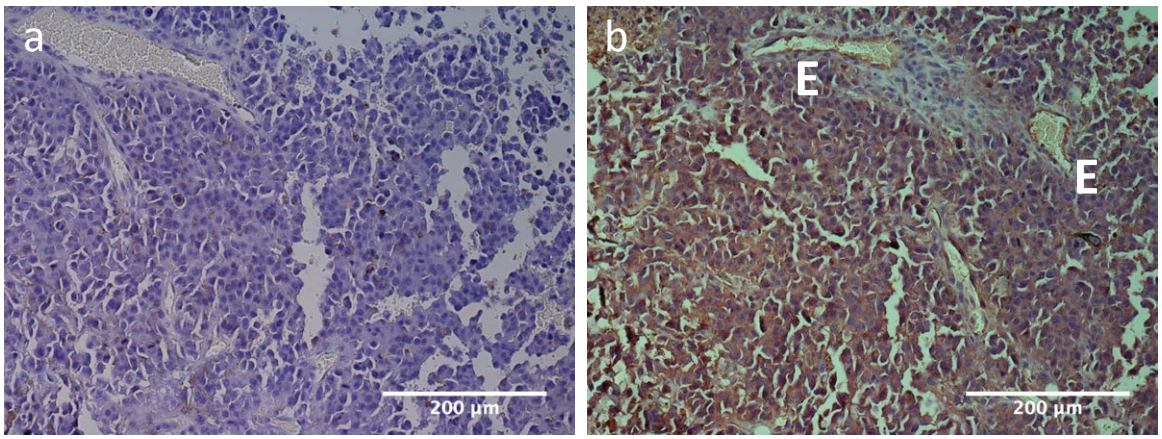

Figure 6-15: Immunohistochemistry of B16-F10-Luc tumours for (a) isotype control antibody and (b) CD31 at the same concentration. Magnification x200. Section from a single tumour shown, representative of sections from 8 different tumours. E = positive endothelial staining for CD31. Unfortunately, no vessels were seen within the majority of tumours, rendering comparison of staining density between control and treatment groups impossible.

CCR6 inhibition

The effects of CCR6 inhibition on tumour growth and Treg infiltration were tested in one experiment. CT26-Luc tumours were established in 10 8-week old female BALB/c mice as before. At day 7, the treatment group received a one-off dose of 100 μg of rat anti-mouse CCR6 antibody in 100 μl of PBS by tail vein injection. The control group received 100 μg of rat IgG2a immunoglobulins (MAB006, R&D Systems) in 100 μl PBS via tail vein injection. The main results from this experiment are shown in Figure 6-16. CCR6 inhibition did not result in any differences in tumour growth or Treg infiltration compared with controls.

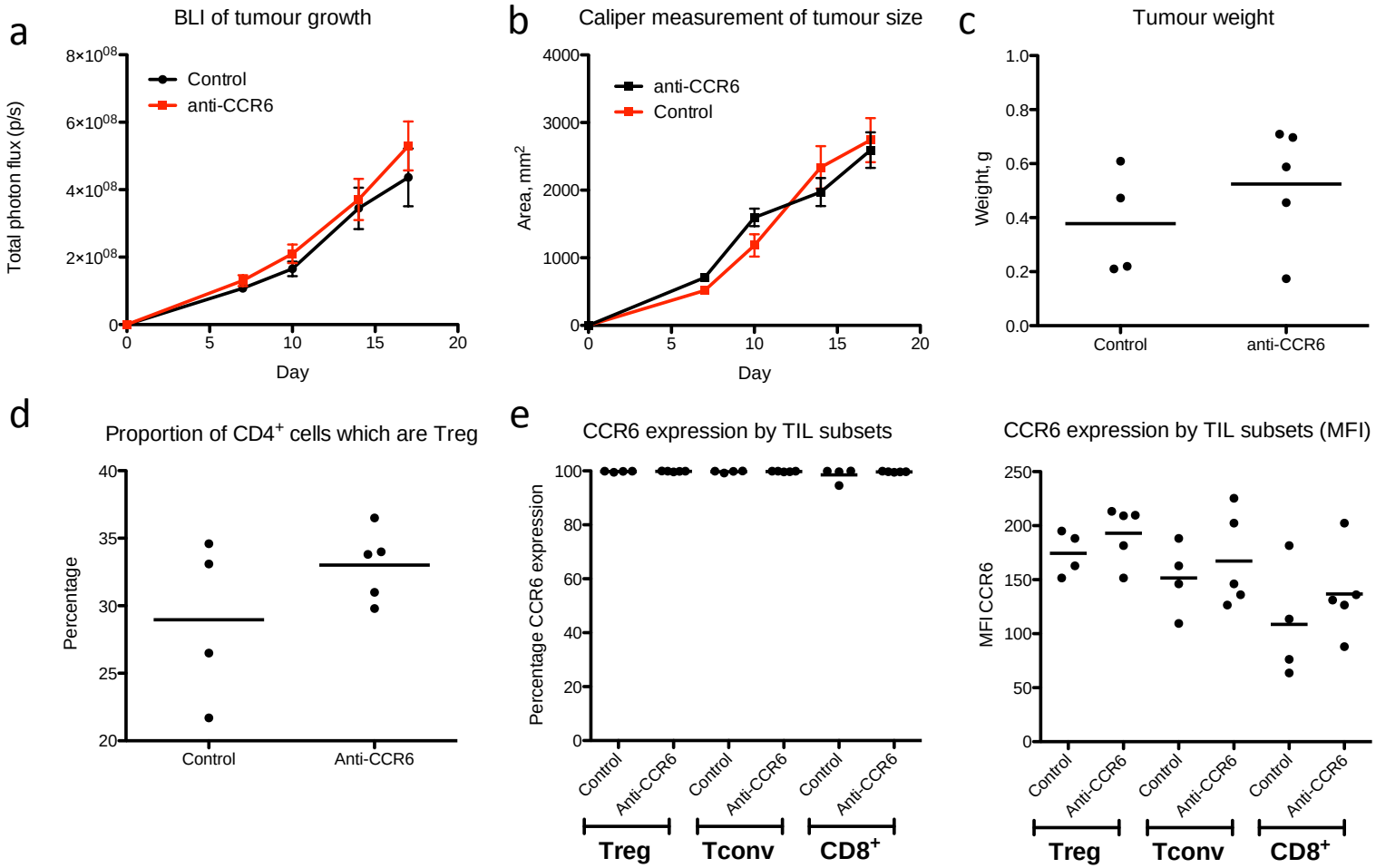

Figure 6-16: One-off tail vein injections of rat IgG2a (control group, n=4) or rat anti-mouse CCR6 antibody (treatment group, n=5) at day 7 in CT26-Luc tumour-bearing BALB/c mice. Tumour growth was measured by (a) BLI, (b) calliper measurements and (c) tumour weight post resection. Mean values are shown. Error bars represent the standard error of the mean.

Discussion

Tumour establishment in mice with the colorectal cancer cell lines, CT26 and CMT93, or with the melanoma cell line B16-F10, resulted in tumour growth that could be measured over a 17-day period. The tumours harboured lymphocytes of which a high proportion were Treg and similar to the findings in human CRC, the Treg expressed significantly more cell surface CCR5 than their Tconv counterparts. Thus, the mouse models used in this chapter appeared appropriate to investigate the role of CCR5 in recruitment of Treg into tumours. Murine CCR5 was antagonised with met-RANTES and TAK-779 while human CCR5 was antagonised with UK-484900 in hCCR5 KI mice. One limitation of these mouse models was the inability to assay drug levels to ensure adequate concentrations in the serum and tissues.

Tumour growth

Both met-RANTES and TAK-779 treatment resulted in significantly smaller tumours compared to controls when given by once daily injection and this is consistent with previous published data based in different murine tumour models (104,267,297,341). The previous studies hypothesised that tumour growth was delayed as a direct result of reduced tumour Treg infiltration. However, in our models, CT26 cells express both CCR5 and CCR1 and therefore a direct effect of met-RANTES and TAK-779 on tumour cell growth cannot be ruled out. Others have shown that in vitro CCL5 treatment of CT26 cells increases proliferation compared to vehicle, an effect that can be inhibited by TAK-779 (267). In vitro experiments presented in this chapter showed that met-RANTES had no effect on CT26 proliferation but direct tumour cell effects are still possible in vivo. To determine if this is indeed the case, tumours could have been

established in immunodeficient mice and then treated with either met-RANTES / TAK-779 or vehicle. This was not done due to the costs of purchasing and maintaining immunodeficient mice. Delayed lung, melanoma and lymphoma tumour growth has been observed in CCR5-/- mice (289,297,354) compared to wildtypes supporting the idea that CCR5 expressed by host cells is responsible for the delayed tumour growth because injected tumour cells may still express CCR5. In a tissue injury mouse model, delayed wound healing is observed in CCR5 -/- mice compared with wildtypes, associated with impaired recruitment of endothelial cells and reduced tissue levels of VEGF (355). There was a trend for lower tumour and serum VEGF levels in mice treated with CCR5 inhibitors (see Figure 6-14c) and this could have contributed to delayed tumour growth.

Delivery of met-RANTES by continuous infusion paradoxically led to increased tumour growth compared to control mice. This may be explained by the partial agonist activity of met-RANTES. The ligands for CCR5 stimulate internalisation of the receptor, but met-RANTES also stimulates internalisation, in a manner that is not consistent with competitive antagonism (352). In this sense, met-RANTES is an atypical antagonist. It has also been shown that cell-surface bound met-RANTES can be metabolised to CCL5 by endogenous aminopeptidases, leading to agonist effects (339,352). Tumour CCL5 expression is associated with tumour growth (104,233) and intratumoral injection of CCL5 leads to an increase in tumour Treg infiltration (297). It is therefore possible that met-RANTES in the osmotic pumps was enzymatically converted to CCL5 over the course of the experiments, leading to the observed increased tumour growth and Treg

infiltration compared with control mice. There are no published reports using delivery of met-RANTES by osmotic pump.

Timing of drug therapy

Treatment of hCCR5 KI mice with UK-484900 led to significantly delayed tumour growth compared to control mice, but only when treatment was commenced at the time of tumour cell injection. No such effect on tumour growth was observed when treatment was delayed until tumour engraftment was established at day 7. Published studies demonstrating delayed tumour growth with met-RANTES treatment compared to controls (297,341) commenced drug at the same time as tumour cell injection whereas reports of delayed tumour growth with TAK-779 commenced drug treatment 2 weeks (104) or 72 hours (267) post-tumour cell injection; although the experiment schedule was notably longer (31 days and 10 weeks, respectively) than the schedule for the experiments described in this chapter. It is thus possible that the lack of difference in tumour growth rates between UK-484900 treated mice and controls when drug treatment was delayed until day 7, can be explained by the relatively rapid and progressive tumour growth and hence, short experiment schedule, of the model.

Lymphocyte infiltration

The proportion of Treg in the CT26-Luc tumours increased with met-RANTES by continuous sc infusion. If met-RANTES was enzymatically modified to CCL5 during the course of this experiment, augmented tumour CCL5 levels may have resulted in increased Treg infiltration. This would be consistent with published data demonstrating increased Treg infiltration in CT26 tumours treated by intratumoral injection of CCL5 (297). Outside of this infusional met-RANTES experiment, there was

no difference in the tumour Treg proportion between treatment and control groups, across 5 different experiments involving 3 different tumour cell lines and 3 different CCR5 inhibitors. This suggests that Treg were not actively recruited to the tumour site by a CCR5-dependent mechanism. These data contradict the findings of Tan et al (104), who demonstrated that CCR5 inhibition with TAK-779 in a murine model of pancreatic cancer led to reduced tumour Treg infiltration compared with PBS treatment. There are however some unanswered questions regarding the Tan et al study. The tumour Treg proportion in control mice was 74% compared with 49% in TAK-779 treated mice. In a different experiment using the same wildtype Pan02 cell line, but with a different experiment duration of 7 more days, control group mice had a tumour Treg proportion of 43%. Quite apart from the extraordinarily high tumour Treg proportion of 74% in control mice, the reduction in Treg proportion to 49% in treatment mice is still higher than the tumour Treg proportion in control mice from other experiments.

Knockdown of CCL5 expression in tumours has also been associated with a reduction in tumour Treg infiltration (104,233). CCL5 knockdown does not necessarily abolish CCR5 signalling because other ligands can activate CCR5 and CCL5 binds to other receptors, notably CCR1 and CCR3. Knockdown of CCL5 will also affect signalling through these receptors with consequent effects on tumour growth and in Treg infiltration. In tumour cell migration experiments, CCR1 and CCR5 were found to act in a redundant manner i.e. both receptors needed to be antagonised to inhibit migration (356). Even though intratumoral injection of CCL5 increases (297) and CCL5 knockdown decreases (104,233) tumour Treg infiltration, inhibition of CCR5 may still have no effect on tumour Treg recruitment, as Treg may be recruited via other CCL5-

binding chemokine receptors. Tumour and serum levels of CCL5 were significantly greater in mice treated with UK-484900 than controls (seeFigure 6-14), an effect which could lead to increased signalling through CCR1 and CCR3. Chemokine receptor-deficient mice are known to exhibit increased tissue and serum levels of cognate chemokines, an effect that has been described as chemokine receptor scavenging (357). In relation to tumour progression rather than Treg infiltration, CCR5 inhibition by TAK-779 only partially inhibited tumour progression compared to anti-CCL5 treatment, suggesting that anti-CCL5 treatment may inhibit more signalling pathways than anti-CCR5 treatment.

Reduced tumour Treg infiltration has been reported in CCR5 -/- models (233,297). While these studies do suggest a role for CCR5 in the recruitment of Treg to tumours, it is important to remember that these mice have developed in the absence of the CCR5 gene. Loss of CCR5 activity may mask the role of the gene in the adult state due to compensatory changes in the expression of other genes during development (358). A general limitation surrounding the use of knockout mice is known as the 'flanking allele problem'. The embryonic stem cells populating the germline transmit their genetic background as well as the null mutation. Thus, the null mutation is flanked by two embryonic stem cell alleles while the wildtype locus is flanked by two C57BL/6 alleles. The possibility therefore exists that an apparent effect of a null mutation could be due to a flanking embryonic stem cell gene (359). While CCR5 -/- mice have a normal lifespan and behaviour, there is an immune phenotype attributed to these mice characterised by an increased number of $CD4^+$ and NKT cells in the gut, associated with increased levels of IL-4, IL-5 and IL-10 and reduced levels of IFN-γ (360). Studies in

CCR5 -/- mice have also demonstrated reduced migration of macrophages and NK cells compared with wildtypes (361,362). In a murine graft-versus-host disease model, T cells from wildtype and CCR5 -/- mice were adoptively transferred to wildtype mice at the time of bone marrow transplant (307). It was demonstrated that CCR5 -/- Treg were suppressive and proliferated in vitro, in a similar manner to wildtype Treg. However, after one week, CCR5 -/- failed to infiltrate target organs while wildtype Treg did not, suggesting that CCR5 is critical to the recruitment of Treg to sites of inflammation. Despite the lack of difference between wildtype and CCR5 -/- Treg in vitro, it is possible that functional differences exist in vivo. For example, CCR5 -/- Treg may have an enhanced propensity to undergo apoptosis.

Treg may be recruited to tumours via CCL5-independent chemokine receptors and it is important to appreciate that 20-50% of the tumour-infiltrating Treg population do not express CCR5 (Figure 6-6). Furthermore, Treg recruitment to tumours may be entirely chemokine-independent and the reduction in tumour Treg proportion observed in CCL5 knock-down tumours and in CCR5 -/- mice may relate to secondary effects that disruption of chemokine signalling has on the tumour microenvironment.

CD8 : CD4 ratio

There was a significantly higher tumoral CD8 : CD4 ratio in mice treated with UK-484900 compared to controls (see Figure 6-11f). This is unlikely to reflect differences in T cell subset recruitment given that CCR5 expression by CD8+ cells was significantly greater than Tconv across tumours from all cell lines and across tissue types (Figure 6-6). One possible explanation for this finding relates to apoptosis. Co-culture of tumour cells with CCL5 leads to apoptosis of CD8+ cells but not CD4+ cells, thereby

decreasing the CD8 : CD4 ratio (363). Other in vitro experiments have demonstrated CCL5-induced apoptosis of peripheral blood T cells, although micromolar concentrations of CCL5 were required (364) - concentrations higher than those found in CRC tissue (259). The addition of Treg cultured in media containing CCL5 to CD8+ cells leads to enhanced CD8+ cell apoptosis, an effect that is mediated by TGF-ß (233). Thus, CCR5 inhibition by UK-484900 may block apoptosis of CD8+ cells and hence, increase the CD8 : CD4 ratio. However, this increase in the tumoral CD8 : CD4 ratio was not observed in a subsequent experiment using UK-484900 to inhibit CCR5 (Figure 6-12) nor in prior experiments using met-RANTES and TAK-779.

Chapter 7
General discussion

Summary of key findings in human CRC

I found that the proportion of tumour-infiltrating $CD4^+$ cells with a Treg phenotype (Treg proportion) was significantly increased in CRC compared with distal, uninvolved colon. This is consistent with published data (52,53,192,195), although reports have published different conclusions regarding the association between tumour Treg enrichment and cancer stage in CRC. I measured CRC-Treg infiltration as a proportion of $CD4^+$ cells with a Treg phenotype by flow cytometry. Consistent with other studies that have taken the same approach, there was no demonstrable association between the Treg proportion and disease stage (56). There may be several reasons to explain this. Firstly, the method we have used is robust making it likely that my conclusions are correct. Measuring the proportion of Treg in the tumour does not assess the absolute numbers of Treg but rather the balance between Treg and other cell types. In other settings, including chronic inflammatory disease, increases in tissue Treg parallel increases in effector cells and it may be the functional balance which is more important in determining outcome rather than absolute or relative numbers. Furthermore, Treg may play different functional roles at different stages of disease progression making it unlikely that there will be a simple linear relationship between Treg numbers and disease stage.

The presence of Treg in tumour tissue is likely to be a consequence of recruitment from blood with a possible contribution also from local proliferation or apoptosis. To

examine the mechanisms by which Treg are recruited to the tumour, I carried out a systematic examination of chemokine receptors expressed on the cell surface of tumour-isolated Treg, Tconv and $CD8^+$ (Chapter 3). Treg expressed significantly more CCR5, in terms of percentage expression and MFI, than Tconv and $CD8^+$ cells and CRC-isolated Treg expressed significantly more CCR5 than Treg isolated from distal colon. Tumour-isolated Treg also expressed significantly more CCR4 than Tconv in terms of both percentage expression and MFI, although there was no difference in CCR4 expression between CRC-isolated and distal colon-isolated Treg. Thus, high levels of CCR5 expression appear to be characteristic of CRC-infiltrating Treg.

Having established the chemokine receptor signature of tumour-infiltrating Treg, the corresponding ligands were measured in CRC and matched distal colon tissue (Chapter 4). RT-PCR analysis of chemokine expression demonstrated that the ligands for CCR4 (CCL17 and CCL22) were not overexpressed by CRC compared with matched distal colon, consistent with the CCR4 expression data that showed no difference between Treg infiltrating CRC and distal colon. Thus, it appears unlikely that CCR4 is involved in the preferential recruitment of Treg to CRC compared with distal colon. However, two of the ligands for CCR5 (CCL3 and CCL4) were significantly overexpressed by CRC compared with distal colon, both at the mRNA and protein levels. CCL4 localised to the tumour endothelium, suggesting that this chemokine may play a key role in the recruitment of $CCR5^+$ lymphocytes to the tumour. The cellular source of the CCR5 ligands was difficult to identify but was probably secreted by tumour cells, fibroblasts and $CD11b^+$ monocytes/macrophages. In Chapter 5, I demonstrated that CRC-isolated T cells migrate towards CCL4 in vitro and that Treg are enriched in the migrating population confirming that CRC-associated Treg show preferential migration in

response to CCR5 activation, and providing more evidence that this pathway is involved in Treg recruitment into CRC. I then went on to demonstrate that the CRC-isolated Treg were able to suppress allogeneic T cell proliferation in vitro and that they had the characteristics of naturally-occurring Treg (nTreg), as demonstrated by the highly unmethylated TSDR locus of Treg DNA.

The active specific recruitment of Treg to CRC

In summary, I found that Treg isolated from CRC were nTreg, capable of suppressing T cell activation in vitro and their expression of high levels of CCR5 allowed them to migrate to CCL4 expressed in tumour tissue, thus providing one explanation for their localisation to tumour. Conditions in CRC therefore exist to support the hypothesis that Treg recruitment to CRC is mediated by specific chemokine receptor interactions with cognate chemokines. A schematic representation of this process is shown in Figure 7-1.

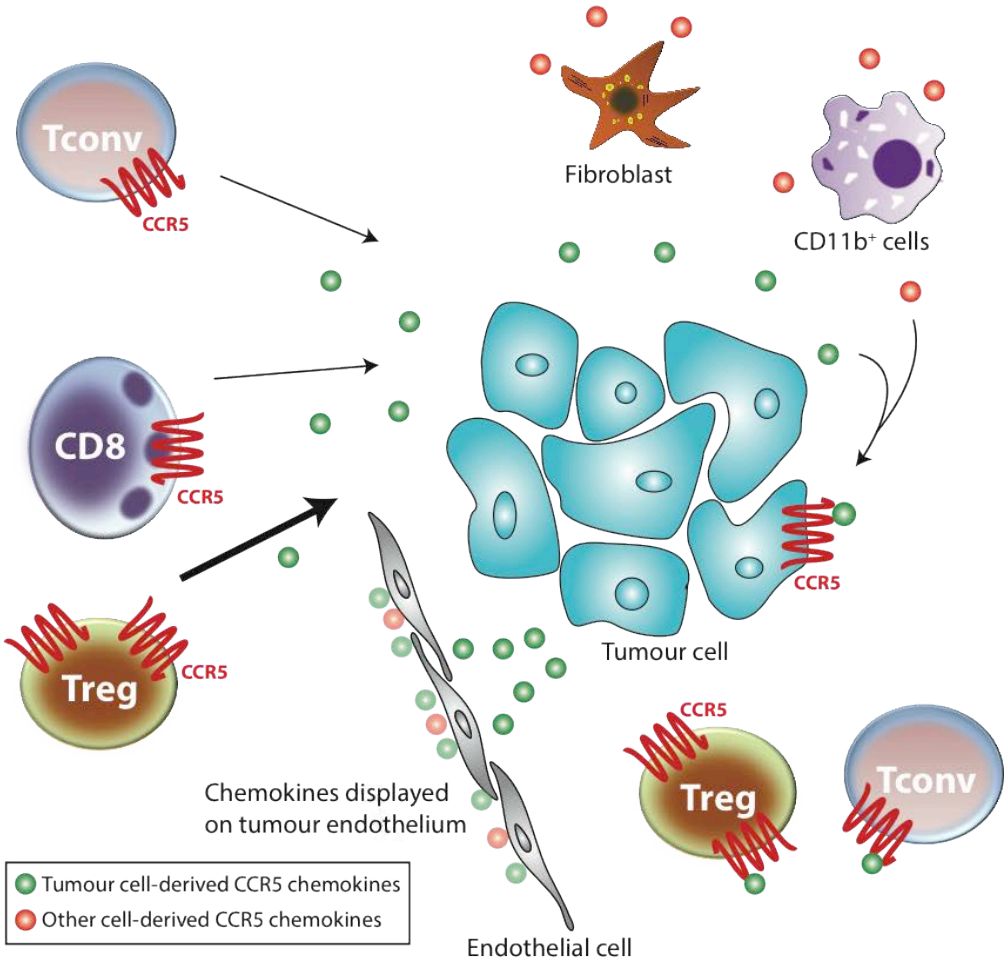

Figure 7-1: The active recruitment of T cells to CRC. Treg express significantly more cell surface CCR5 than Tconv and CD8+ cells. Tumour cells, stromal cells and tumour-associated macrophages (CD11b+ cells) express CCR5 ligands, some of which can be captured and presented by the tumour endothelium.

The data presented so far support a role of CCR5 in recruitment but as they are based on expression studies of tumour tissue and in vitro experiments, they cannot provide proof that this is the important pathway in vivo. For this I used murine cancer models in which CCR5 could be pharmacologically inhibited. CCR5 was inhibited using met-

RANTES and TAK-779 in wildtype mice. Unfortunately, neither of these compounds specifically antagonises CCR5 and the only available specific antagonist of CCR5 (UK-484900) is selective for human and not murine CCR5. To enable me to use UK-484900, I needed mice expressing human CCR5 which I was able to access through a collaboration with Pfizer, who provided mice in which murine CCR5 had been replaced by human CCR5 (hCCR5 KI mice). I implanted B16-F10 (a melanoma cell line) into the hCCR5 KI mice (Chapter 6). Akin to the findings from human CRC, Treg isolated from murine tumours expressed significantly more cell surface CCR5 than Tconv. However, the inhibition of CCR5 using met-RANTES, TAK-779 and UK-484900 did not lead to a significant reduction in tumour Treg infiltration compared with control mice despite resulting in a significant delay in tumour growth. This finding suggests that at least in this model, Treg are not recruited to tumours, to any significant degree, via the CCR5 axis.

Although the expression of high levels of functional CCR5 by Treg and the presence of cognate ligands in the tumour suggest a role for these molecules in the recruitment of Treg to the tumour site, this does not necessarily have to be the case. It is possible that CCR5 expression may be a marker for the expression of other chemokine receptors or integrins involved in the recruitment process. Treg may be recruited by mechanisms independent of chemokine receptors. Selective proliferation of Treg within the tumour tissue, enhanced Treg survival and reduced Treg egress could all explain Treg enrichment in tumours (see Figure 7-2). Others have cited induction of Treg from other T cells as an important mechanism leading to Treg enrichment (365). However, I found that the tumour Treg TSDR locus was highly unmethylated, consistent with the findings

of others (193), suggesting that Treg induction is unlikely to be the sole mechanism leading to Treg enrichment in human CRC.

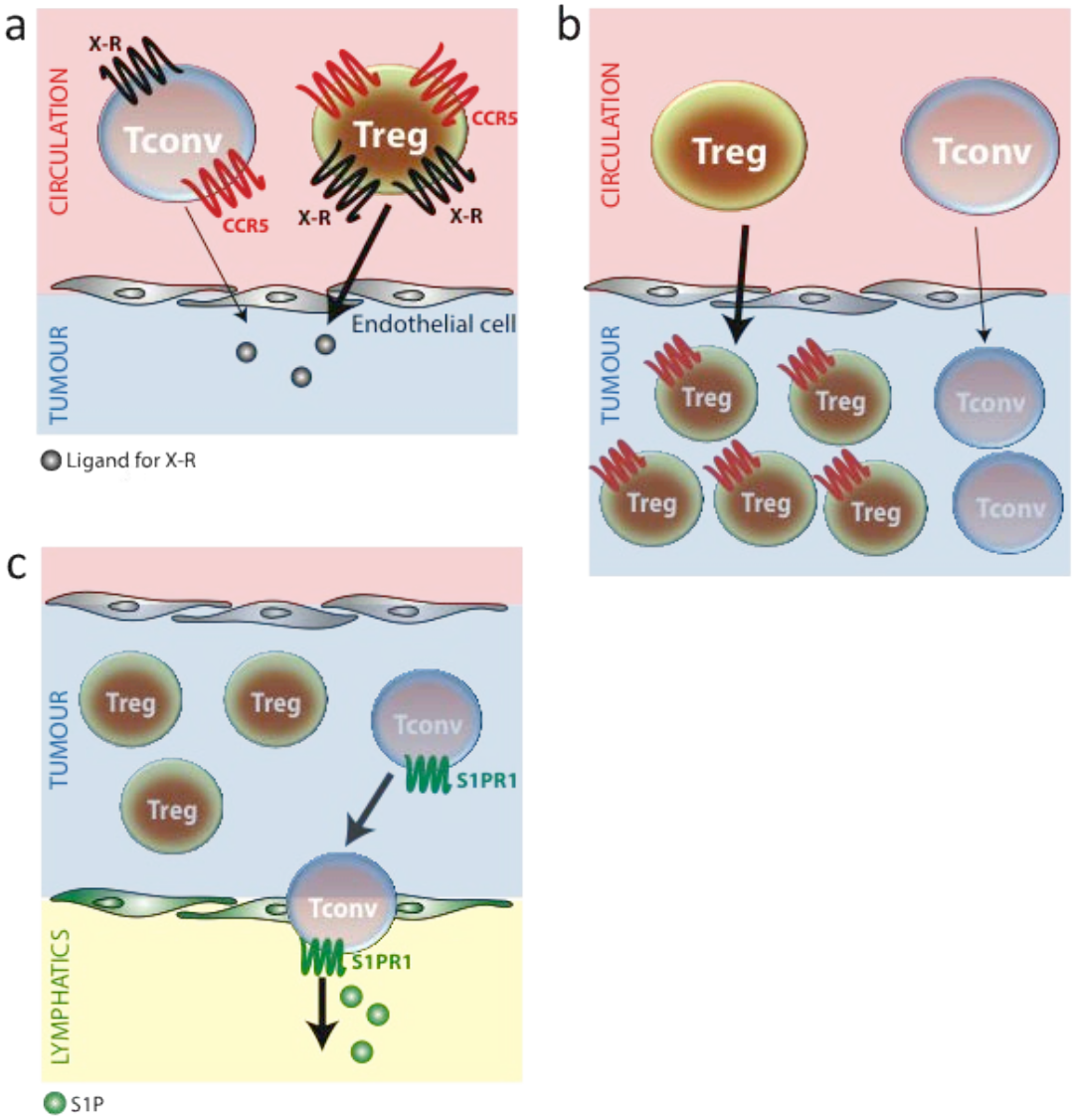

Figure 7-2: Mechanisms of Treg enrichment in CRC. (a) Treg recruitment via enhanced expression of undefined receptors (X-R) by Treg compared with Tconv interacting with cognate ligand. CCR5 expression may be linked to the expression of such receptors. (b) Selective proliferation of Treg within the tumour tissue. Activated proliferating Treg may express CCR5. (c) Enhanced egress of Tconv from the tumour tissue to the lymphatics compared with Treg.

Although I found that CRC-isolated Treg did not proliferate in vitro (see Figure 5-8), I did observe a significantly greater percentage expression of Ki67, a proliferation marker, by Treg compared with Tconv. This suggests that within the tumour tissue in vivo, Treg are proliferating more than Tconv - a process that could lead to the Treg enrichment observed in tumours. Higher levels of Ki67 expression by tumour-resident Treg compared with Tconv have previously been demonstrated both in human cancer (366) and murine cancer models (318). This idea could be tested further in future by an in situ BrdU incorporation experiment, thereby detecting and comparing proliferation of Treg with Tconv, isolated from murine tumours.

Regulation of CCR5 expression

Expression of CCR5 is associated with T cell activation and proliferation (287,367). Treg that have migrated into tumours may become activated and proliferate, thereby leading to both Treg enrichment and upregulation of CCR5 expression. The factors that lead to expression of CCR5 on the cell surface are complex and involve receptor internalisation, receptor recycling and gene transcription. It was shown in Chapter 5 that activation of Tconv, and to a greater extent Treg, increased surface CCR5 expression (see Figure 5-3). Furthermore, my finding that Tconv secreted more CCR5 ligands than Treg cells raises the possibility that ligand-induced internalisation of CCR5 could explain the differences in CCR5 expression between Tconv and Treg (see Figure 5-5). If this were the case, antagonism of CCR5 would be expected to increase surface CCR5 expression and limit the differences in expression between Tconv and Treg. Antagonism did increase Tconv surface expression but not to the levels observed for

Treg. It is therefore likely that other processes regulating CCR5 expression are more important than the autocrine internalisation of CCR5 via its ligands.

There was a two-fold increase in CCR5 mRNA expression by CRC-isolated Treg compared with Tconv (see Figure 3-13). This is consistent with the results of a gene microarray study based on peripheral blood-isolated Treg and Tconv (368). The transcription factors KLF-2 (287) and CREB-1 (367) which regulate CCR5 transcription, were also expressed at higher levels by Treg compared with Tconv. CREB-1 is induced on T cell activation and then binds to the foxp3 promoter, promoting and maintaining the Treg phenotype (369). KLF2 knock-down inhibits CCR5 expression by activated T cells and also controls S1PR1 transcription (370). However, it is not clear why CREB-1 and KLF2 expression were higher in Treg compared with Tconv. S1P1R is the principal S1P receptor regulating T cell trafficking, acting to permit egress of lymphocytes from lymphoid organs into the circulation (371). Interestingly, S1PR1 mRNA was expressed at significantly lower levels by CRC-isolated Treg than by Tconv, suggesting that reduced egress of Treg from CRC may occur, compared with Tconv.

In a murine model of peritonitis, there were significantly higher levels of CCR5 chemokines in the peritoneal exudate of CCR5 -/- mice compared with wildtypes (372). This is similar to the findings from tumour lysates and serum in B16-F10-Luc tumour-bearing hCCR5 KI mice treated with either UK-484900 or control PBS injection (see Figure 6-14). It was shown that apoptotic T cells express more surface CCR5 than live cells and effectively scavenge and sequester CCR5 ligands from sites of inflammation (372). This may serve an important role as part of the resolution phase of inflammation. Annexin-V staining of CRC-isolated T cell subsets was performed, but

only for one sample. The proportion of Annexin-V staining cells in the live Treg and Tconv subsets were equivalent (~9-10%). This experiment would need to be repeated to be certain, but it would appear that differences in the fraction of apoptotic cells within T cell subsets is unlikely to explain the difference in CCR5 expression between Treg and Tconv.

Lack of effect of CCR5 inhibition in the murine model

There are several lines of evidence that CCR5 inhibition would lead to a reduction in Treg infiltration in murine tumours. Firstly, CCL5 knockdown in tumour cell lines has been shown to lead to delayed tumour growth with reduced Treg infiltration compared with wildtype cell lines (104,291). Secondly, tumour growth in CCR5 -/- mice is delayed with associated reduced Treg infiltration compared with wildtype mice. This experiment has been performed using the colorectal cancer cell line CT26 (291) and the melanoma B16 cell line (297). CCR5 -/- mice are also less susceptible to carcinogen-induced lung cancer (354). Thirdly, inhibition of CCR5 using TAK-779 has been shown to reduce tumour Treg infiltration compared with vehicle control in a pancreatic cancer model (104). It was therefore surprising that neither CCR5 inhibition in wildtype mice with met-RANTES or TAK-779 nor with UK-484900 in hCCR5KI mice led to a detectable reduction in tumour Treg infiltration. CCR5 inhibition did however lead to a delay in tumour growth in keeping with previously published findings (104,267,291).

The question that needs to be addressed is therefore how did CCR5 inhibition lead to a delay in tumour growth but no associated reduction in tumour Treg infiltration. The problems with specificity of CCR5 antagonism by met-RANTES and TAK-779 have been

discussed in Chapter 6. It is possible that co-inhibition of CCR1 (met-RANTES) or CXCR3 (TAK-779) could affect the recruitment of other T cell subsets so that the Treg proportion effectively remained unchanged compared with control mice. Experiments designed to test this could involve treating mice with specific inhibitors of CCR1 and CXCR3. Small molecular antagonists to CCR1 (J113863 and BX471, Tocris Bioscience Inc, USA) and neutralising antibodies (CXCR3-173, Biolegend Inc, USA) and small molecular antagonists (AMG487, Tocris Bioscience) to CXCR3 do exist and therefore such experiments are feasible. CXCR3 inhibition has been shown to inhibit the implantation and growth of tumours in a lung metastasis mouse model (139). Similarly, mice treated with a CCR1 antagonist developed less marked metastases in a CRC liver metastasis model associated with reduced tumour infiltration of immature myeloid cells (96). Off-target effects of met-RANTES and TAK-779 treatment could therefore be responsible for the observed delay in tumour growth compared with control mice. This does not explain the delayed tumour growth observed in UK-484900-treated hCCR5KI mice however. B16-F10-Luc cells do obviously not express human CCR5 and there was no difference in the in vitro proliferation of B16-F10-Luc tumour cells when cultured in the presence or absence of UK-484900 (see Figure 6-5). This suggests that UK-484900 does not have a direct inhibitory effect on tumour cell growth, but in order to test this in vivo, the compound would have to be administered to tumour-bearing immunodeficient mice. Inhibition of CCR5 by UK-484900 could lead to changes in migration of other cells into tumours, by inhibition of CCR5-dependent migration. On the other hand, CCR5 inhibition may lead to increased recruitment via other chemokine receptors. Inhibition of CCR5 by UK-484900 led to increased tumour and serum levels of CCL5 (see Figure 6-14). Enhanced migration of other cell types into the tumour via CCR1 may ensue, as

has been shown for NK cells in a murine model of hepatitis (373). Others have shown that there is a significant increase in $CD4^+$, $CD8^+$ and NK cell infiltration into tumours in CCR5 -/- compared to wildtype mice (289), although this was not observed in the UK-484900 / hCCR5KI tumour model. Other studies have shown a reduced number of NK cells infiltrating tumours in CCR5 -/- mice compared to wildtypes (362). In a murine peritonitis model, peritoneal accumulation of macrophages was delayed in CCR5 -/- mice compared with wildtypes (374). There is increased tumour infiltration of $CD19^+$ cells in CCR5 -/- mice compared with wildtypes (289). Such an influx of $CD4^+$, $CD8^+$, NK and $CD19^+$ cells with delayed infiltration of macrophages could result in a reduction in tumour growth while having no effect on the Treg proportion. The infiltration of $CD8^+$ and NK cells was measured in various CRC tumour models and no difference was seen between mice receiving CCR5 inhibitors and controls. However, the infiltration of $CD19^+$ cells and macrophages was not assessed. Inflamed mucosa in CCR5 -/- mice express significantly higher levels of the Th2 cytokines IL-4, IL-5 and IL-10 but significantly less IFN-γ than wildtypes (360). Such a skew to Th2 cytokines may have occurred in the mice treated with CCR5 inhibitors, although this was not measured, and may have led to the observed differences in tumour growth.

As well as a postulated role in Treg recruitment, CCR5 is important for tumour $CD4^+$ and $CD8^+$ cell function (375). In a study comparing tumour growth of Pan02 and LLC cell lines in CCR5 -/- mice versus wildtypes, tumour growth was significantly increased in the CCR5 -/- mice (375), in direct contrast to aforementioned studies (291,297). The presence of intact CCR5 led to increased tumour $CD4^+$ and $CD8^+$ cell infiltration. Intact CCR5 was also necessary for $CD8^+$ cross-priming, a process dependent on CD40L expression by $CD4^+$ cells.

CCR5 also mediates recruitment of endothelial progenitor cells and promotes angiogenesis. Following corneal injury, neovascularisation was inhibited in CCR5 -/- mice compared with wildtypes, associated with lower levels of tissue VEGF (355). Endothelial progenitor cells are recruited to tumours from the bone-marrow in a CCR5-dependent manner, where they lead to the formation of neovessels (376). In a recent study, endothelial progenitor cell recruitment was measured in a wound healing mouse model (377). CCR5 -/- displayed reduced wound healing compared with wildtypes. Furthermore, bone marrow cells from wildtype mice restored normal vascularisation and wound healing when transferred to CCR5 -/- mice. Thus, CCR5 inhibition could reduce tumour neovessel formation through blockade of endothelial cell recruitment, thereby inhibiting tumour growth independent of effects on Treg recruitment. An unsuccessful attempt was made to detect differences in tumour $CD31^{+}$ endothelial cell density between UK-484900 and PBS treated mice by immunohistochemistry. There was however a trend for lower levels of tumour and serum VEGF in UK-484900 treated mice compared with controls, suggesting that CCR5-mediated neovascularisation may indeed be important in the models I studied.

The one published study demonstrating reduced tumour Treg infiltration by pharmacological inhibition of CCR5 used TAK-779 in a murine pancreatic cancer model (104). The results from this study directly contradict the findings presented in Chapter 6 whereby CCR5 antagonism had no demonstrable effect on tumour Treg infiltration. In this pancreatic cancer model however, the tumour Treg proportion in control mice was 74% compared with 49% in TAK-779 treated mice. In a different experiment using the same wildtype Pan02 cell line, albeit with an experiment duration of 7 more days, control group mice had a tumour Treg proportion of 43%. Quite apart from the

extraordinarily high tumour Treg proportion of 74% in control mice, the reduction in Treg proportion to 49% in treatment mice is still higher than the tumour Treg proportion in control mice from other experiments. Aside from this anomaly, there are other potential explanations for the differences between the results from Chapter 6 and published findings. Firstly, Treg recruitment to tumours in the pancreatic cancer model may indeed depend on CCR5, while those in the CRC models do not. Secondly, the CRC/melanoma tumours grow more quickly and thus the CRC models may not have continued for a long enough duration to observe any effects from CCR5 inhibition. By the time CRC/melanoma tumours were established at day 7 and CCR5 inhibition commenced, maximal Treg infiltration may have already occurred whilst it was still an on-going process in the pancreatic cancer model. Nevertheless, no reduction in Treg infiltration from CCR5 inhibition was seen using 3 different cell lines and 3 different CCR5 antagonists. Even if the caveats concerning the finding of reduced Treg infiltration by treatment with TAK-779 in the pancreatic cancer model are accepted, an explanation is still required as to why a reduction in Treg infiltration is observed in CCR5 -/- mice compared with wildtypes. There are at least four potential explanations. Firstly, CCR5 may indeed be important in the recruitment of Treg to tumours and a reduction in tumour Treg infiltration with CCR5 antagonists was not observed for the reasons stated above. Secondly, it has recently been shown that Treg accumulate in the thymus in CCR5 -/- mice, associated with a reduction in S1PR1 expression compared with wildtype mice (378). Without expression of S1P1R, Treg fail to egress from the thymus. A similar effect was demonstrated by inhibition of CCL4 in wildtype mice, although CCR5 antagonism was not tested. Thymic accumulation of Treg was not measured in the CRC/melanoma tumour models. If reduced S1PR1 expression is part of

the CCR5 -/- Treg phenotype and can not be reproduced by CCR5 antagonism, this would explain the reduced tumour Treg infiltration observed in CCR5 -/- mice compared with wildtypes that is not mimicked by CCR5 antagonism. Thirdly, T cells from CCR5 -/- mice secrete lower levels of IL-2 and NFAT following activation compared with T cells from wildtype mice (379). This was also observed for T cells isolated from patients with the CCR5Δ32 mutation compared with healthy subjects. Accordingly, T cell proliferation was noted to be greater in $CCR5^+$ human T cells than $CCR5^-$ T cells. It is therefore entirely possible that tumour-resident Treg are more proliferative in wildtype mice compared to CCR5 -/- mice, leading to the observed differences in Treg infiltration. Fourthly, lower VEGF levels have been reported in CCR5 -/- mice compared to wildtypes (355,377) and Treg have also been shown to express the VEGF receptor (VEGFR) (380). $VEGFR^+$ Treg proliferate in response to VEGF treatment and VEGF blockade inhibits such proliferation.

Limitations

The limitations of the different methods used have been discussed in the relevant chapters. With regard chemokine receptor expression by human CRC-isolated lymphocytes, one limitation relates to the static nature of the assessment. In other words, chemokine receptor expression was measured on lymphocytes that had migrated into the tumour tissue and in the peripheral blood and it is only possible to infer, not prove, the kinetics of chemokine receptor expression and function by lymphocytes as they move from the periphery into the tumour in vivo. Furthermore, changes in expression by retained and egressing lymphocytes cannot be assessed in such a study. High levels of surface chemokine receptor expression by migrated

lymphocytes may indeed point to a role for these receptors in trafficking to the tumour. However, chemokine receptors that have mediated migration may be downregulated or internalised post-migration and thus not be detected by such experiments. The expression of chemokine receptors on migrated lymphocytes may also be functionally neutral markers of activated cells capable of migrating. Nevertheless, systematic examination of chemokine receptor expression in cells from tumour tissue is a useful way to highlight possible important receptors worthy of further study.

CRC-isolated T cells were shown to migrate towards a CCR5 ligand in vitro demonstrating that the CCR5 receptor is functional. However, this may not adequately reflect the situation in vivo. The capacity of T cells to migrate towards CCR5 ligands in vivo may be overwhelmed by the capacity of the cells to migrate towards other ligands. For example, it has been shown that CXCR3 ligands are more chemotactic for T cells than CCR5 ligands, yet in vivo CXCL10 and CCL5 have comparable chemotactic activity and are more potent than other CCR5 and CXCR3 ligands (381). CRC-isolated Treg were able to suppress autologous T cell proliferation showing that they are functional in vitro but this does not prove that they are functional within the tumour microenvironment in vivo. The relative importance of Treg-mediated suppression of effector TILs in vivo is unclear. TILs have a tendency to be anergic as a consequence of several distinct mechanisms, only one of which involves Treg-mediated suppression. Defects in T cell priming occur due to a lack of activating antigen and co-stimulation signals, or an enhanced negative signal, such as signalling through PD-1, TGF-ß or CTLA-4 (382). DC function is deficient in tumours, driven by a variety of different mechanisms. More recently, the hypoxic and acidic environment of tumours has been shown to induce reversible anergic states in T cells (383). The relative contribution of Treg-mediated

suppression to the mix of different processes that lead to defective effector T cell function in the tumour, may be less important than has previously been considered.

The cell surface phenotype ($CD4^+CD25^+CD127^{low}$) was used to define Treg in this thesis. It identifies a population of cells that were able to suppress cell activation in vitro, although in vitro function does not necessarily translate to in vivo activity. Tumours harbour other suppressive T cells that do not conform to the Treg phenotype. For example, within the tumour $CD4^+foxp3^-$ cell population are $LAG3^+$ and LAP^+ cells that are also suppressive. In fact, the majority of CRC-isolated $CD4^+LAP^+$ cells are $foxp3^-$ and have been shown to suppress T cell responses with approximately 50 times as much potency as traditional Treg (384). It is unclear whether $CD4^+LAP^+$ cells are actively recruited to the tumour or are induced from other T cells but they offer another potent mechanism to suppress the anti-tumour immune response, and in the context of this thesis, could be recruited to tumours via a CCR5-independent pathway.

The limitations of the murine tumour models have already been discussed. A failure to observe a reduction in Treg migration with CCR5 inhibition does not necessarily mean that CCR5-dependent Treg migration to tumours is not important. Rather that there was no significant difference in tumour Treg infiltration between treatment and control groups in this chosen tumour model, using this particular tumour cell line, over this time schedule in these specific mice. I was only able to quantify Treg infiltration at one time point and the kinetics of Treg migration, retention and subsequent egress was not measured. Thus, it is possible that CCR5 inhibition did lead to reduced migration of Treg into the tumours, but this did not lead to an overall reduction in Treg numbers due

to changes in Treg egress or proliferation of tumour-resident Treg. None of these effects were measured.

Finally, given the degree of redundancy in the chemokine system, inhibition of one receptor alone may not lead to a dramatic reduction in immune cell recruitment if other receptors then come into play. Furthermore, my finding of increases in tissue and serum CCL5 in UK-484900 treated mice demonstrates the complex consequences of inhibiting the chemokine network. Humans with a CCR5Δ32 mutation are healthy and carry no increased susceptibility to infectious disease, with the exception of West Nile Virus infection despite showing defective CCR5-mediated lymphocyte migration in vitro (385). In order to significantly diminish tumour Treg recruitment, it may be necessary to inhibit a combination of chemokine receptors and integrins. To test this approach in animal experiments requires multiple treatment arms using different combinations of neutralising antibodies or receptor antagonists.

Future work

Despite the lack of reduction in tumour Treg infiltration with CCR5 inhibition, there was an associated delay in tumour growth. Thus CCR5 inhibition may still potentially play an important therapeutic role as part of the armoury against CRC. One possible mechanism by which CCR5 antagonism delays tumour growth is inhibition of endothelial progenitor cell recruitment to the tumour and thus, a disruption in the tumour vasculature. Blocking angiogenesis using anti-VEGF therapy (386) is effective in the treatment of metastatic CRC (9). It would therefore be interesting to explore the effects of CCR5 inhibition in primary and metastatic models of CRC. Targeting the

tumour vasculature through anti-VEGF therapy may have an additive or synergistic effect when combined with CCR5 inhibition. It is also possible that CCR5 inhibition may reduce the local recurrence rates following resection of primary CRC and this could be tested in an animal model. However, CCR5 inhibition in mice delays skin healing (377) and the application of such a therapy may have to occur within a time-frame that avoids delays in the healing of operative wounds and bowel anastomoses.

Regarding Treg recruitment, the phenotype of tumour- and colon- associated endothelium, isolated from human CRC, could be studied to determine differences in the expression of important chemokines and other molecules. Such experiments require successful isolation of endothelial cells, a technically challenging process, which probably explains the limited number of studies in this area previously (387). Whilst chemokine receptor expression on migrating lymphocytes may be downregulated post-migration, there is arguably more stable expression of important endothelial receptors and ligands. Differences in tumour- and colon-associated endothelium have the potential to explain differential recruitment of Treg and Tconv. It is also not understood why Treg may proliferate more than Tconv in the tumour. It has been suggested that Treg may receive stronger antigen signals in tumours than Tconv, driving proliferation (319). $CD11c^+$ DCs have been isolated from murine tumours and shown to stimulate Treg proliferation in a dose-dependent manner, dependent on the presence of TGF-ß (388). Such an effect was not observed for lymph node-isolated DCs. Immunohistochemical studies have demonstrated a correlation between Treg frequency and the ratio of plasmacytoid to myeloid DCs (389). However, the potential role of DCs in selective Treg proliferation and maintenance in human CRC is unclear and would be a suitable topic for further research.

Inhibition of CCR5 reduces the proliferation and migration of serum-starved CRC cells in vitro (267). This has led to a phase I trial, in which patients with hepatic CRC metastases are treated with Maraviroc (390). This trial is primarily designed to assess the safety and tolerability of 8 weeks of continuous Maraviroc therapy in patients with metastatic CRC. Even though the basis for this trial is an inhibitory effect of Maraviroc on the proliferation and migration of CRC tumour cells, such a phase I trial could lead the way for phase II trials investigating the role of Maraviroc in the inhibition of tumour recruitment of immune cells and tumour angiogenesis.

Conclusion

The work presented in this thesis has demonstrated a Treg-specific chemokine receptor signature in human CRC. CCR5 was expressed at higher levels by Treg than by Tconv. The cognate ligands for CCR5 were identified in CRC, at increased levels compared with matched colon. CRC-isolated Treg were chemotactic to CCR5 ligands and were suppressive in vitro. Despite this supportive evidence for the CCR5 axis having a potential role in the recruitment of Treg to tumours, CCR5 inhibition in murine tumour models did not lead to any differences in tumour Treg infiltration. However, CCR5 inhibition did result in delayed tumour growth compared with controls. Possible reasons for the lack of effect of CCR5 inhibition on tumour Treg recruitment, and explanations as to why CCR5 inhibition altered tumour growth, were discussed.

List of References

1. Office for National Statistics. Cancer Statistics registrations: registrations of cancer diagnosed in 2008. http://www.statistics.gov.uk/downloads/theme_health/mb1-39/mb1-no39-2008.pdf (accessed 13 Mar2011).

2. Cancer statistics, 2010. CA Cancer J Clin. 2010 Sep-Oct. http://www.ncbi.nlm.nih.gov/pubmed/20610543 (accessed 12 Mar2011).

3. Vogelstein B, Fearon ER, Hamilton SR, Kern SE, Preisinger AC, Leppert M et al. Genetic alterations during colorectal-tumor development. *N Engl J Med* 1988;**319**:525–532.

4. Markowitz SD, Bertagnolli MM. Molecular origins of cancer: Molecular basis of colorectal cancer. *N Engl J Med* 2009;**361**:2449–2460.

5. Baker SJ, Preisinger AC, Jessup JM, Paraskeva C, Markowitz S, Willson JK et al. p53 gene mutations occur in combination with 17p allelic deletions as late events in colorectal tumorigenesis. *Cancer Res* 1990;**50**:7717–7722.

6. Bass A. Impact of KRAS and BRAF Gene Mutations on Targeted Therapies in Colorectal Cancer. *J Clin Oncol* 2011;**29**:2728 –2729.

7. Di Nicolantonio F, Martini M, Molinari F, Sartore-Bianchi A, Arena S, Saletti P et al. Wild-Type BRAF Is Required for Response to Panitumumab or Cetuximab in Metastatic Colorectal Cancer. *J Clin Oncol* 2008;**26**:5705 –5712.

8. Ellis LM. Mechanisms of action of bevacizumab as a component of therapy for metastatic colorectal cancer. *Semin Oncol* 2006;**33**:S1–7.

9. Tol J, Punt CJA. Monoclonal antibodies in the treatment of metastatic colorectal cancer: A review. *Clin Ther* 2010;**32**:437–453.

10. Lampropoulos P, Zizi-Sermpetzoglou A, Rizos S, Kostakis A, Nikiteas N, Papavassiliou AG. TGF-beta signalling in colon carcinogenesis. *Cancer Lett* 2012;**314**:1–7.

11. Pritchard CC, Grady WM. Colorectal cancer molecular biology moves into clinical practice. *Gut* 2011;**60**:116 –129.

12. Curtin K, Slattery ML, Samowitz WS. CpG Island Methylation in Colorectal Cancer: Past, Present and Future. *Pathol Res Int* 2011;**2011**:902674

13. Johns LE, Houlston RS. A systematic review and meta-analysis of familial colorectal cancer risk. *Am J Gastroenterol* 2001;**96**:2992–3003.

14. Norat T, Bingham S, Ferrari P, Slimani N, Jenab M, Mazuir M et al. Meat, fish, and colorectal cancer risk: the European Prospective Investigation into cancer and nutrition. *J Natl Cancer Inst* 2005;**97**:906–916.

15. Larsson SC, Wolk A. Obesity and colon and rectal cancer risk: a meta-analysis of prospective studies. *Am J Clin Nutr* 2007;**86**:556–565.

16. Wolin KY, Yan Y, Colditz GA. Physical activity and risk of colon adenoma: a meta-analysis. *Br J Cancer* 2011;**104**:882–885.

17. Secretan B, Straif K, Baan R, Grosse Y, El Ghissassi F, Bouvard V et al. A review of human carcinogens--Part E: tobacco, areca nut, alcohol, coal smoke, and salted fish. *Lancet Oncol* 2009;**10**:1033–1034.

18. Kraus S, Arber N. Cancer: Do aspirin and other NSAIDs protect against colorectal cancer? *Nat Rev Gastroenterol Hepatol* 2011;**8**:125–126.

19. Mowat C, Cole A, Windsor A, Ahmad T, Arnott I, Driscoll R et al. Guidelines for the management of inflammatory bowel disease in adults. *Gut* 2011;**60**:571 –607.

20. Galiatsatos P, Foulkes WD. Familial Adenomatous Polyposis. *Am J Gastroenterol* 2006;**101**:385–398.

21. Leslie A, Carey FA, Pratt NR, Steele RJC. The colorectal adenoma-carcinoma sequence. *Br J Surg* 2002;**89**:845–860.

22. Edge S, Byrd D, Compton C. *AJCC Cancer Staging Manual*. 7th Edition. New York, NY: Springer 2010

23. NICE. Capecitabine and oxaliplatin in the adjuvant treatment of stage III (Dukes' C) colon cancer. NICE 2006

24. André T, Boni C, Mounedji-Boudiaf L, Navarro M, Tabernero J, Hickish T et al. Oxaliplatin, fluorouracil, and leucovorin as adjuvant treatment for colon cancer. *N Engl J Med* 2004;**350**:2343–2351.

25. Gray R, Barnwell J, McConkey C, Hills RK, Williams NS, Kerr DJ. Adjuvant chemotherapy versus observation in patients with colorectal cancer: a randomised study. *Lancet* 2007;**370**:2020–2029.

26. Dunn GP, Old LJ, Schreiber RD. The Three Es of Cancer Immunoediting. *Annu Rev Immunol* 2004;**22**:329–360.

27. Birkeland SA, Storm HH, Lamm LU, Barlow L, Blohmé I, Forsberg B et al. Cancer risk after renal transplantation in the Nordic countries, 1964-1986. *Int J Cancer J Int Cancer* 1995;**60**:183–189.

28. Clarke SL, Betts GJ, Plant A, Wright KL, El-Shanawany TM, Harrop R et al. CD4+CD25+FOXP3+ Regulatory T Cells Suppress Anti-Tumor Immune Responses in Patients with Colorectal Cancer. *PLoS ONE* 2006;**1**:e129.

29. Ropponen KM, Eskelinen MJ, Lipponen PK, Alhava E, Kosma V-M. Prognostic value of tumour-infiltrating lymphocytes (TILs) in colorectal cancer. *J Pathol* 1997;**182**:318–324.

30. Popat S. Systematic Review of Microsatellite Instability and Colorectal Cancer Prognosis. *J Clin Oncol* 2004;**23**:609–618.

31. Pagès F, Kirilovsky A, Mlecnik B, Asslaber M, Tosolini M, Bindea G et al. In Situ Cytotoxic and Memory T Cells Predict Outcome in Patients With Early-Stage Colorectal Cancer. *J Clin Oncol* 2009;**27**:5944 –5951.

32. Galon J, Costes A, Sanchez-Cabo F, Kirilovsky A, Mlecnik B, Lagorce-Pagès C et al. Type, Density, and Location of Immune Cells Within Human Colorectal Tumors Predict Clinical Outcome. *Science* 2006;**313**:1960 –1964.

33. Sakaguchi S, Sakaguchi N, Asano M, Itoh M, Toda M. Immunologic self-tolerance maintained by activated T cells expressing IL-2 receptor alpha-chains (CD25). Breakdown of a single mechanism of self-tolerance causes various autoimmune diseases. *J Immunol* 1995;**155**:1151–1164.

34. Sakaguchi S, Miyara M, Costantino CM, Hafler DA. FOXP3+ regulatory T cells in the human immune system. *Nat Rev Immunol* 2010;**10**:490–500.

35. Schmidt A. Molecular mechanisms of Treg-mediated T cell suppression. *Front T Cell Biol* 2012;**3**:51.

36. Cao X, Cai SF, Fehniger TA, Song J, Collins LI, Piwnica-Worms DR et al. Granzyme B and perforin are important for regulatory T cell-mediated suppression of tumor clearance. *Immunity* 2007;**27**:635–646.

37. Qureshi OS, Zheng Y, Nakamura K, Attridge K, Manzotti C, Schmidt EM et al. Trans-Endocytosis of CD80 and CD86: A Molecular Basis for the Cell-Extrinsic Function of CTLA-4. *Science* 2011;**332**:600–603.

38. Seddiki N, Santner-Nanan B, Martinson J, Zaunders J, Sasson S, Landay A et al. Expression of interleukin (IL)-2 and IL-7 receptors discriminates between human regulatory and activated T cells. *J Exp Med* 2006;**203**:1693–1700.

39. Rudensky AY. Regulatory T Cells and Foxp3. *Immunol Rev* 2011;**241**:260–268.

40. Darrasse-Jèze G, Marodon G, Salomon BL, Catala M, Klatzmann D. Ontogeny of CD4+CD25+ regulatory/suppressor T cells in human fetuses. *Blood* 2005;**105**:4715–4721.

41. Fantini MC, Becker C, Monteleone G, Pallone F, Galle PR, Neurath MF. Cutting edge: TGF-beta induces a regulatory phenotype in CD4+CD25- T cells through Foxp3 induction and down-regulation of Smad7. *J Immunol* 2004;**172**:5149–5153.

42. Lin X, Chen M, Liu Y, Guo Z, He X, Brand D et al. Advances in distinguishing natural from induced Foxp3+ regulatory T cells. *Int J Clin Exp Pathol* 2013;**6**:116–123.

43. Sugimoto N, Oida T, Hirota K, Nakamura K, Nomura T, Uchiyama T et al. Foxp3-dependent and -independent molecules specific for CD25+CD4+ natural regulatory T cells revealed by DNA microarray analysis. *Int Immunol* 2006;**18**:1197–1209.

44. Akimova T, Beier UH, Wang L, Levine MH, Hancock WW. Helios Expression Is a Marker of T Cell Activation and Proliferation. *PLoS ONE* 2011;**6**:e24226.

45. Floess S, Freyer J, Siewert C, Baron U, Olek S, Polansky J et al. Epigenetic Control of the foxp3 Locus in Regulatory T Cells. *PLoS Biol* 2007;**5**:e38.

46. Pot C, Apetoh L, Kuchroo VK. Type 1 Regulatory T cells (Tr1) in autoimmunity. *Semin Immunol* 2011;**23**:202–208.

47. Fukaura H, Kent SC, Pietrusewicz MJ, Khoury SJ, Weiner HL, Hafler DA. Induction of circulating myelin basic protein and proteolipid protein-specific transforming growth factor-beta1-secreting Th3 T cells by oral administration of myelin in multiple sclerosis patients. *J Clin Invest* 1996;**98**:70–77.

48. Chaput N, Louafi S, Bardier A, Charlotte F, Vaillant J-C, Ménégaux F et al. Identification of CD8+CD25+Foxp3+ suppressive T cells in colorectal cancer tissue. *Gut* 2009;**58**:520–529.

49. Ha T-Y. The Role of Regulatory T Cells in Cancer. *Immune Netw* 2009;**9**:209.

50. Danke NA, Koelle DM, Yee C, Beheray S, Kwok WW. Autoreactive T Cells in Healthy Individuals. *J Immunol* 2004;**172**:5967 –5972.

51. Betts G, Jones E, Junaid S, El-Shanawany T, Scurr M, Mizen P et al. Suppression of tumour-specific CD4+ T cells by regulatory T cells is associated with progression of human colorectal cancer. *Gut* 2012;**61**:1163–1171.

52. Ling KL, Pratap SE, Bates GJ, Singh B, Mortensen NJ, George BD et al. Increased frequency of regulatory T cells in peripheral blood and tumour infiltrating lymphocytes in colorectal cancer patients. *Cancer Immun* 2007;**7**:7.

53. Frey DM, Droeser RA, Viehl CT, Zlobec I, Lugli A, Zingg U et al. High frequency of tumor-infiltrating FOXP3 regulatory T cells predicts improved survival in mismatch repair-proficient colorectal cancer patients. *Int J Cancer* 2010;**126**:2635–2643.

54. Loddenkemper C, Schernus M, Noutsias M, Stein H, Thiel E, Nagorsen D. In situ analysis of FOXP3+ regulatory T cells in human colorectal cancer. *J Transl Med* 2006;**4**:52.

55. Matera L, Sandrucci S, Mussa A, Boffa C, Castellano I, Cassoni P. Low Foxp3 expression in negative sentinel lymph nodes is associated with node metastases in colorectal cancer. *Gut* 2010;**59**:419 –420.

56. Deng L, Zhang H, Luan Y, Zhang J, Xing Q, Dong S et al. Accumulation of Foxp3+ T Regulatory Cells in Draining Lymph Nodes Correlates with Disease Progression and Immune Suppression in Colorectal Cancer Patients. *Clin Cancer Res* 2010;**16**:4105 –4112.

57. Curiel TJ, Coukos G, Zou L, Alvarez X, Cheng P, Mottram P et al. Specific recruitment of regulatory T cells in ovarian carcinoma fosters immune privilege and predicts reduced survival. *Nat Med* 2004;**10**:942–949.

58. Hiraoka N, Onozato K, Kosuge T, Hirohashi S. Prevalence of FOXP3+ Regulatory T Cells Increases During the Progression of Pancreatic Ductal Adenocarcinoma and Its Premalignant Lesions. *Clin Cancer Res* 2006;**12**:5423 –5434.

59. Gao Q, Qiu S-J, Fan J, Zhou J, Wang X-Y, Xiao Y-S et al. Intratumoral balance of regulatory and cytotoxic T cells is associated with prognosis of hepatocellular carcinoma after resection. *J Clin Oncol* 2007;**25**:2586–2593.

60. James E, Yeh A, King C, Korangy F, Bailey I, Boulanger DS et al. Differential Suppression of Tumor-Specific CD8+ T Cells by Regulatory T Cells. *J Immunol* 2010;**185**:5048 –5055.

61. Morse MA, Hobeika AC, Osada T, Serra D, Niedzwiecki D, Lyerly HK et al. Depletion of human regulatory T cells specifically enhances antigen-specific immune responses to cancer vaccines. *Blood* 2008;**112**:610–618.

62. Cahill RN, Poskitt DC, Frost DC, Trnka Z. Two distinct pools of recirculating T lymphocytes: migratory characteristics of nodal and intestinal T lymphocytes. *J Exp Med* 1977;**145**:420 –428.

63. Adams DH, Eksteen B. Aberrant homing of mucosal T cells and extra-intestinal manifestations of inflammatory bowel disease. *Nat Rev Immunol* 2006;**6**:244–251.

64. Hosoe N, Miura S, Watanabe C, Tsuzuki Y, Hokari R, Oyama T et al. Demonstration of functional role of TECK/CCL25 in T lymphocyte-endothelium interaction in inflamed and uninflamed intestinal mucosa. *Am J Physiol - Gastrointest Liver Physiol* 2004;**286**:G458 –G466.

65. DeNucci CC, Mitchell JS, Shimizu Y. Integrin function in t cell homing to lymphoid and non-lymphoid sites: getting there and staying there. *Crit Rev Immunol* 2009;**29**:87–109.

66. Tomura M, Honda T, Tanizaki H, Otsuka A, Egawa G, Tokura Y et al. Activated regulatory T cells are the major T cell type emigrating from the skin during a cutaneous immune response in mice. *J Clin Invest* 2010;**120**:883–893.

67. Matsushima H, Takashima A. Bidirectional homing of Tregs between the skin and lymph nodes. *J Clin Invest* 2010;**120**:653–656.

68. Eksteen B, Miles A, Curbishley SM, Tselepis C, Grant AJ, Walker LSK et al. Epithelial Inflammation Is Associated with CCL28 Production and the Recruitment of Regulatory T Cells Expressing CCR10. *J Immunol* 2006;**177**:593 –603.

69. Oo YH, Weston CJ, Lalor PF, Curbishley SM, Withers DR, Reynolds GM et al. Distinct Roles for CCR4 and CXCR3 in the Recruitment and Positioning of Regulatory T Cells in the Inflamed Human Liver. *J Immunol* 2010;**184**:2886–2898.

70. Barthel SR, Gavino JD, Descheny L, Dimitroff CJ. Targeting selectins and selectin ligands in inflammation and cancer. *Expert Opin Ther Targets* 2007;**11**:1473–1491.

71. Ley K, Laudanna C, Cybulsky MI, Nourshargh S. Getting to the site of inflammation: the leukocyte adhesion cascade updated. *Nat Rev Immunol* 2007;**7**:678–689.

72. Zipin A, Israeli-Amit M, Meshel T, Sagi-Assif O, Yron I, Lifshitz V et al. Tumor-microenvironment interactions: the fucose-generating FX enzyme controls adhesive properties of colorectal cancer cells. *Cancer Res* 2004;**64**:6571–6578.

73. Ermann J, Hoffmann P, Edinger M, Dutt S, Blankenberg FG, Higgins JP et al. Only the CD62L+ subpopulation of CD4+CD25+ regulatory T cells protects from lethal acute GVHD. *Blood* 2005;**105**:2220–2226.

74. Gorfu G, Rivera-Nieves J, Ley K. Role of β7 integrins in intestinal lymphocyte homing and retention. *Curr Mol Med* 2009;**9**:836–850.

75. Paschos KA, Canovas D, Bird NC. The role of cell adhesion molecules in the progression of colorectal cancer and the development of liver metastasis. *Cell Signal* 2009;**21**:665–674.

76. Koretz K, Schlag P, Boumsell L, Möller P. Expression of VLA-alpha 2, VLA-alpha 6, and VLA-beta 1 chains in normal mucosa and adenomas of the colon, and in colon carcinomas and their liver metastases. *Am J Pathol* 1991;**138**:741–750.

77. Wang J, Zhang Z, Xu K, Sun X, Yang G, Niu W et al. Suppression of integrin αυβ6 by RNA interference in colon cancer cells inhibits extracellular matrix degradation through the MAPK pathway. *Int J Cancer* 2008;**123**:1311–1317.

78. Mook ORF, Van Marie J, Jonges R, Vreeling-Sindelarova H, Frederiks WM, Van Noorden CJF. Interactions between colon cancer cells and hepatocytes in rats in relation to metastasis. *J Cell Mol Med* 2008;**12**:2052–2061.

79. Rott LS, Briskin MJ, Andrew DP, Berg EL, Butcher EC. A fundamental subdivision of circulating lymphocytes defined by adhesion to mucosal addressin cell adhesion molecule-1. Comparison with vascular cell adhesion molecule-1 and correlation with beta 7 integrins and memory differentiation. *J Immunol* 1996;**156**:3727–3736.

80. Cepek KL, Parker CM, Madara JL, Brenner MB. Integrin alpha E beta 7 mediates adhesion of T lymphocytes to epithelial cells. *J Immunol* 1993;**150**:3459–3470.

81. Denning TL, Kim G, Kronenberg M. Cutting Edge: CD4+CD25+ Regulatory T Cells Impaired for Intestinal Homing Can Prevent Colitis. *J Immunol* 2005;**174**:7487 – 7491.

82. Stassen M, Fondel S, Bopp T, Richter C, Müller C, Kubach J et al. Human CD25+ regulatory T cells: two subsets defined by the integrins alpha 4 beta 7 or alpha 4 beta 1 confer distinct suppressive properties upon CD4+ T helper cells. *Eur J Immunol* 2004;**34**:1303–1311.

83. Lehmann J, Huehn J, de la Rosa M, Maszyna F, Kretschmer U, Krenn V et al. Expression of the integrin αEβ7 identifies unique subsets of CD25+ as well as CD25– regulatory T cells. *Proc Natl Acad Sci* 2002;**99**:13031–13036.

84. Tran DQ, Glass DD, Uzel G, Darnell DA, Spalding C, Holland SM et al. Analysis of adhesion molecules, target cells and role of interleukin-2 in human FOXP3+ regulatory T cell suppressor function. *J Immunol* 2009;**182**:2929–2938.

85. Pigott R, Dillon LP, Hemingway IH, Gearing AJH. Soluble forms of E-selectin, ICAM-1 and VCAM-1 are present in the supernatants of cytokine activated cultured endothelial cells. *Biochem Biophys Res Commun* 1992;**187**:584–589.

86. Alexiou D, Karayiannakis A., Syrigos K., Zbar A, Kremmyda A, Bramis I et al. Serum levels of E-selectin, ICAM-1 and VCAM-1 in colorectal cancer patients: correlations with clinicopathological features, patient survival and tumour surgery. *Eur J Cancer* 2001;**37**:2392–2397.

87. Cepek KL, Shaw SK, Parker CM, Russell GJ, Morrow JS, Rimm DL et al. Adhesion between epithelial cells and T lymphocytes mediated by E-cadherin and the alpha E beta 7 integrin. *Nature* 1994;**372**:190–193.

88. Anz D, Mueller W, Golic M, Kunz WG, Rapp M, Koelzer VH et al. CD103 is a hallmark of tumor-infiltrating regulatory T cells. *Int J Cancer* 2011;**129**:2417–2426.

89. Franciszkiewicz K, Le Floc'h A, Jalil A, Vigant F, Robert T, Vergnon I et al. Intratumoral Induction of CD103 Triggers Tumor-Specific CTL Function and CCR5-Dependent T-Cell Retention. *Cancer Res* 2009;**69**:6249 –6255.

90. Murphy PM, Baggiolini M, Charo IF, Hébert CA, Horuk R, Matsushima K et al. International Union of Pharmacology. XXII. Nomenclature for Chemokine Receptors. *Pharmacol Rev* 2000;**52**:145 –176.

91. Balkwill F. Chemokine biology in cancer. *Semin Immunol* 2003;**15**:49–55.

92. Honczarenko M, Douglas RS, Mathias C, Lee B, Ratajczak MZ, Silberstein LE. SDF-1 responsiveness does not correlate with CXCR4 expression levels of developing human bone marrow B cells. *Blood* 1999;**94**:2990–2998.

93. Mitra P, De A, Ethier MF, Mimori K, Kodys K, Shibuta K et al. Loss of chemokine SDF-1alpha-mediated CXCR4 signalling and receptor internalization in human hepatoma cell line HepG2. *Cell Signal* 2001;**13**:311–319.

94. Erreni M, Bianchi P, Laghi L, Mirolo M, Fabbri M, Locati M et al. Chapter 5 Expression of Chemokines and Chemokine Receptors in Human Colon Cancer. In: *Chemokines, Part A*. Academic Press 2009: 105–121.

95. Robinson SC, Scott KA, Wilson JL, Thompson RG, Proudfoot AEI, Balkwill FR. A chemokine receptor antagonist inhibits experimental breast tumor growth. *Cancer Res* 2003;**63**:8360–8365.

96. Kitamura T, Fujishita T, Loetscher P, Revesz L, Hashida H, Kizaka-Kondoh S et al. Inactivation of chemokine (C-C motif) receptor 1 (CCR1) suppresses colon cancer liver metastasis by blocking accumulation of immature myeloid cells in a mouse model. *Proc Natl Acad Sci* 2010;**107**:13063–13068.

97. Yoong KF, Afford SC, Jones R, Aujla P, Qin S, Price K et al. Expression and function of CXC and CC chemokines in human malignant liver tumors: a role for human monokine induced by gamma-interferon in lymphocyte recruitment to hepatocellular carcinoma. *Hepatology* 1999;**30**:100–111.

98. Xanthou G, Duchesnes CE, Williams TJ, Pease JE. CCR3 functional responses are regulated by both CXCR3 and its ligands CXCL9, CXCL10 and CXCL11. *Eur J Immunol* 2003;**33**:2241–2250.

99. Baatar D, Olkhanud P, Sumitomo K, Taub D, Gress R, Biragyn A. Human peripheral blood T regulatory cells (Tregs), functionally primed CCR4+ Tregs and unprimed CCR4- Tregs, regulate effector T cells using FasL. *J Immunol* 2007;**178**:4891–4900.

100. Kanagawa N, Niwa M, Hatanaka Y, Tani Y, Nakagawa S, Fujita T et al. CC-chemokine ligand 17 gene therapy induces tumor regression through augmentation of tumor-infiltrating immune cells in a murine model of preexisting CT26 colon carcinoma. *Int J Cancer J Int Cancer* 2007;**121**:2013–2022.

101. Mizukami Y, Kono K, Kawaguchi Y, Akaike H, Kamimura K, Sugai H et al. CCL17 and CCL22 chemokines within tumor microenvironment are related to accumulation of Foxp3+ regulatory T cells in gastric cancer. *Int J Cancer* 2008;**122**:2286–2293.

102. Musha H, Ohtani H, Mizoi T, Kinouchi M, Nakayama T, Shiiba K et al. Selective infiltration of CCR5(+)CXCR3(+) T lymphocytes in human colorectal carcinoma. *Int J Cancer J Int Cancer* 2005;**116**:949–956.

103. Zimmermann T, Moehler M, Gockel I, Sgourakis GG, Biesterfeld S, Müller M et al. Low expression of chemokine receptor CCR5 in human colorectal cancer correlates with lymphatic dissemination and reduced CD8+ T-cell infiltration. *Int J Colorectal Dis* 2010;**25**:417–424.

104. Tan MCB, Goedegebuure PS, Belt BA, Flaherty B, Sankpal N, Gillanders WE et al. Disruption of CCR5-dependent homing of regulatory T cells inhibits tumor growth in a murine model of pancreatic cancer. *J Immunol* 2009;**182**:1746–1755.

105. Rubie C, Frick VO, Wagner M, Weber C, Kruse B, Kempf K et al. Chemokine expression in hepatocellular carcinoma versus colorectal liver metastases. *World J Gastroenterol WJG* 2006;**12**:6627–6633.

106. Xu L, Xu W, Qiu S, Xiong S. Enrichment of CCR6+Foxp3+ regulatory T cells in the tumor mass correlates with impaired CD8+ T cell function and poor prognosis of breast cancer. *Clin Immunol Orlando Fla* 2010;**135**:466–475.

107. Mumtaz M, Wågsäter D, Löfgren S, Hugander A, Zar N, Dimberg J. Decreased expression of the chemokine CCL21 in human colorectal adenocarcinomas. *Oncol Rep* 2009;**21**:153–158.

108. Hoffmann P, Eder R, Kunz-Schughart LA, Andreesen R, Edinger M. Large-scale in vitro expansion of polyclonal human CD4(+)CD25high regulatory T cells. *Blood* 2004;**104**:895–903.

109. Soler D, Chapman TR, Poisson LR, Wang L, Cote-Sierra J, Ryan M et al. CCR8 expression identifies CD4 memory T cells enriched for FOXP3+ regulatory and Th2 effector lymphocytes. *J Immunol* 2006;**177**:6940–6951.

110. Hoelzinger DB, Smith SE, Mirza N, Dominguez AL, Manrique SZ, Lustgarten J. Blockade of CCL1 Inhibits T Regulatory Cell Suppressive Function Enhancing Tumor Immunity without Affecting T Effector Responses. *J Immunol* 2010;**184**:6833 –6842.

111. Wurbel MA, Philippe JM, Nguyen C, Victorero G, Freeman T, Wooding P et al. The chemokine TECK is expressed by thymic and intestinal epithelial cells and attracts double- and single-positive thymocytes expressing the TECK receptor CCR9. *Eur J Immunol* 2000;**30**:262–271.

112. Hadeiba H, Sato T, Habtezion A, Oderup C, Pan J, Butcher EC. CCR9 expression defines tolerogenic plasmacytoid dendritic cells able to suppress acute graft-versus-host disease. *Nat Immunol* 2008;**9**:1253–1260.

113. Kunkel EJ, Campbell JJ, Haraldsen G, Pan J, Boisvert J, Roberts AI et al. Lymphocyte CC chemokine receptor 9 and epithelial thymus-expressed chemokine (TECK) expression distinguish the small intestinal immune compartment: Epithelial expression of tissue-specific chemokines as an organizing principle in regional immunity. *J Exp Med* 2000;**192**:761–768.

114. Wurbel M-A, McIntire MG, Dwyer P, Fiebiger E. CCL25/CCR9 Interactions Regulate Large Intestinal Inflammation in a Murine Model of Acute Colitis. *PLoS ONE* 2011;**6**:e16442.

115. Pan J, Kunkel EJ, Gosslar U, Lazarus N, Langdon P, Broadwell K et al. Cutting Edge: A Novel Chemokine Ligand for CCR10 And CCR3 Expressed by Epithelial Cells in Mucosal Tissues. *J Immunol* 2000;**165**:2943 –2949.

116. Dimberg J, Hugander A, Wågsäter D. Protein expression of the chemokine, CCL28, in human colorectal cancer. *Int J Oncol* 2006;**28**:315–319.

117. Facciabene A, Peng X, Hagemann IS, Balint K, Barchetti A, Wang L-P et al. Tumour hypoxia promotes tolerance and angiogenesis via CCL28 and Treg cells. *Nature* 2011;**475**:226–230.

118. Li A, Varney ML, Singh RK. Expression of interleukin 8 and its receptors in human colon carcinoma cells with different metastatic potentials. *Clin Cancer Res Off J Am Assoc Cancer Res* 2001;**7**:3298–3304.

119. Oladipo O, Conlon S, O'Grady A, Purcell C, Wilson C, Maxwell PJ et al. The expression and prognostic impact of CXC-chemokines in stage II and III colorectal cancer epithelial and stromal tissue. *Br J Cancer* 2011;**104**:480–487.

120. Eikawa S, Ohue Y, Kitaoka K, Aji T, Uenaka A, Oka M et al. Enrichment of Foxp3+ CD4 Regulatory T Cells in Migrated T Cells to IL-6– and IL-8–Expressing Tumors through Predominant Induction of CXCR1 by IL-6. *J Immunol* 2010;**185**:6734 – 6740.

121. Lacotte S, Brun S, Muller S, Dumortier H. CXCR3, Inflammation, and Autoimmune Diseases. *Ann N Y Acad Sci* 2009;**1173**:310–317.

122. Oo YH, Weston CJ, Lalor PF, Curbishley SM, Withers DR, Reynolds GM et al. Distinct roles for CCR4 and CXCR3 in the recruitment and positioning of regulatory T cells in the inflamed human liver. *J Immunol* 2010;**184**:2886–2898.

123. Hoerning A, Koss K, Datta D, Boneschansker L, Jones CN, Wong IY et al. Subsets of human CD4+ regulatory T cells express the peripheral homing receptor CXCR3. *Eur J Immunol* 2011;**41**:2291–2302.

124. Yang S, Wang B, Guan C, Wu B, Cai C, Wang M et al. Foxp3+IL-17+ T cells promote development of cancer-initiating cells in colorectal cancer. *J Leukoc Biol* 2011;**89**:85–91.

125. Shimizu Y, Dobashi K, Imai H, Sunaga N, Ono A, Sano T et al. CXCR4+FOXP3+CD25+ lymphocytes accumulate in CXCL12-expressing malignant pleural mesothelioma. *Int J Immunopathol Pharmacol* 2009;**22**:43–51.

126. Zou L, Barnett B, Safah H, LaRussa VF, Evdemon-Hogan M, Mottram P et al. Bone Marrow Is a Reservoir for CD4+CD25+ Regulatory T Cells that Traffic through CXCL12/CXCR4 Signals. *Cancer Res* 2004;**64**:8451 –8455.

127. Lim HW, Hillsamer P, Kim CH. Regulatory T cells can migrate to follicles upon T cell activation and suppress GC-Th cells and GC-Th cell-driven B cell responses. *J Clin Invest* 2004;**114**:1640–1649.

128. Lim HW, Broxmeyer HE, Kim CH. Regulation of Trafficking Receptor Expression in Human Forkhead Box P3+ Regulatory T Cells. *J Immunol* 2006;**177**:840 –851.

129. Hirahara K, Liu L, Clark RA, Yamanaka K, Fuhlbrigge RC, Kupper TS. The Majority of Human Peripheral Blood CD4+CD25highFoxp3+ Regulatory T Cells Bear Functional Skin-Homing Receptors. *J Immunol* 2006;**177**:4488–4494.

130. Hojo S, Koizumi K, Tsuneyama K, Arita Y, Cui Z, Shinohara K et al. High-level expression of chemokine CXCL16 by tumor cells correlates with a good prognosis and increased tumor-infiltrating lymphocytes in colorectal cancer. *Cancer Res* 2007;**67**:4725–4731.

131. Meijer J, Ogink J, Roos E. Effect of the chemokine receptor CXCR7 on proliferation of carcinoma cells in vitro and in vivo. *Br J Cancer* 2008;**99**:1493–1501.

132. Ohta M, Tanaka F, Yamaguchi H, Sadanaga N, Inoue H, Mori M. The high expression of Fractalkine results in a better prognosis for colorectal cancer patients. *Int J Oncol* 2005;**26**:41–47.

133. Miyara M, Amoura Z, Parizot C, Badoual C, Dorgham K, Trad S et al. The immune paradox of sarcoidosis and regulatory T cells. *J Exp Med* 2006;**203**:359–370.

134. Hadis U, Wahl B, Schulz O, Hardtke-Wolenski M, Schippers A, Wagner N et al. Intestinal Tolerance Requires Gut Homing and Expansion of FoxP3+ Regulatory T Cells in the Lamina Propria. *Immunity* 2011;**34**:237–246.

135. Nguyen KD, Fohner A, Booker JD, Dong C, Krensky AM, Nadeau KC. XCL1 Enhances Regulatory Activities of CD4+CD25highCD127low/– T Cells in Human Allergic Asthma. *J Immunol* 2008;**181**:5386–5395.

136. Yamazaki C, Miyamoto R, Hoshino K, Fukuda Y, Sasaki I, Saito M et al. Conservation of a chemokine system, XCR1 and its ligand, XCL1, between human and mice. *Biochem Biophys Res Commun* 2010;**397**:756–761.

137. Rubie C, Oliveira V, Kempf K, Wagner M, Tilton B, Rau B et al. Involvement of Chemokine Receptor CCR6 in Colorectal Cancer Metastasis. *Tumor Biol* 2006;**27**:166–174.

138. Matsusue R, Kubo H, Hisamori S, Okoshi K, Takagi H, Hida K et al. Hepatic Stellate Cells Promote Liver Metastasis of Colon Cancer Cells by the Action of SDF-1/CXCR4 Axis. *Ann Surg Oncol* 2009;**16**:2645–2653.

139. Cambien B, Karimdjee BF, Richard-Fiardo P, Bziouech H, Barthel R, Millet MA et al. Organ-specific inhibition of metastatic colon carcinoma by CXCR3 antagonism. *Br J Cancer* 2009;**100**:1755–1764.

140. Amersi FF, Terando AM, Goto Y, Scolyer RA, Thompson JF, Tran AN et al. Activation of CCR9/CCL25 in Cutaneous Melanoma Mediates Preferential Metastasis to the Small Intestine. *Clin Cancer Res* 2008;**14**:638–645.

141. Nocentini G, Ronchetti S, Cuzzocrea S, Riccardi C. GITR/GITRL: more than an effector T cell co-stimulatory system. *Eur J Immunol* 2007;**37**:1165–1169.

142. Stephens GL, McHugh RS, Whitters MJ, Young DA, Luxenberg D, Carreno BM et al. Engagement of glucocorticoid-induced TNFR family-related receptor on effector T cells by its ligand mediates resistance to suppression by CD4+CD25+ T cells. *J Immunol* 2004;**173**:5008–5020.

143. Lutsiak MEC, Tagaya Y, Adams AJ, Schlom J, Sabzevari H. Tumor-Induced Impairment of TCR Signaling Results in Compromised Functionality of Tumor-Infiltrating Regulatory T Cells. *J Immunol* 2008;**180**:5871–5881.

144. McCoy KD, Le Gros G. The role of CTLA-4 in the regulation of T cell immune responses. *Immunol Cell Biol* 1999;**77**:1–10.

145. Wing K, Onishi Y, Prieto-Martin P, Yamaguchi T, Miyara M, Fehervari Z et al. CTLA-4 control over Foxp3+ regulatory T cell function. *Science* 2008;**322**:271–275.

146. Peggs KS, Quezada SA, Chambers CA, Korman AJ, Allison JP. Blockade of CTLA-4 on both effector and regulatory T cell compartments contributes to the antitumor activity of anti–CTLA-4 antibodies. *J Exp Med* 2009;**206**:1717–1725.

147. Watts TH. TNF/TNFR family members in costimulation of T cell responses. *Annu Rev Immunol* 2005;**23**:23–68.

148. Nagorsen D, Scheibenbogen C, Marincola FM, Letsch A, Keilholz U. Natural T Cell Immunity against Cancer. *Clin Cancer Res* 2003;**9**:4296–4303.

149. Rogers PR, Song J, Gramaglia I, Killeen N, Croft M. OX40 promotes Bcl-xL and Bcl-2 expression and is essential for long-term survival of CD4 T cells. *Immunity* 2001;**15**:445–455.

150. Bansal-Pakala P, Jember AG, Croft M. Signaling through OX40 (CD134) breaks peripheral T-cell tolerance. *Nat Med* 2001;**7**:907–912.

151. Vu MD, Xiao X, Gao W, Degauque N, Chen M, Kroemer A et al. OX40 costimulation turns off Foxp3+ Tregs. *Blood* 2007;**110**:2501–2510.

152. Deaglio S, Dwyer KM, Gao W, Friedman D, Usheva A, Erat A et al. Adenosine generation catalyzed by CD39 and CD73 expressed on regulatory T cells mediates immune suppression. *J Exp Med* 2007;**204**:1257–1265.

153. Dwyer KM, Hanidziar D, Putheti P, Hill PA, Pommey S, McRae JL et al. Expression of CD39 by Human Peripheral Blood CD4+CD25+ T Cells Denotes a Regulatory Memory Phenotype. *Am J Transplant* 2010;**10**:2410–2420.

154. Naganuma M, Wiznerowicz EB, Lappas CM, Linden J, Worthington MT, Ernst PB. Cutting Edge: Critical Role for A2A Adenosine Receptors in the T Cell-Mediated Regulation of Colitis. *J Immunol* 2006;**177**:2765–2769.

155. Ernst PB, Garrison JC, Thompson LF. Much ado about adenosine: adenosine synthesis and function in regulatory T cell biology. *J Immunol* 2010;**185**:1993–1998.

156. Fletcher JM, Lonergan R, Costelloe L, Kinsella K, Moran B, O'Farrelly C et al. CD39+Foxp3+ Regulatory T Cells Suppress Pathogenic Th17 Cells and Are Impaired in Multiple Sclerosis. *J Immunol* 2009;**183**:7602–7610.

157. Tosolini M, Kirilovsky A, Mlecnik B, Fredriksen T, Mauger S, Bindea G et al. Clinical impact of different classes of infiltrating T cytotoxic and helper cells (Th1, th2, treg, th17) in patients with colorectal cancer. *Cancer Res* 2011;**71**:1263–1271.

158. Sun X, Wu Y, Gao W, Enjyoji K, Csizmadia E, Müller CE et al. CD39/ENTPD1 expression by CD4+Foxp3+ regulatory T cells promotes hepatic metastatic tumor growth in mice. *Gastroenterology* 2010;**139**:1030–1040.

159. Feng L, Sun X, Csizmadia E, Han L, Bian S, Murakami T et al. Vascular CD39/ENTPD1 directly promotes tumor cell growth by scavenging extracellular adenosine triphosphate. *Neoplasia N Y N* 2011;**13**:206–216.

160. Alam MS, Kurtz CC, Rowlett RM, Reuter BK, Wiznerowicz E, Das S et al. CD73 is expressed by human regulatory T helper cells and suppresses proinflammatory cytokine production and Helicobacter felis-induced gastritis in mice. *J Infect Dis* 2009;**199**:494–504.

161. Stagg J, Divisekera U, McLaughlin N, Sharkey J, Pommey S, Denoyer D et al. Anti-CD73 antibody therapy inhibits breast tumor growth and metastasis. *Proc Natl Acad Sci U S A* 2010;**107**:1547–1552.

162. Stagg J, Divisekera U, Duret H, Sparwasser T, Teng MW, Darcy PK et al. CD73-deficient mice have increased anti-tumor immunity and are resistant to experimental metastasis. *Cancer Res* 2011;**71**:2892–2900.

163. Jungblut M, Oeltze K, Zehnter I, Hasselmann D, Bosio A. Preparation of Single-Cell Suspensions from Mouse Spleen with the gentleMACS Dissociator. *J Vis Exp* doi:10.3791/1029

164. Van Ree JH, Jeganathan KB, Malureanu L, van Deursen JM. Overexpression of the E2 ubiquitin–conjugating enzyme UbcH10 causes chromosome missegregation and tumor formation. *J Cell Biol* 2010;**188**:83–100.

165. Hardt, O, Parker, LL, Dudley, ME, Bosio, A. Isolation of tumor cell subpopulations using semi-automated tissue dissociation and magnetic cell separation. *Cancer Res* 2010:**70**:S1 (Abstract 3357).

166. Mulder WMC, Koenen H, Muysenberg AJC, Bloemena E, Wagsfaff J, Scheper RJ. Reduced expression of distinct T-cell CD molecules by collagenase/DNase treatment. *Cancer Immunol Immunother* 1994;**38**:253–258.

167. Diederichsen ACP, Zeuthen J, Christensen PB, Kristensen T. Characterisation of tumour infiltrating lymphocytes and correlations with immunological surface molecules in colorectal cancer. *Eur J Cancer* 1999;**35**:721–726.

168. Shields PL, Morland CM, Salmon M, Qin S, Hubscher SG, Adams DH. Chemokine and Chemokine Receptor Interactions Provide a Mechanism for Selective T Cell Recruitment to Specific Liver Compartments Within Hepatitis C-Infected Liver. *J Immunol* 1999;**163**:6236–6243.

169. Ford AL, Foulcher E, Goodsall AL, Sedgwick JD. Tissue digestion with dispase substantially reduces lymphocyte and macrophage cell-surface antigen expression. *J Immunol Methods* 1996;**194**:71–75.

170. Grange C, Létourneau J, Forget M-A, Godin-Ethier J, Martin J, Liberman M et al. Phenotypic characterization and functional analysis of human tumor immune infiltration after mechanical and enzymatic disaggregation. *J Immunol Methods* 2011;**372**:119–126.

171. Autissier P, Soulas C, Burdo TH, Williams KC. Evaluation of a 12-color flow cytometry panel to study lymphocyte, monocyte, and dendritic cell subsets in humans. *Cytom Part J Int Soc Anal Cytol* 2010;**77**:410–419.

172. Bull DM, Bookman MA. Isolation and functional characterization of human intestinal mucosal lymphoid cells. *J Clin Invest* 1977;**59**:966–974.

173. Saccani A, Saccani S, Orlando S, Sironi M, Bernasconi S, Ghezzi P et al. Redox regulation of chemokine receptor expression. *Proc Natl Acad Sci* 2000;**97**:2761–2766.

174. Burmeister Y, Lischke T, Dahler AC, Mages HW, Lam K-P, Coyle AJ et al. ICOS Controls the Pool Size of Effector-Memory and Regulatory T Cells. *J Immunol* 2008;**180**:774–782.

175. McMurchy AN, Levings MK. Suppression assays with human T regulatory cells: A technical guide. *Eur J Immunol* 2012;**42**:27–34.

176. Arnold LW, Lannigan J. Practical Issues in High-Speed Cell Sorting. In: *Current Protocols in Cytometry*. John Wiley & Sons, Inc. 2001http://onlinelibrary.wiley.com/doi/10.1002/0471142956.cy0124s51/abstract (accessed 6 Nov2013).

177. Ariel A, Yavin EJ, Hershkoviz R, Avron A, Franitza S, Hardan I et al. IL-2 Induces T Cell Adherence to Extracellular Matrix: Inhibition of Adherence and Migration by IL-2 Peptides Generated by Leukocyte Elastase. *J Immunol* 1998;**161**:2465–2472.

178. Hershkoviz R, Schor H, Ariel A, Hecht I, Cohen IR, Lider O et al. Disaccharides generated from heparan sulphate or heparin modulate chemokine-induced T-cell adhesion to extracellular matrix. *Immunology* 2000;**99**:87–93.

179. Caradec J, Sirab N, Revaud D, Keumeugni C, Loric S. Is GAPDH a relevant housekeeping gene for normalisation in colorectal cancer experiments? *Br J Cancer* 2010;**103**:1475–1476.

180. Kheirelseid EA, Chang KH, Newell J, Kerin MJ, Miller N. Identification of endogenous control genes for normalisation of real-time quantitative PCR data in colorectal cancer. *BMC Mol Biol* 2010;**11**:12.

181. Rubie C, Kempf K, Hans J, Su T, Tilton B, Georg T et al. Housekeeping gene variability in normal and cancerous colorectal, pancreatic, esophageal, gastric and hepatic tissues. *Mol Cell Probes* 2005;**19**:101–109.

182. Sørby LA, Andersen SN, Bukholm IR, Jacobsen MB. Evaluation of suitable reference genes for normalization of real-time reverse transcription PCR analysis in colon cancer. *J Exp Clin Cancer Res*;**29**:144–144.

183. Bustin SA, Benes V, Garson JA, Hellemans J, Huggett J, Kubista M et al. The MIQE guidelines: minimum information for publication of quantitative real-time PCR experiments. *Clin Chem* 2009;**55**:611–622.

184. Vandesompele J, Preter KD, Pattyn F, Poppe B, Roy NV, Paepe AD et al. Accurate normalization of real-time quantitative RT-PCR data by geometric averaging of multiple internal control genes. *Genome Biol* 2002;**3**:research0034.

185. Andersen CL, Jensen JL, Ørntoft TF. Normalization of real-time quantitative reverse transcription-PCR data: a model-based variance estimation approach to identify genes suited for normalization, applied to bladder and colon cancer data sets. *Cancer Res* 2004;**64**:5245–5250.

186. Pfaffl MW, Tichopad A, Prgomet C, Neuvians TP. Determination of stable housekeeping genes, differentially regulated target genes and sample integrity: BestKeeper – Excel-based tool using pair-wise correlations. *Biotechnol Lett* 2004;**26**:509–515.

187. Frommer M, McDonald LE, Millar DS, Collis CM, Watt F, Grigg GW et al. A genomic sequencing protocol that yields a positive display of 5-methylcytosine residues in individual DNA strands. *Proc Natl Acad Sci U S A* 1992;**89**:1827–1831.

188. Tatura R, Zeschnigk M, Adamzik M, Probst-Kepper M, Buer J, Kehrmann J. Quantification of Regulatory T Cells in Septic Patients by Real-Time PCR–Based Methylation Assay and Flow Cytometry. *PLoS ONE* 2012;**7**:e49962.

189. Weiss W, Görg A. Sample solublization buffers for two-dimensional electrophoresis. *Methods Mol Biol Clifton NJ* 2008;**424**:35–42.

190. Kaufmann SH, Ewing CM, Shaper JH. The erasable Western blot. *Anal Biochem* 1987;**161**:89–95.

191. Salama P, Phillips M, Grieu F, Morris M, Zeps N, Joseph D et al. Tumor-Infiltrating FOXP3+ T Regulatory Cells Show Strong Prognostic Significance in Colorectal Cancer. *J Clin Oncol* 2009;**27**:186–192.

192. Yoon HH, Orrock JM, Foster NR, Sargent DJ, Smyrk TC, Sinicrope FA. Prognostic impact of FoxP3+ regulatory T cells in relation to CD8+ T lymphocyte density in human colon carcinomas. *PloS One* 2012;**7**:e42274.

193. Svensson H, Olofsson V, Lundin S, Yakkala C, Björck S, Börjesson L et al. Accumulation of CCR4+ CTLA-4hi FOXP3+CD25hi Regulatory T Cells in Colon Adenocarcinomas Correlate to Reduced Activation of Conventional T Cells. *PLoS ONE* 2012;**7**:e30695.

194. Williams G, Philip Quirke, Neil Shepherd. Standards and Datasets for Reporting Cancers: Dataset for colorectal cancer. The Royal College of Pathologists 2007.

195. Sinicrope FA, Rego RL, Ansell SM, Knutson KL, Foster NR, Sargent DJ. Intraepithelial effector (CD3+)/regulatory (FoxP3+) T-cell ratio predicts a clinical outcome of human colon carcinoma. *Gastroenterology* 2009;**137**:1270–1279.

196. Le Gouvello S, Bastuji-Garin S, Aloulou N, Mansour H, Chaumette M-T, Berrehar F et al. High prevalence of Foxp3 and IL17 in MMR-proficient colorectal carcinomas. *Gut* 2008;**57**:772–779.

197. Woo EY, Chu CS, Goletz TJ, Schlienger K, Yeh H, Coukos G et al. Regulatory CD4(+)CD25(+) T cells in tumors from patients with early-stage non-small cell lung cancer and late-stage ovarian cancer. *Cancer Res* 2001;**61**:4766–4772.

198. Tao H, Mimura Y, Aoe K, Kobayashi S, Yamamoto H, Matsuda E et al. Prognostic potential of FOXP3 expression in non-small cell lung cancer cells combined with tumor-infiltrating regulatory T cells. *Lung Cancer Amst Neth* 2012;**75**:95–101.

199. Liyanage UK, Moore TT, Joo H-G, Tanaka Y, Herrmann V, Doherty G et al. Prevalence of Regulatory T Cells Is Increased in Peripheral Blood and Tumor Microenvironment of Patients with Pancreas or Breast Adenocarcinoma. *J Immunol* 2002;**169**:2756–2761.

200. Merlo A, Casalini P, Carcangiu ML, Malventano C, Triulzi T, Mènard S et al. FOXP3 expression and overall survival in breast cancer. *J Clin Oncol Off J Am Soc Clin Oncol* 2009;**27**:1746–1752.

201. Andaloussi AE, Lesniak MS. An increase in CD4+CD25+FOXP3+ regulatory T cells in tumor-infiltrating lymphocytes of human glioblastoma multiforme. *Neuro-Oncol* 2006;**8**:234–243.

202. Strauss L, Bergmann C, Szczepanski M, Gooding W, Johnson JT, Whiteside TL. A unique subset of CD4+CD25highFoxp3+ T cells secreting interleukin-10 and transforming growth factor-beta1 mediates suppression in the tumor microenvironment. *Clin Cancer Res Off J Am Assoc Cancer Res* 2007;**13**:4345–4354.

203. Ichihara F, Kono K, Takahashi A, Kawaida H, Sugai H, Fujii H. Increased populations of regulatory T cells in peripheral blood and tumor-infiltrating lymphocytes in patients with gastric and esophageal cancers. *Clin Cancer Res Off J Am Assoc Cancer Res* 2003;**9**:4404–4408.

204. Kono K, Kawaida H, Takahashi A, Sugai H, Mimura K, Miyagawa N et al. CD4(+)CD25high regulatory T cells increase with tumor stage in patients with gastric and esophageal cancers. *Cancer Immunol Immunother* 2006;**55**:1064–1071.

205. Unitt E, Rushbrook SM, Marshall A, Davies S, Gibbs P, Morris LS et al. Compromised lymphocytes infiltrate hepatocellular carcinoma: the role of T-regulatory cells. *Hepatology* 2005;**41**:722–730.

206. Suzuki H, Chikazawa N, Tasaka T, Wada J, Yamasaki A, Kitaura Y et al. Intratumoral CD8+ T/FOXP3+ cell ratio is a predictive marker for survival in patients with colorectal cancer. *Cancer Immunol Immunother* 2009;**59**:653–661.

207. Zeestraten ECM, Hoesel AQV, Speetjens FM, Menon AG, Putter H, Velde CJH van de et al. FoxP3- and CD8-positive Infiltrating Immune Cells Together Determine Clinical Outcome in Colorectal Cancer. *Cancer Microenviron* 2013;**6**:31–39.

208. Correale P, Rotundo MS, Del Vecchio MT, Remondo C, Migali C, Ginanneschi C et al. Regulatory (FoxP3+) T-cell Tumor Infiltration Is a Favorable Prognostic Factor in Advanced Colon Cancer Patients Undergoing Chemo or Chemoimmunotherapy. *J Immunother* 2010;**33**:435–441.

209. Tougeron D, Maby P, Elie N, Fauquembergue E, Le Pessot F, Cornic M et al. Regulatory T lymphocytes are associated with less aggressive histologic features in microsatellite-unstable colorectal cancers. *PloS One* 2013;**8**:e61001.

210. Erdman SE, Poutahidis T. Roles for Inflammation and Regulatory T Cells in Colon Cancer. *Toxicol Pathol* 2010;**38**:76 –87.

211. Blatner NR, Bonertz A, Beckhove P, Cheon EC, Krantz SB, Strouch M et al. In colorectal cancer mast cells contribute to systemic regulatory T-cell dysfunction. *Proc Natl Acad Sci* 2010;**107**:6430 –6435.

212. Jobin C. COLORECTAL CANCER CRC--all about microbial products and barrier function? *Nat Rev Gastroenterol Hepatol* 2012;**9**:694–696.

213. Lee AM, Clear AJ, Calaminici M, Davies AJ, Jordan S, MacDougall F et al. Number of CD4+ cells and location of forkhead box protein P3-positive cells in diagnostic follicular lymphoma tissue microarrays correlates with outcome. *J Clin Oncol Off J Am Soc Clin Oncol* 2006;**24**:5052–5059.

214. Badoual C, Hans S, Rodriguez J, Peyrard S, Klein C, Agueznay NEH et al. Prognostic value of tumor-infiltrating CD4+ T-cell subpopulations in head and neck cancers. *Clin Cancer Res Off J Am Assoc Cancer Res* 2006;**12**:465–472.

215. Nosho K, Baba Y, Tanaka N, Shima K, Hayashi M, Meyerhardt JA et al. Tumour-infiltrating T-cell subsets, molecular changes in colorectal cancer and prognosis: cohort study and literature review. *J Pathol* 2010;**222**:350–366.

216. Camus M, Tosolini M, Mlecnik B, Pagès F, Kirilovsky A, Berger A et al. Coordination of intratumoral immune reaction and human colorectal cancer recurrence. *Cancer Res* 2009;**69**:2685–2693.

217. Ropponen KM, Eskelinen MJ, Lipponen PK, Alhava E, Kosma VM. Prognostic value of tumour-infiltrating lymphocytes (TILs) in colorectal cancer. *J Pathol* 1997;**182**:318–324.

218. Drescher KM, Sharma P, Watson P, Gatalica Z, Thibodeau SN, Lynch HT. Lymphocyte recruitment into the tumor site is altered in patients with MSI-H colon cancer. *Fam Cancer* 2009;**8**:231–239.

219. Walker MR, Kasprowicz DJ, Gersuk VH, Benard A, Van Landeghen M, Buckner JH et al. Induction of FoxP3 and acquisition of T regulatory activity by stimulated human CD4+CD25- T cells. *J Clin Invest* 2003;**112**:1437–1443.

220. Roncador G, Brown PJ, Maestre L, Hue S, Martínez-Torrecuadrada JL, Ling K-L et al. Analysis of FOXP3 protein expression in human CD4+CD25+ regulatory T cells at the single-cell level. *Eur J Immunol* 2005;**35**:1681–1691.

221. Kim M, Grimmig T, Grimm M, Lazariotou M, Meier E, Rosenwald A et al. Expression of Foxp3 in colorectal cancer but not in Treg cells correlates with disease progression in patients with colorectal cancer. *PloS One* 2013;**8**:e53630.

222. Jang TJ. Progressive Increase of Regulatory T Cells and Decrease of CD8+ T Cells and CD8+ T Cells/Regulatory T Cells Ratio during Colorectal Cancer Development. *Korean J Pathol* 2013;**47**:443.

223. Kocián P, Šedivcová M, Drgáč J, Cerná K, Hoch J, Kodet R et al. Tumor-infiltrating lymphocytes and dendritic cells in human colorectal cancer: their relationship to KRAS mutational status and disease recurrence. *Hum Immunol* 2011;**72**:1022–1028.

224. Liu X, Jakubowski M, Hunt JL. KRAS gene mutation in colorectal cancer is correlated with increased proliferation and spontaneous apoptosis. *Am J Clin Pathol* 2011;**135**:245–252.

225. Sekar D, Hahn C, Brüne B, Roberts E, Weigert A. Apoptotic tumor cells induce IL-27 release from human DCs to activate Treg cells that express CD69 and attenuate cytotoxicity. *Eur J Immunol* 2012;**42**:1585–1598.

226. Michel S, Benner A, Tariverdian M, Wentzensen N, Hoefler P, Pommerencke T et al. High density of FOXP3-positive T cells infiltrating colorectal cancers with microsatellite instability. *Br J Cancer* 2008;**99**:1867–1873.

227. Diederichsen ACP, Hjelmborg J v B, Christensen PB, Zeuthen J, Fenger C. Prognostic value of the CD4+/CD8+ ratio of tumour infiltrating lymphocytes in colorectal cancer and HLA-DR expression on tumour cells. *Cancer Immunol Immunother CII* 2003;**52**:423–428.

228. Michael-Robinson JM, Biemer-Hüttmann A-E, Purdie DM, Walsh MD, Simms LA, Biden KG et al. Tumour infiltrating lymphocytes and apoptosis are independent features in colorectal cancer stratified according to microsatellite instability status. *Gut* 2001;**48**:360–366.

229. Koch M, Beckhove P, op den Winkel J, Autenrieth D, Wagner P, Nummer D et al. Tumor Infiltrating T Lymphocytes in Colorectal Cancer. *Ann Surg* 2006;**244**:986–993.

230. Lee B, Sharron M, Blanpain C, Doranz BJ, Vakili J, Setoh P et al. Epitope mapping of CCR5 reveals multiple conformational states and distinct but overlapping structures involved in chemokine and coreceptor function. *J Biol Chem* 1999;**274**:9617–9626.

231. Wu L, LaRosa G, Kassam N, Gordon CJ, Heath H, Ruffing N et al. Interaction of Chemokine Receptor CCR5 with its Ligands: Multiple Domains for HIV-1 gp120 Binding and a Single Domain for Chemokine Binding. *J Exp Med* 1997;**186**:1373–1381.

232. Berro R, Klasse PJ, Lascano D, Flegler A, Nagashima KA, Sanders RW et al. Multiple CCR5 Conformations on the Cell Surface Are Used Differentially by Human Immunodeficiency Viruses Resistant or Sensitive to CCR5 Inhibitors ▽. *J Virol* 2011;**85**:8227–8240.

233. Chang L-Y, Lin Y-C, Mahalingam J, Huang C-T, Chen T-W, Kang C-W et al. Tumor-derived chemokine CCL5 enhances TGF-ß mediated killing of CD8+ T cells in colon cancer by T regulatory cells. *Cancer Res* 2012;**72**:1092–1102.

234. Erreni M, Bianchi P, Laghi L, Mirolo M, Fabbri M, Locati M et al. Expression of chemokines and chemokine receptors in human colon cancer. *Methods Enzymol* 2009;**460**:105–121.

235. Parsonage G, Machado LR, Hui JW-Y, McLarnon A, Schmaler T, Balasothy M et al. CXCR6 and CCR5 Localize T Lymphocyte Subsets in Nasopharyngeal Carcinoma. *Am J Pathol* 2012;**180**:1215–1222.

236. Oldham KA, Parsonage G, Bhatt RI, Wallace DMA, Deshmukh N, Chaudhri S et al. T lymphocyte recruitment into renal cell carcinoma tissue: a role for chemokine receptors CXCR3, CXCR6, CCR5, and CCR6. *Eur Urol* 2012;**61**:385–394.

237. Liu J, Zhang N, Li Q, Zhang W, Ke F, Leng Q et al. Tumor-associated macrophages recruit CCR6+ regulatory T cells and promote the development of colorectal cancer via enhancing CCL20 production in mice. *PloS One* 2011;**6**:e19495.

238. Kleinewietfeld M, Puentes F, Borsellino G, Battistini L, Rötzschke O, Falk K. CCR6 expression defines regulatory effector/memory-like cells within the CD25+CD4+ T-cell subset. *Blood* 2005;**105**:2877–2886.

239. Kunkel EJ, Boisvert J, Murphy K, Vierra MA, Genovese MC, Wardlaw AJ et al. Expression of the Chemokine Receptors CCR4, CCR5, and CXCR3 by Human Tissue-Infiltrating Lymphocytes. *Am J Pathol* 2002;**160**:347–355.

240. Qin S, Rottman JB, Myers P, Kassam N, Weinblatt M, Loetscher M et al. The chemokine receptors CXCR3 and CCR5 mark subsets of T cells associated with certain inflammatory reactions. *J Clin Invest* 1998;**101**:746–754.

241. Van Lelyveld SFL, Wensing AMJ, Hoepelman AIM. The MOTIVATE trials: maraviroc therapy in antiretroviral treatment-experienced HIV-1-infected patients. *Expert Rev Anti Infect Ther* 2012;**10**:1241–1247.

242. Glass WG, McDermott DH, Lim JK, Lekhong S, Yu SF, Frank WA et al. CCR5 deficiency increases risk of symptomatic West Nile virus infection. *J Exp Med* 2006;**203**:35–40.

243. Prahalad S. Negative association between the chemokine receptor CCR5-Δ32 polymorphism and rheumatoid arthritis: A meta-analysis. *Genes Immun* 2006;**7**:264–268.

244. Kaimen-Maciel DR, Reiche EMV, Brum Souza DG, Frota Comini ER, Bobroff F, Morimoto HK et al. CCR5-Delta32 genetic polymorphism associated with benign clinical course and magnetic resonance imaging findings in Brazilian patients with multiple sclerosis. *Int J Mol Med* 2007;**20**:337–344.

245. Petrek M, Cermáková Z, Hutyrová B, Miceková D, Drábek J, Rovensky J et al. CC chemokine receptor 5 and interleukin-1 receptor antagonist gene polymorphisms in patients with primary Sjögren's syndrome. *Clin Exp Rheumatol* 2002;**20**:701–703.

246. Fischereder M, Luckow B, Hocher B, Wüthrich RP, Rothenpieler U, Schneeberger H et al. CC chemokine receptor 5 and renal-transplant survival. *Lancet* 2001;**357**:1758–1761.

247. Mañes S, Mira E, Colomer R, Montero S, Real LM, Gómez-Moutón C et al. CCR5 Expression Influences the Progression of Human Breast Cancer in a p53-dependent Manner. *J Exp Med* 2003;**198**:1381–1389.

248. Pereira RW, Pires ER, Duarte APM, Moura RP de, Monteiro E, Torloni H et al. Frequency of the CCRdelta32 allele in Brazilians: a study in colorectal cancer and in HTLV-I infection. *Genet Mol Biol* 2000;**23**:523–526.

249. Blanquicett C, Johnson MR, Heslin M, Diasio RB. Housekeeping Gene Variability in Normal and Carcinomatous Colorectal and Liver Tissues: Applications in Pharmacogenomic Gene Expression Studies. *Anal Biochem* 2002;**303**:209–214.

250. Samson M, Labbe O, Mollereau C, Vassart G, Parmentier M. Molecular cloning and functional expression of a new human CC-chemokine receptor gene. *Biochemistry (Mosc)* 1996;**35**:3362–3367.

251. Petkovic V, Moghini C, Paoletti S, Uguccioni M, Gerber B. I-TAC/CXCL11 is a natural antagonist for CCR5. *J Leukoc Biol* 2004;**76**:701–708.

252. Hillyer P, Male D. Expression of chemokines on the surface of different human endothelia. *Immunol Cell Biol* 2005;**83**:375–382.

253. Eberlein J, Nguyen TT, Victorino F, Golden-Mason L, Rosen HR, Homann D. Comprehensive assessment of chemokine expression profiles by flow cytometry. *J Clin Invest* 2010;**120**:907–923.

254. Zlotnik A. Chemokines and cancer. *Int J Cancer* 2006;**119**:2026–2029.

255. Berin MC, Dwinell MB, Eckmann L, Kagnoff MF. Production of MDC/CCL22 by human intestinal epithelial cells. *Am J Physiol - Gastrointest Liver Physiol* 2001;**280**:G1217 –G1226.

256. Wågsäter D, Dienus O, Löfgren S, Hugander A, Dimberg J. Quantification of the chemokines CCL17 and CCL22 in human colorectal adenocarcinomas. *Mol Med Rep* 2008;**1**:211–217.

257. Maruyama T, Kono K, Izawa S, Mizukami Y, Kawaguchi Y, Mimura K et al. CCL17 and CCL22 chemokines within tumor microenvironment are related to infiltration of regulatory T cells in esophageal squamous cell carcinoma. *Dis Esophagus Off J Int Soc Dis Esophagus ISDE* 2010;**23**:422–429.

258. Mizukami Y, Kono K, Kawaguchi Y, Akaike H, Kamimura K, Sugai H et al. CCL17 and CCL22 chemokines within tumor microenvironment are related to accumulation of Foxp3+ regulatory T cells in gastric cancer. *Int J Cancer* 2008;**122**:2286–2293.

259. Baier PK, Eggstein S, Wolff-Vorbeck G, Baumgartner U, Hopt UT. Chemokines in human colorectal carcinoma. *Anticancer Res* 2005;**25**:3581–3584.

260. Langenes V, Svensson H, Börjesson L, Gustavsson B, Bemark M, Sjöling Å et al. Expression of the chemokine decoy receptor D6 is decreased in colon adenocarcinomas. *Cancer Immunol Immunother CII* 2013;**62**:1687–1695.

261. Uhlen M, Oksvold P, Fagerberg L, Lundberg E, Jonasson K, Forsberg M et al. Towards a knowledge-based Human Protein Atlas. *Nat Biotechnol* 2010;**28**:1248–1250.

262. Da Silva CC, Lamerant-Fayel N, Paprocka M, Mitterrand M, Gosset D, Dus D et al. Selective human endothelial cell activation by chemokines as a guide to cell homing. *Immunology* 2009;**126**:394–404.

263. Netelenbos T, Dräger AM, van het Hof B, Kessler FL, Delouis C, Huijgens PC et al. Differences in sulfation patterns of heparan sulfate derived from human bone marrow and umbilical vein endothelial cells. *Exp Hematol* 2001;**29**:884–893.

264. Hansell CAH, Hurson CE, Nibbs RJB. DARC and D6: silent partners in chemokine regulation? *Immunol Cell Biol* 2011;**89**:197–206.

265. Gao J, Kuhns D, Tiffany H, McDermott D, Li X, Francke U et al. Structure and functional expression of the human macrophage inflammaotry protein 1 alpha/RANTES receptor. *J Exp Med* 1993;**177**:1421–1427.

266. Blanpain C, Migeotte I, Lee B, Vakili J, Doranz BJ, Govaerts C et al. CCR5 Binds Multiple CC-Chemokines: MCP-3 Acts as a Natural Antagonist. *Blood* 1999;**94**:1899–1905.

267. Cambien B, Richard-Fiardo P, Karimdjee BF, Martini V, Ferrua B, Pitard B et al. CCL5 Neutralization Restricts Cancer Growth and Potentiates the Targeting of PDGFRβ in Colorectal Carcinoma. *PLoS ONE* 2011;**6**:e28842.

268. Xu BJ, An QA, Srinivasa Gowda S, Yan W, Pierce LA, Abel TW et al. Identification of blood protein biomarkers that aid in the clinical assessment of patients with malignant glioma. *Int J Oncol* 2012;**40**:1995–2003.

269. Carvalho Batista A, Mendonça EF, Rodrigues Leles C, Queiroz Cunha F, Fukada SY, De Cassia Gonçalves Alencar R et al. Dual role of CCL3/CCR1 in oral squamous cell carcinoma: Implications in tumor metastasis and local host defense. *Oncol Rep* 2007;**18**:1107–1113.

270. Rajkumar T, Vijayalakshmi N, Gopal G, Sabitha K, Shirley S, Raja UM et al. Identification and validation of genes involved in gastric tumorigenesis. *Cancer Cell Int* 2010;**10**:45.

271. Lu P, Nakamoto Y, Nemoto-Sasaki Y, Fujii C, Wang H, Hashii M et al. Potential interaction between CCR1 and its ligand, CCL3, induced by endogenously produced interleukin-1 in human hepatomas. *Am J Pathol* 2003;**162**:1249–1258.

272. Negus RP, Stamp GW, Hadley J, Balkwill FR. Quantitative assessment of the leukocyte infiltrate in ovarian cancer and its relationship to the expression of C-C chemokines. *Am J Pathol* 1997;**150**:1723–1734.

273. Wolf M, Clark-Lewis I, Buri C, Langen H, Lis M, Mazzucchelli L. Cathepsin D specifically cleaves the chemokines macrophage inflammatory protein-1 alpha, macrophage inflammatory protein-1 beta, and SLC that are expressed in human breast cancer. *Am J Pathol* 2003;**162**:1183–1190.

274. Saito S, Kitayama J, Jin ZX, Tsuno N, Kaisaki S, Seto Y et al. Beta-chemokine, macrophage inflammatory protein-1beta (MIP-1beta), is highly expressed in diffuse type human gastric cancers. *J Exp Clin Cancer Res CR* 2003;**22**:453–459.

275. Moran CJ, Arenberg DA, Huang C-C, Giordano TJ, Thomas DG, Misek DE et al. RANTES expression is a predictor of survival in stage I lung adenocarcinoma. *Clin Cancer Res Off J Am Assoc Cancer Res* 2002;**8**:3803–3812.

276. Luboshits G, Shina S, Kaplan O, Engelberg S, Nass D, Lifshitz-Mercer B et al. Elevated expression of the CC chemokine regulated on activation, normal T cell expressed and secreted (RANTES) in advanced breast carcinoma. *Cancer Res* 1999;**59**:4681–4687.

277. Niwa Y, Akamatsu H, Niwa H, Sumi H, Ozaki Y, Abe A. Correlation of tissue and plasma RANTES levels with disease course in patients with breast or cervical cancer. *Clin Cancer Res Off J Am Assoc Cancer Res* 2001;**7**:285–289.

278. König JE, Senge T, Allhoff EP, König W. Analysis of the inflammatory network in benign prostate hyperplasia and prostate cancer. *The Prostate* 2004;**58**:121–129.

279. Mueller A, Strange PG. Mechanisms of internalization and recycling of the chemokine receptor, CCR5. *Eur J Biochem FEBS* 2004;**271**:243–252.

280. Ubogu EE, Callahan MK, Tucky BH, Ransohoff RM. CCR5 expression on monocytes and T cells: modulation by transmigration across the blood-brain barrier in vitro. *Cell Immunol* 2006;**243**:19–29.

281. Hsu C-J, Wu M-H, Chen C-Y, Tsai C-H, Hsu H-C, Tang C-H. AMP-activated protein kinase activation mediates CCL3-induced cell migration and matrix metalloproteinase-2 expression in human chondrosarcoma. *Cell Commun Signal* 2013;**11**:68.

282. Choi W, Li Z, Oh H-J, Im S-K, Lee S-H, Park S-H et al. Expression of CCR5 and its ligands CCL3, -4, and -5 in the tear film and ocular surface of patients with dry eye disease. *Curr Eye Res* 2012;**37**:12–17.

283. Repeke CE, Ferreira SB Jr, Claudino M, Silveira EM, de Assis GF, Avila-Campos MJ et al. Evidences of the cooperative role of the chemokines CCL3, CCL4 and CCL5 and its receptors CCR1+ and CCR5+ in RANKL+ cell migration throughout experimental periodontitis in mice. *Bone* 2010;**46**:1122–1130.

284. Kmieciak M, Gowda M, Graham L, Godder K, Bear HD, Marincola FM et al. Human T cells express CD25 and Foxp3 upon activation and exhibit effector/memory phenotypes without any regulatory/suppressor function. *J Transl Med* 2009;**7**:89.

285. Karanikas V, Speletas M, Zamanakou M, Kalala F, Loules G, Kerenidi T et al. Foxp3 expression in human cancer cells. *J Transl Med* 2008;**6**:19.

286. Ghadjar P, Rubie C, Aebersold DM, Keilholz U. The chemokine CCL20 and its receptor CCR6 in human malignancy with focus on colorectal cancer. *Int J Cancer J Int Cancer* 2009;**125**:741–745.

287. Richardson MW, Jadlowsky J, Didigu CA, Doms RW, Riley JL. KLF2 Modulates CCR5 Expression and Susceptibility to HIV-1 Infection. *J Immunol* 2012;**189**:3815–3821.

288. Zengel P, Nguyen-Hoang A, Schildhammer C, Zantl R, Kahl V, Horn E. μ-Slide Chemotaxis: A new chamber for long-term chemotaxis studies. *BMC Cell Biol* 2011;**12**:21.

289. Song JK, Park MH, Choi D-Y, Yoo HS, Han SB, Yoon DY et al. Deficiency of C-C Chemokine Receptor 5 Suppresses Tumor Development via Inactivation of NF-κB and Upregulation of IL-1Ra in Melanoma Model. *PLoS ONE* 2012;**7**:e33747.

290. Wang J, Guan E, Roderiquez G, Norcross MA. Synergistic Induction of Apoptosis in Primary CD4+ T Cells by Macrophage-Tropic HIV-1 and TGF-β1. *J Immunol* 2001;**167**:3360–3366.

291. Chang. CCL5 secreted by tumor could not only attract tumor-protecting regulatory T cells but also enhance the killing ability of regulatory T cells on CD8+ T cells.

292. Ishida Y, Kimura A, Kuninaka Y, Inui M, Matsushima K, Mukaida N et al. Pivotal role of the CCL5/CCR5 interaction for recruitment of endothelial progenitor cells in mouse wound healing. *J Clin Invest* 2012;**122**:711–721.

293. Suffee N, Hlawaty H, Meddahi-Pelle A, Maillard L, Louedec L, Haddad O et al. RANTES/CCL5-induced pro-angiogenic effects depend on CCR1, CCR5 and glycosaminoglycans. *Angiogenesis* 2012;**15**:727–744.

294. Scholzen T, Gerdes J. The Ki-67 protein: from the known and the unknown. *J Cell Physiol* 2000;**182**:311–322.

295. Green DR, Reed JC. Mitochondria and Apoptosis. *Science* 1998;**281**:1309–1312.

296. Dilek N, Poirier N, Usal C, Martinet B, Blancho G, Vanhove B. Control of Transplant Tolerance and Intragraft Regulatory T Cell Localization by Myeloid-Derived Suppressor Cells and CCL5. *J Immunol* 2012;**188**:4209–4216.

297. Schlecker E, Stojanovic A, Eisen C, Quack C, Falk CS, Umansky V et al. Tumor-Infiltrating Monocytic Myeloid-Derived Suppressor Cells Mediate CCR5-Dependent Recruitment of Regulatory T Cells Favoring Tumor Growth. *J Immunol* 2012;**189**:5602–5611.

298. Reshef R, Luger SM, Hexner EO, Loren AW, Frey NV, Nasta SD et al. Blockade of lymphocyte chemotaxis in visceral graft-versus-host disease. *N Engl J Med* 2012;**367**:135–145.

299. Zucchetto A, Benedetti D, Tripodo C, Bomben R, Dal Bo M, Marconi D et al. CD38/CD31, the CCL3 and CCL4 chemokines, and CD49d/vascular cell adhesion molecule-1 are interchained by sequential events sustaining chronic lymphocytic leukemia cell survival. *Cancer Res* 2009;**69**:4001–4009.

300. Calabrese EJ. Cell migration/chemotaxis: biphasic dose responses. *Crit Rev Toxicol* 2001;**31**:615–624.

301. Iellem A, Mariani M, Lang R, Recalde H, Panina-Bordignon P, Sinigaglia F et al. Unique Chemotactic Response Profile and Specific Expression of Chemokine Receptors Ccr4 and Ccr8 by Cd4+Cd25+ Regulatory T Cells. *J Exp Med* 2001;**194**:847 –854.

302. Chen H-C. Boyden chamber assay. *Methods Mol Biol* 2005;**294**:15–22.

303. Yang YF, Tomura M, Iwasaki M, Mukai T, Gao P, Ono S et al. IL-12 as well as IL-2 upregulates CCR5 expression on T cell receptor-triggered human CD4+ and CD8+ T cells. *J Clin Immunol* 2001;**21**:116–125.

304. Riley JL, Levine BL, Craighead N, Francomano T, Kim D, Carroll RG et al. Naïve and Memory CD4 T Cells Differ in Their Susceptibilities to Human Immunodeficiency Virus Type 1 Infection following CD28 Costimulation: Implications for Transmission and Pathogenesis. *J Virol* 1998;**72**:8273–8280.

305. Trickett A, Kwan YL. T cell stimulation and expansion using anti-CD3/CD28 beads. *J Immunol Methods* 2003;**275**:251–255.

306. Duarte RF, Chen FE, Lowdell MW, Potter MN, Lamana ML, Prentice HG et al. Functional impairment of human T-lymphocytes following PHA-induced expansion and retroviral transduction: implications for gene therapy. *Gene Ther* 2002;**9**:1359–1368.

307. Wysocki CA, Jiang Q, Panoskaltsis-Mortari A, Taylor PA, McKinnon KP, Su L et al. Critical role for CCR5 in the function of donor CD4+CD25+ regulatory T cells during acute graft-versus-host disease. *Blood* 2005;**106**:3300–3307.

308. Stoddart CA, Keir ME, McCune JM. IFN-α-Induced Upregulation of CCR5 Leads to Expanded HIV Tropism In Vivo. *PLoS Pathog* 2010;**6**:e1000766.

309. Hornung F, Scala G, Lenardo MJ. TNF-alpha-induced secretion of C-C chemokines modulates C-C chemokine receptor 5 expression on peripheral blood lymphocytes. *J Immunol* 2000;**164**:6180–6187.

310. WANG CR, LIU MF. Regulation of CCR5 expression and MIP-1? production in CD4+ T cells from patients with rheumatoid arthritis. *Clin Exp Immunol* 2003;**132**:371–378.

311. Pharoah DS, Varsani H, Tatham RW, Newton KR, Jager W de, Prakken BJ et al. Expression of the inflammatory chemokines CCL5, CCL3 and CXCL10 in juvenile idiopathic arthritis, and demonstration of CCL5 production by an atypical subset of CD8+ T cells. *Arthritis Res Ther* 2006;**8**:R50.

312. Chakraborty R, Rooney C, Dotti G, Savoldo B. Changes in chemokine receptor expression of regulatory T cells after ex vivo culture. *J Immunother* 2012;**35**:329–336.

313. Taams LS, Smith J, Rustin MH, Salmon M, Poulter LW, Akbar AN. Human anergic/suppressive CD4(+)CD25(+) T cells: a highly differentiated and apoptosis-prone population. *Eur J Immunol* 2001;**31**:1122–1131.

314. Chang L-Y, Lin Y-C, Kang C-W, Hsu C-Y, Chu Y-Y, Huang C-T et al. The Indispensable Role of CCR5 for In Vivo Suppressor Function of Tumor-Derived CD103+ Effector/Memory Regulatory T Cells. *J Immunol* 2012;**189**:567–574.

315. Zhang N, Schröppel B, Lal G, Jakubzick C, Mao X, Chen D et al. Regulatory T cells sequentially migrate from inflamed tissues to draining lymph nodes to suppress the alloimmune response. *Immunity* 2009;**30**:458–469.

316. Soler DC, Sugiyama H, Young AB, Massari JV, McCormick TS, Cooper KD. Psoriasis patients exhibit impairment of the high potency CCR5(+) T regulatory cell subset. *Clin Immunol* 2013;**149**:111–118.

317. Walker LSK, Chodos A, Eggena M, Dooms H, Abbas AK. Antigen-dependent proliferation of CD4+ CD25+ regulatory T cells in vivo. *J Exp Med* 2003;**198**:249–258.

318. Wainwright DA, Sengupta S, Han Y, Lesniak MS. Thymus-derived rather than tumor-induced regulatory T cells predominate in brain tumors. *Neuro-Oncol* 2011;**13**:1308–1323.

319. Ondondo B, Jones E, Godkin A, Gallimore A. Home sweet home: the tumor microenvironment as a haven for regulatory T cells. *Front Immunol* 2013;**4**:197.

320. Chung DJ, Rossi M, Romano E, Ghith J, Yuan J, Munn DH et al. Indoleamine 2,3-dioxygenase-expressing mature human monocyte-derived dendritic cells expand potent autologous regulatory T cells. *Blood* 2009;**114**:555–563.

321. Thornton AM, Korty PE, Tran DQ, Wohlfert EA, Murray PE, Belkaid Y et al. Expression of Helios, an Ikaros Transcription Factor Family Member, Differentiates Thymic-Derived from Peripherally Induced Foxp3+ T Regulatory Cells. *J Immunol* 2010;**184**:3433 –3441.

322. Gottschalk RA, Corse E, Allison JP. Expression of Helios in Peripherally Induced Foxp3+ Regulatory T Cells. *J Immunol* 2012;**188**:976–980.

323. Hindley JP, Ferreira C, Jones E, Lauder SN, Ladell K, Wynn KK et al. Analysis of the T-cell receptor repertoires of tumor-infiltrating conventional and regulatory T cells reveals no evidence for conversion in carcinogen-induced tumors. *Cancer Res* 2011;**71**:736–746.

324. Heijstek MW, Kranenburg O, Borel Rinkes IHM. Mouse Models of Colorectal Cancer and Liver Metastases. *Dig Surg* 2005;**22**:16–25.

325. Yamada Y, Mori H. Multistep carcinogenesis of the colon in ApcMin/+ mouse. *Cancer Sci* 2007;**98**:6–10.

326. Rosenberg MP, Bortner D. Why transgenic and knockout animal models should be used (for drug efficacy studies in cancer). *Cancer Metastasis Rev* 1998;**17**:295–299.

327. Wilmanns C, Fan D, O'Brian CA, Bucana CD, Fidler IJ. Orthotopic and ectopic organ environments differentially influence the sensitivity of murine colon carcinoma cells to doxorubicin and 5-fluorouracil. *Int J Cancer J Int Cancer* 1992;**52**:98–104.

328. Zhang Y, Davis C, Ryan J, Janney C, Peña MMO. Development and characterization of a reliable mouse model of colorectal cancer metastasis to the liver. *Clin Exp Metastasis* 2013;**30**:903–918.

329. Zigmond E, Halpern Z, Elinav E, Brazowski E, Jung S, Varol C. Utilization of Murine Colonoscopy for Orthotopic Implantation of Colorectal Cancer. *PLoS ONE* 2011;**6**:e28858.

330. Donigan M, Norcross LS, Aversa J, Colon J, Smith J, Madero-Visbal R et al. Novel Murine Model for Colon Cancer: Non-Operative Trans-Anal Rectal Injection. *J Surg Res* 2009;**154**:299–303.

331. Paroo Z, Bollinger RA, Braasch DA, Richer E, Corey DR, Antich PP et al. Validating bioluminescence imaging as a high-throughput, quantitative modality for assessing tumor burden. *Mol Imaging* 2004;**3**:117–124.

332. Edinger M, Sweeney TJ, Tucker AA, Olomu AB, Negrin RS, Contag CH. Noninvasive assessment of tumor cell proliferation in animal models. *Neoplasia N Y N* 1999;**1**:303–310.

333. Gheysens O, Mottaghy FM. Method of bioluminescence imaging for molecular imaging of physiological and pathological processes. *Methods* 2009;**48**:139–145.

334. Puaux A-L, Ong LC, Jin Y, Teh I, Hong M, Chow PKH et al. A Comparison of Imaging Techniques to Monitor Tumor Growth and Cancer Progression in Living Animals. *Int J Mol Imaging* 2011;**2011**:321538.

335. Mansfield R, Able S, Griffin P, Irvine B, James I, Macartney M et al. CCR5 pharmacology methodologies and associated applications. *Methods Enzymol* 2009;**460**:17–55.

336. Ray N. Maraviroc in the treatment of HIV infection. *Drug Des Devel Ther* 2009;**2**:151–161.

337. Dorr P, Westby M, Dobbs S, Griffin P, Irvine B, Macartney M et al. Maraviroc (UK-427,857), a potent, orally bioavailable, and selective small-molecule inhibitor of chemokine receptor CCR5 with broad-spectrum anti-human immunodeficiency virus type 1 activity. *Antimicrob Agents Chemother* 2005;**49**:4721–4732.

338. Saita Y, Kondo M, Shimizu Y. Species selectivity of small-molecular antagonists for the CCR5 chemokine receptor. *Int Immunopharmacol* 2007;**7**:1528–1534.

339. Proudfoot AE, Power CA, Hoogewerf AJ, Montjovent MO, Borlat F, Offord RE et al. Extension of recombinant human RANTES by the retention of the initiating methionine produces a potent antagonist. *J Biol Chem* 1996;**271**:2599–2603.

340. Song E, Zou H, Yao Y, Proudfoot A, Antus B, Liu S et al. Early application of Met-RANTES ameliorates chronic allograft nephropathy. *Kidney Int* 2002;**61**:676–685.

341. Robinson SC, Scott KA, Wilson JL, Thompson RG, Proudfoot AEI, Balkwill FR. A Chemokine Receptor Antagonist Inhibits Experimental Breast Tumor Growth. *Cancer Res* 2003;**63**:8360 –8365.

342. Kiss DL, Longden J, Fechner GA, Avery VM. The functional antagonist Met-RANTES: a modified agonist that induces differential CCR5 trafficking. *Cell Mol Biol Lett* 2009;**14**:537–547.

343. Elsner J, Petering H, Höchstetter R, Kimmig D, Wells TN, Kapp A et al. The CC chemokine antagonist Met-RANTES inhibits eosinophil effector functions through the chemokine receptors CCR1 and CCR3. *Eur J Immunol* 1997;**27**:2892–2898.

344. Baba M, Nishimura O, Kanzaki N, Okamoto M, Sawada H, Iizawa Y et al. A small-molecule, nonpeptide CCR5 antagonist with highly potent and selective anti-HIV-1 activity. *Proc Natl Acad Sci U S A* 1999;**96**:5698–5703.

345. Gao P, Zhou X-Y, Yashiro-Ohtani Y, Yang Y-F, Sugimoto N, Ono S et al. The unique target specificity of a nonpeptide chemokine receptor antagonist: selective blockade of two Th1 chemokine receptors CCR5 and CXCR3. *J Leukoc Biol* 2003;**73**:273–280.

346. Tokuyama H, Ueha S, Kurachi M, Matsushima K, Moriyasu F, Blumberg RS et al. The simultaneous blockade of chemokine receptors CCR2, CCR5 and CXCR3 by a non-peptide chemokine receptor antagonist protects mice from dextran sodium sulfate-mediated colitis. *Int Immunol* 2005;**17**:1023–1034.

347. Ni J, Zhu Y-N, Zhong X-G, Ding Y, Hou L-F, Tong X-K et al. The chemokine receptor antagonist, TAK-779, decreased experimental autoimmune encephalomyelitis by reducing inflammatory cell migration into the central nervous system, without affecting T cell function. *Br J Pharmacol* 2009;**158**:2046–2056.

348. Tsutahara K, Okumi M, Kakuta Y, Abe T, Yazawa K, Miyagawa S et al. The blocking of CXCR3 and CCR5 suppresses the infiltration of T lymphocytes in rat renal ischemia reperfusion. *Nephrol Dial Transplant* 2012;**27**:3799–3806.

349. Dorr P. Maraviroc outlook in HIV and non-HIV diseases. HIV-Infection and Organ Transplantation Symposium, University Medical Center, Hamburg-Eppendorf, Hamburg, Germany 2008.

350. Hirota K, Yoshitomi H, Hashimoto M, Maeda S, Teradaira S, Sugimoto N et al. Preferential Recruitment of CCR6-Expressing Th17 Cells to Inflamed Joints Via CCL20 in Rheumatoid Arthritis and Its Animal Model. *J Exp Med* 2007;**204**:2803–2812.

351. Madi L, Bar-Yehuda S, Barer F, Ardon E, Ochaion A, Fishman P. A3 adenosine receptor activation in melanoma cells: association between receptor fate and tumor growth inhibition. *J Biol Chem* 2003;**278**:42121–42130.

352. Longden J, Cooke E-L, Hill SJ. Effect of CCR5 receptor antagonists on endocytosis of the human CCR5 receptor in CHO-K1 cells. *Br J Pharmacol* 2008;**153**:1513–1527.

353. Wong M, Uddin S, Majchrzak B, Huynh T, Proudfoot AE, Platanias LC et al. Rantes activates Jak2 and Jak3 to regulate engagement of multiple signaling pathways in T cells. *J Biol Chem* 2001;**276**:11427–11431.

354. Lee NJ, Choi DY, Song JK, Jung YY, Kim DH, Kim TM et al. Deficiency of C–C chemokine receptor 5 suppresses tumor development via inactivation of NF–κB and inhibition of monocyte chemoattractant protein-1 in urethane-induced lung tumor model. *Carcinogenesis* 2012;**33**:2520-2528.

355. Ambati BK, Anand A, Joussen AM, Kuziel WA, Adamis AP, Ambati J. Sustained inhibition of corneal neovascularization by genetic ablation of CCR5. *Invest Ophthalmol Vis Sci* 2003;**44**:590–593.

356. Pham K, Luo D, Liu C, Harrison JK. CCL5, CCR1 and CCR5 in murine glioblastoma: immune cell infiltration and survival rates are not dependent on individual expression of either CCR1 or CCR5. *J Neuroimmunol* 2012;**246**:10–17.

357. Cardona AE, Sasse ME, Liu L, Cardona SM, Mizutani M, Savarin C et al. Scavenging roles of chemokine receptors: chemokine receptor deficiency is associated with increased levels of ligand in circulation and tissues. *Blood* 2008;**112**:256–263.

358. Crawley JN. Behavioral phenotyping of transgenic and knockout mice: experimental design and evaluation of general health, sensory functions, motor abilities, and specific behavioral tests. *Brain Res* 1999;**835**:18–26.

359. Wolfer DP, Crusio WE, Lipp HP. Knockout mice: simple solutions to the problems of genetic background and flanking genes. *Trends Neurosci* 2002;**25**:336–340.

360. Andres PG, Beck PL, Mizoguchi E, Mizoguchi A, Bhan AK, Dawson T et al. Mice with a selective deletion of the CC chemokine receptors 5 or 2 are protected from dextran sodium sulfate-mediated colitis: lack of CC chemokine receptor 5 expression results in a NK1.1+ lymphocyte-associated Th2-type immune response in the intestine. *J Immunol* 2000;**164**:6303–6312.

361. Passos GF, Figueiredo CP, Prediger RDS, Pandolfo P, Duarte FS, Medeiros R et al. Role of the macrophage inflammatory protein-1alpha/CC chemokine receptor 5 signaling pathway in the neuroinflammatory response and cognitive deficits induced by beta-amyloid peptide. *Am J Pathol* 2009;**175**:1586–1597.

362. Liu C, Lou Y, Lizée G, Qin H, Liu S, Rabinovich B et al. Plasmacytoid dendritic cells induce NK cell-dependent, tumor antigen-specific T cell cross-priming and tumor regression in mice. *J Clin Invest* 2008;**118**:1165–1175.

363. Sugasawa H, Ichikura T, Kinoshita M, Ono S, Majima T, Tsujimoto H et al. Gastric cancer cells exploit CD4+ cell-derived CCL5 for their growth and prevention of CD8+ cell-involved tumor elimination. *Int J Cancer* 2008;**122**:2535–2541.

364. Murooka TT, Wong MM, Rahbar R, Majchrzak-Kita B, Proudfoot AEI, Fish EN. CCL5-CCR5-mediated apoptosis in T cells: Requirement for glycosaminoglycan binding and CCL5 aggregation. *J Biol Chem* 2006;**281**:25184–25194.

365. Liu VC, Wong LY, Jang T, Shah AH, Park I, Yang X et al. Tumor evasion of the immune system by converting CD4+CD25- T cells into CD4+CD25+ T regulatory cells: role of tumor-derived TGF-beta. *J Immunol* 2007;**178**:2883–2892.

366. Gobert M, Treilleux I, Bendriss-Vermare N, Bachelot T, Goddard-Leon S, Arfi V et al. Regulatory T Cells Recruited through CCL22/CCR4 Are Selectively Activated in Lymphoid Infiltrates Surrounding Primary Breast Tumors and Lead to an Adverse Clinical Outcome. *Cancer Res* 2009;**69**:2000–2009.

367. Wierda RJ, Kuipers HF, van Eggermond MCJA, Benard A, van Leeuwen JC, Carluccio S et al. Epigenetic control of CCR5 transcript levels in immune cells and modulation by small molecules inhibitors. *J Cell Mol Med* 2012;**16**:1866–1877.

368. Pfoertner S, Jeron A, Probst-Kepper M, Guzman CA, Hansen W, Westendorf AM et al. Signatures of human regulatory T cells: an encounter with old friends and new players. *Genome Biol* 2006;**7**:R54.

369. Wen AY, Sakamoto KM, Miller LS. The role of the transcription factor CREB in immune function. *J Immunol* 2010;**185**:6413–6419.

370. Weinreich MA, Takada K, Skon C, Reiner SL, Jameson SC, Hogquist KA. KLF2 Transcription-Factor Deficiency in T Cells Results in Unrestrained Cytokine

Production and Upregulation of Bystander Chemokine Receptors. *Immunity* 2009;**31**:122–130.

371. Chi H, Flavell RA. Cutting edge: regulation of T cell trafficking and primary immune responses by sphingosine 1-phosphate receptor 1. *J Immunol* 2005;**174**:2485–2488.

372. Ariel A, Fredman G, Sun Y-P, Kantarci A, Van Dyke TE, Luster AD et al. Apoptotic neutrophils and T cells sequester chemokines during immune response resolution through modulation of CCR5 expression. *Nat Immunol* 2006;**7**:1209–1216.

373. Ajuebor MN, Wondimu Z, Hogaboam CM, Le T, Proudfoot AEI, Swain MG. CCR5 deficiency drives enhanced natural killer cell trafficking to and activation within the liver in murine T cell-mediated hepatitis. *Am J Pathol* 2007;**170**:1975–1988.

374. Kuziel WA, Dawson TC, Quinones M, Garavito E, Chenaux G, Ahuja SS et al. CCR5 deficiency is not protective in the early stages of atherogenesis in apoE knockout mice. *Atherosclerosis* 2003;**167**:25–32.

375. González-Martín A, Gómez L, Lustgarten J, Mira E, Mañes S. Maximal T cell-mediated antitumor responses rely upon CCR5 expression in both CD4(+) and CD8(+) T cells. *Cancer Res* 2011;**71**:5455–5466.

376. Spring H, Schüler T, Arnold B, Hämmerling GJ, Ganss R. Chemokines direct endothelial progenitors into tumor neovessels. *Proc Natl Acad Sci U S A* 2005;**102**:18111–18116.

377. Ishida Y, Kimura A, Kuninaka Y, Inui M, Matsushima K, Mukaida N et al. Pivotal role of the CCL5/CCR5 interaction for recruitment of endothelial progenitor cells in mouse wound healing. *J Clin Invest* 2012;**122**:711–721.

378. Kroetz DN, Deepe GS. An Aberrant Thymus in CCR5(-/-) Mice Is Coupled with an Enhanced Adaptive Immune Response in Fungal Infection. *J Immunol* 2011;**186**:5949–5955.

379. Camargo JF, Quinones MP, Mummidi S, Srinivas S, Gaitan AA, Begum K et al. CCR5 expression levels influence NFAT translocation, IL-2 production, and subsequent signaling events during T lymphocyte activation. *J Immunol* 2009;**182**:171–182.

380. Terme M, Pernot S, Marcheteau E, Sandoval F, Benhamouda N, Colussi O et al. VEGFA-VEGFR pathway blockade inhibits tumor-induced regulatory T-cell proliferation in colorectal cancer. *Cancer Res* 2013;**73**:539–549.

381. Stanford MM, Issekutz TB. The relative activity of CXCR3 and CCR5 ligands in T lymphocyte migration: concordant and disparate activities in vitro and in vivo. *J Leukoc Biol* 2003;**74**:791–799.

382. Frey AB. Cancer-Induced Signaling Defects in Antitumor T Cells. *Immunol Rev* 2008;**222**:192–205.

383. Calcinotto A, Filipazzi P, Grioni M, Iero M, De Milito A, Ricupito A et al. Modulation of microenvironment acidity reverses anergy in human and murine tumor-infiltrating T lymphocytes. *Cancer Res* 2012;**72**:2746–2756.

384. Scurr M, Ladell K, Besneux M, Christian A, Hockey T, Smart K et al. Highly prevalent colorectal cancer-infiltrating LAP(+) Foxp3(-) T cells exhibit more potent immunosuppressive activity than Foxp3(+) regulatory T cells. *Mucosal Immunol* 2014;**7**:428–439.

385. Lim JK, Glass WG, McDermott DH, Murphy PM. CCR5: no longer a 'good for nothing' gene--chemokine control of West Nile virus infection. *Trends Immunol* 2006;**27**:308–312.

386. Ellis LM, Hicklin DJ. VEGF-targeted therapy: mechanisms of anti-tumour activity. *Nat Rev Cancer* 2008;**8**:579–591.

387. Schellerer VS, Croner RS, Weinländer K, Hohenberger W, Stürzl M, Naschberger E. Endothelial cells of human colorectal cancer and healthy colon reveal phenotypic differences in culture. *Lab Investig J Tech Methods Pathol* 2007;**87**:1159–1170.

388. Xu L, Xu W, Wen Z, Xiong S. In Situ Prior Proliferation of CD4 CCR6 Regulatory T Cells Facilitated by TGF-β Secreting DCs Is Crucial for Their Enrichment and Suppression in Tumor Immunity. *PloS One* 2011;**6**:e20282.

389. Gai XD, Song Y, Li C, Lei YM, Yang B. Potential role of plasmacytoid dendritic cells for FOXP3+ regulatory T cell development in human colorectal cancer and tumor draining lymph node. *Pathol - Res Pract* 2013;**209**:774–778.

390. ClinicalTrials.gov. CCR5-blockade in Metastatic Colorectal Cancer (MARACON). NCT01736813. 2013.http://clinicaltrials.gov/ct2/show/NCT01736813 (accessed 24 Feb 2014).

Appendix I: Abbreviations

ACTB	ß-actin
ADAMTS	A disintegrin and metalloproteinase with thrombospondin motifs
AJCC	American Joint Committee on Cancer
Akt	From AKT8, the transforming retrovirus responsible for formation of thymoma in AKR mice
ANG	Angiogenin
Ang-1/2	Angiopoietin-1/2
APC	Adenomatous polyposis coli
APC	Allophycocyanin
ATCC	American Type Culture Collection
B cell	Lymphocytes which mature in the bone marrow (or Bursa of Fabricus in birds)
B16-F10-Luc	Luciferase-expressing B16-F10 cells
BCL2	B-cell lymphoma 2
BLI	Bioluminescent imaging
BMI	Body mass index
BMPR1A	Bone morphogenetic protein receptor, type 1A
BRAF	v-Raf murine sarcoma viral oncogene homologue B1
BSA	Bovine serum albumin
CAM	Cell adhesion molecules
CD	Cluster of differentiation
CIMP	CpG island methylator phenotype
CMT93	Colon mouse tumour 93
CMT93-Luc	Luciferase-expressing CMT93 cells
cPBS	Complete PBS: PBS containing 10% foetal calf serum and 1% Glutamine-Penicillin-Streptomycin.
CRC	Colorectal cancer

Cre	Causes recombination
CREB1	cAMP responsive element binding protein 1
cRPMI	Complete RPMI media: RPMI containing 1% foetal calf serum, 5 mg Gentamicin, 125 µg Amphotericin B and 1% Glutamine-Penicillin-Streptomycin.
CT26	Colon tumour 26
CT26-Luc	Luciferase-expressing CT26 cells
DAPI	4',6-diamidino-2-phenylindole
DARC	Duffy antigen/chemokine receptor
DC	Dendritic cell
DC	Distal colon
DCC	Deleted in colorectal cancer
DMEM	Dulbecco's modified Eagle's medium
DMSO	Dimethyl sulfoxide
DPPIV	Dipeptidyl peptidase-4
DPX	Di-N-Butyle Phthalate in Xylene
DTT	Dithiothreitol
E-selectin	Endothelium-selectin
ECM	Extra-cellular matrix (gel)
EDTA	Ethylenediaminetetraacetic acid
EG-VEGF	Endocrine gland-derived vascular endothelial growth factor
EGF	Epidermal growth factor
EGFR	Epidermal growth factor
EMVI	Extramural vascular invasion
Env	Envelope (gene)
EPIC	European Prospective Investigation into Cancer and Nutrition
ERK	Extracellular signal-regulated kinase
ES	Embryonic stem (cells)
FAM	6-carboxyfluorescein

FAP	Familial adenomatous polyposis
FCS	Foetal calf serum
FFPE	Formal saline-fixed paraffin embedded
FGF	Fibroblast growth factor
FITC	Fluorescein isothiocyanate
FL	Fluorescence channel (of flow cytometer)
FMO	Fluorescence-Minus-One control
FOB	Faecal occult blood
Foxp3	Forkhead box P3
g	Acceleration of gravity (9.8 ms^{-2} on Earth)
g	Grams
G-CSF	Granulocyte colony-stimulating factor
G6PD	Glucose-6-phosphate dehydrogenase
Gag	Group antigens
GAPD	Glyceraldehyde-3-phosphate dehydrogenase
GlyCAM-1	Glycosylation-dependent cell adhesion molecule 1
GM-CSF	Granulocyte-macrophage colony-stimulating factor
GPS	Glutamine-Penicillin-Streptomycin
GSK-3	Glycogen synthase kinase-3
GUSB	ß-glucuronidase
HB-EGF	Heparin-binding EGF-like growth factor
hCCR5	Human CCR5
hCCR5 KI	Human CCR5 knock-in (mouse)
HFE	Haemochromatosis. From *H*igh iron (*Fe*)
HGF	Hepatocyte growth factor
hMLH1	Human MutL homologue 1
hMSH1	Human MutS homologue 1
hMSH6	Human MutS homologue 6

hMYH	Human MutY homologue
HNPCC	Hereditary non-polyposis colorectal cancer
HPRT	Hypoxanthine phosphoribosyltransferase
HRP	Horseradish peroxidase
ICAM-1	Intercellular adhesion molecule 1
Ig	Immunoglobulin
IGFBP	Insulin-like growth factor-binding protein
IL	Interleukin
IMC	Isotype-matched control
IMDM	Iscove's modified Dulbecco's medium
Inc	Incorporated
Ip	Intraperitoneal
IPEX	Immunodysregulation polyendocrinopathy X-linked syndrome
IPO8	Importin 8
IQR	Inter-quartile range
iTreg	Induced Treg
KLF2	Kruppel-like factor 2
KRAS	Kirsten rat sarcoma viral oncogene
l	Litre
L-selectin	Leukocyte-selectin
LAG-3	Lymphocyte activation gene 3
LAP	Latency associated peptide
LINE-1	Long interspersed nucleotide element-1
LLC	Lewis lung carcinoma
LPS	Lipopolysaccharide
LREC	Local research and ethics committee
Ltd	Limited company
M	Molar concentration

MAdCAM-1	Mucosal addressin cell adhesion molecule 1
MAPK	Mitogen-activated protein kinase
mCCR5	Murine CCR5
MEK	(MAPK) ERK kinase
MFI	Median fluorescent intensity
mg	Milligrams
MHC	Major Histocompatibility Complex
MIF	Macrophage migration inhibitory factor
MIQE	Minimum Information for Publication of Quantitative Real-Time PCR Experiments
ml	Millilitre
MMP	Matrix metalloproteinase
Ms	Mouse
MSCV	Murine stem cell virus
MSI	Microsatellite instability
mTOR	Mammalian target of rapamycin
MTT	3-(4,5-Dimethylthiazol-2-yl)-2,5-diphenyltetrazolium bromide
MVC	Maraviroc
N	Normality of a solution
n	Number (of subjects / cases)
ng	Nanograms
NICE	National Institute for Health and Care Excellence
NRG1	Neuregulin
NSAID	Non-steroidal anti-inflammatory drug
nTreg	Naturally-occurring Treg
ORF	Open-reading frame
P-selectin	Platelet-selectin
PAC	Puromycin N-acetyl transferase

PBGD	Porphobilinogen deaminase
PBMC	Peripheral blood mononuclear cell
PBS	Phosphate-buffered saline
PCR	Polymerase chain reaction
PD-ECGF	Platelet-derived endothelial cell growth factor
PDGF	Platelet-derived growth factor
PE	Phycoerythrin
PGK1	Phosphoglycerate kinase 1
PHA	Phytohaemagglutinin
PI3K	Phosphoinositide 3-kinase
PIGF	Placental growth factor
PLC	Public limited company
PMS2	Post-meiotic segregation 2
PNAd	Peripheral node addressin
Pol	Polymerase gene
PPIA	Peptidylprolyl Isomerase A
PSGL-1	P-selectin glycoprotein ligand 1
PTEN	Phosphatase and tensin homologue
PTX3	Pentraxin-3
QAMA	Quantitative analysis of methylated alleles
QEHB	Queen Elizabeth Hospital Birmingham, UK
RAF	Rapidly accelerated fibrosarcoma
RPMI	Roswell Park Memorial Institute (cell media)
RT	Reverse transcriptase
S1P	Sphingosine-1-phosphate
S1PR1	Sphingosine-1-phosphate receptor 1
Sc	Subcutaneous
SD	Standard deviation

SDS	Sodium dodecyl sulphate
SDS-PAGE	Sodium dodecyl sulphate polyacrylamide gel electrophoresis
sICAM1	Soluble ICAM-1
Smad	SMA (small body size) – MAD (mothers against decapentaplegic)
ß2M	ß2-microglobulin
STK11	Serine/threonine kinase 11
sTREM-1	Soluble TREM-1
T cell	Lymphocytes which mature in the thymus
TBP	TATA box binding protein
TBS	Tris-buffered saline
Tconv	Conventional T cell
TDLN	Tumour-draining lymph node
TEMED	N,N,N',N'-tetramethylethylenediamine
TGF	Tansforming growth factor
Th3	T helper 3 cell
TIL	Tumour infiltrating lymphocyte
TIMP	Tissue inhibitor of metalloproteinases
TNF	Tumour necrosis factor
TP53	Tumour protein p53
Tr1	Type 1 regulatory cell
Treg	Regulatory T cell
TREM-1	Triggering receptor expressed on myeloid cells-1
Tresp	Responder T cells (labelled $CD4^+CD25^-$ cells used in suppression assays)
TSDR	Treg-specific determining region
TSP-1/2	Thrombospondin-1/2
UC	Ulcerative colitis
UICC	International Union Against Cancer

UK	United Kingdom
uPA	Urinary plasminogen activator
V	Volts
VAP-1	Vascular adhesion protein-1
VCAM-1	Vascular cell adhesion molecule 1
VCAM-1	Vascular cell adhesion protein 1
VEGF	Vascular endothelial growth factor
VIC	4,7,2'-trichloro-7'phenyl-6-carboxyfluorescein
VLA-4	Very late antigen-4
Wnt	Wingless-related integration site
µg	Micrograms
µl	Microlitre

Appendix II: Sample data

Neo	Neo-adjuvant chemo- or radiotherapy
Pos LN	Number of positive lymph nodes / total number of lymph nodes
KRAS	Presence or absence of a KRAS mutation
Died	Patient died during the follow-up period
CRC-related	Death was related to CRC
LR	Local recurrence during follow-up period
DR	Distant recurrence during follow-up period
AdenoCa	Adenocarcinoma
Mod	Moderate
Mdys	Moderate dysplasia
WB	Western blot
PCR	Used to obtain RNA for real-time PCR
IHC	Immunohistochemistry (FFPE); -c for chemokines using frozen sections
P	Phenotyping (flow cytometry)
B	Matched blood sample used for phenotyping
LN	Matched TDLN used for phenotyping
Super	Used to obtain supernatant; * supernatant used in protein array
Supp	Suppression assay
Transwell	Transwell migration (chemotaxis) assays
RNA	Cell-sorted to obtain RNA
DNA	Cell-sorted to obtain DNA for TSDR analysis

Sample	Sex	Age	Neo	Position	Type	Grade	Dukes	T	N	M	EMVI	Pos LN	Margins	KRAS	MSI	mm^3 Volume	Died	CRC-related	LR	DR	Sample used for
1392	M	79		Left	Adenoma	Mdys															
1400	F	64	No	Left	AdenoCa	Mod	B	3	0	0	Positive	0/24	Clear	Unknown	Unknown	42000	No		No	No	WB, PCR
1409	M	58	No	Rectum	AdenoCa	Mod	C	4	1	1	Positive	2/26	Clear	Wildtype	Unknown	36000	Yes	Yes	No	No	WB, PCR
1422	M	80	No	Right	AdenoCa	Poor	C	3	1	0	Positive	1/11	Clear	Wildtype	Unknown	126000	No		No	No	
1423	F	74	No	Right	AdenoCa	Mod	C	3	1	0	Positive	1/28	Clear	Unknown	Unknown	24000	No		No	No	PCR
1432	M	73	No	Left	AdenoCa	Mod	D	4	0	1	Positive	0/24	Clear	Wildtype	Unknown	144000	No		No	No	IHC, PCR
1447	F	81	No	Right	Mucinous	Mod	D	4	2	1	Positive	7/10	Clear	Unknown	Unknown	78000	Yes	Yes	No	No	WB, IHC, PCR
1489	M	72	No	Left	AdenoCa	Mod	B	2	0	0	Negative	0/18	Clear	Unknown	Unknown	1800	Yes	No	No	No	
1490	M	36	No	Left	AdenoCa	Poor	B	4	0	0	Negative	0/44	Clear	Unknown	MSI	29700	No		No	No	PCR
1522	M	76	No	Right	AdenoCa	Mod	A	2	0	0	Negative	0/24	Clear	Unknown	Unknown	2500	No		No	No	WB
1523	M	60	No	Rectum	AdenoCa	Mod	B	3	0	0	Negative	0/7	Clear	Unknown	MSS	5000	Yes	No	No	No	
1536	F	64	No	Rectum	AdenoCa	Mod	D	3	0	1	Positive	0/30	Clear	Wildtype	Unknown	38350	No		No	No	PCR
1569	F	84	No	Right	AdenoCa	Poor	B	4	0	0	Negative	0/21	Clear	Unknown	Unknown	198000	No		No	No	
1586	M	80	Yes	Rectum	AdenoCa	Mod	C	3	1	0	Negative	1/10	Clear	Unknown	Unknown	15750	No		No	Yes	
1588	M	64	No	Left	AdenoCa	Mod	C	3	1	0	Negative	2/14	Clear	Unknown	Unknown	15540	No		No	No	P
1622	F	85	No	Right	AdenoCa	Poor	B	4	0	0	Negative	0/19	Clear	Unknown	Unknown	78000	Yes	No			P
1645	F	63	No	Right	AdenoCa	Mod	C	4	2	0	Positive	4/23	Clear	Wildtype	Unknown	9000	No		No	Yes	P
1673	F	87	No	Left	AdenoCa	Mod	C	3	1	0	Positive	3/20	Clear	Unknown	Unknown	13440	No		No	No	P
1680	F	52	No	Left	AdenoCa	Mod	D	4	2	1	Positive	4/13	Involved	Unknown	Unknown	9800	No		No	No	

1691	M	76	Yes	Left	AdenoCa	Mod	D	3	1	1	Negative	1/17	Clear	Unknown	Unknown	7000	No		No	Yes	P
1692	M	78	No	Rectum	AdenoCa	Mod	B	4	0	0	Positive	0/23	Clear	Unknown	Unknown	33000	No		No	No	P
1712	F	86	No	Right	Mucinous	Mod	C	4	1	0	Negative	2/24	Clear	Unknown	Unknown	26400	Yes	No	No	No	P
1733	M	66	No	Left	AdenoCa	Mod	C	3	1	0	Positive	1/25	Clear	Wildtype	Unknown	13000	No		No	Yes	P
1753	F	88	No	Right	AdenoCa	Mod	B	4	0	0	Negative	0/24	Clear	Unknown	Unknown	204000	No		No	No	P
1757	M	68	Yes	Rectum	AdenoCa	Poor	D	4	2	1	Positive	4/8	Involved	Mutation	Unknown	20000	Yes	Yes			P
1793	F	79	No	Right	AdenoCa	Mod	B	4	0	0	Negative	0/26	Clear	Unknown	Unknown	30000	No		No	No	IHC, PCR
1798	M	60		Left	Adenoma	Mdys															
1861	M	63	No	Left	AdenoCa	Mod	B	3	0	0	Negative	0/14	Clear	Unknown	Unknown	5250	No		No	No	P, PCR
1877	F	31	No	Rectum	AdenoCa	Poor	C	2	2	0	Positive	13/28	Clear	Unknown	MSS	7500	No		No	No	P, IHC, PCR
1912	F	65	No	Right	Mucinous	Mod	B	3	0	0	Negative	0/30	Clear	Unknown	Unknown	56000	No		No	No	P, PCR
1931	M	69	No	Right	AdenoCa	Mod	B	3	0	0	Negative	0/29	Clear	Unknown	Unknown	26400	Yes	No			
1932	F	69	No	Rectum	AdenoCa	Mod	B	3	0	0	Negative	0/26	Clear	Unknown	Unknown	13860	Yes	Yes	Yes	Yes	P, PCR
1945	M	65	No	Rectum	AdenoCa	Mod	B	3	0	0	Negative	0/44	Clear	Unknown	Unknown	61875	No		No	No	P, PCR
1970	M	73	No	Rectum	AdenoCa	Mod	A	1	0	0	Negative	0/35	Clear	Unknown	Unknown	2925	No		No	No	P
2014	F	71	No	Rectum	AdenoCa	Mod	A	2	0	0	Negative	0/18	Clear	Unknown	Unknown	2250	No		No	No	P
2052	F	78	No	Right	Mucinous	Mod	B	3	0	0		0/23	Clear	Unknown	Unknown	61875	No		No	No	P, IHC
2062	M	66	No	Right	AdenoCa	Mod	B	3	0	0		0/24	Clear	Unknown	MSI	390000	No		No	No	IHC
2069	M	75	No	Right	AdenoCa	Mod	C	4	2	0	Negative	7/18	Clear	Unknown	Unknown	13500	No		No	No	
2141	M	73	No	Right	AdenoCa	Mod	A	2	0	0	Negative	0/10	Clear	Unknown	Unknown	4050	No		No	No	P
2186	M	54	No	Rectum	AdenoCa	Mod	B	4	0	0	Positive	0/21	Clear	Unknown	Unknown	56000	No		No	No	P, PCR

2220	M	52	No	Left	AdenoCa	Mod	D	4	2	1	Positive	10/65	Clear	Wildtype	Unknown	61200	Yes	Yes	No	No	WB
2239		80	No	Rectum	Adenoma	Mdys															
2242	F	56	No	Right	AdenoCa	Poor	C	2	1	0	Negative	1/11	Clear	Wildtype	MSI	7875	No		No	No	WB, IHC
2255	M	78	No	Left	AdenoCa	Mod	D	4	2	1	Positive	6/12	Clear	Wildtype	Unknown	1512	No		No	No	P
2265	M	83	No	Rectum	AdenoCa	Mod	B	3	0	0	Negative	0/20	Clear	Unknown	Unknown	76950	No		No	No	P
2268	M	32	No	Right	AdenoCa	Mod	C	4	2	0	Positive	9/24	Clear	Wildtype	MSI	72000	No		No	No	Super
2287	F	70	No	Right	AdenoCa	Poor	D	3	2	1	Negative	9/13	Clear	Wildtype	MSI	1331000	Yes	Yes	No	No	P, WB
2291	F	79	No	Right	AdenoCa	Poor	C	3	1	0	Negative	3/16	Clear	Wildtype	MSI	78400	No		No	No	
2312	F	29	No	Rectum	AdenoCa	Mod	D	3	1	1	Positive	2/20	Clear	Mutation	MSS	147000	Yes	Yes	No	No	
2315	F	85	No	Right	Mucinous	Mod	B	3	0	0	Negative	0/29	Clear	Mutation	MSS	12500	No		No	No	P
2337	M	82	No	Rectum	AdenoCa	Mod	C	2	1	0	Negative	1/25	Clear	Wildtype	MSS	18480	No		No	No	P, WB, PCR
2359	M	80	Yes	Rectum	AdenoCa	Mod	C	3	1	0	Positive	1/20	Clear	Unknown	Unknown	30375	No		No	No	PCR
2381	M	64	No	Rectum	AdenoCa	Mod	C	3	1	0	Negative	1/69	Clear	Unknown	Unknown	13750	No		No	No	P, PCR
2385a	F	73	No	Right	AdenoCa	Poor	C	4	1	0	Negative	2/24	Clear	Mutation	MSI	27000	Yes	Yes	Yes	Yes	P
2385b	F	73	No	Rectum	AdenoCa	Mod	C	2	1	0	Negative	2/24	Clear	Unknown	MSI	4375	Yes	Yes	Yes	Yes	P, WB
2431	F	78	No	Right	Mucinous	Mod	C	4	2	0	Positive	4/28	Clear	Unknown	Unknown	135000	No		No	No	WB
2449	F	70	No	Left	AdenoCa	Mod	C	4	1	0	Negative	1/37	Clear	Mutation	Unknown	17500	No		No	No	P, B
2450	F	70	No	Left	AdenoCa	Mod	C	4	1	0	Negative	1/37	Clear	Mutation	Unknown	17500	No		No	No	WB
2455	F	67	No	Rectum	AdenoCa	Poor	D	3	1	1	Positive	1/10	Clear	Mutation	Unknown	30000	Yes	Yes	No	No	
2492	F	82	No	Right	AdenoCa	Poor	C	3	2	0	Negative	10/17	Clear	Wildtype	Unknown	47500	Yes	Yes	No	Yes	
2493	M	89	No	Rectum	AdenoCa	Mod	B	3	0	0	Negative	0/7	Clear	Unknown	Unknown	50000	No		No	No	Supp

2578	F	75	No	Left	AdenoCa	Mod	B	3	0	0	Positive	3/35	Clear	Mutation	MSS	36000	No		No	No	P
2623	M	56	Yes	Rectum	Mucinous	Mod	C	3	1	0	Negative	1/20	Clear	Mutation	MSS	11040	No		Yes	No	Supp
2691	M	63	No	Left	AdenoCa	Mod	C	3	1	0	Positive	2/35	Clear	Mutation	Unknown	56400	No		No	No	P, B
2731	M	50	No	Left	AdenoCa	Mod	C	3	1	0	Positive	1/12	Clear	Wildtype	MSS	52500	No		No	No	P, PCR
2732	M	83	No	Right	AdenoCa	Mod	B	3	0	0	Negative	0/29	Clear	Wildtype	Unknown	110400	No		No	No	
2742	M	76	No	Right	AdenoCa	Mod	A	2	0	0		0/23	Clear	Wildtype	MSI	481500	No		No	No	P, B, PCR, LN
2767	F	61	No	Left	AdenoCa	Mod	A	2	0	0	Positive	0/17	Clear	Wildtype	Unknown	10080	No		No	No	P
2768	F	85	No	Right	AdenoCa	Mod	A	2	0	0	Negative	0/12	Clear	Wildtype	Unknown	73125	No		No	No	P
2787	M	52	No	Rectum	AdenoCa	Mod	A	2	0	0	Negative	0/22	Clear	Mutation	Unknown	7500	No		No	No	P, B
2799	M	76	No	Left	AdenoCa	Mod	B	3	0	0	Negative	0/26	Clear	Wildtype	MSS	25200	No		No	No	P
2815	M	69	No	Rectum	AdenoCa	Mod	C	3	2	0	Positive	7/23	Clear	Wildtype	Unknown	6480	No		No	No	P
2896	M	44	No	Rectum	AdenoCa	Poor	B	4	0	0	Negative	0/23	Clear	Wildtype	MSI	56250	No		No	No	P
2928	M	62	No	Rectum	AdenoCa	Mod	C	2	1	x	Negative	1/13	Clear	Wildtype	Unknown	5400	No		No	No	P
2929	M	71	No	Rectum	AdenoCa	Mod	B	3	0	0	Positive	0/15	Clear	Mutation	Unknown	16000	No		No	No	P
2996	M	71	No	Right	AdenoCa	Mod	C	4	1	0	Positive	3/17	Clear	Mutation	Unknown	364000	No		No	No	P, PCR, LN
3047	F	81	No	Right	AdenoCa	Mod	C	4	1	0	Negative	1/26	Clear	Mutation	Unknown	135000	No		No	No	P, Supp
3086	F	87	No	Right	AdenoCa	Poor	C	3	1	0	Negative	1/39	Clear	Wildtype	MSI	300000	No		No	No	P, Transwell, PCR
3152	F	59	No	Rectum	AdenoCa	Mod	A	2	0	0	Negative	0/29	Clear	Wildtype	Unknown	36000	No		No	No	P, Transwell
3161	F	83	No	Rectum	AdenoCa	Mod	C	3	1	0	Positive	1/16	Clear	Wildtype	Unknown	10500	No		No	No	P, Transwell
3192	M	61	No	Rectum	AdenoCa	Mod	C	4	2	0	Positive	7/19	Clear	Mutation	Unknown	31500	No		No	No	P, Transwell
3205	F	63	No	Left	AdenoCa	Mod	B	3	0	0	Positive	0/36	Clear	Wildtype	Unknown	57750	No		No	No	P, Transwell, PCR

3216	F	45		Right	AdenoCa	Mod	C	4	2	0	Positive	6/25	Clear	Mutation	MSS	11200	No		No	No	P, LN
3217	F	57		Right	AdenoCa	Mod	B	3	0	0	Negative	0/29	Clear	Mutation	Unknown	31500	No		No	No	P
3218	M	60	No	Left	AdenoCa	Poor	B	3	0	0	Negative	0/19	Clear	Unknown	Unknown	33800	No		No	No	P
3280	M	65		Right	AdenoCa	Mod	B	3	0	0	Positive	0/15	Clear	Wildtype	Unknown	16800	No		No	No	P, Transwell, IHC-c, LN
3319	M	62		Left	AdenoCa	Mod	B	4	0	0	Negative	0/28	Clear	Mutation	Unknown	232875	No		No	No	P, Transwell, IHC-c
3340	M	63		Rectum	AdenoCa	Mod	C	3	2	0	Positive	4/13	Clear	Wildtype	Unknown	11200	No		No	No	Super
3351	F	62		Right	AdenoCa	Poor	B	3	0	0	Positive	0/38	Clear	Wildtype	MSI	42000	No		No	No	P, Transwell, LN
3355	M	78		Right	AdenoCa	Poor	A	2	0	0	Positive	0/21	Clear	Wildtype	MSI	50000	No		No	No	P, Supp, IHC-c, B, LN
3359	M	60		Left	AdenoCa	Mod	C	3	1	0	Negative	1/27	Clear	Mutation	Unknown	23625	No		No	No	P, Super*, IHC-c, B
3407	M	61		Left	AdenoCa	Mod	D	3	0	1	Positive	0/15	Clear	Wildtype	Unknown	20000	No		No	No	P, LN
3609	F	80		Right	AdenoCa	Poor	C	4	1	0	Positive	3/15		Wildtype	Unknown	126000	No		Yes	No	RNA
3616	M	55		Left	AdenoCa	Mod	D	3	2	1	Positive	6/16	Clear	Wildtype	Unknown	4900	No		No	No	P, RNA
3628	M	62		Right	AdenoCa	Mod	C	3	2	0	Negative	5/28	Clear	Mutation	Unknown	36000	No		No	No	RNA
3654	F	87	No	Right	AdenoCa	Mod	C	3	2	0	Negative	5/14	Clear	Unknown	MSI	128800	Yes	Yes	No	No	P, RNA
3705	M	71		Rectum	AdenoCa	Mod	C	3	1	0	Negative	1/26	Clear	Mutation	Unknown	16800	No		No	No	P, PCR, LN
3729	M	64		Right	AdenoCa	Mod	C	1	1	0	Negative	3/14	Clear	Unknown	Unknown	35100	No		No	No	
3741	F	51		Left	AdenoCa	Mod	C	4	1	0	Negative	1/15	Clear	Wildtype	MSS	1800	No		No	No	P
3906	M	77		Left	AdenoCa	Mod	C	3	1	0	Negative	1/18	Clear	Unknown	Unknown	13500	No		No	No	P, PCR
3948	M	48		Right	AdenoCa	Mod	D	4	2	1	Positive	8/13	Clear	Mutation	Unknown	63000	No		No	No	P
3970	F	73		Rectum	AdenoCa	Mod	B	4	0	0	Negative	0/13	Clear	Mutation	Unknown	9408	No		No	No	P

3995	M	75		Left	AdenoCa	Mod	B	4	0	0	Negative	0/21	Clear	Unknown	Unknown	200200	No	Yes	No	P, B
4137	F	48		Left	AdenoCa	Mod	C	3	1	0	Positive	3/16	Clear	Wildtype	MSS	2100	No	No	No	P
4145	F	86		Right	AdenoCa	Poor	C	4	1	0	Positive	2/30	Clear	Wildtype	MSI	191250	No	No	No	P
4262	M	63		Left	AdenoCa	Mod	B	3	0	0	Negative	0/20	Clear	Wildtype	Unknown	4000	No	No	No	Super*
4294	F	77		Right	AdenoCa	Mod	B	3	0	0	Negative	0/19	Clear	Mutation	Unknown	18360	No	No	No	Supp, P-c
4418	F	66		Right	AdenoCa	Mod	D	4	2	1	Positive	6/13	Clear	Unknown	Unknown	67500	No	No	No	P-c
4474	M	78		Left	AdenoCa	Mod	A	2	0	0	Negative	0/31	Clear	Wildtype	Unknown	9720	No	No	No	P-c
4545	M	71		Right	AdenoCa	Mod	B	3	0	0	Positive	0/34	Clear	Unknown	Unknown	68000	No	No	No	DNA
4500	M	50		Right	AdenoCa	Mod	C	4	2	0	Positive	12/55	Clear	Mutation	Unknown	39600	No	No	No	P, Supp
4519	F	73		Right	AdenoCa	Mod	C	4	1	0	Negative	1/35	Clear	Wildtype	Unknown	75000	No	No	No	P, Supp, DNA
4545	M	71		Right	AdenoCa	Mod	B	3	0	0	Positive	0/34	Clear	Unknown	Unknown	68000	No	No	No	P, Supp
4571	F	71		Rectum	AdenoCa	Mod	B	3	0	0	Positive	0/27	Clear	Mutation	Unknown	17150	No	No	No	P, DNA
4682	F	48		Right	AdenoCa	Mod	C	3	1	0	Positive	3/30	Clear	Unknown	Unknown	16000	No	No	No	Supp, RNA, DNA
1678	M	65	No		AdenoCa															P
1897	F	49	No		AdenoCa															P
2746	M	62	No		AdenoCa															P

Appendix III:
Antibodies used for flow cytometry

Antigen	Clone	Fluorochrome	Isotype	Manufacturer	Code
CD3	UCHT1	Alexa-Fluor 750	Ms IgG1	Serotec	MCA463P750
CD4	RPA-T4	V500	Ms IgG1	BD	560768
CD25	M-A251	V450	Ms IgG1	BD	560355
CD127	HIL-7R-M21	FITC	Ms IgG1	BD	560549
CD127	eBioRDR5	APC	Ms IgG1	eBioscience	17-1278-42
CD8	RPA-T8	PE-CF594	Ms IgG1	BD	562282
CCR1	53504	APC	Ms IgG2b	R&D Systems	FAB145A
CCR2	48607	APC	Ms IgG2b	R&D Systems	FAB151A
CCR3	61828	APC	Rat IgG2a	R&D Systems	FAB155A
CCR4	205410	APC	Ms IgG2b	R&D Systems	FAB1567A
CCR5	CTC5	APC	Ms IgG1	R&D Systems	FAB1802A
CCR5	CTC5	PE	Ms IgG1	R&D Systems	FAB1802P
CCR5	2D7-CCR5	PE	Ms IgG2a	BD	560935
CCR6	11A9	PE	Ms IgG1	BD	551773
CCR7	150503	APC	Ms IgG2a	R&D Systems	FAB197A
CCR8	191704	APC	Rat IgG2b	R&D Systems	FAB1429A
CCR9	112509	Alexa-Fluor 647	Ms IgG2a	BD	557975
CCR10	314305	PE	RatIgG2a	R&D Systems	FAB3478P
CXCR1	42705	APC	MsIgG2a	R&D Systems	FAB330A
CXCR2	48311	APC	MsIgG2a	R&D Systems	FAB331A
CXCR3	49801	APC	MsIgG1	R&D Systems	FAB160A
CXCR4	12G5	PE	MsIgG2a	R&D Systems	FAB170P
CXCR5	51505	APC	MsIgG2b	R&D Systems	FAB190A
CXCR6	K041E5	APC	MsIgG2a	Biolegend	356006
CX3CR1	528728	FITC	MsIgG1	R&D Systems	FAB5204F

XCR1	Polyclonal	FITC	Goat	R&D Systems	FAB857F
CD27	CLB-27/1	PE	MsIgG2a	Caltag	MHCD2704
CD39	eBioA1	PE	MsIgG1	eBioscience	12-0399
CD45RA	F8-11-13	PE	MsIgG1	Serotec	MCA88PE
CD62L	DREG-56	PE	MsIgG1	BD	555544
CD69	FN50	APC	MsIgG1	BD	555533
CD73	AD2	PE	MsIgG1	BD	550257
PD-1	EH12.1	PECy7	MsIgG1	BD	561272
GARP	855151	PE	RatIgG2a	R&D Systems	FAB6055P
GITR	110416	APC	MsIgG1	R&D Systems	FAB689A
OX40	ACT35	PE	MsIgG1	BD	555838
TGF-LAP	27232	PE	MsIgG1	R&D Systems	FAB2463P
CD103	Ber-ACT8	PE	MsIgG1	BD	550260
α1	SR84	PE	MsIgG1	BD	559596
α2	HAS3	PE	MsIgG2a	R&D Systems	FAB1233P
α3	IA3	PE	MsIgG1	R&D Systems	FAB1345P
α4	7.2R	APC	MsIgG1	R&D Systems	FAB1354A
α5	238307	PE	MsIgG1	R&D Systems	FAB1864P
α6	GoH3	PE	RatIgG2a	R&D Systems	FAB13501P
αL	345913	APC	MsIgG1	R&D Systems	FAB3595A
αM	238446	APC	MsIgG2b	R&D Systems	FAB16991A
αV	13C2	PE	MsIgG1	Abcam	Ab82530
αX	ICRF 3.9	APC	MsIgG1	R&D Systems	FAB1777A
ß1	P5D2	PE	MsIgG1	R&D Systems	FAB17781P
ß2	212701	PE	MsIgG1	R&D Systems	FAB1730P
ß3	256809	PE	MsIgG2a	R&D Systems	FAB2266P
ß7	473207	PE	MsIgG1	R&D Systems	FAB4669P
Foxp3	PCH101	PE	Rat IgG2a	eBioscience	12-4776-42
CTLA-4	BNI3	APC	Ms IgG2a	BD	560938
Helios	22F6	APC	Hamster IgG	Biolegend	137222

Ki67	35/Ki-67	FITC	Ms IgG1	BD	612472
CD3	UCHT1	PE	Ms IgG1	BD	555333
CD4	RPA-T4	FITC	Ms IgG1	BD	555346
CD11b	ICRF44	PECy7	Ms IgG1	BD	557743
CD31	9G11	FITC	Ms IgG1	R&D Systems	FAB3567F
CD90	Thy-1A1	PE	Ms IgG2a	R&D Systems	FAB2067P
EpCAM	158206	PE	Ms IgG2b	R&D Systems	FAB9601P
IMC	MOPC-21	PECy7	MsIgG1	BD	557872
IMC	-	Alexa-Fluor 750	Ms IgG1	Serotec	MCA928P750
IMC	X40	V500	Ms IgG1	BD	560787
IMC	MOPC-21	V450	Ms IgG1	BD	560373
IMC	11711	FITC	Ms IgG1	R&D Systems	IC002F
IMC	X40	PE-CF594	Ms IgG1	BD	562292
IMC	-	FITC	Goat	R&D Systems	IC108F
IMC	11711	PE	Ms IgG1	R&D Systems	IC002P
IMC	20102	PE	Ms IgG2a	R&D Systems	IC003P
IMC	133303	PE	Ms IgG2b	R&D Systems	IC0041P
IMC	eBR2a	PE	Rat IgG2a	eBioscience	12-4321
IMC	11711	APC	Ms IgG1	R&D Systems	IC002A
IMC	20102	APC	Ms IgG2a	R&D Systems	IC003A
IMC	133303	APC	Ms IgG2b	R&D Systems	IC0041A
IMC	54447	APC	Rat IgG2a	R&D Systems	IC006A
IMC	141945	APC	Rat IgG2b	R&D Systems	IC013A

Appendix IV: ImageJ macro

ImageJ macro to read Proteome Profiler™ spots (R&D systems)

```
// ImageJ macro to read Proteome Profiler spots (Cytokine A panel)
by Steve Ward, 2013

myImageID=getImageID();
if (isOpen("Results")) {
       selectWindow("Results");
       run("Close");
   }
 if (isOpen("ROI Manager")) {
     selectWindow("ROI Manager");
     run("Close");
  }
run("8-bit");

        if (getPixel(0, 0) != 0)
                run("Invert");
setTool("Point");
beep();
waitForUser("Steve Ward's Protein Array Plug-in","Please click in
centre of TOP LEFT dot then click on OK…");
s = selectionType();
if( s != 10 ) {
    exit("The selection wasn't a point selection.");
} else {
    getSelectionCoordinates(xPoints,yPoints);
    xstart = xPoints[0];
    ystart = yPoints[0];
}

beep();
waitForUser("Steve Ward's Protein Array Plug-in","Please click in
centre of TOP RIGHT dot then click on OK…");
s = selectionType();
if( s != 10 ) {
    exit("The selection wasn't a point selection.");
} else {
    getSelectionCoordinates(xPoints,yPoints);
    xend = xPoints[0];
    yend = yPoints[0];
}
startl = sqrt(((xend-xstart)*(xend-xstart)) + ((yend-ystart)*(yend-
ystart)));
diffh = (yend-ystart);
rang = -(asin(diffh / startl)*57.2957795);
```

```
rangrad=-(asin(diffh / startl));

run("Rotate... ", "angle=rang grid=1 interpolation=Bilinear");

selectImage(myImageID);
x=477/startl*getWidth();
//y=475.5591/startl*getHeight();
run("Size...", "width=x constrain interpolation=Bilinear");

beep();
waitForUser("Steve Ward's Protein Array Plug-in","Please click in
centre of TOP LEFT dot again then click on OK…");
s = selectionType();
if( s != 10 ) {
    exit("The selection wasn't a point selection.");
} else {
    getSelectionCoordinates(xPoints,yPoints);
    xoffset = xPoints[0];
    yoffset = yPoints[0];
}

setTool("oval");
makeOval(5+(xoffset-13),  13+(yoffset-20),  16,  19);  run("Add  to
Manager"); roiManager("Add");
roiManager("Show All");
run("Set  Measurements...",  "    mean  redirect=None  decimal=0");
roiManager("Select",0);
roiManager("Rename", "Ref");
makeOval(26+(xoffset-13),       13+(yoffset-20),       16,       19);
roiManager("Add");   roiManager("Select",1);   roiManager("Rename",
"Ref");
makeOval(60+(xoffset-13),       13+(yoffset-20),       16,       19);
roiManager("Add");   roiManager("Select",2);   roiManager("Rename",
"C5/C5a");
makeOval(81+(xoffset-13),       13+(yoffset-20),       16,       19);
roiManager("Add");   roiManager("Select",3);   roiManager("Rename",
"C5/C5a");
makeOval(103+(xoffset-13),       13+(yoffset-20),       16,       19);
roiManager("Add");   roiManager("Select",4);   roiManager("Rename",
"CD40L");
makeOval(126+(xoffset-13),       13+(yoffset-20),       16,       19);
roiManager("Add");   roiManager("Select",5);   roiManager("Rename",
"CD40L");
makeOval(159+(xoffset-13),       13+(yoffset-20),       16,       19);
roiManager("Add"); roiManager("Select",6); roiManager("Rename", "G-
CSF");
makeOval(182+(xoffset-13),       13+(yoffset-20),       16,       19);
roiManager("Add"); roiManager("Select",7); roiManager("Rename", "G-
CSF");
makeOval(204+(xoffset-13),       13+(yoffset-20),       16,       19);
roiManager("Add"); roiManager("Select",8); roiManager("Rename", "GM-
CSF");
makeOval(225+(xoffset-13),       13+(yoffset-20),       16,       19);
roiManager("Add"); roiManager("Select",9); roiManager("Rename", "GM-
CSF");
```

```
makeOval(259+(xoffset-13),      13+(yoffset-20),      16,      19);
roiManager("Add");   roiManager("Select",10);   roiManager("Rename",
"GROa");
makeOval(281+(xoffset-13),      13+(yoffset-20),      16,      19);
roiManager("Add");   roiManager("Select",11);   roiManager("Rename",
"GROa");
makeOval(304+(xoffset-13),      13+(yoffset-20),      16,      19);
roiManager("Add");   roiManager("Select",12);   roiManager("Rename",
"I309");
makeOval(328+(xoffset-13),      13+(yoffset-20),      16,      19);
roiManager("Add");   roiManager("Select",13);   roiManager("Rename",
"I309");
makeOval(359+(xoffset-13),      13+(yoffset-20),      16,      19);
roiManager("Add");   roiManager("Select",14);   roiManager("Rename",
"sICAM1");
makeOval(382+(xoffset-13),      13+(yoffset-20),      16,      19);
roiManager("Add");   roiManager("Select",15);   roiManager("Rename",
"sICAM1");
makeOval(403+(xoffset-13),      13+(yoffset-20),      16,      19);
roiManager("Add");   roiManager("Select",16);   roiManager("Rename",
"IFNg");
makeOval(425+(xoffset-13),      13+(yoffset-20),      16,      19);
roiManager("Add");   roiManager("Select",17);   roiManager("Rename",
"IFNg");
makeOval(459+(xoffset-13),      13+(yoffset-20),      16,      19);
roiManager("Add");   roiManager("Select",18);   roiManager("Rename",
"Ref");
makeOval(482+(xoffset-13),      13+(yoffset-20),      16,      19);
roiManager("Add");   roiManager("Select",19);   roiManager("Rename",
"Ref");
makeOval(60+(xoffset-13),      44+(yoffset-20),      16,      19);
roiManager("Add");   roiManager("Select",20);   roiManager("Rename",
"IL-1a");
makeOval(81+(xoffset-13),      44+(yoffset-20),      16,      19);
roiManager("Add");   roiManager("Select",21);   roiManager("Rename",
"IL-1a");
makeOval(103+(xoffset-13),      44+(yoffset-20),      16,      19);
roiManager("Add");   roiManager("Select",22);   roiManager("Rename",
"IL-1b");
makeOval(126+(xoffset-13),      44+(yoffset-20),      16,      19);
roiManager("Add");   roiManager("Select",23);   roiManager("Rename",
"IL-1b");
makeOval(159+(xoffset-13),      44+(yoffset-20),      16,      19);
roiManager("Add");   roiManager("Select",24);   roiManager("Rename",
"IL-1ra");
makeOval(182+(xoffset-13),      44+(yoffset-20),      16,      19);
roiManager("Add");   roiManager("Select",25);   roiManager("Rename",
"IL-1ra");
makeOval(204+(xoffset-13),      44+(yoffset-20),      16,      19);
roiManager("Add");   roiManager("Select",26);   roiManager("Rename",
"IL-2");
makeOval(225+(xoffset-13),      44+(yoffset-20),      16,      19);
roiManager("Add");   roiManager("Select",27);   roiManager("Rename",
"IL-2");
makeOval(259+(xoffset-13),      44+(yoffset-20),      16,      19);
```

```
roiManager("Add");   roiManager("Select",28);   roiManager("Rename",
"IL-4");
makeOval(281+(xoffset-13),       44+(yoffset-20),       16,       19);
roiManager("Add");   roiManager("Select",29);   roiManager("Rename",
"IL-4");
makeOval(304+(xoffset-13),       44+(yoffset-20),       16,       19);
roiManager("Add");   roiManager("Select",30);   roiManager("Rename",
"IL-5");
makeOval(328+(xoffset-13),       44+(yoffset-20),       16,       19);
roiManager("Add");   roiManager("Select",31);   roiManager("Rename",
"IL-5");
makeOval(359+(xoffset-13),       44+(yoffset-20),       16,       19);
roiManager("Add");   roiManager("Select",32);   roiManager("Rename",
"IL-6");
makeOval(382+(xoffset-13),       44+(yoffset-20),       16,       19);
roiManager("Add");   roiManager("Select",33);   roiManager("Rename",
"IL-6");
makeOval(403+(xoffset-13),       44+(yoffset-20),       16,       19);
roiManager("Add");   roiManager("Select",34);   roiManager("Rename",
"IL-8");
makeOval(425+(xoffset-13),       44+(yoffset-20),       16,       19);
roiManager("Add");   roiManager("Select",35);   roiManager("Rename",
"IL-8");
makeOval(60+(xoffset-13),       66+(yoffset-20),       16,       19);
roiManager("Add");   roiManager("Select",36);   roiManager("Rename",
"IL-10");
makeOval(81+(xoffset-13),       66+(yoffset-20),       16,       19);
roiManager("Add");   roiManager("Select",37);   roiManager("Rename",
"IL-10");
makeOval(103+(xoffset-13),       66+(yoffset-20),       16,       19);
roiManager("Add");   roiManager("Select",38);   roiManager("Rename",
"IL-12p70");
makeOval(126+(xoffset-13),       66+(yoffset-20),       16,       19);
roiManager("Add");   roiManager("Select",39);   roiManager("Rename",
"IL-12p70");
makeOval(159+(xoffset-13),       66+(yoffset-20),       16,       19);
roiManager("Add");   roiManager("Select",40);   roiManager("Rename",
"IL-13");
makeOval(182+(xoffset-13),       66+(yoffset-20),       16,       19);
roiManager("Add");   roiManager("Select",41);   roiManager("Rename",
"IL-13");
makeOval(204+(xoffset-13),       66+(yoffset-20),       16,       19);
roiManager("Add");   roiManager("Select",42);   roiManager("Rename",
"IL-16");
makeOval(225+(xoffset-13),       66+(yoffset-20),       16,       19);
roiManager("Add");   roiManager("Select",43);   roiManager("Rename",
"IL-16");
makeOval(259+(xoffset-13),       66+(yoffset-20),       16,       19);
roiManager("Add");   roiManager("Select",44);   roiManager("Rename",
"IL-17");
makeOval(281+(xoffset-13),       66+(yoffset-20),       16,       19);
roiManager("Add");   roiManager("Select",45);   roiManager("Rename",
"IL-17");
makeOval(304+(xoffset-13),       66+(yoffset-20),       16,       19);
roiManager("Add");   roiManager("Select",46);   roiManager("Rename",
```

```
"IL-17E");
makeOval(328+(xoffset-13),       66+(yoffset-20),       16,       19);
roiManager("Add");   roiManager("Select",47);   roiManager("Rename",
"IL-17E");
makeOval(359+(xoffset-13),       66+(yoffset-20),       16,       19);
roiManager("Add");   roiManager("Select",48);   roiManager("Rename",
"IL-23");
makeOval(382+(xoffset-13),       66+(yoffset-20),       16,       19);
roiManager("Add");   roiManager("Select",49);   roiManager("Rename",
"IL-23");
makeOval(403+(xoffset-13),       66+(yoffset-20),       16,       19);
roiManager("Add");   roiManager("Select",50);   roiManager("Rename",
"IL-27");
makeOval(425+(xoffset-13),       66+(yoffset-20),       16,       19);
roiManager("Add");   roiManager("Select",51);   roiManager("Rename",
"IL-27");
makeOval(60+(xoffset-13),       89+(yoffset-20),       16,       19);
roiManager("Add");   roiManager("Select",52);   roiManager("Rename",
"IL-32a");
makeOval(81+(xoffset-13),       89+(yoffset-20),       16,       19);
roiManager("Add");   roiManager("Select",53);   roiManager("Rename",
"IL-32a");
makeOval(103+(xoffset-13),       89+(yoffset-20),       16,       19);
roiManager("Add");   roiManager("Select",54);   roiManager("Rename",
"IP-10");
makeOval(126+(xoffset-13),       89+(yoffset-20),       16,       19);
roiManager("Add");   roiManager("Select",55);   roiManager("Rename",
"IP-10");
makeOval(159+(xoffset-13),       89+(yoffset-20),       16,       19);
roiManager("Add"); roiManager("Select",56); roiManager("Rename", "I-
TAC");
makeOval(182+(xoffset-13),       89+(yoffset-20),       16,       19);
roiManager("Add"); roiManager("Select",57); roiManager("Rename", "I-
TAC");
makeOval(204+(xoffset-13),       89+(yoffset-20),       16,       19);
roiManager("Add");   roiManager("Select",58);   roiManager("Rename",
"MCP-1");
makeOval(225+(xoffset-13),       89+(yoffset-20),       16,       19);
roiManager("Add");   roiManager("Select",59);   roiManager("Rename",
"MCP-1");
makeOval(259+(xoffset-13),       89+(yoffset-20),       16,       19);
roiManager("Add");   roiManager("Select",60);   roiManager("Rename",
"MIF");
makeOval(281+(xoffset-13),       89+(yoffset-20),       16,       19);
roiManager("Add");   roiManager("Select",61);   roiManager("Rename",
"MIF");
makeOval(304+(xoffset-13),       89+(yoffset-20),       16,       19);
roiManager("Add");   roiManager("Select",62);   roiManager("Rename",
"MIP-1a");
makeOval(328+(xoffset-13),       89+(yoffset-20),       16,       19);
roiManager("Add");   roiManager("Select",63);   roiManager("Rename",
"MIP-1a");
makeOval(359+(xoffset-13),       89+(yoffset-20),       16,       19);
roiManager("Add");   roiManager("Select",64);   roiManager("Rename",
"MIP-1b");
```

```
makeOval(382+(xoffset-13),       89+(yoffset-20),       16,       19);
roiManager("Add");   roiManager("Select",65);   roiManager("Rename",
"MIP-1b");
makeOval(403+(xoffset-13),       89+(yoffset-20),       16,       19);
roiManager("Add");   roiManager("Select",66);   roiManager("Rename",
"SerpinE1");
makeOval(425+(xoffset-13),       89+(yoffset-20),       16,       19);
roiManager("Add");   roiManager("Select",67);   roiManager("Rename",
"SerpinE1");
makeOval(5+(xoffset-13),       109+(yoffset-20),       16,       19);
roiManager("Add");   roiManager("Select",68);   roiManager("Rename",
"Ref");
makeOval(28+(xoffset-13),       109+(yoffset-20),       16,       19);
roiManager("Add");   roiManager("Select",69);   roiManager("Rename",
"Ref");
makeOval(60+(xoffset-13),       109+(yoffset-20),       16,       19);
roiManager("Add");   roiManager("Select",70);   roiManager("Rename",
"RANTES");
makeOval(81+(xoffset-13),       109+(yoffset-20),       16,       19);
roiManager("Add");   roiManager("Select",71);   roiManager("Rename",
"RANTES");
makeOval(103+(xoffset-13),       109+(yoffset-20),       16,       19);
roiManager("Add");   roiManager("Select",72);   roiManager("Rename",
"SDF-1a");
makeOval(126+(xoffset-13),       109+(yoffset-20),       16,       19);
roiManager("Add");   roiManager("Select",73);   roiManager("Rename",
"SDF-1a");
makeOval(159+(xoffset-13),       109+(yoffset-20),       16,       19);
roiManager("Add");   roiManager("Select",74);   roiManager("Rename",
"TNFa");
makeOval(182+(xoffset-13),       109+(yoffset-20),       16,       19);
roiManager("Add");   roiManager("Select",75);   roiManager("Rename",
"TNFa");
makeOval(204+(xoffset-13),       109+(yoffset-20),       16,       19);
roiManager("Add");   roiManager("Select",76);   roiManager("Rename",
"sTREM-1");
makeOval(225+(xoffset-13),       109+(yoffset-20),       16,       19);
roiManager("Add");   roiManager("Select",77);   roiManager("Rename",
"sTREM-1");
makeOval(460+(xoffset-13),       109+(yoffset-20),       16,       19);
roiManager("Add");   roiManager("Select",78);   roiManager("Rename",
"Negative");
makeOval(483+(xoffset-13),       109+(yoffset-20),       16,       19);
roiManager("Add");   roiManager("Select",79);   roiManager("Rename",
"Negative");

array1 = newArray("0");;
for (i=1;i<roiManager("count");i++){
        array1 = Array.concat(array1,i);

}
roiManager("select", array1);

roiManager("Multi Measure");
selectWindow("Results");
```

```
//headings=String.getResultsHeadings;  replace(headings,  "Mean\\(",
""); replace(headings, "\\)",""); print(headings);
text = getInfo();
lines = split(text, "\n");
columns = split(lines[0], "\t");
bkground=getResult("Mean(Negative)",0); print(bkground);
refspot=getResult("Mean(Ref)",0); print(refspot);
refstd=refspot-bkground;
arrayR=newArray("0");
for (i=1;i<columns.length;i++) {
arrayR = Array.concat(arrayR,getResult(columns[i],0));
columns[i]=replace(columns[i], "Mean\\(", "");
columns[i]=replace(columns[i], "\\)","");
}
for (i=0;i<columns.length;i++) {print(columns[i]);}
for (i=0;i<columns.length;i++) {print(arrayR[i]);}

selectWindow("Results");
  run("Close");
for (i=1;i<columns.length-1;i++) {
subbk= (arrayR[i])-bkground;
if (subbk >= 0.0)
     setResult(columns[i], 0, subbk);
else setResult(columns[i], 0,0);
}



//  ImageJ  macro  to  read  Proteome  Profiler  spots  (Angiogenesis
Array), by Steve Ward 2013
myImageID=getImageID();
if (isOpen("Results")) {
       selectWindow("Results");
       run("Close");
   }
 if (isOpen("ROI Manager")) {
     selectWindow("ROI Manager");
     run("Close");
  }
//selectWindow(myImageID);
run("8-bit");

        if (getPixel(0, 0) != 0)
                run("Invert");
setTool("Point");
beep();
waitForUser("Steve  Ward's  Protein  Array  Plug-in","Please  click  in
centre of TOP LEFT dot then click on OK…");
s = selectionType();
if( s != 10 ) {
    exit("The selection wasn't a point selection.");
} else {
    getSelectionCoordinates(xPoints,yPoints);
    xstart = xPoints[0];
    ystart = yPoints[0];
```

```
}

beep();
waitForUser("Steve Ward's Protein Array Plug-in","Please click in
centre of TOP RIGHT dot then click on OK…");
s = selectionType();
if( s != 10 ) {
    exit("The selection wasn't a point selection.");
} else {
    getSelectionCoordinates(xPoints,yPoints);
    xend = xPoints[0];
    yend = yPoints[0];
}
startl = sqrt(((xend-xstart)*(xend-xstart)) + ((yend-ystart)*(yend-
ystart)));
diffh = (yend-ystart);
rang = -(asin(diffh / startl)*57.2957795);
rangrad=-(asin(diffh / startl));

run("Rotate... ", "angle=rang grid=1 interpolation=Bilinear");

selectImage(myImageID);
x=477/startl*getWidth();
//y=475.5591/startl*getHeight();
run("Size...", "width=x constrain interpolation=Bilinear");

beep();
waitForUser("Steve Ward's Protein Array Plug-in","Please click in
centre of TOP LEFT dot again then click on OK…");
s = selectionType();
if( s != 10 ) {
    exit("The selection wasn't a point selection.");
} else {
    getSelectionCoordinates(xPoints,yPoints);
    xoffset = xPoints[0];
    yoffset = yPoints[0];
}

setTool("oval");
makeOval(5+(xoffset-13),  12+(yoffset-20),  16,  19);  run("Add  to
Manager"); roiManager("Add");
roiManager("Show All");
run("Set  Measurements...",  "    mean  redirect=None  decimal=0");
roiManager("Select",0);
roiManager("Rename", "Ref");
makeOval(24+(xoffset-13),       12+(yoffset-20),       16,       19);
roiManager("Add");   roiManager("Select",1);   roiManager("Rename",
"Ref");
makeOval(43+(xoffset-13),       12+(yoffset-20),       16,       19);
roiManager("Add");   roiManager("Select",2);   roiManager("Rename",
"BLANK");
makeOval(62+(xoffset-13),       12+(yoffset-20),       16,       19);
roiManager("Add");   roiManager("Select",3);   roiManager("Rename",
"BLANK");
makeOval(88+(xoffset-13),       12+(yoffset-20),       16,       19);
```

```
roiManager("Add");   roiManager("Select",4);   roiManager("Rename",
"Activin-A");
makeOval(107+(xoffset-13),      12+(yoffset-20),      16,      19);
roiManager("Add");   roiManager("Select",5);   roiManager("Rename",
"Activin-A");
makeOval(126+(xoffset-13),      12+(yoffset-20),      16,      19);
roiManager("Add");   roiManager("Select",6);   roiManager("Rename",
"ADAMTS-1");
makeOval(145+(xoffset-13),      12+(yoffset-20),      16,      19);
roiManager("Add");   roiManager("Select",7);   roiManager("Rename",
"ADAMTS-1");
makeOval(172+(xoffset-13),      12+(yoffset-20),      16,      19);
roiManager("Add");   roiManager("Select",8);   roiManager("Rename",
"ANG");
makeOval(191+(xoffset-13),      12+(yoffset-20),      16,      19);
roiManager("Add");   roiManager("Select",9);   roiManager("Rename",
"ANG");
makeOval(210+(xoffset-13),      12+(yoffset-20),      16,      19);
roiManager("Add");   roiManager("Select",10);   roiManager("Rename",
"Ang-1");
makeOval(229+(xoffset-13),      12+(yoffset-20),      16,      19);
roiManager("Add");   roiManager("Select",11);   roiManager("Rename",
"Ang-1");
makeOval(256+(xoffset-13),      12+(yoffset-20),      16,      19);
roiManager("Add");   roiManager("Select",12);   roiManager("Rename",
"Ang-2");
makeOval(275+(xoffset-13),      12+(yoffset-20),      16,      19);
roiManager("Add");   roiManager("Select",13);   roiManager("Rename",
"Ang-2");
makeOval(294+(xoffset-13),      12+(yoffset-20),      16,      19);
roiManager("Add");   roiManager("Select",14);   roiManager("Rename",
"Plasminogen");
makeOval(313+(xoffset-13),      12+(yoffset-20),      16,      19);
roiManager("Add");   roiManager("Select",15);   roiManager("Rename",
"Plasminogen");
makeOval(340+(xoffset-13),      12+(yoffset-20),      16,      19);
roiManager("Add");   roiManager("Select",16);   roiManager("Rename",
"AR");
makeOval(359+(xoffset-13),      12+(yoffset-20),      16,      19);
roiManager("Add");   roiManager("Select",17);   roiManager("Rename",
"AR");
makeOval(378+(xoffset-13),      12+(yoffset-20),      16,      19);
roiManager("Add");   roiManager("Select",18);   roiManager("Rename",
"Artemin");
makeOval(397+(xoffset-13),      12+(yoffset-20),      16,      19);
roiManager("Add");   roiManager("Select",19);   roiManager("Rename",
"Artemin");
makeOval(423+(xoffset-13),      12+(yoffset-20),      16,      19);
roiManager("Add");   roiManager("Select",20);   roiManager("Rename",
"BLANK");
makeOval(442+(xoffset-13),      12+(yoffset-20),      16,      19);
roiManager("Add");   roiManager("Select",21);   roiManager("Rename",
"BLANK");
makeOval(461+(xoffset-13),      12+(yoffset-20),      16,      19);
roiManager("Add");   roiManager("Select",22);   roiManager("Rename",
```

```
"Ref");
makeOval(480+(xoffset-13),       12+(yoffset-20),       16,       19);
roiManager("Add");   roiManager("Select",23);   roiManager("Rename",
"Ref");

// Row B
makeOval(5+(xoffset-13),       38+(yoffset-20),       16,       19);
roiManager("Add");   roiManager("Select",24);   roiManager("Rename",
"CoagF3");
makeOval(24+(xoffset-13),       38+(yoffset-20),       16,       19);
roiManager("Add");   roiManager("Select",25);   roiManager("Rename",
"CoagF3");
makeOval(43+(xoffset-13),       38+(yoffset-20),       16,       19);
roiManager("Add");   roiManager("Select",26);   roiManager("Rename",
"CXCL16");
makeOval(62+(xoffset-13),       38+(yoffset-20),       16,       19);
roiManager("Add");   roiManager("Select",27);   roiManager("Rename",
"CXCL16");
makeOval(88+(xoffset-13),       38+(yoffset-20),       16,       19);
roiManager("Add");   roiManager("Select",28);   roiManager("Rename",
"DPPIV");
makeOval(107+(xoffset-13),       38+(yoffset-20),       16,       19);
roiManager("Add");   roiManager("Select",29);   roiManager("Rename",
"DPPIV");
makeOval(126+(xoffset-13),       38+(yoffset-20),       16,       19);
roiManager("Add");   roiManager("Select",30);   roiManager("Rename",
"EGF");
makeOval(145+(xoffset-13),       38+(yoffset-20),       16,       19);
roiManager("Add");   roiManager("Select",31);   roiManager("Rename",
"EGF");
makeOval(172+(xoffset-13),       38+(yoffset-20),       16,       19);
roiManager("Add");   roiManager("Select",32);   roiManager("Rename",
"EG-VEGF");
makeOval(191+(xoffset-13),       38+(yoffset-20),       16,       19);
roiManager("Add");   roiManager("Select",33);   roiManager("Rename",
"EG-VEGF");
makeOval(210+(xoffset-13),       38+(yoffset-20),       16,       19);
roiManager("Add");   roiManager("Select",34);   roiManager("Rename",
"Endoglin");
makeOval(229+(xoffset-13),       38+(yoffset-20),       16,       19);
roiManager("Add");   roiManager("Select",35);   roiManager("Rename",
"Endoglin");
makeOval(256+(xoffset-13),       38+(yoffset-20),       16,       19);
roiManager("Add");   roiManager("Select",36);   roiManager("Rename",
"Endostatin");
makeOval(275+(xoffset-13),       38+(yoffset-20),       16,       19);
roiManager("Add");   roiManager("Select",37);   roiManager("Rename",
"Endostatin");
makeOval(294+(xoffset-13),       38+(yoffset-20),       16,       19);
roiManager("Add");   roiManager("Select",38);   roiManager("Rename",
"Endothelin-1");
makeOval(313+(xoffset-13),       38+(yoffset-20),       16,       19);
roiManager("Add");   roiManager("Select",39);   roiManager("Rename",
"Endothelin-1");
makeOval(340+(xoffset-13),       38+(yoffset-20),       16,       19);
```

```
roiManager("Add");   roiManager("Select",40);   roiManager("Rename",
"FGF-1");
makeOval(359+(xoffset-13),       38+(yoffset-20),       16,       19);
roiManager("Add");   roiManager("Select",41);   roiManager("Rename",
"FGF-1");
makeOval(378+(xoffset-13),       38+(yoffset-20),       16,       19);
roiManager("Add");   roiManager("Select",42);   roiManager("Rename",
"FGF-2");
makeOval(397+(xoffset-13),       38+(yoffset-20),       16,       19);
roiManager("Add");   roiManager("Select",43);   roiManager("Rename",
"FGF-2");
makeOval(423+(xoffset-13),       38+(yoffset-20),       16,       19);
roiManager("Add");   roiManager("Select",44);   roiManager("Rename",
"FGF-4");
makeOval(442+(xoffset-13),       38+(yoffset-20),       16,       19);
roiManager("Add");   roiManager("Select",45);   roiManager("Rename",
"FGF-4");
makeOval(461+(xoffset-13),       38+(yoffset-20),       16,       19);
roiManager("Add");   roiManager("Select",46);   roiManager("Rename",
"FGF-7");
makeOval(480+(xoffset-13),       38+(yoffset-20),       16,       19);
roiManager("Add");   roiManager("Select",47);   roiManager("Rename",
"FGF-7");

// Row C
makeOval(5+(xoffset-13),       57+(yoffset-20),       16,       19);
roiManager("Add");   roiManager("Select",48);   roiManager("Rename",
"GDNF");
makeOval(24+(xoffset-13),       57+(yoffset-20),       16,       19);
roiManager("Add");   roiManager("Select",49);   roiManager("Rename",
"GDNF");
makeOval(43+(xoffset-13),       57+(yoffset-20),       16,       19);
roiManager("Add");   roiManager("Select",50);   roiManager("Rename",
"GM-CSF");
makeOval(62+(xoffset-13),       57+(yoffset-20),       16,       19);
roiManager("Add");   roiManager("Select",51);   roiManager("Rename",
"GM-CSF");
makeOval(88+(xoffset-13),       57+(yoffset-20),       16,       19);
roiManager("Add");   roiManager("Select",52);   roiManager("Rename",
"HB-EGF");
makeOval(107+(xoffset-13),       57+(yoffset-20),       16,       19);
roiManager("Add");   roiManager("Select",53);   roiManager("Rename",
"HB-EGF");
makeOval(126+(xoffset-13),       57+(yoffset-20),       16,       19);
roiManager("Add");   roiManager("Select",54);   roiManager("Rename",
"HGF");
makeOval(145+(xoffset-13),       57+(yoffset-20),       16,       19);
roiManager("Add");   roiManager("Select",55);   roiManager("Rename",
"HGF");
makeOval(172+(xoffset-13),       57+(yoffset-20),       16,       19);
roiManager("Add");   roiManager("Select",56);   roiManager("Rename",
"IGFBP-1");
makeOval(191+(xoffset-13),       57+(yoffset-20),       16,       19);
roiManager("Add");   roiManager("Select",57);   roiManager("Rename",
"IGFBP-1");
```

```
makeOval(210+(xoffset-13),       57+(yoffset-20),       16,       19);
roiManager("Add");   roiManager("Select",58);   roiManager("Rename",
"IGFBP-2");
makeOval(229+(xoffset-13),       57+(yoffset-20),       16,       19);
roiManager("Add");   roiManager("Select",59);   roiManager("Rename",
"IGFBP-2");
makeOval(256+(xoffset-13),       57+(yoffset-20),       16,       19);
roiManager("Add");   roiManager("Select",60);   roiManager("Rename",
"IGFBP-3");
makeOval(275+(xoffset-13),       57+(yoffset-20),       16,       19);
roiManager("Add");   roiManager("Select",61);   roiManager("Rename",
"IGFBP-3");
makeOval(294+(xoffset-13),       57+(yoffset-20),       16,       19);
roiManager("Add");   roiManager("Select",62);   roiManager("Rename",
"IL-1b");
makeOval(313+(xoffset-13),       57+(yoffset-20),       16,       19);
roiManager("Add");   roiManager("Select",63);   roiManager("Rename",
"IL-1b");
makeOval(340+(xoffset-13),       57+(yoffset-20),       16,       19);
roiManager("Add");   roiManager("Select",64);   roiManager("Rename",
"IL-8");
makeOval(359+(xoffset-13),       57+(yoffset-20),       16,       19);
roiManager("Add");   roiManager("Select",65);   roiManager("Rename",
"IL-8");
makeOval(378+(xoffset-13),       57+(yoffset-20),       16,       19);
roiManager("Add");   roiManager("Select",66);   roiManager("Rename",
"LAP (TGF-b1)");
makeOval(397+(xoffset-13),       57+(yoffset-20),       16,       19);
roiManager("Add");   roiManager("Select",67);   roiManager("Rename",
"LAP (TGF-b1)");
makeOval(423+(xoffset-13),       57+(yoffset-20),       16,       19);
roiManager("Add");   roiManager("Select",68);   roiManager("Rename",
"Leptin");
makeOval(442+(xoffset-13),       57+(yoffset-20),       16,       19);
roiManager("Add");   roiManager("Select",69);   roiManager("Rename",
"Leptin");
makeOval(461+(xoffset-13),       57+(yoffset-20),       16,       19);
roiManager("Add");   roiManager("Select",70);   roiManager("Rename",
"MCP-1");
makeOval(480+(xoffset-13),       57+(yoffset-20),       16,       19);
roiManager("Add");   roiManager("Select",71);   roiManager("Rename",
"MCP-1");


//Row D
makeOval(5+(xoffset-13),       76+(yoffset-20),       16,       19);
roiManager("Add");   roiManager("Select",72);   roiManager("Rename",
"MIP-1a");
makeOval(24+(xoffset-13),       76+(yoffset-20),       16,       19);
roiManager("Add");   roiManager("Select",73);   roiManager("Rename",
"MIP-1a");
makeOval(43+(xoffset-13),       76+(yoffset-20),       16,       19);
roiManager("Add");   roiManager("Select",74);   roiManager("Rename",
"MMP-8");
makeOval(62+(xoffset-13),       76+(yoffset-20),       16,       19);
```

```
roiManager("Add");   roiManager("Select",75);   roiManager("Rename",
"MMP-8");
makeOval(88+(xoffset-13),       76+(yoffset-20),       16,       19);
roiManager("Add");   roiManager("Select",76);   roiManager("Rename",
"MMP-9");
makeOval(107+(xoffset-13),       76+(yoffset-20),       16,       19);
roiManager("Add");   roiManager("Select",77);   roiManager("Rename",
"MMP-9");
makeOval(126+(xoffset-13),       76+(yoffset-20),       16,       19);
roiManager("Add");   roiManager("Select",78);   roiManager("Rename",
"NRG1-b1");
makeOval(145+(xoffset-13),       76+(yoffset-20),       16,       19);
roiManager("Add");   roiManager("Select",79);   roiManager("Rename",
"NRG1-b1");
makeOval(172+(xoffset-13),       76+(yoffset-20),       16,       19);
roiManager("Add");   roiManager("Select",80);   roiManager("Rename",
"PTX3");
makeOval(191+(xoffset-13),       76+(yoffset-20),       16,       19);
roiManager("Add");   roiManager("Select",81);   roiManager("Rename",
"PTX3");
makeOval(210+(xoffset-13),       76+(yoffset-20),       16,       19);
roiManager("Add");   roiManager("Select",82);   roiManager("Rename",
"PD-ECGF");
makeOval(229+(xoffset-13),       76+(yoffset-20),       16,       19);
roiManager("Add");   roiManager("Select",83);   roiManager("Rename",
"PD-ECGF");
makeOval(256+(xoffset-13),       76+(yoffset-20),       16,       19);
roiManager("Add");   roiManager("Select",84);   roiManager("Rename",
"PDGF-AA");
makeOval(275+(xoffset-13),       76+(yoffset-20),       16,       19);
roiManager("Add");   roiManager("Select",85);   roiManager("Rename",
"PDGF-AA");
makeOval(294+(xoffset-13),       76+(yoffset-20),       16,       19);
roiManager("Add");   roiManager("Select",86);   roiManager("Rename",
"PDGF-AB/BB");
makeOval(313+(xoffset-13),       76+(yoffset-20),       16,       19);
roiManager("Add");   roiManager("Select",87);   roiManager("Rename",
"PDGF-AB/BB");
makeOval(340+(xoffset-13),       76+(yoffset-20),       16,       19);
roiManager("Add");   roiManager("Select",88);   roiManager("Rename",
"Persephin");
makeOval(359+(xoffset-13),       76+(yoffset-20),       16,       19);
roiManager("Add");   roiManager("Select",89);   roiManager("Rename",
"Persephin");
makeOval(378+(xoffset-13),       76+(yoffset-20),       16,       19);
roiManager("Add");   roiManager("Select",90);   roiManager("Rename",
"CXCL4");
makeOval(397+(xoffset-13),       76+(yoffset-20),       16,       19);
roiManager("Add");   roiManager("Select",91);   roiManager("Rename",
"CXCL4");
makeOval(423+(xoffset-13),       76+(yoffset-20),       16,       19);
roiManager("Add");   roiManager("Select",92);   roiManager("Rename",
"PIGF");
makeOval(442+(xoffset-13),       76+(yoffset-20),       16,       19);
roiManager("Add");   roiManager("Select",93);   roiManager("Rename",
```

```
"PIGF");
makeOval(461+(xoffset-13),       76+(yoffset-20),       16,       19);
roiManager("Add");   roiManager("Select",94);   roiManager("Rename",
"Prolactin");
makeOval(480+(xoffset-13),       76+(yoffset-20),       16,       19);
roiManager("Add");   roiManager("Select",95);   roiManager("Rename",
"Prolactin");


// Row E
makeOval(5+(xoffset-13),       96+(yoffset-20),       16,       19);
roiManager("Add");   roiManager("Select",96);   roiManager("Rename",
"Serpin-B5");
makeOval(24+(xoffset-13),       96+(yoffset-20),       16,       19);
roiManager("Add");   roiManager("Select",97);   roiManager("Rename",
"Serpin-B5");
makeOval(43+(xoffset-13),       96+(yoffset-20),       16,       19);
roiManager("Add");   roiManager("Select",98);   roiManager("Rename",
"Serpin-E1");
makeOval(62+(xoffset-13),       96+(yoffset-20),       16,       19);
roiManager("Add");   roiManager("Select",99);   roiManager("Rename",
"Serpin-E1");
makeOval(88+(xoffset-13),       96+(yoffset-20),       16,       19);
roiManager("Add");   roiManager("Select",100);   roiManager("Rename",
"Serpin-F1");
makeOval(107+(xoffset-13),       96+(yoffset-20),       16,       19);
roiManager("Add");   roiManager("Select",101);   roiManager("Rename",
"Serpin-F1");
makeOval(126+(xoffset-13),       96+(yoffset-20),       16,       19);
roiManager("Add");   roiManager("Select",102);   roiManager("Rename",
"TIMP-1");
makeOval(145+(xoffset-13),       96+(yoffset-20),       16,       19);
roiManager("Add");   roiManager("Select",103);   roiManager("Rename",
"TIMP-1");
makeOval(172+(xoffset-13),       96+(yoffset-20),       16,       19);
roiManager("Add");   roiManager("Select",104);   roiManager("Rename",
"TIMP-4");
makeOval(191+(xoffset-13),       96+(yoffset-20),       16,       19);
roiManager("Add");   roiManager("Select",105);   roiManager("Rename",
"TIMP-4");
makeOval(210+(xoffset-13),       96+(yoffset-20),       16,       19);
roiManager("Add");   roiManager("Select",106);   roiManager("Rename",
"TSP-1");
makeOval(229+(xoffset-13),       96+(yoffset-20),       16,       19);
roiManager("Add");   roiManager("Select",107);   roiManager("Rename",
"TSP-1");
makeOval(256+(xoffset-13),       96+(yoffset-20),       16,       19);
roiManager("Add");   roiManager("Select",108);   roiManager("Rename",
"TSP-2");
makeOval(275+(xoffset-13),       96+(yoffset-20),       16,       19);
roiManager("Add");   roiManager("Select",109);   roiManager("Rename",
"TSP-2");
makeOval(294+(xoffset-13),       96+(yoffset-20),       16,       19);
roiManager("Add");   roiManager("Select",110);   roiManager("Rename",
"uPA");
```

```
makeOval(313+(xoffset-13),      96+(yoffset-20),      16,      19);
roiManager("Add");  roiManager("Select",111);  roiManager("Rename",
"uPA");
makeOval(340+(xoffset-13),      96+(yoffset-20),      16,      19);
roiManager("Add");  roiManager("Select",112);  roiManager("Rename",
"Vasohibin");
makeOval(359+(xoffset-13),      96+(yoffset-20),      16,      19);
roiManager("Add");  roiManager("Select",113);  roiManager("Rename",
"Vasohibin");
makeOval(378+(xoffset-13),      96+(yoffset-20),      16,      19);
roiManager("Add");  roiManager("Select",114);  roiManager("Rename",
"VEGF");
makeOval(397+(xoffset-13),      96+(yoffset-20),      16,      19);
roiManager("Add");  roiManager("Select",115);  roiManager("Rename",
"VEGF");
makeOval(423+(xoffset-13),      96+(yoffset-20),      16,      19);
roiManager("Add");  roiManager("Select",116);  roiManager("Rename",
"VEGF-C");
makeOval(442+(xoffset-13),      96+(yoffset-20),      16,      19);
roiManager("Add");  roiManager("Select",117);  roiManager("Rename",
"VEGF-C");
makeOval(461+(xoffset-13),      96+(yoffset-20),      16,      19);
roiManager("Add");  roiManager("Select",118);  roiManager("Rename",
"BLANK");
makeOval(480+(xoffset-13),      96+(yoffset-20),      16,      19);
roiManager("Add");  roiManager("Select",119);  roiManager("Rename",
"BLANK");


//Row F
makeOval(5+(xoffset-13),      122+(yoffset-20),      16,      19);
roiManager("Add");  roiManager("Select",120);  roiManager("Rename",
"Ref");
makeOval(24+(xoffset-13),      122+(yoffset-20),      16,      19);
roiManager("Add");  roiManager("Select",121);  roiManager("Rename",
"Ref");
makeOval(461+(xoffset-13),      122+(yoffset-20),      16,      19);
roiManager("Add");  roiManager("Select",122);  roiManager("Rename",
"Negative");
makeOval(480+(xoffset-13),      122+(yoffset-20),      16,      19);
roiManager("Add");  roiManager("Select",123);  roiManager("Rename",
"Negative");

array1 = newArray("0");;
for (i=1;i<roiManager("count");i++){
        array1 = Array.concat(array1,i);

}
roiManager("select", array1);

roiManager("Multi Measure");
selectWindow("Results");
//headings=String.getResultsHeadings;  replace(headings,  "Mean\\(",
""); replace(headings, "\\)",""); print(headings);
text = getInfo();
```

```
lines = split(text, "\n");
columns = split(lines[0], "\t");
bkground=getResult("Mean(Negative)",0); print(bkground);
refspot=getResult("Mean(Ref)",0); print(refspot);
refstd=refspot-bkground;
arrayR=newArray("0");
for (i=1;i<columns.length;i++) {
arrayR = Array.concat(arrayR,getResult(columns[i],0));
columns[i]=replace(columns[i], "Mean\\(", "");
columns[i]=replace(columns[i], "\\)","");
}
for (i=0;i<columns.length;i++) {print(columns[i]);}
for (i=0;i<columns.length;i++) {print(arrayR[i]);}


selectWindow("Results");
run("Close");
for (i=1;i<columns.length-1;i++) {
subbk= (arrayR[i])-bkground;
if (subbk >= 0.0)
     setResult(columns[i], 0, subbk);
else setResult(columns[i], 0,0);
```